PETROLOGICAL, GEOCHEMICAL AND DIAGENETIC STUDIES OF THE EUPHRATES LIMESTONE FORMATION (LOWER MIOCENE) OF THE JAMBUR AREA, NORTHEAST IRAQ

Ibrahim Abdul Karim Rashid

A Thesis Submitted for the Degree of PhD
at the
University of St Andrews

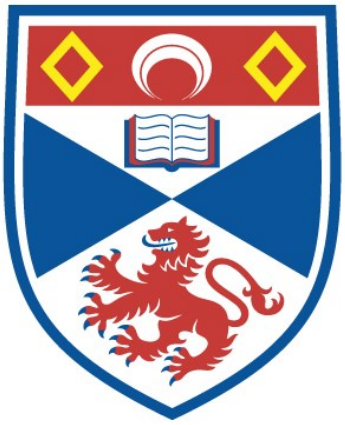

1989

Petrological, geochemical, and diagenetic studies of the Euphrates Limestone Formation (Lower Miocene) of the Jambur area, northeast Iraq.

Thesis submitted for the degree of the Doctor of Philosophy at the University of ST. Andrews.

By

IBRAHIM ABDUL KARIM RASHID
1989

ProQuest LLC.
789 East Eisenhower Parkway
P.O. Box 1346
Ann Arbor, MI 48106 – 1346

UNIVERSITY OF ST. ANDREWS

Thesis Copyright Declaration Form.

A UNRESTRICTED

"In submitting this thesis to the University of St. Andrews I understand that I am giving permission for it to be made available for public use in accordance with the regulations of the University Library for the time being in force, subject to any copyright vested in the work not being affected thereby. I also understand that the title and abstract will be published, and that a copy of the work may be made and supplied to any bona fide library or research worker."

B RESTRICTED

"In submitting this thesis to the University of St. Andrews I wish access to it to be subject to the following conditions:
for a period of Three years [maximum 5] from the date of submission the thesis shall be

a) withheld from public use.

b) made available for public use only with consent of the head or chairman of the department in which the work was carried out.

I understand, however, that the title and abstract of the thesis will be published during this period of restricted access; and that after the expiry of this period the thesis will be made available for public use in accordance with the regulations of the University Library for the time being in force, subject to any copyright in the work not being affected thereby, and a copy of the work may be made and supplied to any bona fide library or research worker."

Declaration

I wish to exercise option Ba [i.e. A, Ba or Bb] of the above options.

Signature

Date 22.6.1989

This thesis is dedicated to
my mother
and
to my wife, my chlidren, Mustafa, Sara, Nadia

AKNOWLEDGEMENTS

I would like to take this opportunity to express my sincere thanks and gratitude to Professor E. K. Walton, my supervisor for his encouragement, suggestions, and critical review of the manuscript.

My thanks also go to my wife and children for their patience, and encouragement without which this work could not be completed.

I also extend my gratitude to Dr R. A. MacGregor and Dr P. Bowden for their help and cooperation during my research. Sincere thanks are due to Dr. A. E. Fallick, S.U.R.R.C., East Kilbride, for his help in respect of stable isotope analyses.

Thanks also due to the technical staff of St. Andrews University, particularly, Jim Allen, Andy Mackie, Angus Calder, and Sandy Edwards for their help and efforts over the last three years. I am also thankful to Mrs Galloway and miss Kit Finlay for general help.

I gratefully acknowledge the receipt of the grant from the Iraqi Ministry of Higher Education and Scientific Research, and sincere thanks are due to the Department of Geology, the Northern Petroleum Organization (NPO) for their help and supply of the core samples and documents.

CERTIFICATE

I hereby certify that IBRAHIM ABDUL KARIM RASHID has been engaged in research for nine terms at the University of St. Andrews, that he has fulfilled the conditions of Ordinance No. 12 and resolution of the University Court, 1967, No.1, and that he is qualified to submit the accompanying thesis in application for the degree of Doctor of Philosophy.

Signed.....Date 22/6/89.

I certify that the following thesis is of my own composition, that it is based on the result of research carried out by me, and that it has not previously been presented in application for a higher degree.

Signed.....Date 22/6/1989

ABSTRACT

The Euphrates Limestone Formation in north Iraq is encountered at depth in Jambur Field and eight cores were studied in this work. The formation is overlain by Dhiban Anhydrite Formation and underlain by the basinal Serikagni Formation. The formation was deposited in a shallow lagoonal environment.

Three types of dolomites have been observed in the Euphrates Limestone Formation. The first type is class A which is very fine (4-10 microns) and associated with anhydrite and gypsum. Its origin is presumed to be of contemporaneous primary dolomite formed in a supratidal environment.

The second type is class B (10-30 microns in grain size) formed as a replacement of pre-existing carbonate sediments. Reflux of hypersaline brines is presumed to have been the source of magnesium for this type of dolomite. The third type of dolomite is formed of larger crystals 50-100 microns. This type is formed of euhedral and inclusion-free rhombs filling pores and vugs, and sometimes disseminated between other types of dolomite. This dolomite probably formed by mixing of meteoric water with sea water.

The dolomite in the Euphrates Limestone Formation is mainly stoichiometric and well ordered in the southern part of the studied area. Eight types of dolomitization fabrics are observed in the formation. These types range between partial

to complete dolomitization with complete obliteration of the original textures.

The degree of dolomitization is very extensive in the southeast part of the studied area, and decreases in the northwest direction. Dolomitization also decreases with depth. Therefore three different areas are recognized during the present work, these areas are; the southeastern (A), the central (B), and the northwestern (C).

Euphrates Limestone Formation dolomite has $\acute{O}^{18}O$ values ranging between 0.23 to 3.37 ‰, which is heavier than most normal marine waters today and very close to modern sabkha dolomites. These heavy values of oxygen isotopes indicates a hypersaline environment as a source for most of the dolomite in the formation

Strontium contents in the dolomite are relatively high (500-700 ppm) compared with most ancient dolomites, and similar to the concentration in Holocene dolomite.

Different types of diagenetic processes which were responsible for cementation, compaction, dissolution, precipitation of anhydrite, and dolomitization are recognized in the formation. Different types of cements have been identified in the formation, namely isopachous crusts, micritic envelopes, ferroan and non-ferroan calcite. Very high moldic porosity in the oolitic fossilifeous grainstone facies are detected. The overall porosity of the formation in the dolomitized part is high and very low in undolomitized parts.

CONTENTS Page

LIST OF FIGURES

LIST OF APPENDICES

CHAPTER 1
INTRODUCTION

1.1 AIM AND MOTIVATIONS

The objective of the present study is to gain an understanding of the diagenesis and the diagenetic processes and their effects on the textures, structures, compositions and the porosity of the Euphrates Limestone Formation in the Jambur Field, also to establish the origin of the dolomite and its environment of deposition. The study deals with petrography, porosity, stable isotopes and the trace element distribution in the formation.

The area examined in the present study represents approximately 140 Km^2. The Euphrates Limestone Formation is encountered at depths between 1000-2000m below sea level in the Jambur Field (**Fig 1.2**). Cores were taken from eight wells through the Euphrates Formation, Lower Miocene.

The Euphrates Limestone Formation is overlain by the Dhiban Anhydrite Formation deposited during the regression which occurred during the Lower Miocene. The present study places emphasis on the vertical and horizontal variation of the sequence, the diagenetic processes involved and their relationship to the products.

1.2 LOCATION

The present study is mainly concerned with the limestone, dolomite, and dolomitic limestone sequences within the Euphrates Limestone Formation, northeast Iraq, in the Jambur

area. Eight wells were cored through the formation. The Jambur Field is situated 20 Km southeast of Kirkuk City in the northeast of Iraq. The field is about 40 Km long and 3.5 Km wide (**Fig 1.1, 1.2**).

1.3 SAMPLING

A total of 170 rock samples were collected from subsurface cores recovered from eight wells in the Jambur Field at 1m intervals. A total of more than 200 thin sections were stained and impregnated with coloured epoxy resin. Seventy one samples were prepared and analysed by x-ray diffraction both quantitatively and qualitatively. Thirty three samples were analysed to estimate the dolomite ordering and stoichiometry. Seventy samples were prepared and analysed by x-ray fluorescence to measure the trace element concentrations in the Formation, finally twenty six samples were prepared and analysed for isotopic composition of calcite, dolomite, and calcite dolomite pairs, both for oxygen and carbon isotopes. A few analyses were made by the microprobe to measure the compositional differences across the dolomite rhombs.

1.4 METHODS

A combination of various methods and techniques are used during the present study. Thin sections are stained in order to differentiate between the carbonate minerals and impregnated with coloured epoxy resin to facilitate porosity identification. X-ray diffraction methods are used to estimate the mineralogical composition of the samples both quantitatively and

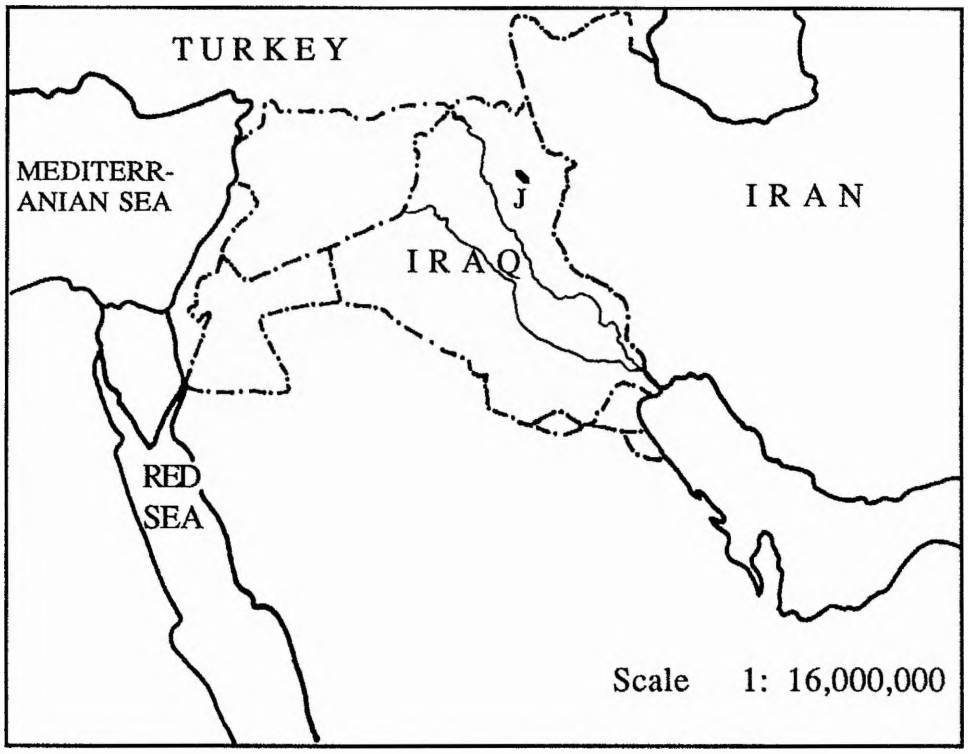

Fig 1.1 Map showing the location of Jambur Field (J), Northeast of Iraq.

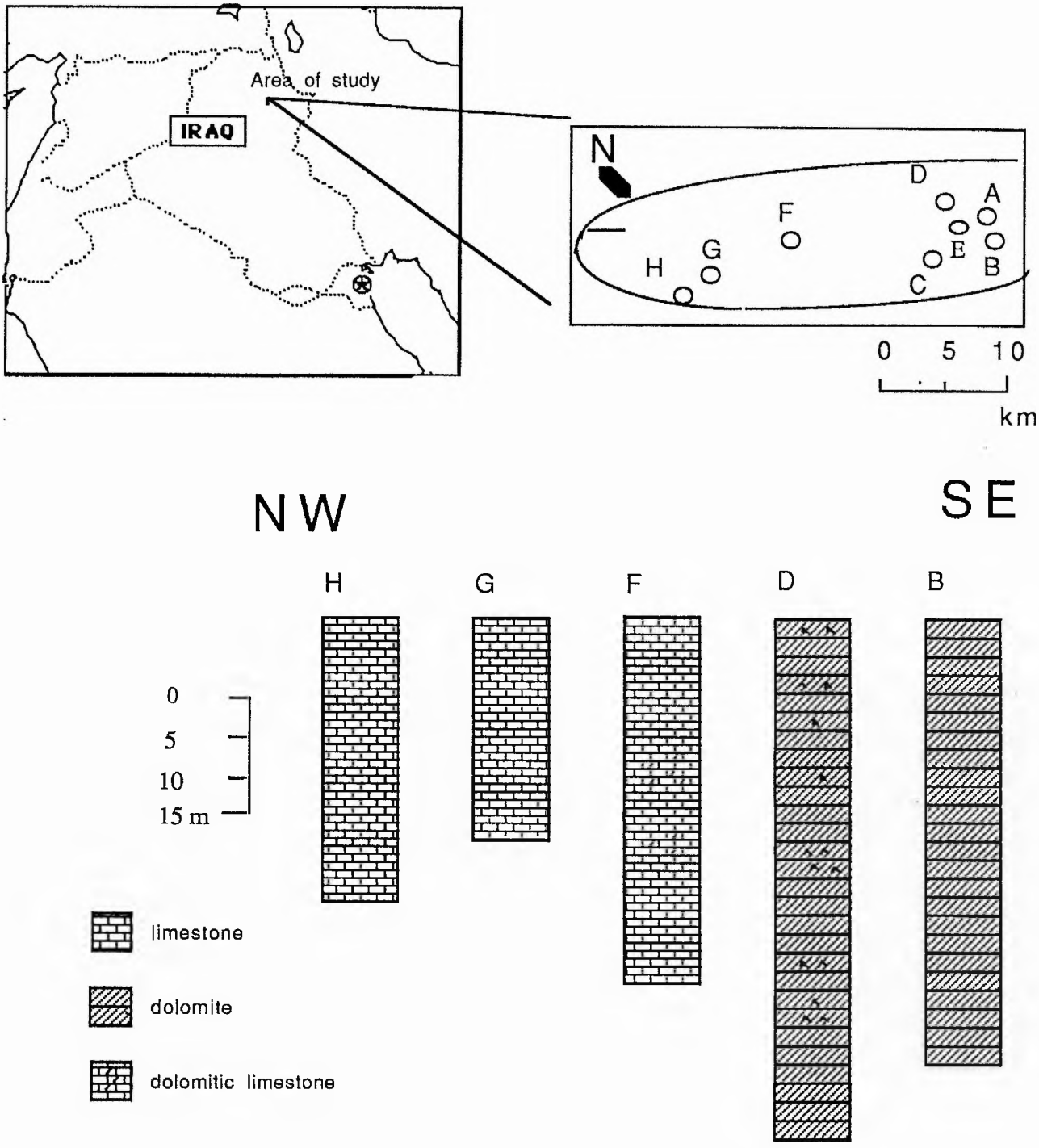

Fig.1.2 A map showing the location of the studied area and a sketch showing the location of the cored wells in Jambur, and lithosratigraphic sections of the Jambur wells show dolomitization which is complete in the SE area but incomplete in the NW. Lithology in wells A, B and D is similar, so too is that in wells G, H , and C.

qualitatively, and to estimate the dolomite ordering and stoichiometry. Trace element analyses are carried out using the x-ray fluorescence technique. Isotopic composition analyses is carried out in East Kilbride using the mass spectrometer to measure the isotopic composition of the dolomite and the calcite in the formation. SEM is used extensively and proved very useful in the identifications of the microstrucres, microporosity, dissolution features and clay minerals (**Appendix 1**).

1.5 PREVIOUS WORK

The Jambur Field and its region have been a subject of continuous concern, since oil accumulation was discovered early this century. Drilling assumed in 1927 and oil was produced in the 1950s in the region. The most distinctive work concerning the geology, and the stratigraphy of the region has been published by **Bellen (1959)**.

Dunnington (1958) published his work which was mainly concerned with stratigraphy, sedimentation and hydrocarbon accumulation, generation, migration and dissipation.

A regional stratigraphic correlation study concerned with environmental setting, fossil assemblages and age of the Tertiary rocks has been published by **Bellen (1959)**.

The geology of the southern area of Kirkuk (including the area of the study) has been studied in detail, with a regional correlation diagram summarizing the geological knowledge (**Al Naquib, 1967**). Many other works dealing with various aspects of the geology of the area have been published

contributing to the knowledge of the structure and stratigraphy of the region (**Henson, 1951; Dunnington, 1967**).

CHAPTER 2
GENERAL GEOLOGY

2.1 Structure

Iraq lies in the border between two main Precambrian Units of the Middle East. These units are 1. Part of the African platform (Nubio-Arabian) and 2. The Asian branch of the Alpine geosyncline. The border between these two units has been placed on the northern border of the folded zone (**Buday, 1980**) (**Fig 2.1**).

The North Iraq basin has been divided into three main interrelated structural zones (**Fig 2.1**) (**Dunnington, 1958**). Each zone has its own characteristic tectonics and geological history.

The zones are 1. **Zone of major complex overthrusting** 2. **Zone of authochthonous folding**, and 3. **The Unfolded zone**. These zones were clearly differentiated during the later Tertiary (mainly Pliocene). The Alpine Orogeny raised the high Zagros mountains close to and beyond the northeastern borders of Iraq, and produced the large elongated anticlinal folds of the folded zone.

Henson (1951b) stressed that the late Tertiary folding in the folded zone was intimately affected by a preexisting complex of faults, which left residual features to deflect folding and which pre-disposed the region to react in irregular and complex fashion to simple tangential pressure.

The first zone (zone of major complex overthrusting) forms a narrow belt in the remote northeastern part of Iraq, mainly consisting of a complex tectonic area, with extensive overthrusting. Rocks in this zone show a low grade of metamorphism. Extensive igneous activity is represented by basalt, andesite, dolerite and other basic rocks, and granite. The second zone (zone of Authochthonous folding) comprises a wider area (100 miles) in which the folds extend in a general NW-SE direction in the northeastern part of the country. In the north and the northwest part, the trend gradually changed to East-west (**Fig 2.1**).

The area is made up of sharp folds with or without faulting and subordinate thrusting. Anticlines in this area run en echelon and are separated by broad synclines. There is a tendency for the anticlines to increase in the amplitude and tightness in the direction of the thrusted zone (Nappe zone) but there are many departures from this phenomenon. Another phenomenon noticed in this zone is the existence of great elevational differences between adjacent anticlines of similar dimension. These anomalies among others led **Henson (1950)** to believe in deep seated block faulting along NW-SE, NE-SW, E-W, and N-S trends.

The last zone (Unfolded Zone) includes a large area of western Iraq, characterised by the absence of surface structures, except for a few folds of small amplitude. Studies have shown the existence of important buried structures throughout the zone.

The later variation in sedimentary thickness over a small distances in this zone are believed to be controlled by pre-

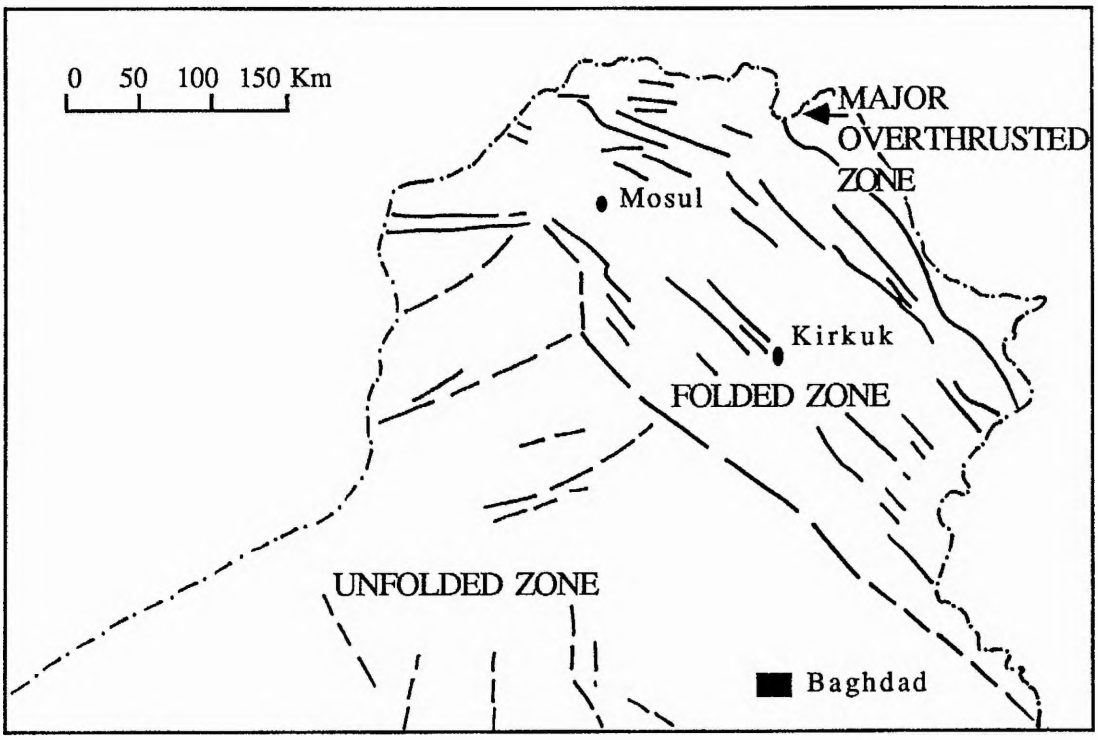

Fig 2.1 Map showing the structural zones of northern Iraq .

Miocene faulting. The boundary between the folded and unfolded zones is abrupt and follows a more or less arcuate line from northwest-southeast in the south to east-west in the northwest but is offset sharply in the area west of Qaiyara.

The Jambur structure lies within the zone of autochthonous folding (zone 2). The structures in this zone are mainly of Late Tertiary origin, and most of them exhibit thrusting of one flank over the other, the structures show disharmony between the surface shape and the subsurface cores of the anticlines (**Fig 2.2**). Structures in this zone trend in a general NW-SE direction and are separated by broad synclines.

Later the platform of part of Iraqi territory was divided into two main structural Units, the Stable and the Unstable Shelf. (**Buday, 1980**). (**Fig 2.3**).

The Stable Shelf is characterized by a reduced thickness of sedimentary cover, and lack of folding. The Unstable Shelf is characterized by a thick and folded sedimentary cover, the intensity of folding as mentioned before increasing in a northeastern direction.These two major units are farther subdivided into subzones (**Fig. 2.4**).

2.2 Jambur Structure

The Jambur structure extends in the general regional direction (Zagros trend) NW-SE and it is en echelon with the Pulkhana structure. The structure appears as a gentle asymmetrical anticline. The southwestern flank is the steepest,

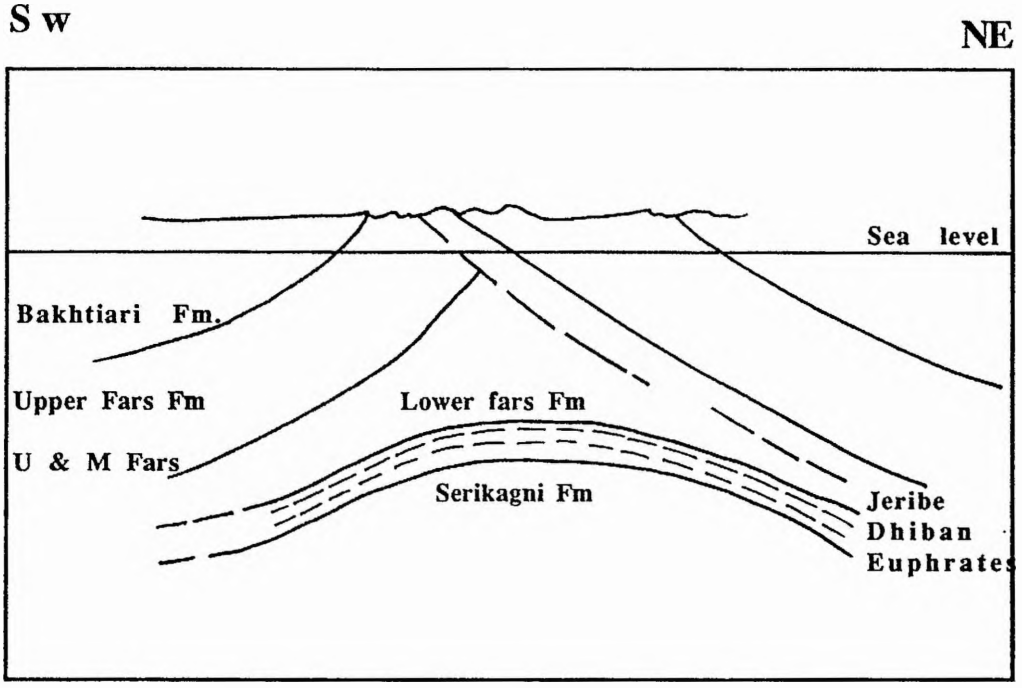

Fig 2.2 Structural cross section of Jambur Field. Shows the disharmony between the surface shape and the subsurface core of the anticline.

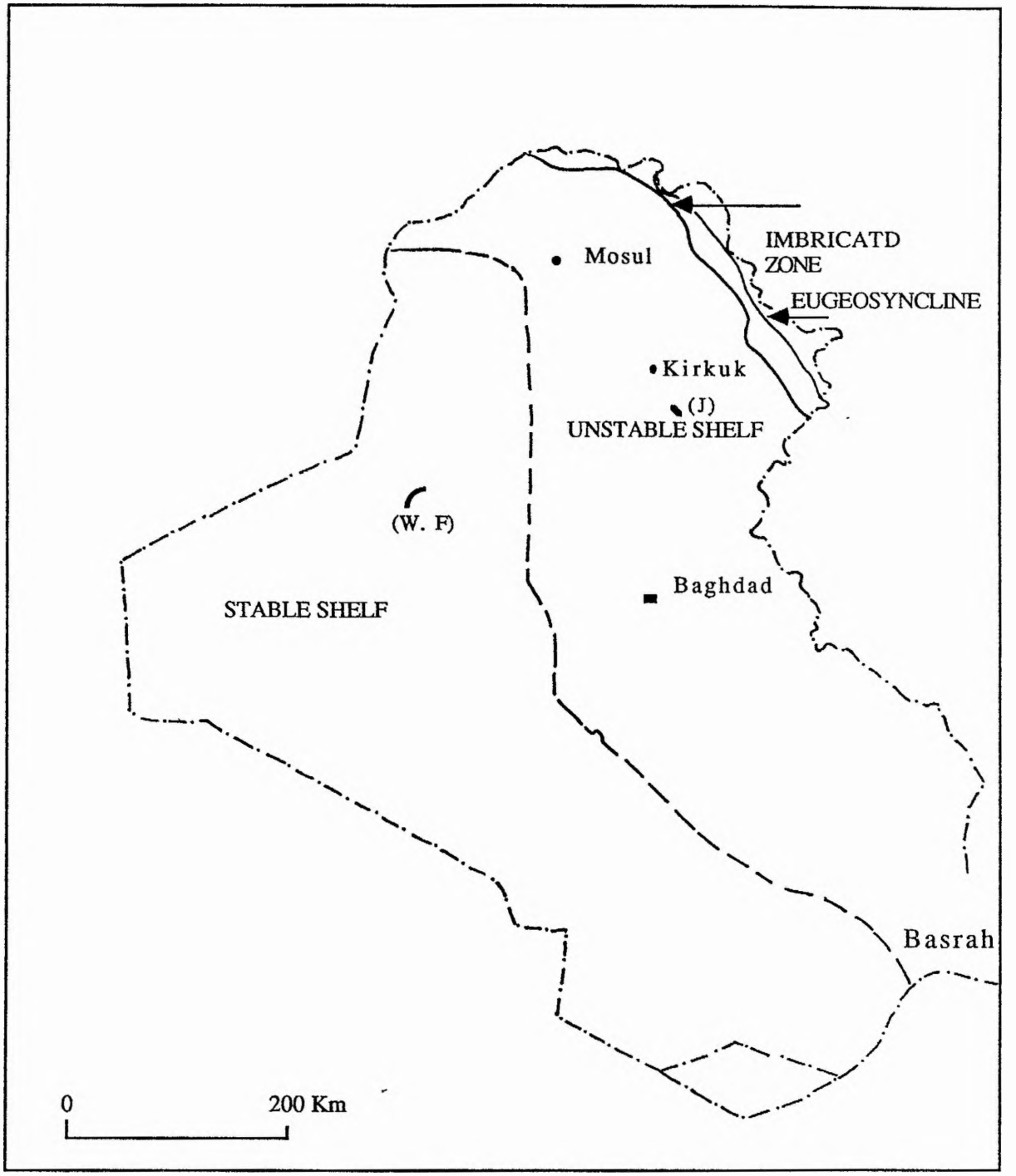

Fig 2.3 Map showing the major structural units in Iraq after Buday (1980).

(W.F) Type section of the Euphrates Limestone Formation

(J) Jambur structure

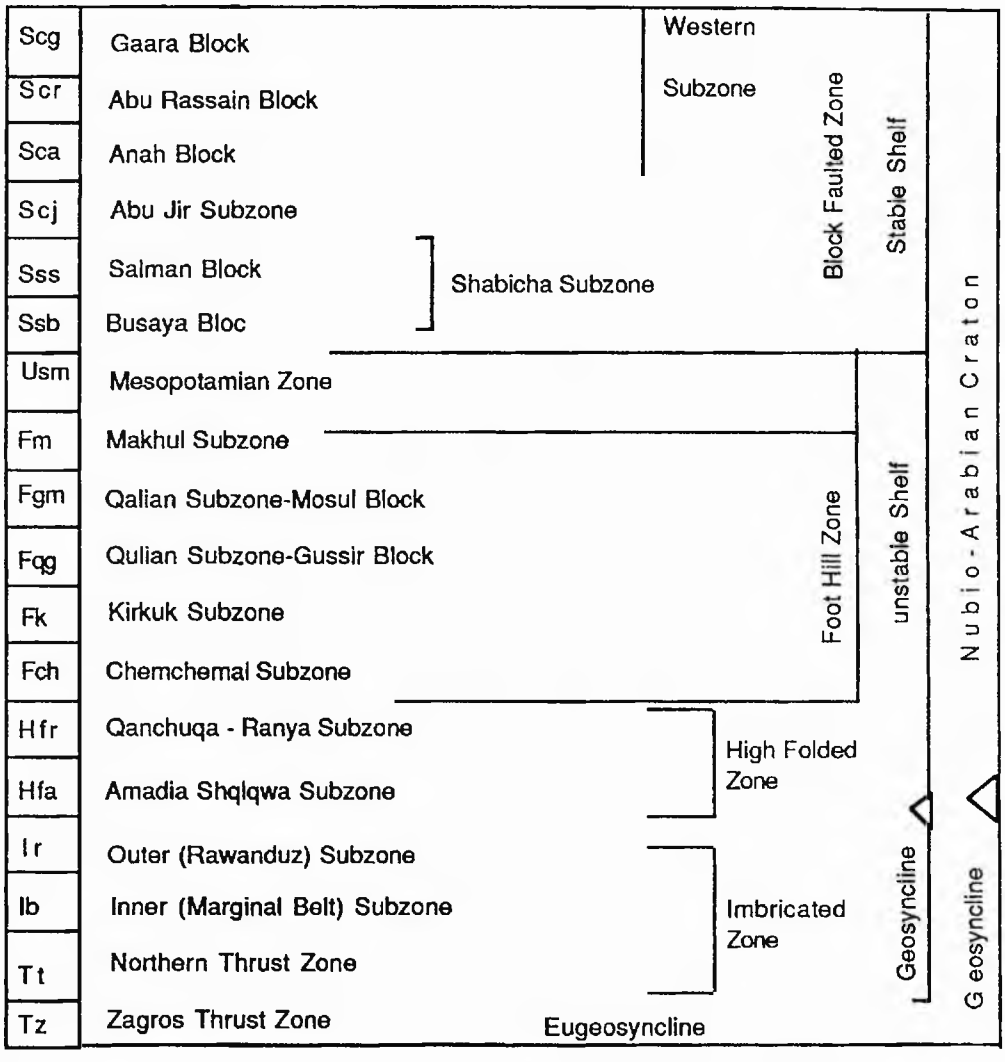

Fig 2.4 Main structural divisions of Iraq. After Buday (1980)

in some places the SW limb approaches verticality even locally overturned. A difference in strike between the higher and lower beds of the southwestern limb has been noticed in places southeastward and a distinct displacements occurs, which reaches about 300m away from the axis. In Jambur the Lower Fars of the northeastern flank with a dip of 30° is thrustover the upper Fars which shows very high to vertical dip (**Fig 2.2**). Some oblique faults are developed and extend across the axis. The structure is separated from the Pulkhana structure by a narrow syncline.

2.3 STRATIGRAPHY

The stratigraphic sequence drilled in the Jambur structure is mainly of limestone of Cretaceous and Tertiary ages with minor shales in the lower part, and anhydrite at the upper part of the Miocene (**Fig 2.5**). The uppermost sequence Fars and Backhtiari (Middle Miocene-Pliocene) is composed of sandstone, siltstone, shale with minor carbonate of evaporitic nature (**Fig 2.5**). For the purpose of the present study only the stratigraphy of the lower Miocene will be dealt with briefly. The Serikagni Formation which represents the base of the Lower Miocene sequence in Jambur is underlain by the Basal Anhydrite Formation (Lower Miocene) which is composed entirely of massive anhydrite bed approximately 5-6 metres thick.

The Serikagni Formation has a restricted areal distribution compared with the Euphrates Limestone Formation, and it represents basinal and offshore sediments mainly composed of globigerinal

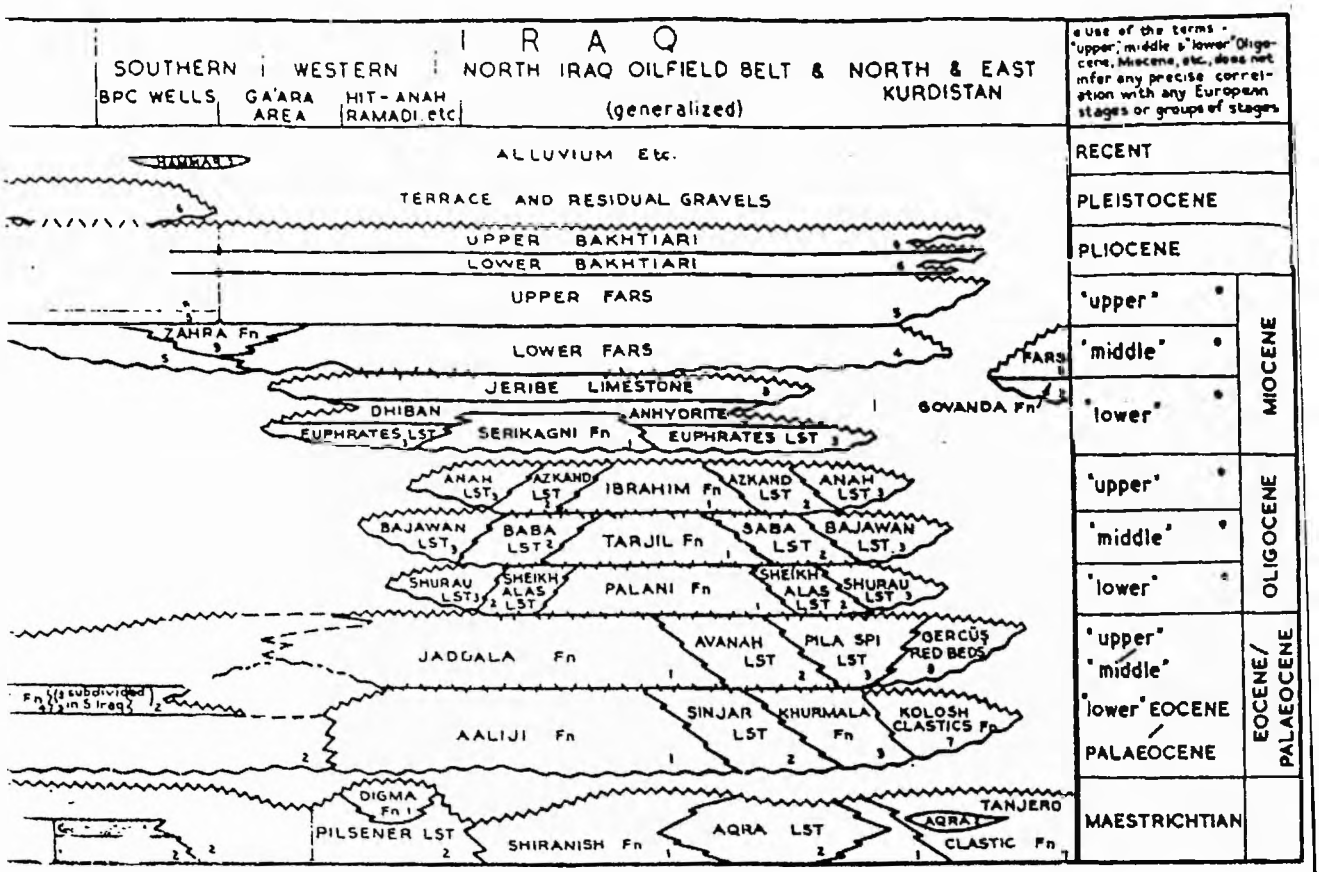

NUMBER - KEY TO LITHOLOGIES OF UNITS

1 "Basinal" marls, shales and limestones
2 Neritic, shoal and shelf limestones.
3 Backreef and lagoonal limestones (including reef limestones in Oligocene)
4 Anhydrites and salt (with limestones, etc.)
5 Marine sandstones, siltstones and variegated clastics
6 Continental sandstones, lacustrine clastics, etc.
7 "Flysch"-like calcareous clastics.
8 Red beds.
9 "Fresh water" sandy limestone

KEY TO BOUNDARY SYMBOLS

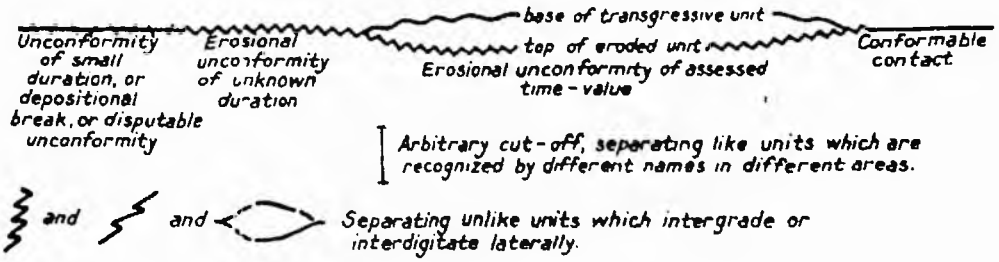

Fig 2.5 Stratigraphy of Tertiary Rocks in Iraq showing lateral relations of lithologies.(After Al Naqib, 1967).

chalky limestone. This formation is thought to have been deposited in the central part of the Miocene basin and at its maximum thickness reaches 150m (**Al Naquib, 1967**). From both lithological and fauna facies point of view this Formation ranges from purely globigerinal marly sediments to algal/reef limestone with all the intermediate gradations (**Bellen , 1959**). The relation between this formation and the overlying Euphrates Limestone Formation is one of interfingering and intergradation.

The Euphrates Limestone Formation which overlies this formation in Jambur is composed of lagoonal limestone which very strongly recrystallised and dolomitized with occasional anhydrite and chert nodules. A varied fauna includes gastropods, miliolids, chilostomallids, peneroplids and crustacean debris. The thickness of the Euphrates Limestone Formation varies over the Jambur area from 5-85m. Normally this formation is overlain by the Dhiban Anhydrite Formation in most places or sometimes it is replaced by it.

The Dhiban Anhydrite Formation of the Lower Miocene age shows a remarkable variation in thickness over the Jambur area. Lithologicaly it mainly consists of massive anhydrite interbedded with limestone, and occasional thin blue marl. This limestone contains a variety of fauna (rotalids, chilostomallids, molluscs and crustacean debris) and it is a lagoonal limestone.

The Formation passes laterally and downward into the Euphrates Limestone Formation, But it is overlain transgressivelly by the Jeribe limestone. The Jeribe Limestone

Formation has been clearly recorded over Jambur and adjacent structures, and probably covers a wider area than the Euphrates Limestone Formation. Again this formation shows great variation in thickness (**Fig 2.6**) with the thickest section recorded in the northwest part of the structure. Lithologically the formation consists of marly, lagoonal limestone, finely crystalline and in some places dolomitized.

Anhydrite nodules and replacement occurred throughout the formation, chert nodules and secondary silica are present. Miliolids, rotalids, Rotalia biicarii, Miogypsina, and chilostomallids, were common fauna in this formation in addition to echinoids, crustaceans and ostracods.

In Jambur the Jeribe Limestone Formation rests on the Dhiban Anhydrite Formation, but it may rest over the Euphrates Limestone Formation, or older formations when the Dhiban Anhydrite Formation is absent. Jeribe itself is overlain trasgressivelly by the Lower Fars Formation of the Middle Miocene age.

2.3.1 EUPHRATES LIMESTONE FORMATION

The Euphrates Limestone Formation is the most superficially widespread formations and one of the earliest described formations in Iraq (**Bellen, 1959**).

The type locality of the formation lies nearWadi Fuhami (**Fig 2.3**) in the Anah Trough on the Stable Shelf. Extremely reduced thickness of the formation in the type locality means that probably only part of the section comprising the formation is present there (**Buday, 1980**). At the type locality, the

Formation is shelly, chalky, well bedded and recrystallized limestone (**Bellen, 1959**) and it does contain sand in the subsurface section (**Bellen, 1959**).

Oolitic limestone and conglomerate were reported from Anah wells and from surface sections around the type locality area (**Hay and Hart, 1959; Bellen, 1959**). A great lithological variability of the formation has been recognized during field survey carried out by parties of the State Organization for minerals (**S O M**) over the last years (**Jumaily, 1974**). The survey revealed that the Euphrates Limestone Formation contains several beds of greenish marl, marly limestone and conglomerates. The limestone thickness varies greatly and the rocks are often recrystallized, mostly oolitic chalky and shelly limestone (**Buday, 1980**).

The thickness at the type locality is only eight metres, whereas the thickness in the surrounding areas as well as in the bore holes is usually many times more reaching a maximum of one hundred metres. The average thickness is about sixty metres, whereas the thickness of the formation in the Jambur area averages only forty five metres.

The Formation was deposited under shallow marine and lagoonal conditions, with local coral and lithophyllid reefs and with intermittently occurring fore reef conditions, on one side, and lagoonal conditions on the other side (**Buday, 1980**).

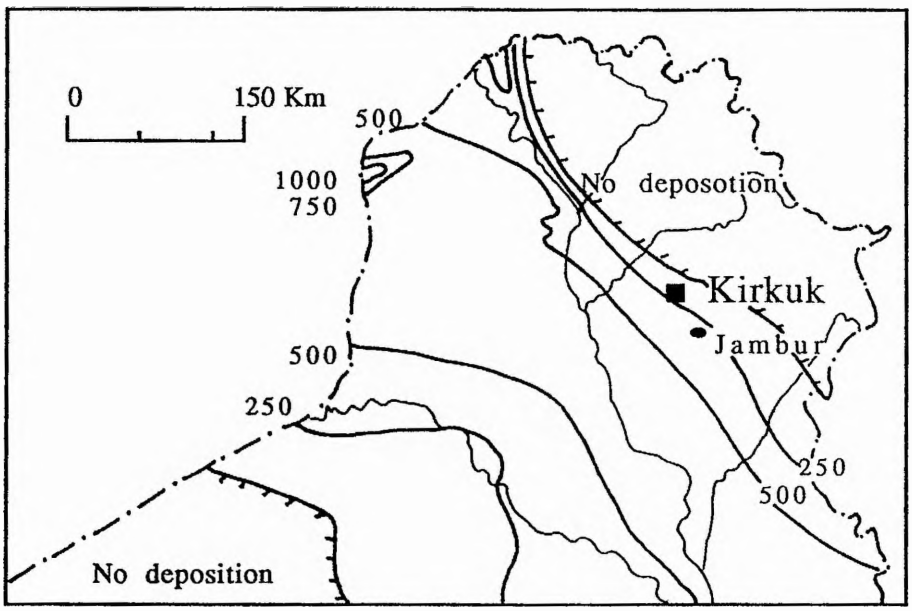

Fig 2.6 Isopach map of the Euphrates Limestone Formation.

According to a detailed evaluation of the fuana (**Cytroky and Karim, 1971**), a later Miocene age and early Middle Miocene was determined for the Euphrates Limestone Formation. But a more detailed investigation proved that only Lower Miocene is present (**Prazak, 1974**).

The lower contact of the formation is usually unconformable and the formation in the type locality area overlies a horizon of conglomerate and residual clay filling the uneven Oligocene Anah Formation. In many areas the formation overlies different Oligocene and Eocene Formations, but in areas where the underlying unit is Sarikagni, the lower contact is conformable e.g. Jambur area.

The upper boundary at the type locality is not exposed. **Bellen *et al* (1959)** suggested that the limestone on the surrounding hillocks belong to the Jeribe Formation. It seems , therefore, that the upper contact is conglomeratic marking the errosional termination or at least an emergent phase at the top of the formation. In the Jambur area from the present study the top part of the formation in most cases is marked by dolomite, and dolomitic limestone associated with anhydrite nodules. The top of the Formation is covered with a massive anhydrite bed of the Dhiban Anhydrite Formation.

In general the formation is formed of various kinds of rocks, mudstone, wackestone, packstone and grainstone limestone and dolostone, in some cases formed of dolomitic limestone.

Bellen *et al* (1959) reported that the Euphrates Limestone Formation is either overlain and replaced by partially

contemporaneous Dhiban Anhydrite Formation, in this case the upper boundary is gradational and conformable as in the Jambur area; or it is overlain by the Jeribe Limestone Formation, in which case the boundary is subconglomeratic and unconformable.

2.3. GENERAL PALEOGEOGRAPHY

The Tertiary sediments were laid down in broad basin trending in general NW-SE direction; this trough was formed during the Upper Cretaceous times and continued throughout the Tertiary times. The trough is bordered in the southwest by the Ga'ara Uplift, and on the northeast by a steep updip slope.

The facies distribution within the Lower Miocene sequence was controlled by a series of shoals and islands along the eastern shore of the trough which separated the open sea in the west from a more or less lagoonal area at the east or northeast.The islands and shoals are believed to have been represented by a low area of bryozoan and algal reefs.

At the end of the Oligocene a regression occurred in the Kirkuk area, marked by conglomerates which separates the Euphrates Limestone Formation (Lower Miocene) from the Anah Limestone Formation (Oligocene). An important transgression followed this regression and introduced the Lower Miocene sediments.

During the Miocene the coast line of the gulf or lagoon ran from Mosul to the north of Kirkuk and extended southwestward to Chiasurkh. Along this shore line in Bai Hassan and Khormor the Lower Miocene lagoonal Euphrates Formation was deposited

in a belt varying in width between 10-20 Km. From this area toward the central basin the equivalent off shore sediment (The Serikagni Limestone Formation) was laid down.

A good deal of interfingering and interdigitation between these two formations is indicated both laterally and vertically.

Bellen (1959) reported that these two formations were deposited in a shallow sea which was bordered by fairly wide lagoon, that was effectively separated by a series of shoals and islands of lithophyllids-bryozoan and algal reefs. To the west of the coast line, and seawards, the top of the Euphrates Limestone Formation passes laterally into the Dhiban Anhydrite Formation which is evidenced in the Jambur and Injana areas. West of this area the Euphrates Limestone Formation is completely absent and the sediments of the Dhiban Anhydrite Formation rest directly on the basinal Serikagni Limestone Formation.

Precipitation of the Dhiban Anhydrite Formation from the Lower Miocene lagoon is thought to be due to the partial or complete closure of the exit between the lagoon and the open sea **(Bellen,1959)**.

Dhiban Anhydrite Formation shows frequent facies change and interfingering. These changes are believed to be caused by major oscillations in the depth of the sea, which were probably controlled by a local change in the rate of sedimentation.

Evaporite sedimentation (Dhiban Anhydrite Formation) was ended by the introduction of a transgressive Jeribe Limestone Formation. This was probably caused by the opening of the barrier between the lagoon and the open sea. At the end of the

Lower Miocene the Kirkuk area experienced a short period of regression which resulted in the erosion of exposed Eocene and some Oligocene formations. This regression is indicated by the thick conglomerates which cover the Lower Miocene and entire Oligocene. This regression was followed by a major transgression which covered a large area of northern Iraq. This large transgression which introduced the Lower Fars Formation (**Middle Miocene**) is marked by the Basal Fars Conglomerate (BFC).

CHAPTER 3
PETROGRAPHY

3.1. LIMESTONE

The Euphrates Limestone Formation is composed of grainstone, wackestone, mudstone and packstone but varying degrees of dolomitization have occurred. The result is that limestones are dominant in the northwestern part of the study area (cores **H** and **G**), with dolomite in the southeast cores **A**, **B**, and **D**, and core **F** represents a transitional area.

Although dolomitization is extensive, the calcareous components in the surviving limestone are of the following types:-

1- Calcite skeletal fragments.

2- Fine crystalline groundmass carbonates.

3- Various kinds of cements.

3.1.1 Calcite skeletal fragments

Generally the skeletal fragments present include brachiopods, gastropods, ostracods, echinoderms, red and green algae, crinoids, foraminifera, and bivalves. The grains are surrounded by micritic envelopes that are also surrounded in most cases by an isopachous crust cement. These kinds of cements are characteristic of marine phreatic diagenesis **(Bathurst, 1966; Bricker, 1971; and Longman, 1980)**. The micritic envelopes indicate the role of microorganisms; sometimes extensive boring has occurred presumably produced by mechanisms described by **Bathurst, 1966; Friedman,**

1964; Friedman etal, 1971; Kobluk and Kahl, 1978, and Kobluk and Risk, 1977. The isopachous crust cement is often recrystallized to coarser crystals. Selective dolomitization has sometimes affected the groundmass leaving the bioclastic grains undolomitized (**Fig 3.1**) whereas in other cases the skeletal fragments have been partially dolomitized (**Fig 3.2**). In the ultimate case the grains become totally dolomitized (**Fig 3.3**).

In general, the fossils, lithoclasts, and the skeletal fragments show signs of compaction as indicated by the breakage of the grains before cementation (**Fig 3.4**).

Replacement of the grains (bioclastic) by dolomite or anhydrite sometimes leaves the internal texture unaltered (**Fig 3.5**), on the other hand it may be totally altered.

3.1.2 Fine crystalline groundmass carbonates

This type of carbonate is very finely crystalline and in most cases is cryptocrystalline. The individual crystals are very difficult to recognize under the microscope (**Fig 3.6**). The porosity of this type of carbonate is very low or negligible.

This type includes micritic envelopes, formed of crystals of low magnesian calcite (**Bathurst, 1975; Monty, 1967**). The carbonates of the groundmass contain different types of quartz of various sizes which are very abundant sometimes and form up to 5% of the total sediment. Mega, micro and flamboyant quartz of different sizes are present in the groundmass (**Fig 3.7**). Feldspar crystals are present (**Fig 3.8**) and may be replaced by gypsum lozenges. Pyrite is present in the form of

Fig 3.1 Photomicrograph of a foraminiferal test composed of calcite in a completely dolomitized groundmass. The chamber of the test is filled with dolomite crystals. Plane polarized light. Scale bar is 0.35mm.

Fig 3.2 Photomicrograph of a brachiopod fragment which is partially dolomitized in a completely dolomitized groundmass. Internal structure of the fragment remained unaltered. Plane polarized light. Scale bar is 0.17mm.

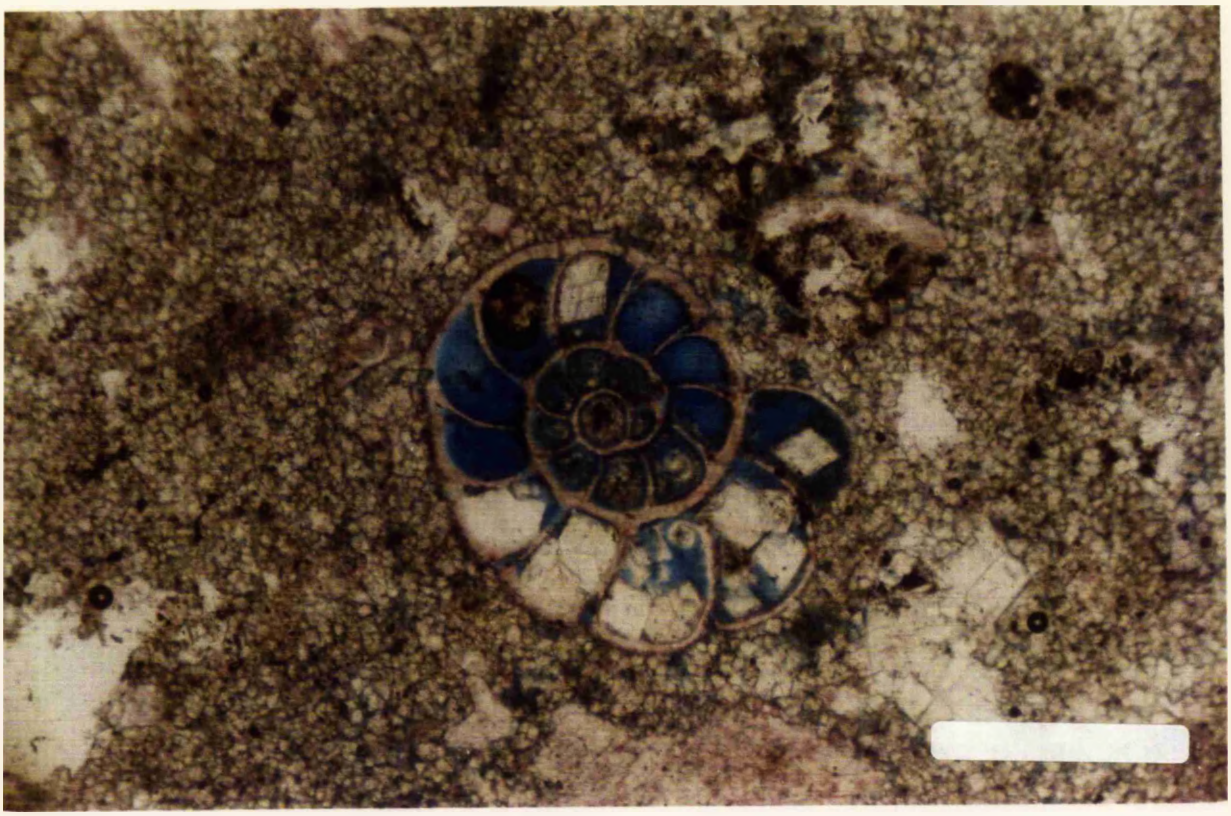

Fig 3.3 Photomicrograph of bioclastic and lithoclastic grains which are completely dolomitized as well as the groundmass. The boundaries between the grains are still recognizable. White areas are anhydrite cement, whereas the dark areas represent moldic pores. Plane polarized light. Scale bar is 0.875mm.

Fig 3.4 Photomicrograph of a half moon shape oolite indicates that compaction occurred at an early stage, and before the lithification of the sediments. Plane polarized light. Scale bar is.0.35mm.

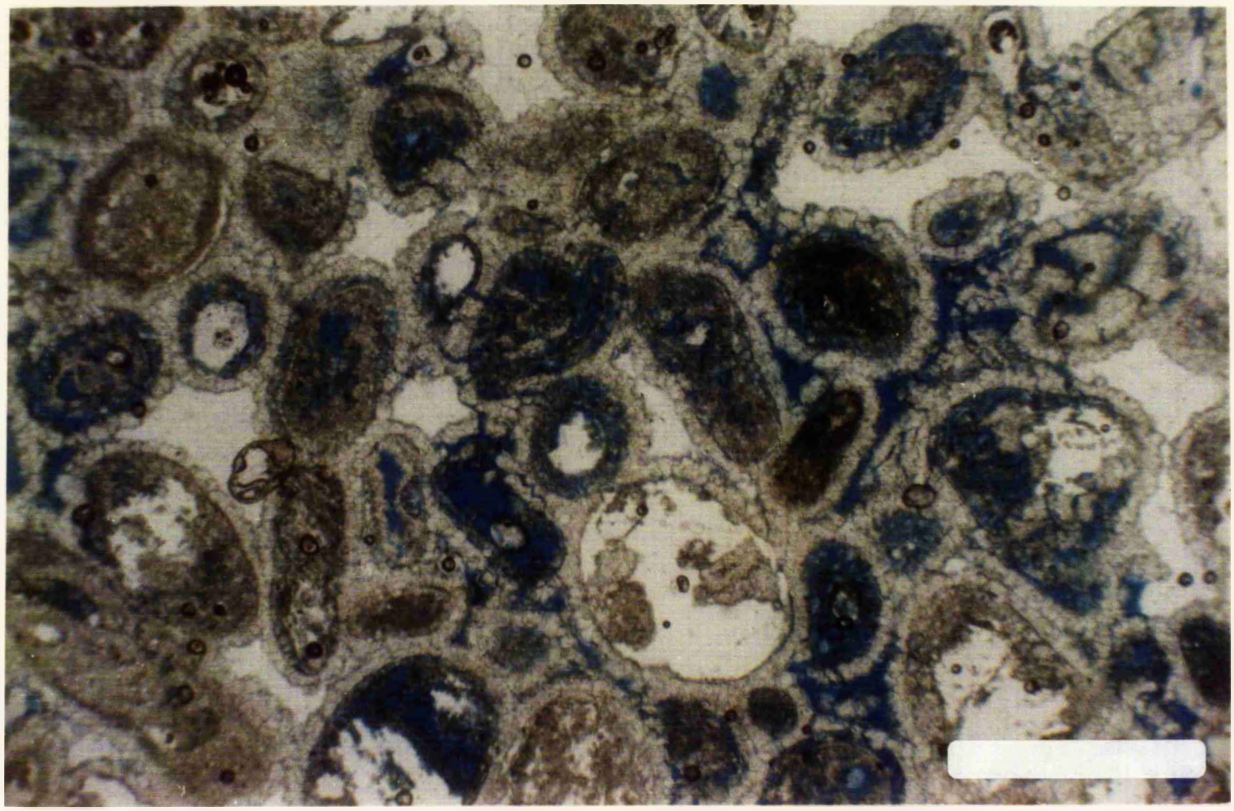

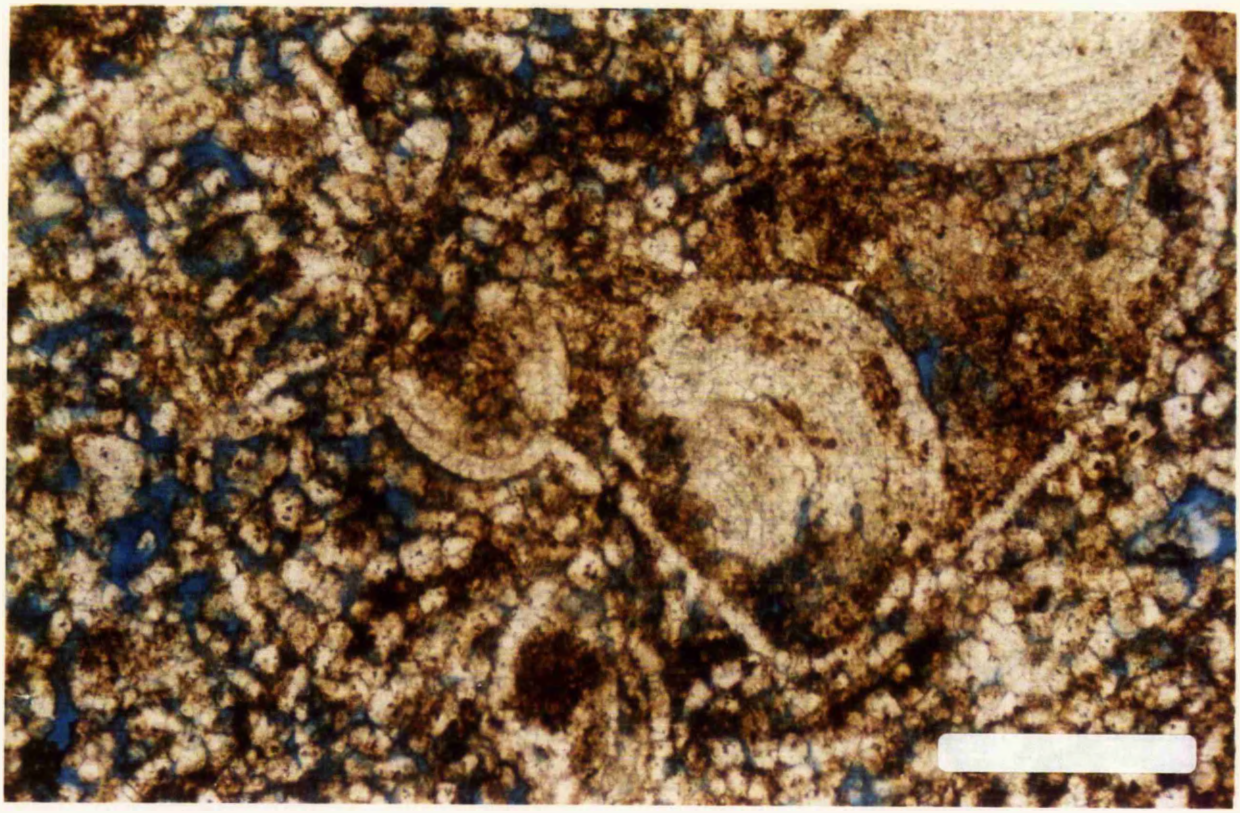

Fig 3.5 Photomicrograph of a totally dolomitized foraminiferal test with its internal structure still identifiable, the boundary is not obliterated by dolomitization. White areas are anhydrite cement filling. Plane polarized light. Scale bar is 0.35mm.

Fig 3.6 Photomicrograph of very fine crystalline carbonates, the individual crystals are very difficult to recognize. Plane polarized light. Scale bar is 0.875mm.

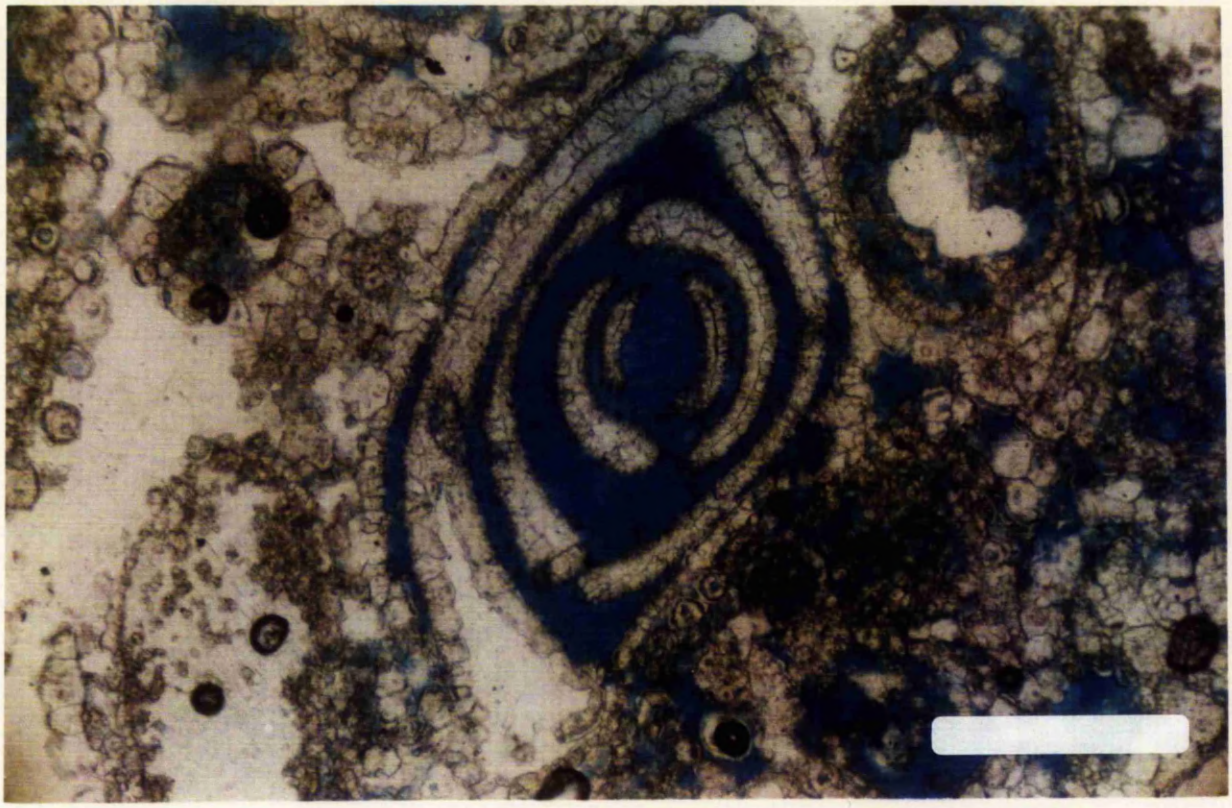

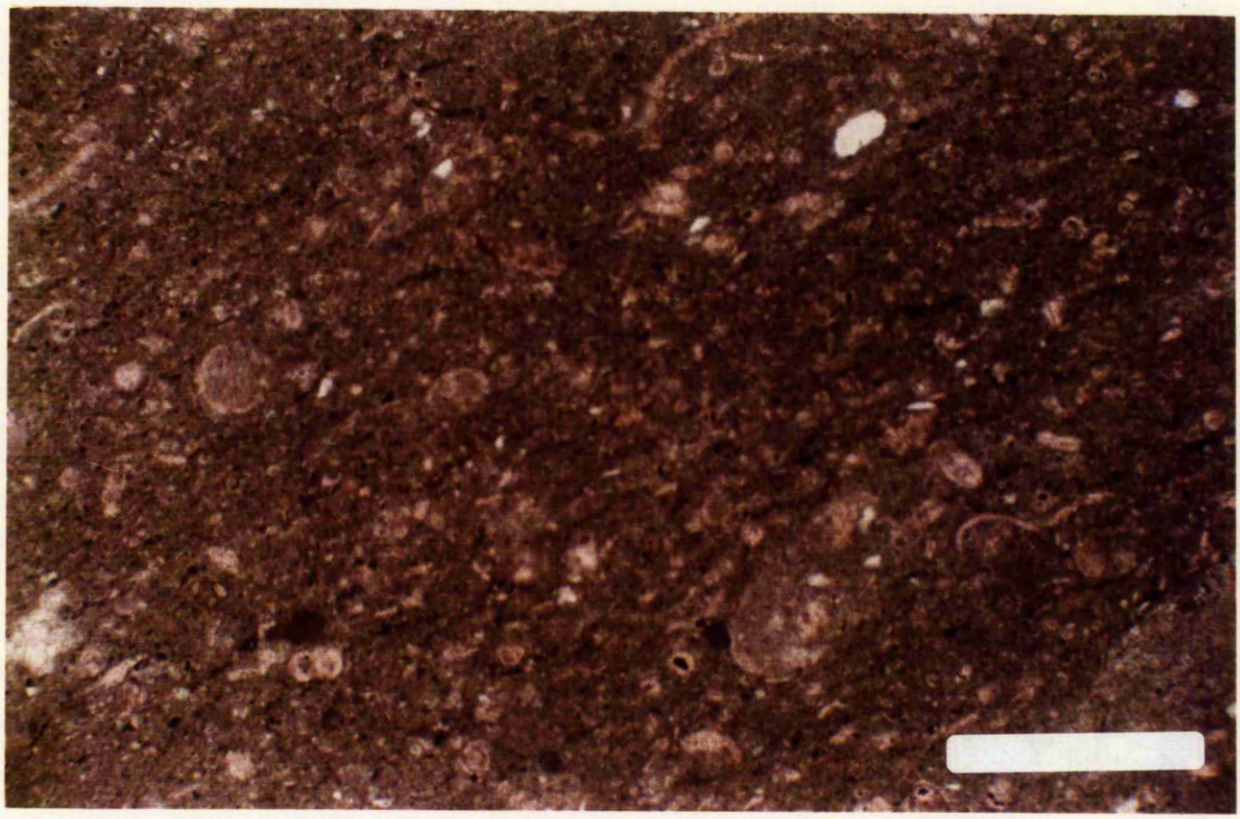

framboids scattered in the groundmass and some other forms which fill the chamber of the fossils.

Microstylolites of different sizes are present in the limestone (**Dunnington,1967; Dorbeck and Read, 1986**). These stylolites are filled with black carbonaceous materials (**Fig 3.9**). Amorphous organic materials are embedded in the groundmass and form a black opaque material.

Scattered dolomite rhombs of euhedral shape and various sizes are found very commonly in the groundmass. Sometimes the groundmass is totally dolomitized leaving only the bioclastic grains undolomitised. Sometimes the grains (bioclastic) are oriented horizontally. Signs of bioturbation are noticed in this facies (**Fig 3.10**).

3.1.3 Calcite cement

Cement has been defined as " *all the primary precipitated space-filling carbonate crystals which grow attached to free surfaces*" (**Bathurst, 1975**).

Petrographic investigation of the Euphrates Limestone Formation reveals that cement occurs in burrows, fractures, molds as well as within the matrix.

Usually two generations of sparry calcite cements are present (**Oldershaw and Scoffin, 1967**). The first, is as sparry non ferroan calcite cement usually found attached to the wall of vugs in the form of small crystals or of larger crystals occupying the centres of the vugs and the dissolved fossil chambers; the second is sparry ferroan calcite cement of coarser crystals which in most cases occupies the centres of

Fig 3.7 SEM photomicrograph showing a large quartz crystal filling a large pore in a carbonate matrix.

Fig 3.8 SEM photomicrograph shows a feldspar crystal found embedded in the dolomite matrix. This crystal is surrounded by anhydrite crystals and dolomite rhombs.

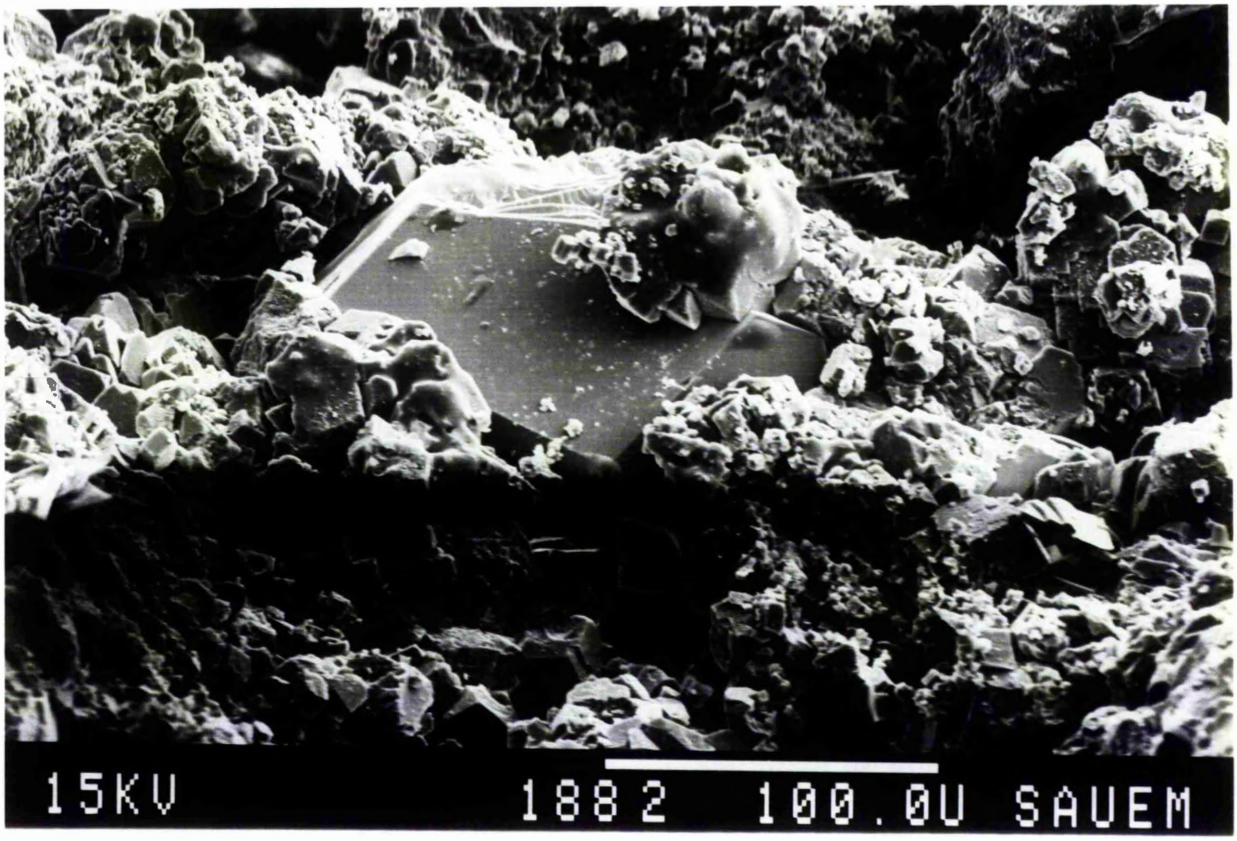
15KV
1882
100.0U SAUEM

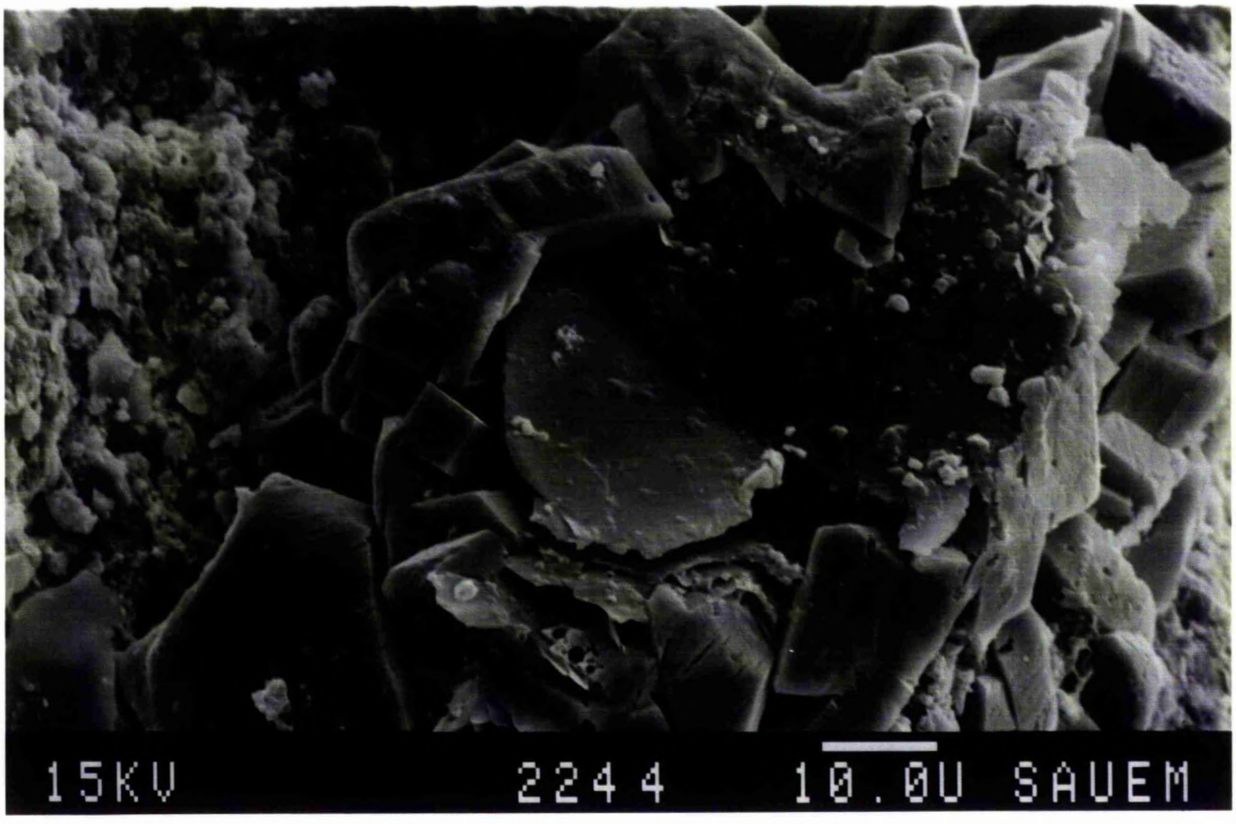
15KV
2244
10.0U SAUEM

Fig 3.9 Photomicrograph shows a microstylolite in the wackestone and mudstone facies. These stylolites are usually filled with black materials .Plane polarized light. Scale bar is o.875mm.

Fig 3.10 A photograph of a core sample showing the signs of bioturbation in the Euphrates Limestone Formation. Scale bar is 2.2cm.

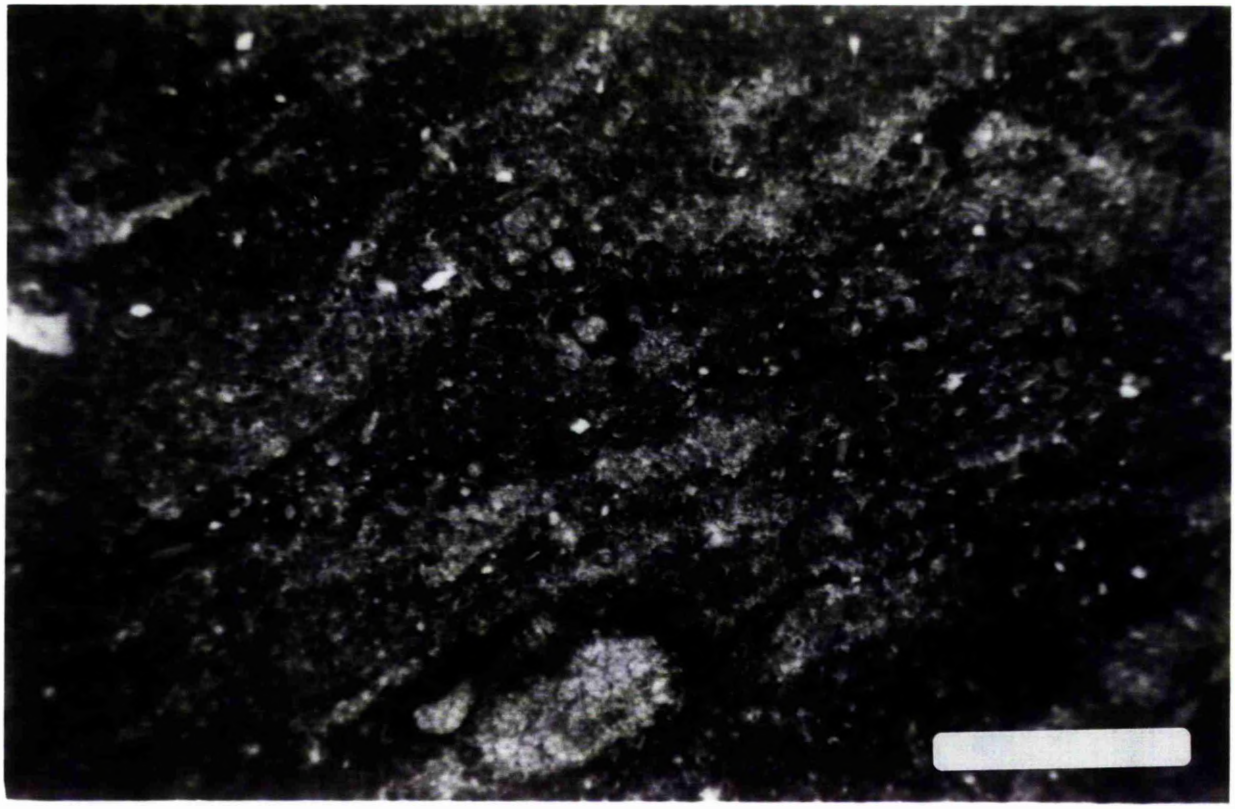

vugs. Sparry cement is found in pores which were once open and not in those filled with mud. The two generations of cements indicate a change in the chemistry of the solution that precipitated the cements (**Fig 3.11**) (**Bathurst, 1975**).

The ferroan calcite cement in this formation is formed of large euhedral crystals (their sizes averaging 270 microns in some cases) tapering from the wall of the fractures and the crystals always have plane straight edges. It is known that not all the sparry cement in the limestone is cement, some of it may be neomorphic (**Bathurst, 1975**), but in the Euphrates Limestone Formation it is found that the sparry calcite was precipitated as a cement. Large crystals of calcite cement both ferroan and non ferroan formed in vugs, chambers etc.; sometimes the sparry cement is formed of ferroan calcite especially in the fractures (**Fig 3.12**).

The blocky non-ferroan calcite cement fills the centres of dissolved grains such as ooids and bioclasts. It is sometimes replaced by anhydrite (**Fig 3.13**) or in other cases by silicate (**Fig 3.14**). Therefore the formation of the cement postdates the leaching of the interior of the oolites and bioclastic grains but some of the calcite cement show signs of dissolution and form a new type of porosity, for which I suggest the name of "*cement porosity*" (**Fig 3.15**). The ferroan calcite that has been replaced by anhydrite takes the shape of the original texture and cleavage of the anhydrite . Thick isopachous cement of 5 microns thick or larger is also common (**Fig 3.16**). Thick blocky non ferroan calcite cement is sometimes replaced by dolomite. Druzy cement is present as a fibrous druzy and druzy mosaic.

Fig 3.11 Photomicrograph shows two generations of calcite cement, One of ferroan calcite and the other is non-ferroan calcite .The non-ferroan is formed earlier.and it is nearer to the void walls. Plane polarized light. Scale bar is 0.35mm.

Fig 3.12 Photomicrograph shows ferroan calcite cement filling a fracture, indicates that cementation by ferroan calcite is postdates the fracture formation. Plane polarized light.Scale bar is 0.35mm..

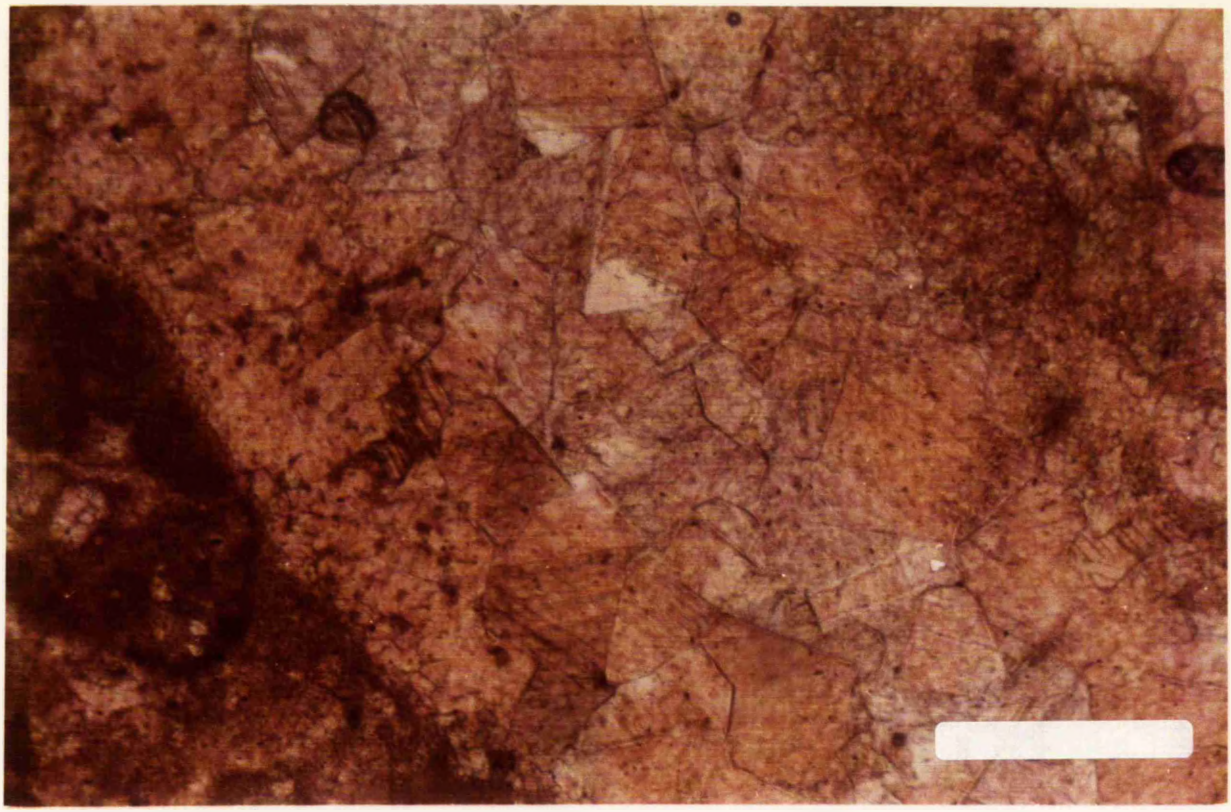

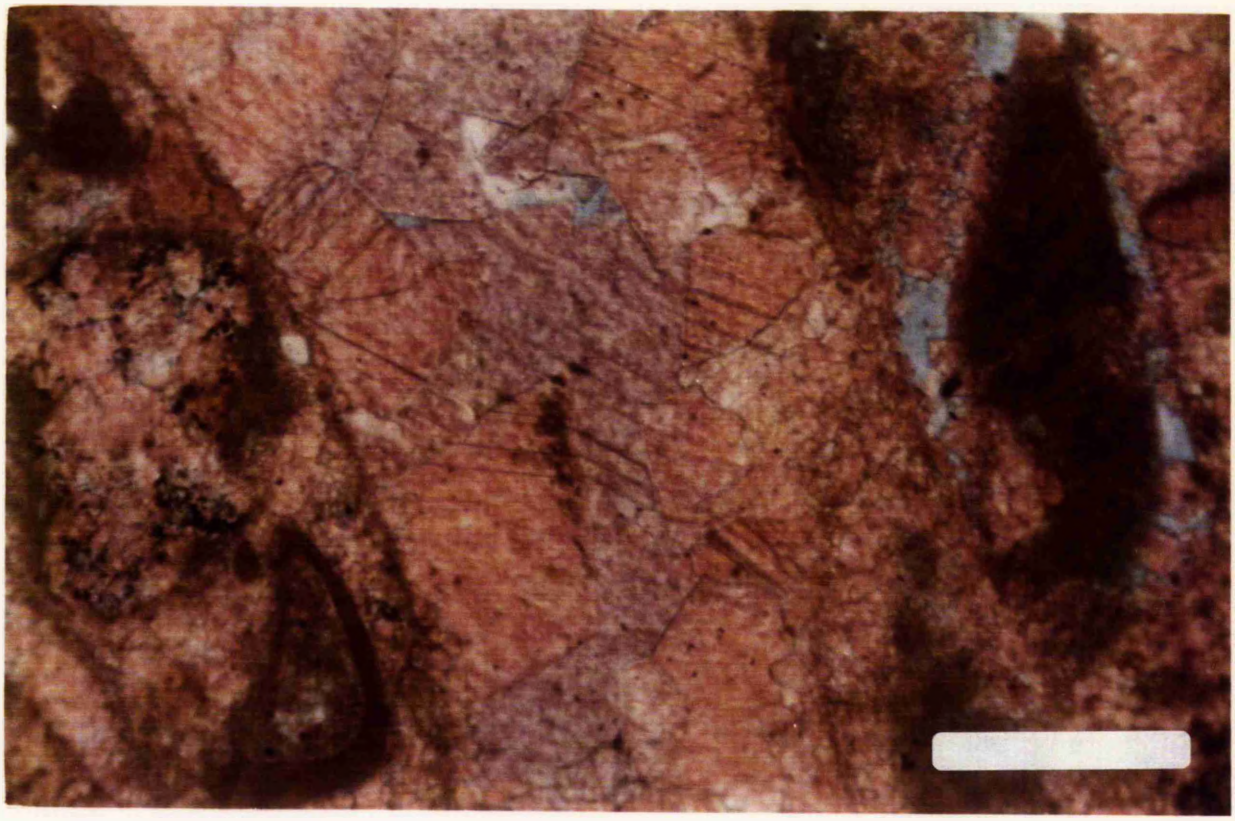

Fig 3.13 Photomicrograph of ferroan calcite in a fracture. This type of cement may be replaced by anhydrite cement. The anhydrite takes the same texture as the ferroan calcite crystals. Plane polarized light. Scale bar is 0.35mm.

Fig 3.14 Photomicrograph of a ferroan calcite cement in a fracture replaced by feldspar crystals, note the zigzag contact between the two minerals. Plane polarized light. Scale bar is 0.17mm.

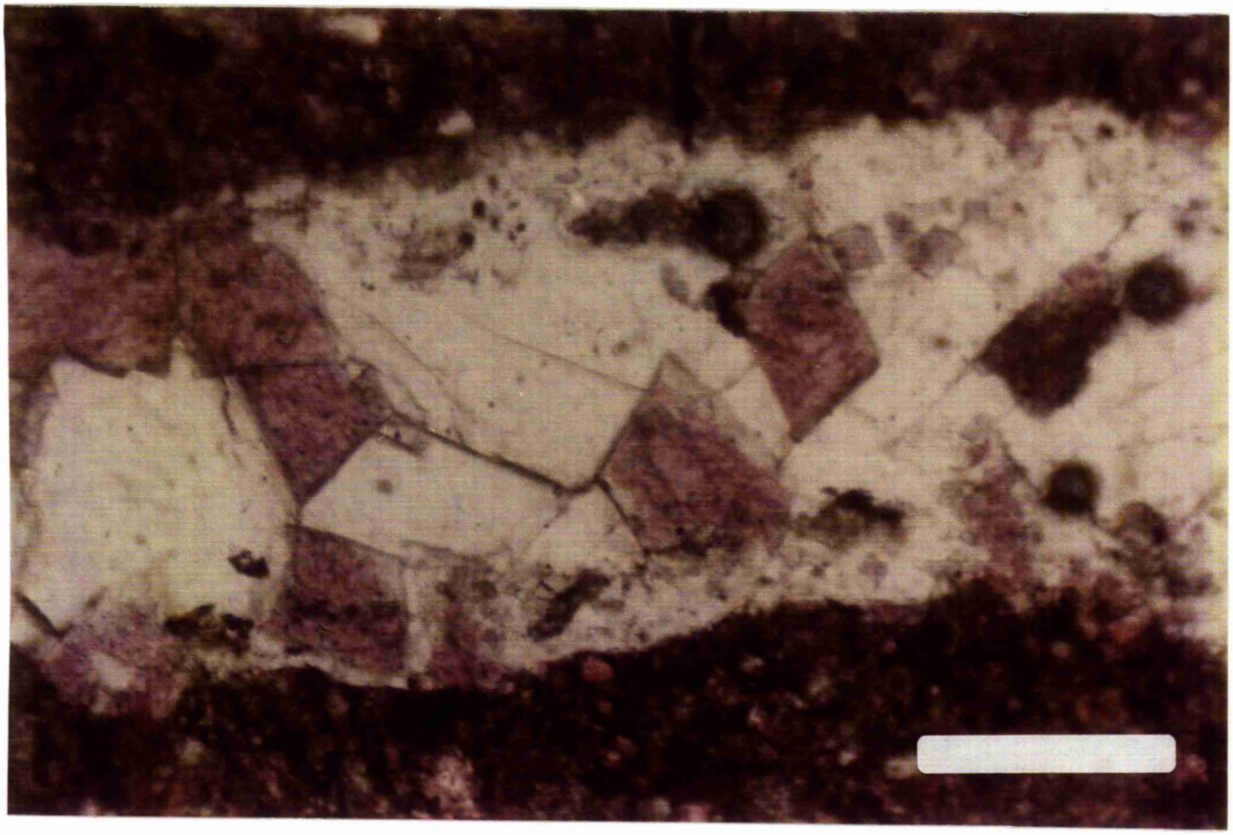

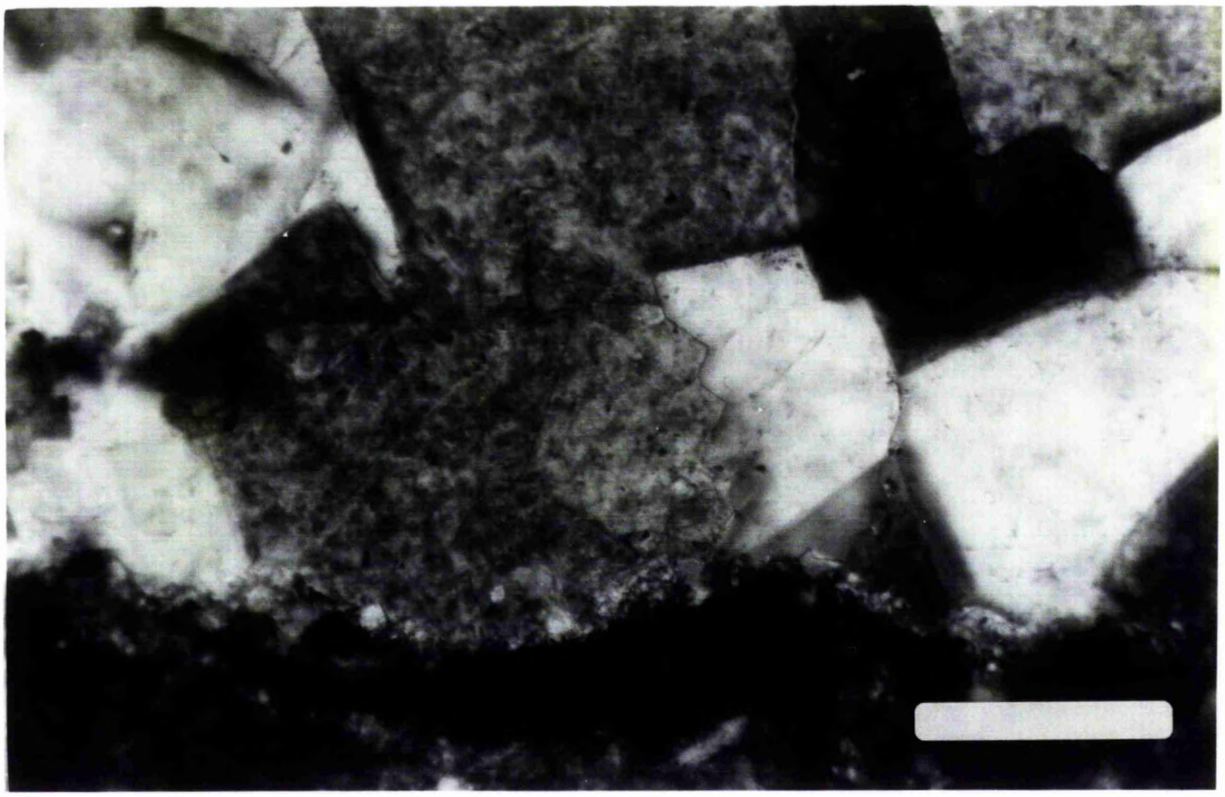

3.2 Limestone facies

The Limestone facies of the Euphrates Limestone Formation are formed of grainstone, mudstone, wackestone, mudstone, and packstone facies which are in all cases fossiliferous, except at the top of the formation, and in some cases, where the mudstone facies is formed of very fine crystalline dolomite.

3,.2.1 Grainstone facies (shoal facies)

This facies is composed of different types of well sorted grains (skeletal fragments, ooids and lithoclasts) in which the grains are normally overpacked. Overpacking has caused the breakage of the grains, a phenomenon that is abundant and very well recognized in this facies (**Fig 3.17**). The grains are surrounded with micritic envelopes and with isopachous crust cement which is formed of uneven and even thickness of large crystals (40 microns) which probably became coarser by recrystallization.

The grains of this facies (fossils and oolites, and in some cases peloids) are completely or strongly dolomitized to the extent that their original textures or structure may be unidentifiable. Dolomitization is quite strong in this facies due probably, as will be discussed later, to interparticle porosity which permitted the percolation of the supersaline brines through the sediments. The interior of these grains has been leached out and filled with anhydrite (**Fig 3.18**) or in some cases left empty forming moldic porosity (**Fig 3.19**). The interparticle porosity may be filled with dolomite and/or anhydrite but in some cases the porosity is preserved. When the

Fig 3.15 SEM photomicrograph of calcite cement filling a pore. The cement was leached and microvugs were created in the cement. These vugs form a new type of porosity called cement porosity.

Fig 3.16 SEM photomicrograph of an isopachous crust cement formed around an oolite . This cement remained unaffected after the dissolution of the grain. Later a dolomite cement has grown on the inside the oolite. A large dolomite rhombs formed later inside the mold.

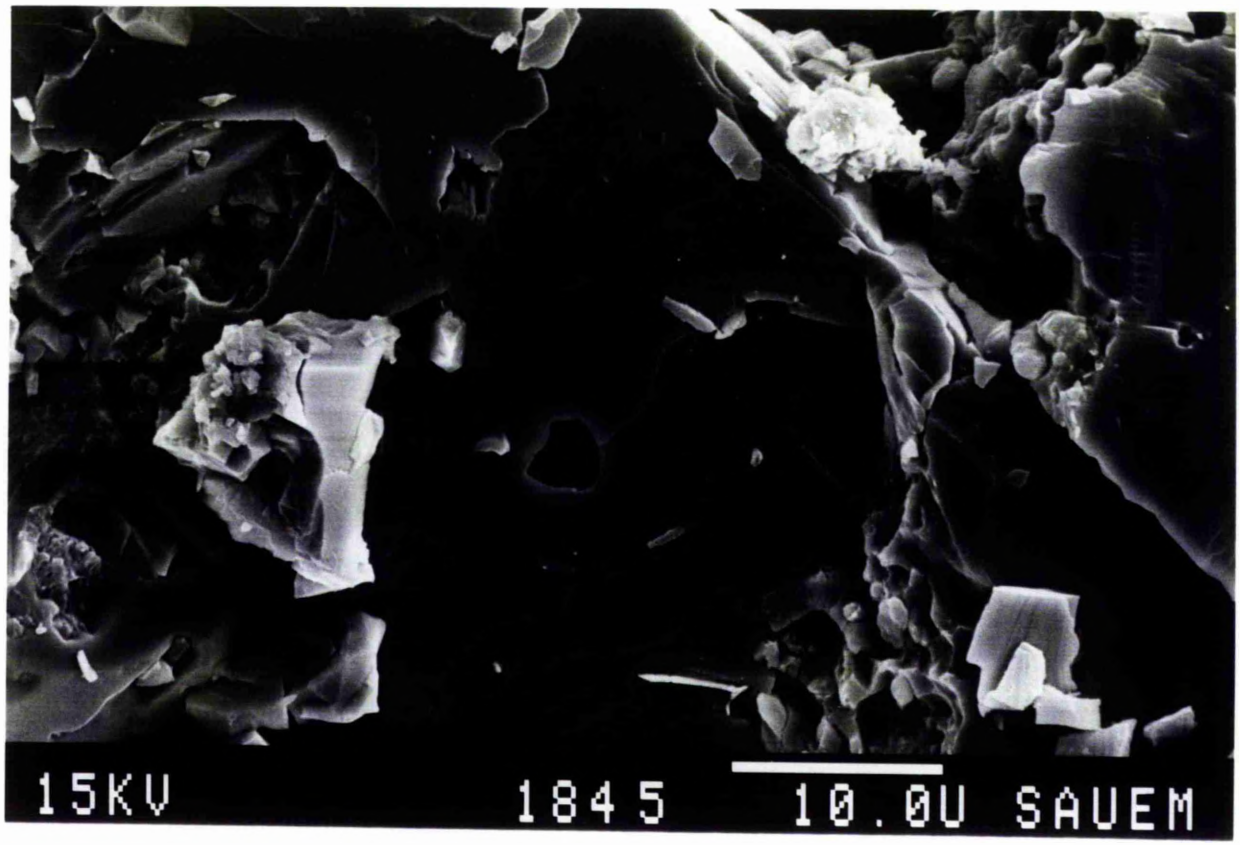
15KV
1845
10.0U SAUEM

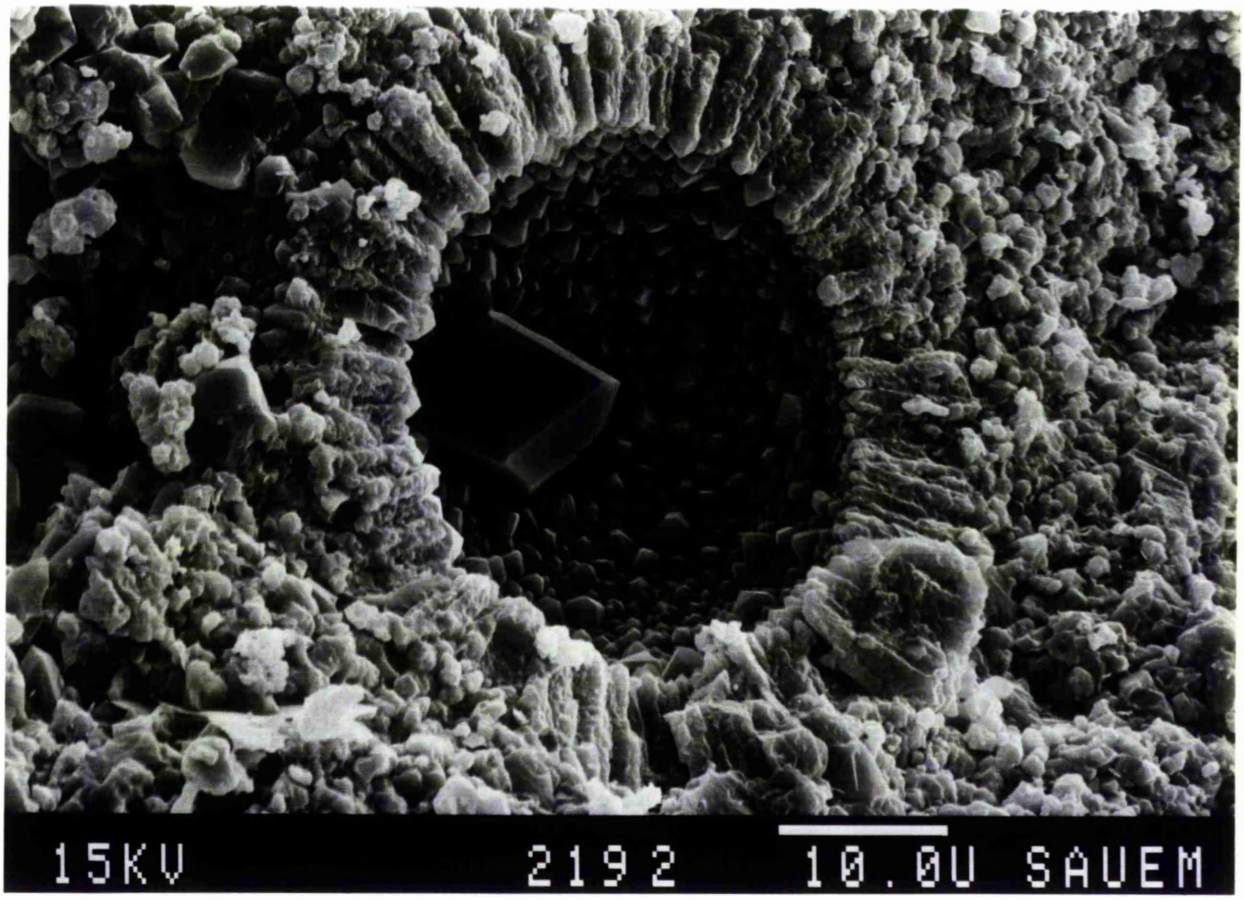
15KV
2192
10.0U SAUEM

Fig 3.17 Photomicrograph of a broken ooid due to compaction with its centre filled with later anhydrite cement. Plane polarized light. Scale bar is 0.35mm.

Fig 3.18 Photomicrograph of anhydrite cement filling a mold pore in a completely dolomitized facies. The dolomite rhombs in the surrounding matrix are very small and less than 10 microns. Plane polarized light. Scale bar is 0.875mm.

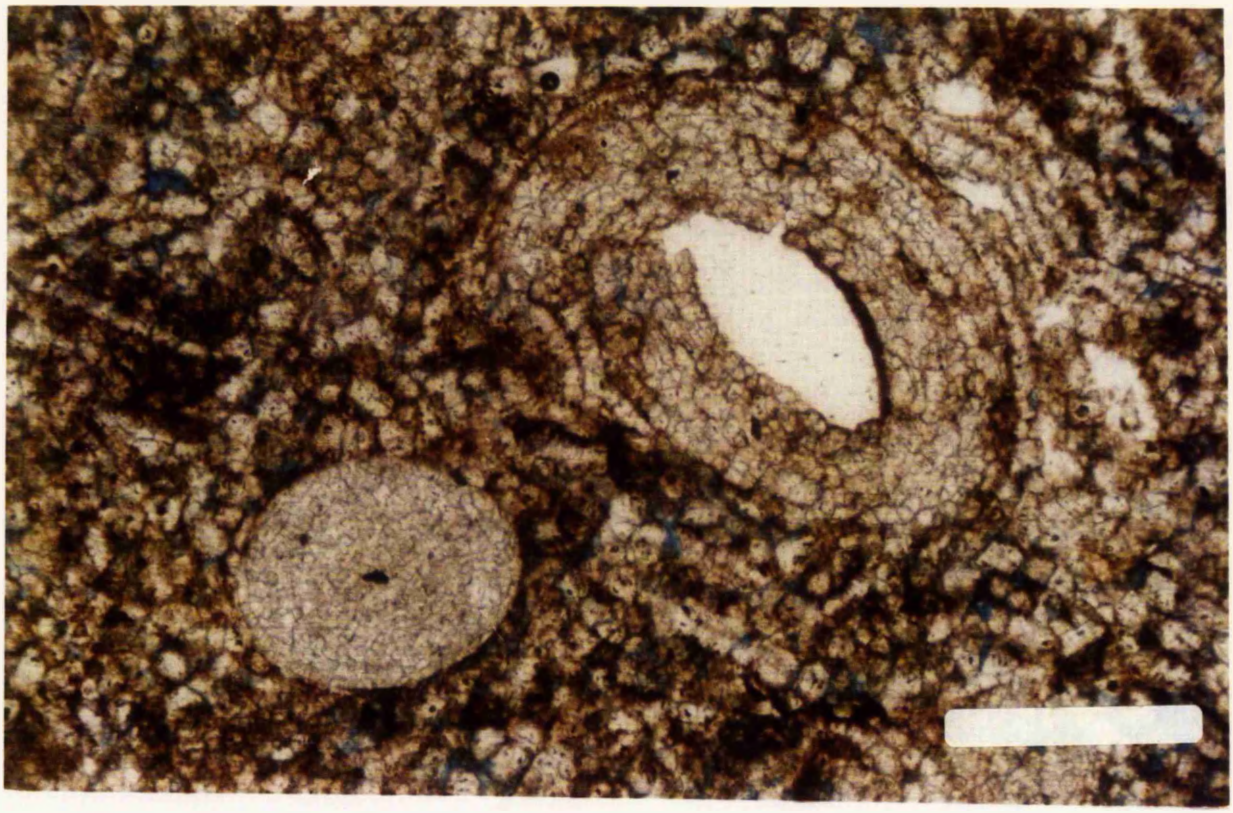

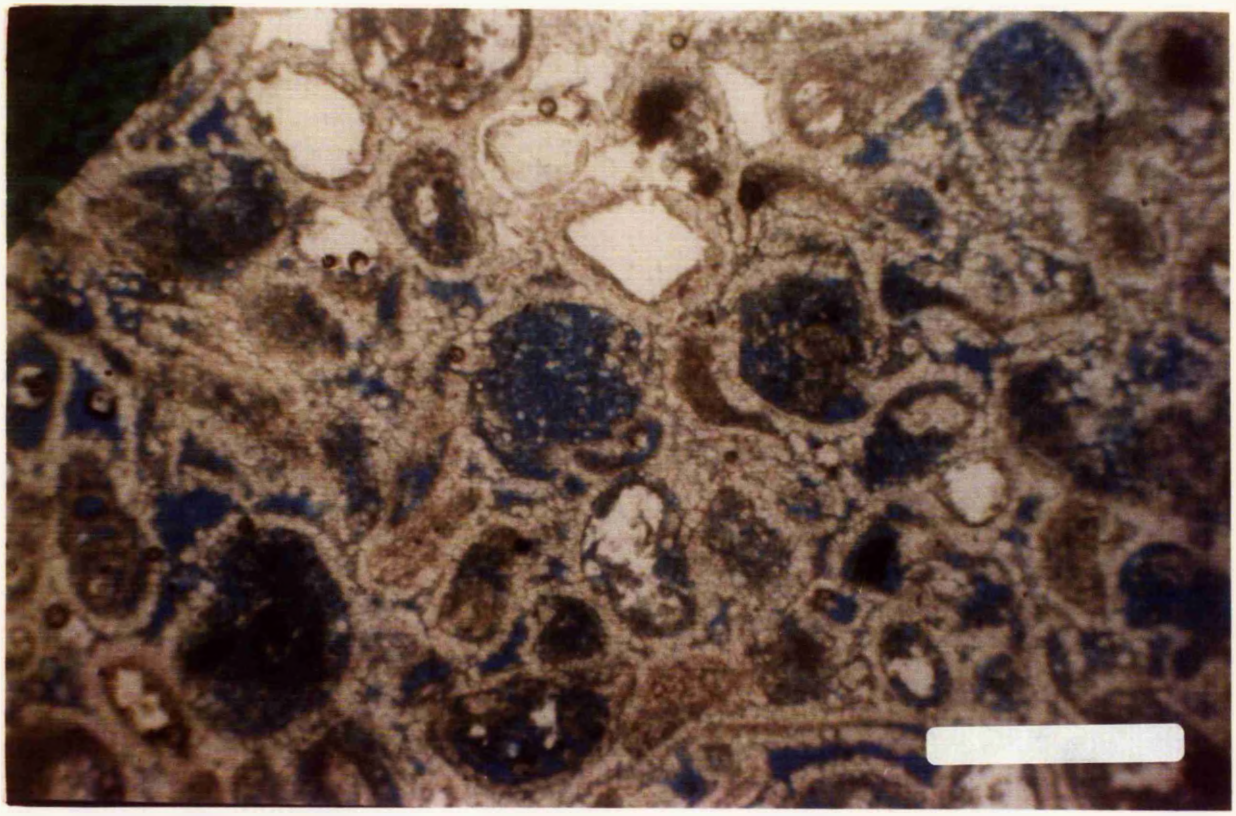

interior of the grains remains unleached they are formed of very fine crystals (micritic dolomite). In other cases the dolomite crystals occupying the interior of the grains are coarser and reach 20 microns in size. This type of facies is extensively dolomitized in cores **A, B, D, E** and partly in **F**.

3.2.2 Packstone facies

This facies is formed of bioclastic grains of echinoderms, molluscs and other unidentified fossils cemented by micritic carbonate mud which recrystallized in places (**Fig 3.20**). Quartz grains form about 2 to 3 %; they are of various sizes and in some cases reach up to 50 microns.

Most of the grains forming this facies have identifiable micritic envelopes and isopachous cement crust (**Fig 3.21**). The micritic mud has been recrystallized to coarser crystals when dolomitized; some of the skeletal fragments are also neomorphosed and some changed to low magnesian calcite with the original texture remaining unaltered. Fibrous druzy cement crusts around the grains is abundant as mentioned before.

Druz blocky calcite cement fills some fossil chambers and fractures although some small open microfractures have been noticed in this facies. Black opaque materials probably representing amorphous materials is present.

Pyrite grains of various sizes and types are also present in abundance. Similar to the grainstone facies this type of facies is strongly dolomitized in cores **A, B, D, E,** and partly in **F**.

3.2.3 Wackestone facies (basinal facies)

This facies shows slight bioturbation with grains set in a

Fig 3.19 SEM photomicrograph of a foraminiferal test with its isopachous crust cement preserved. The interior of the grain is partially filled with calcite crystals of different sizes.

Fig 3.20 Photomicrograph shows an example of packstone facies. Plane polarized light. Scale bar is 0.35mm.

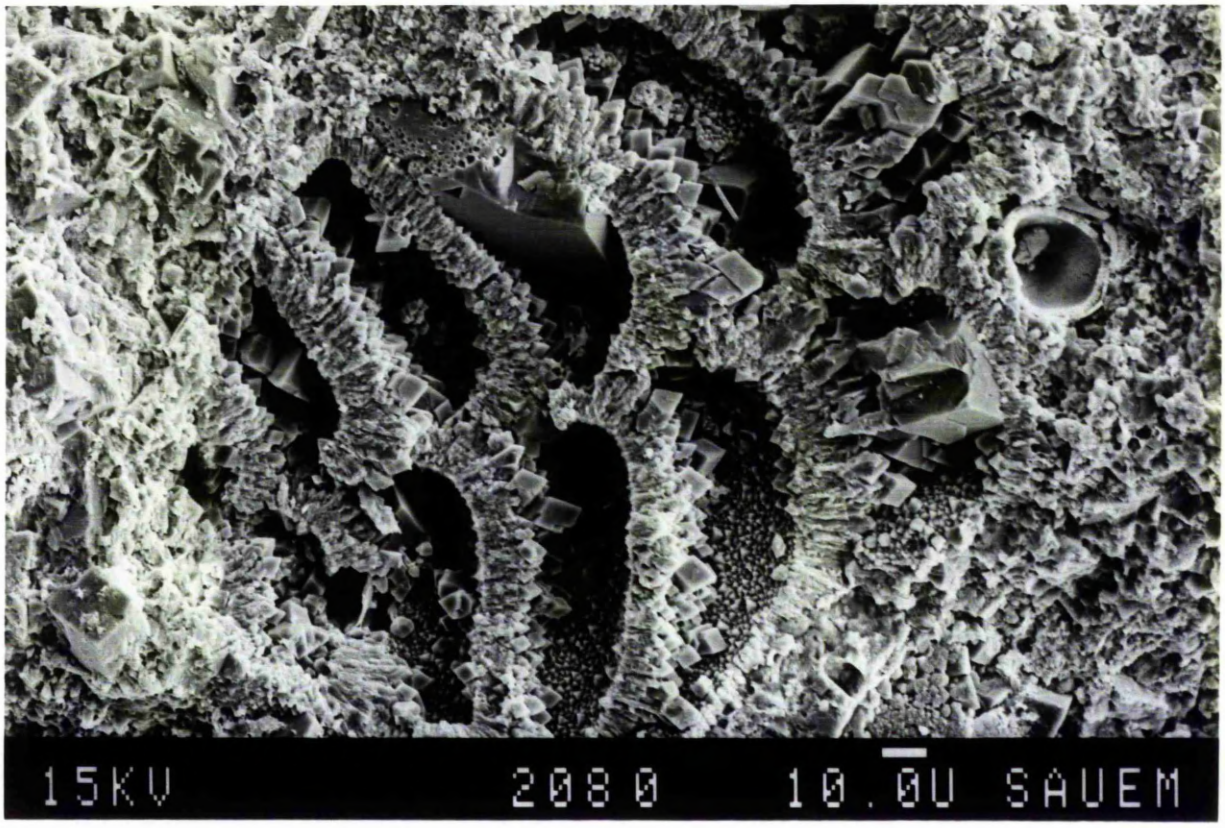
15KV 2080 10.0U SAUEM

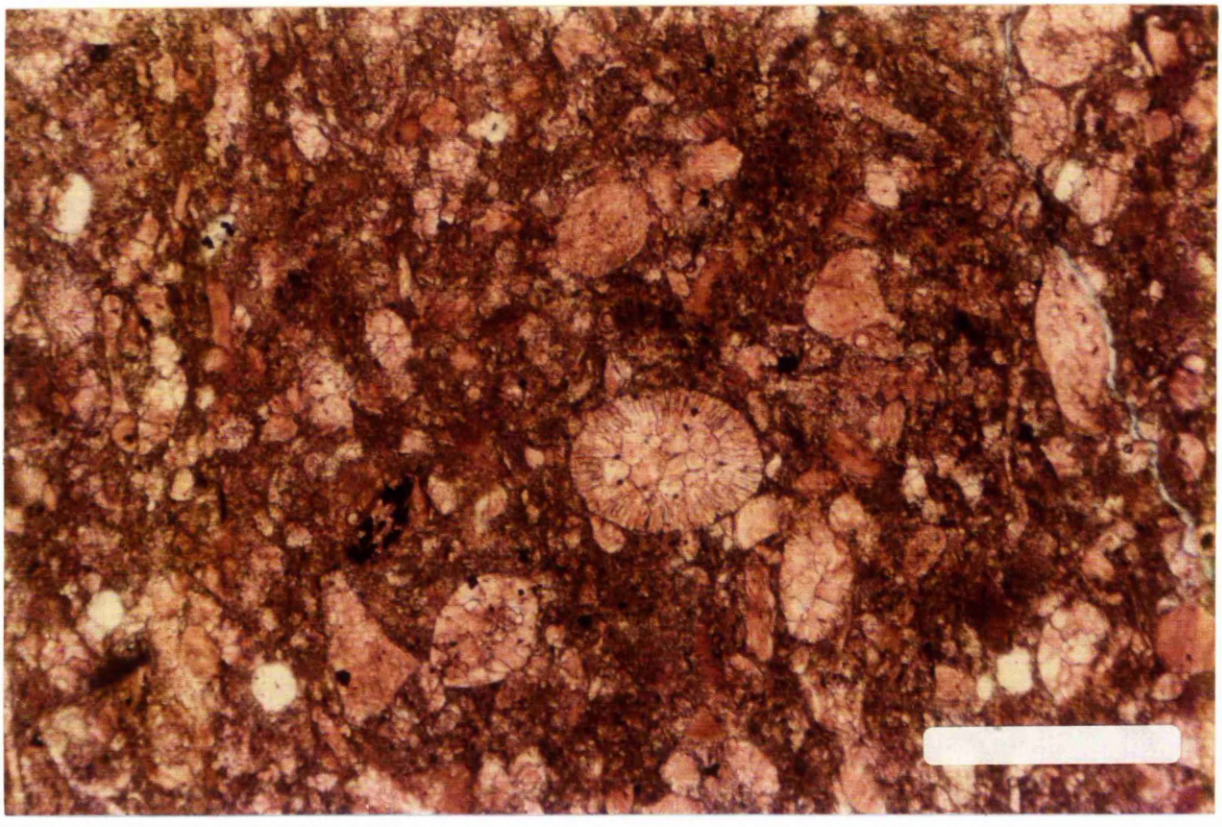

Fig 3.21 Photomicrograph of isopachous crust cement surrounding ooids (note the centre of the photograph) associated with very fine black micritic envelope. A sign of compaction can be seen on the grain in the upper right of the photograph. White areas are anhydrite cement. Plane polarized light. Scale bar is 0.875mm.

Fig 3.22 Photomicrograph shows an example of wackestone facies. Plane polarized light. Scale bar is 0.875mm.

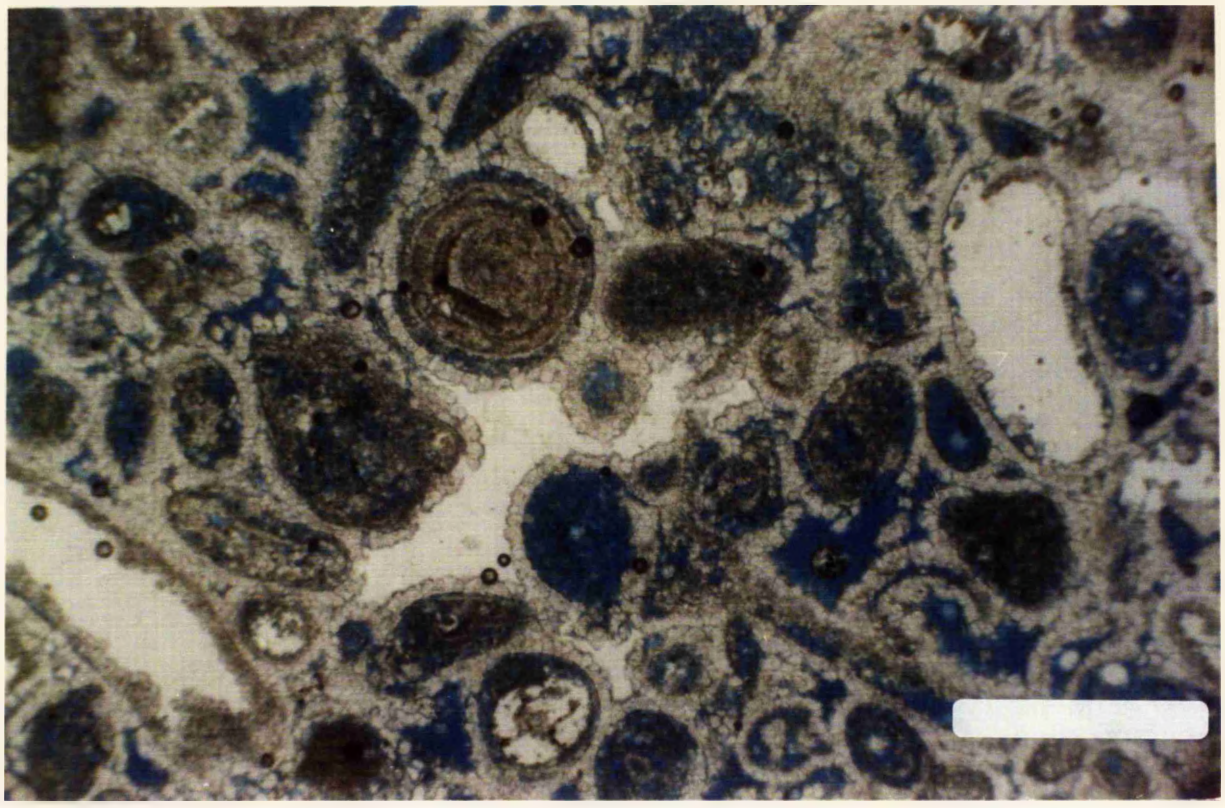

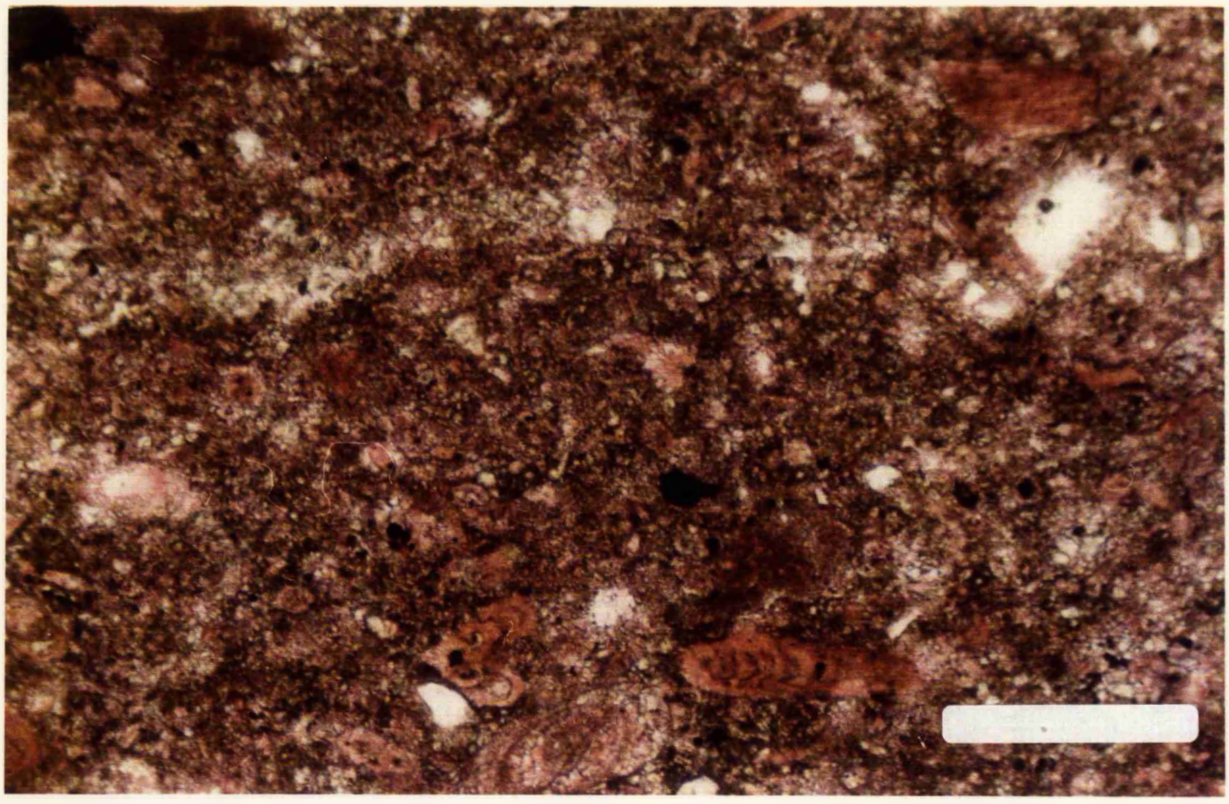

very fine grained groundmass. The bioclastic grains are composed of foraminifera (Miliolids), bivalves, echinoderms, gastropods, brachiopods, calcispheres, bryozoa, corals, and algae (**Fig 3.22**). In certain instances the grains are very heavily micritized with thick micritic envelopes.

Recrystallization of the grains has occurred leading to a total alteration of the original texture and structure.

In some cases the grains were dolomitized without altering the original texture. Some of the grains are surrounded by a very thick envelope probably a form of organic matter. Quartz grains are abundant and vary in size; chert also is not uncommon.

Blocky calcite cement fills the chambers of fossils, in some cases forming a large single block of calcite filling the void (**Fig 3.23**), whereas in other cases smaller crystals are found on the interior walls of the grains as a substrate and increase in size towards the centre of the pore (**Bathurst, 1975**) (**Fig 3.24**). Ferroan calcite cement is present on a very limited scale. Partial dolomitization is noticed in this facies as euhedral dolomite rhombs scattered in the groundmass (**Fig 3.25**).

3.2.4 Mudstone facies (open marine)

This facies is formed of very fine crystalline groundmass, and it is very dense with very poor porosity. Various kinds of fossils are found in this facies including foraminifera, brachipods, green and red algae, and corals.

Blocky calcite crystals are common. Open fractures are noticed. This facies is characterized by the abundance of quartz grains, high percentages of pyrites and amorphous organic

Fig 3.23 SEM photomicrograph of a pore filled with a single crystal of calcite. This crystal is formed of several layers like a stair steps, this probably indicates several stages of deposition.

Fig 3.24 Microphotograph shows an increase in the crystal size toward the pore centre. Plane polarized light. Scale bar is 0.17mm.

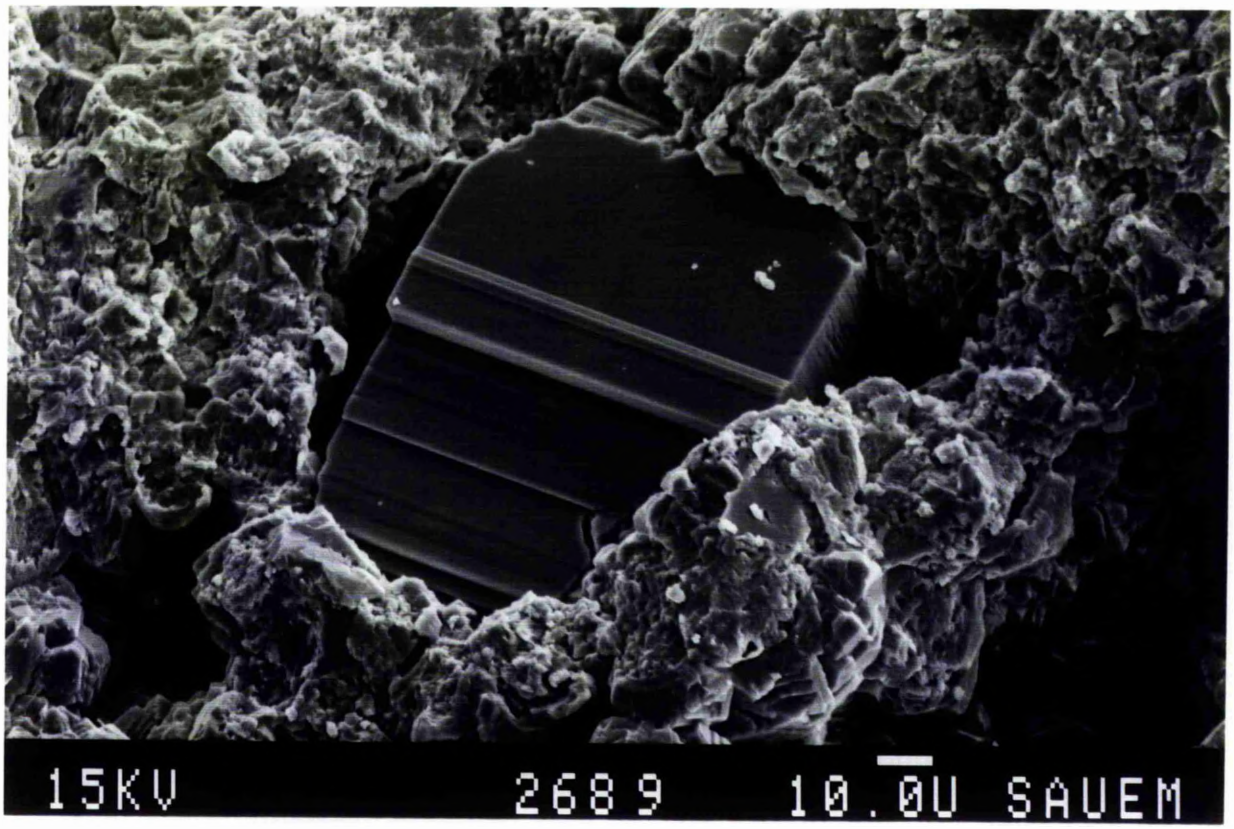
15KV
2689
10.0U SAUEM

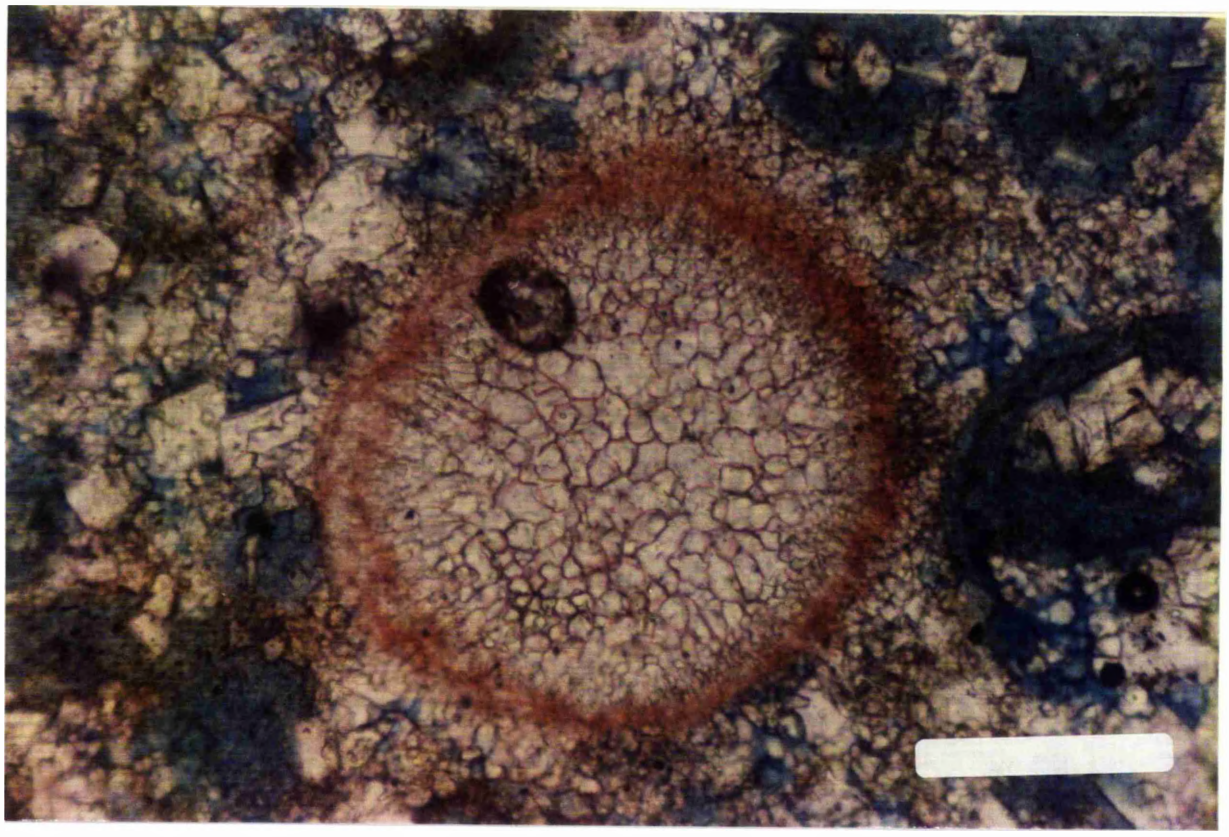

materials. Chert grains are also not uncommon. Dolomitization in this type of facies is partial.

Bioturbation of this facies is significant and breakage of grains is evident in some cases where it has occurred before any cementation because the fractures caused by compaction are healed by the later blocky calcite cement.

3.2.5 Boundstone facies (biological)

This facies is formed of very fine crystalline sediments bound together by green and red algae associated with fragmental debris of bryozoa, bivalves, foraminifera (miliolids) and locally globigerina (**Fig 3.26**). The limestone is made up of very fine crystals (cryptocrystalline) as groundmass and calcite skeletal fragments, as well as a secondary calcite cement (blocky calcite cement, druz fibrous).

This limestone shows some degree of recrystallization. The crystal size of the groundmass ranges from cryptocrystalline to microcrystalline. The limestone is dolomitized and dolomitization shows all the grades from partial up to total dolomitization.

3.3. DOLOMITE

Dolomitization of the Euphrates Limestone Formation has affected and altered and replaced all the carbonate components of the precursor limestone (oolites, peloids, and skeletal fragments) to one degree or another.

Replacement of the components has to some extent sometimes preserved the original fabrics, on the other hand it may have completely altered the fabric which is no longer recognizable.

Different dolomite textures and dolomitization fabrics are identified.

Fig 3.25 SEM photomicrograph of scattered dolomite rhombs in carbonate groundmass. This shows the first stage of dolomitization. Note the bryozoan fragment which is very slightly affected by dolomitization.

Fig 3.26 Photomicrograph shows an eaxample of the boundstone facies. Plane polarized light. Scale bar is 0.875mm.

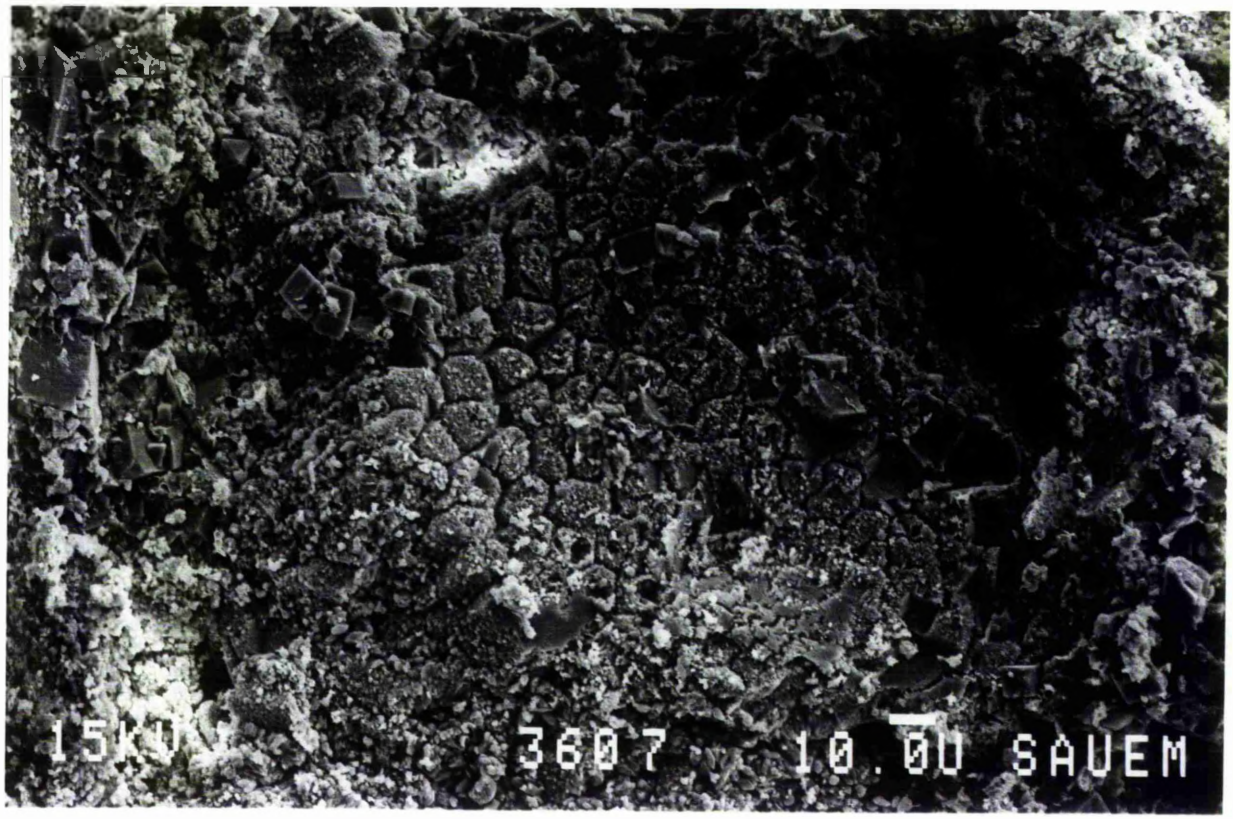
15KV
3607
10.0U SAUEM

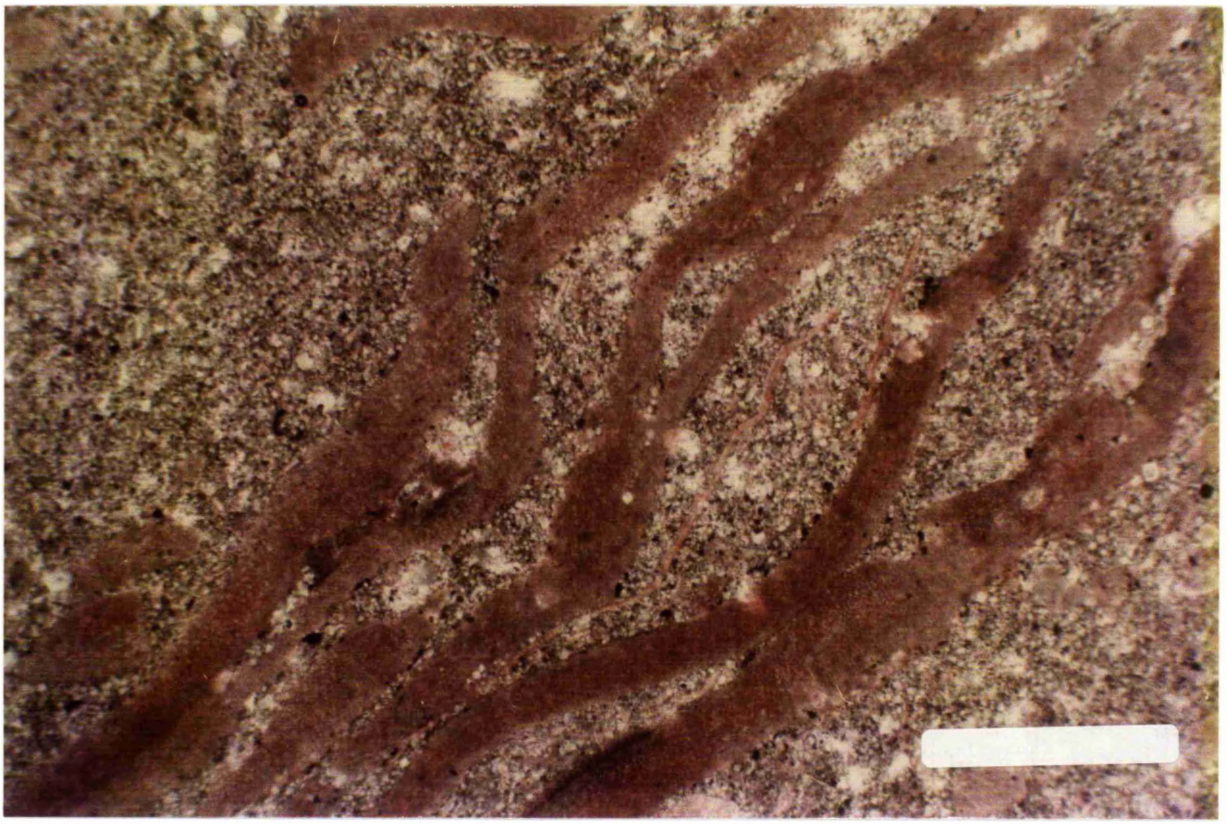

Fig 3.27 Photomicrograph shows a very fine dolomite texture associated with anhydrite. Plane polarized light. Scale bar is 0.875mm.

Fig 3.28 SEM photomicrograph of two textures of dolomite, the first is very fine euhedral and filling the chamber of an unidentified grain. This probably represents the replacement of the original aragonite composition. The second texture is formed of large anhedral to subhedral dolomite crystals.

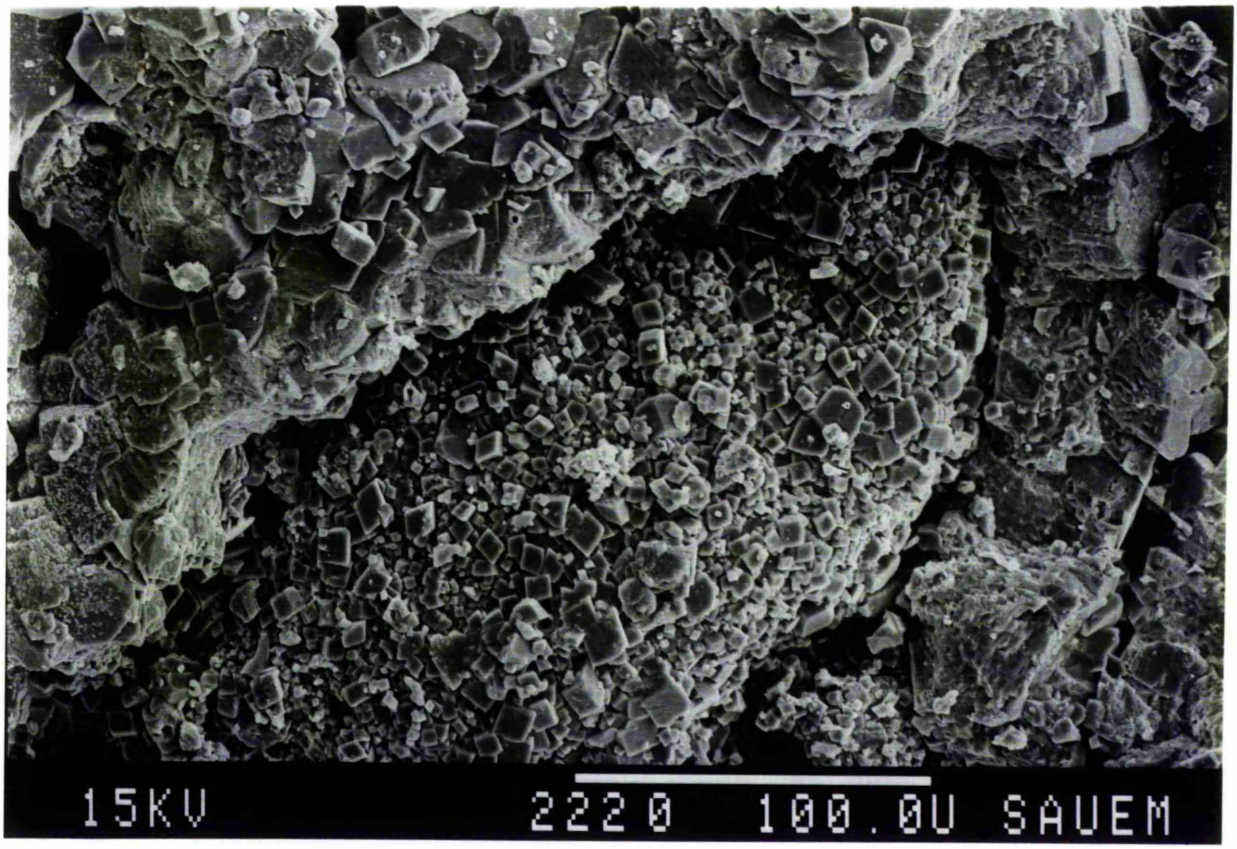
15KV
2220
100.0U SAUEM

3.3.1 DOLOMITE TEXTURES

In the Euphrates Limestone Formation different types of dolomite texture are present and these textures can be grouped in three main classes, class **A**, class **B**, and class **C**.

3.3.1.1. Class A

In this class the dolomite is formed of very fine crystals ranging in size between 0 to 10 microns (**Fig 3.27**), similar to the micron size of **Gidman (1978)**. The finer fraction of this type is very difficult to recognize under the microscope.

The general colour of this dolomite is grey to dark grey, and it is formed of interlocking equigranular fine crystals with very low intercrystalline porosity. The crystal boundaries are not clear but the shapes of the crystals are anhedral to subhedral, but coarser crystals are of euhedral shape. Clear dolomite is present in the intercrystalline pores; usually this class of texture is associated with anhydrite cement, anhydrite nodules and/or other sulphate minerals. Normally in this type of dolomite the skeletal fragments are absent, but in some cases ghosts are not uncommon. In most cases class **A** dolomite is found just below the top of the Euphrates Limestone Formation (below the evaporite and carbonate-evaporite facies) and associated with chicken-wire texture which is a significant feature of sabkha and supersaline environments. However in other cases it is present within the Euphrates Limestone Formation core **D** at different depths.

Fig 3.29 SEM photomicrograph of medium grained dolomite texture (20-30 microns) filling a vug in a fine dolomite matrix. The dolomite rhombs are highly leached, and an intracrystalline porosity.is produced.

Fig 3.30 SEM photomicrograph shows the first stage of dolomitization, where only scattered dolomite rhombs appear in the groundmass of the calcite matrix. Plane polarized light. Scale bar is 86 μm.

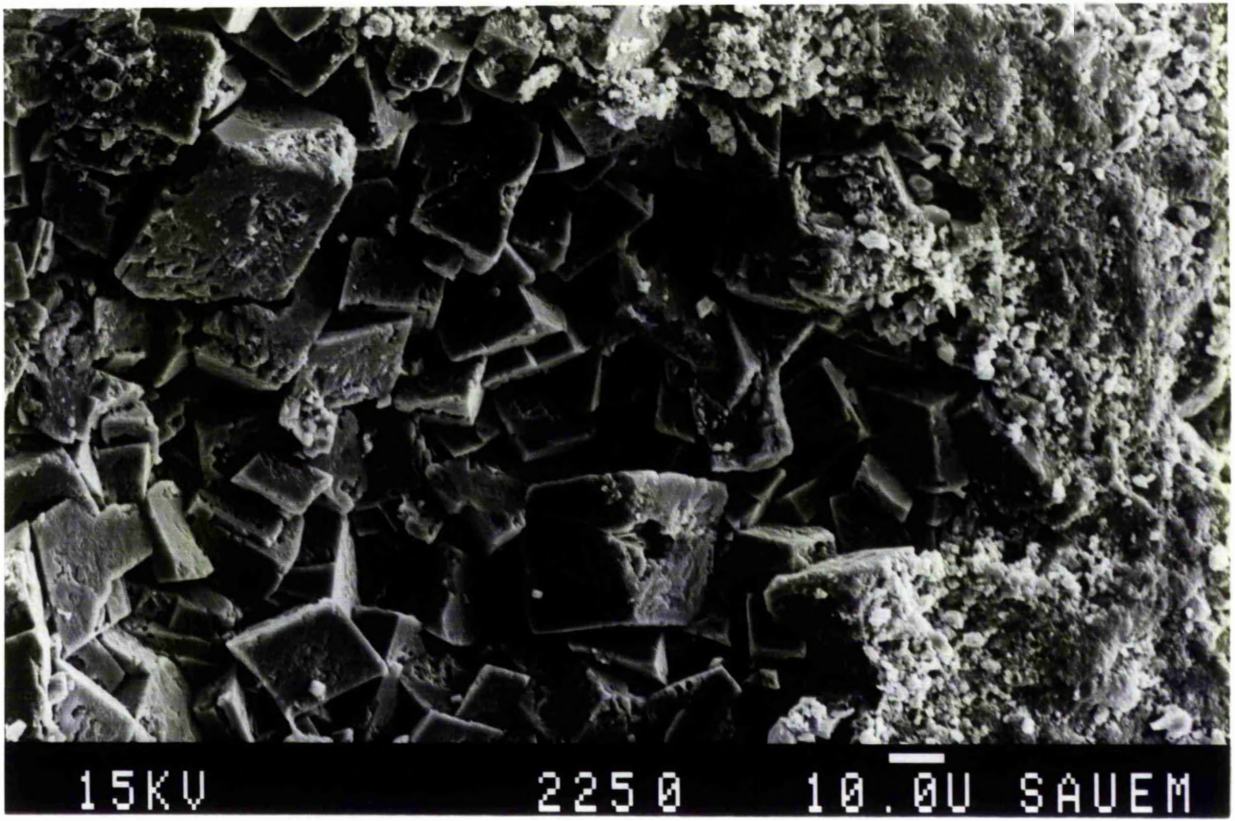
15KV
2250
10.0U SAUEM

Fig 3.31 Microphotograph shows foraminiferal tests embedded in a completely dolomitized matrix. These tests are not dolomitized and composed of calcite. White area in the upper right represents a dolomite crystal. Plane polarized light. Scale bar is 0.35mm.

Fig 3.32 SEM photomicrograph of a very fine dolomite (2-10 microns) which may have replaced the original component of the grain wall. The original structure is totally obliterated.

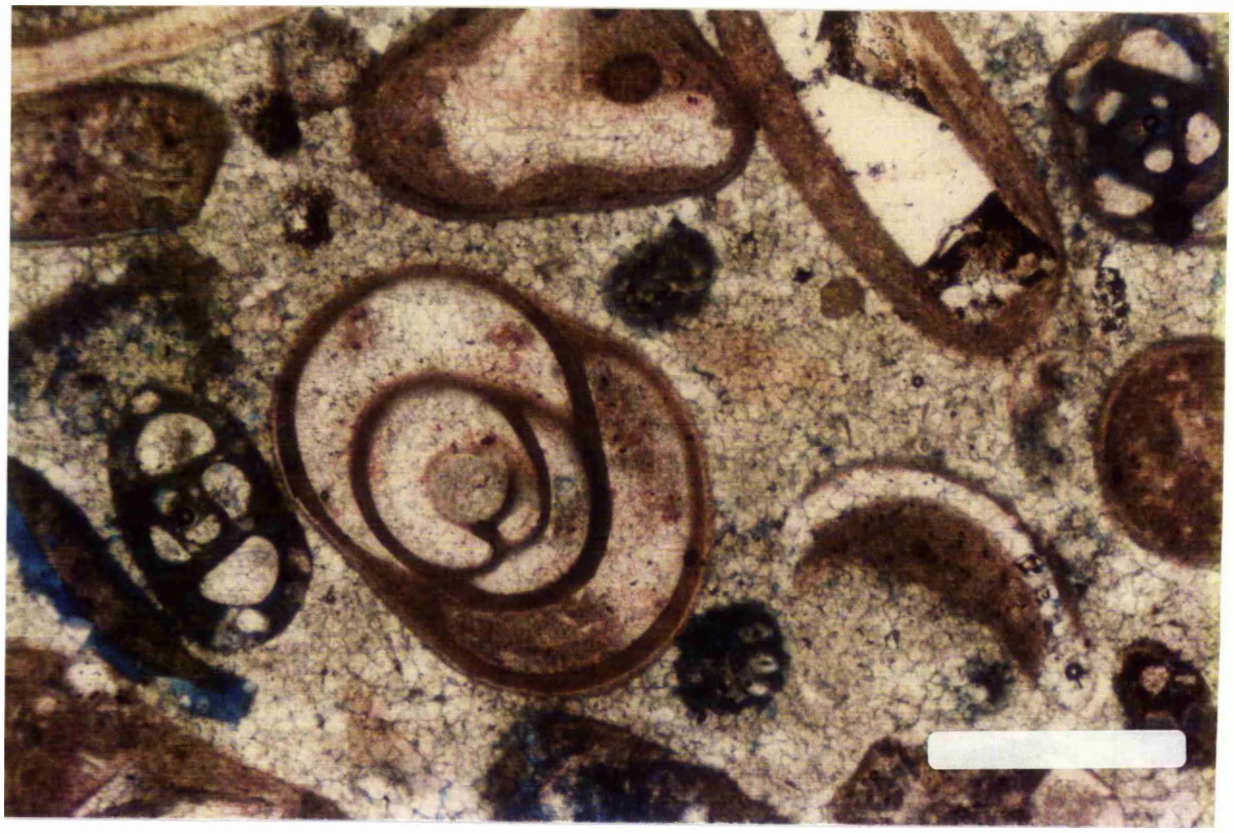

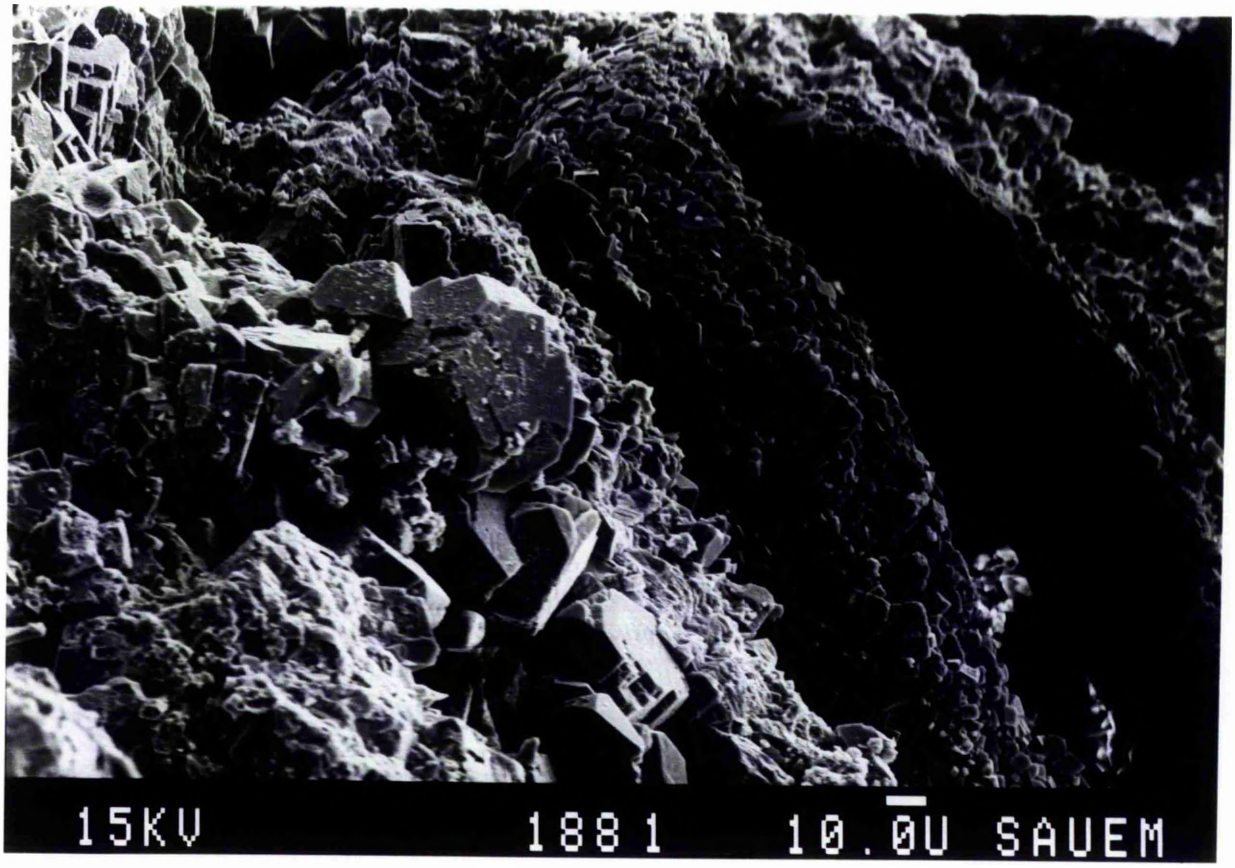
15KV 1881 10.0U SAUEM

3.3.1.2. Class B

This class of texture is formed of medium size crystals ranging between 10 to 30 microns. The dolomite crystals are anhedral to subhedral (**Fig 3.28, 3.29**)) and they are unequal in size (inequigranular) (**Friedman, 1964**) but euhedral crystals are not uncommon. This class of dolomite in most cases has a brownish dirty appearance which is probably in some instances due to inclusions from the precursor replaced carbonates. This type of dolomite has the phenomenon of hollow dolomite rhombs which will be described later in a forthcoming section. Some of the dolomite crystals have clear rims of 5 microns thick. These rims are very clear and take the outer shape of the crystals, as circular, square, triangular, or irregular in shape. It is noticed that these rims are present in the crystals which abut the voids or pores, whereas they are not found in the crystals which are away from pores. It is interesting to note that some of the crystals have rims on the pore sides but they do not have rims on the opposite side. The rims are broken in some instances. This type of dolomite will be called "**rimmed dolomite**". Spherulitic dolomite is also present in this type of textures.

Class B dolomite forms the groundmass of the dolomite section and even sometimes replaced the lithoclasts or bioclasts and forms a coarse dolomite. This class of dolomite is associated with very good porosity of various types (intercrystalline, intracrystalline interparticle, vuggy and moldic).

Detrital quartz is present in this type of dolomite with irregular shapes, but euhedral shapes are present possibly formed as neomorphic crystals after gypsum (**Friedman,**

1980). The size of this quartz ranges between 60 to 130 microns. Sulphate minerals are associated with this type of dolomite for example celestite ($SrSO_4$).

3.3.1.3. Class C

This class of dolomite texture comprises dolomite crystals of larger size (50- 100 microns); in most cases the crystals have euhedral shape and straight edges; they are clear and inclusion free, and found in the pores, fractures, fossil chambers or disseminated between smaller dolomite crystals. This class of dolomite is a limpid dolomite (**Folk and Land, 1974: 1975; Siedlecka, 1972; Land, 1973**). The phenomenon of the hollow dolomite is found in this type of dolomite as well. Class C is regarded as a cement rather than replacement dolomite and it fills the vugs, fractures, molds, pores and fossil chambers.

3.3.2. DOLOMITE CLASSIFICATION

The classification introduced by **Shukla (1980), Shukla and Friedman, (1983)** is more relevant to the Euphrates Limestone Formation than any other kind of classification (**cf Friedman and Sanders, 1967 p308; Sibley and Gregg, 1987**).

The following types of dolomitization fabrics are recognized in the Euphrates Formation; in each case the comparable Shukla type is noted.

3.3.2.1. Type 1

In this type the dolomite euhedra of 10 to 30 microns are scattered in the groundmass and this represents the onset of dolomitization. The skeletal fragments and the grains are not

affected by dolomitization (**Fig 3.30**). This type led to the formation of the dolomitic limestone in which the dolomite is less than 10%. This type of dolomite is comparable to Shuklas "incipient dolomitization "(**I-D**).

3.3.2.2. Type 2

In this type of dolomite the groundmass is usually completely dolomitized leaving the skeletal fragments unaltered (**Fig 3.31**) and undolomitized, but rarely some of the original groundmass remained undolomitized. It is similar to the type " groundmass dolomitization " (**G-D**).

3.3.2.3. Type 3

When dolomitization has progressed, the skeletal fragments are also affected by dolomitization (**Fig 3.32**) and the structure of them replaced by dolomite, but the detail of the structure (except the ultrastructural details) are preserved (ooids, skeletal fragments etc.), which is similar to the " Allochems (detail) dolomitization" fabric "**A(d)**" .

3.3.2.4. Type 4

In this type the dolomitization is so intense that the internal details of the grains are completely obliterated and only the outer boundaries of the grains are preserved. Grains are easily recognizable (**Fig 3.33**) such as ooids, and skeletal fragments, (" Allochems" boundary " dolomitization fabric" **A" b** " type).

3.3.2.5. Type 5

The dolomitization of this type has obliterated the internal structure as well as the boundaries of the grains (**Fig 3.34**) which are very poorly preserved, but identification is still

possible. (Allochems incomplete (Boundary) dolomitization, A "1b").

3.3.2.6. Type 6

In this type, the dolomitization is intensive to the extent that all the details of the allochems have been obliterated and only ghosts or dusty lines remain (**Fig 3.35**) to indicate the former presence of the allochems. Identification of this type may be very difficult. It is very similar to the Allochems"vuque" dolomitization fabric (A"v").

3.3.2.7. Type 7

In this type of dolomitization the original texture (bioclastic or lithoclastic) is completely altered (**Fig 3.36**)
and sometimes it is very difficult to determine whether the original limestone had any allochems or not, or whether the dolomite is primary penecontemporaneous dolomite, or whether it formed according to the dissolution-precipitation model. This type is very similar to General dolomitization fabric ("**D**").

3.3.2.8. Type 8

This type is that in which the dolomite fills voids or vugs of various shapes. Voids may contain a normal dolomite (**Fig 3.37**) or a saddle dolomite (**Matthews, 1971; Radke, 1978**). This type is very rare in the Euphrates Limestone Formation. This type is called void filling dolomitization fabric ("**V**").

Fig 3.33 Photomicrograph shows an ooid that still has its original shape with unaltered boundary. Plane polarized light. Scale bar is 0.35mm.

Fig 3.34 Photomicrograph of completely dolomitized facies. The boundary of the bioclast is obliterated by dolomitization. Its mold is filled with large clear crystals. Plane polarized light. Scale bar is 0.35mm.

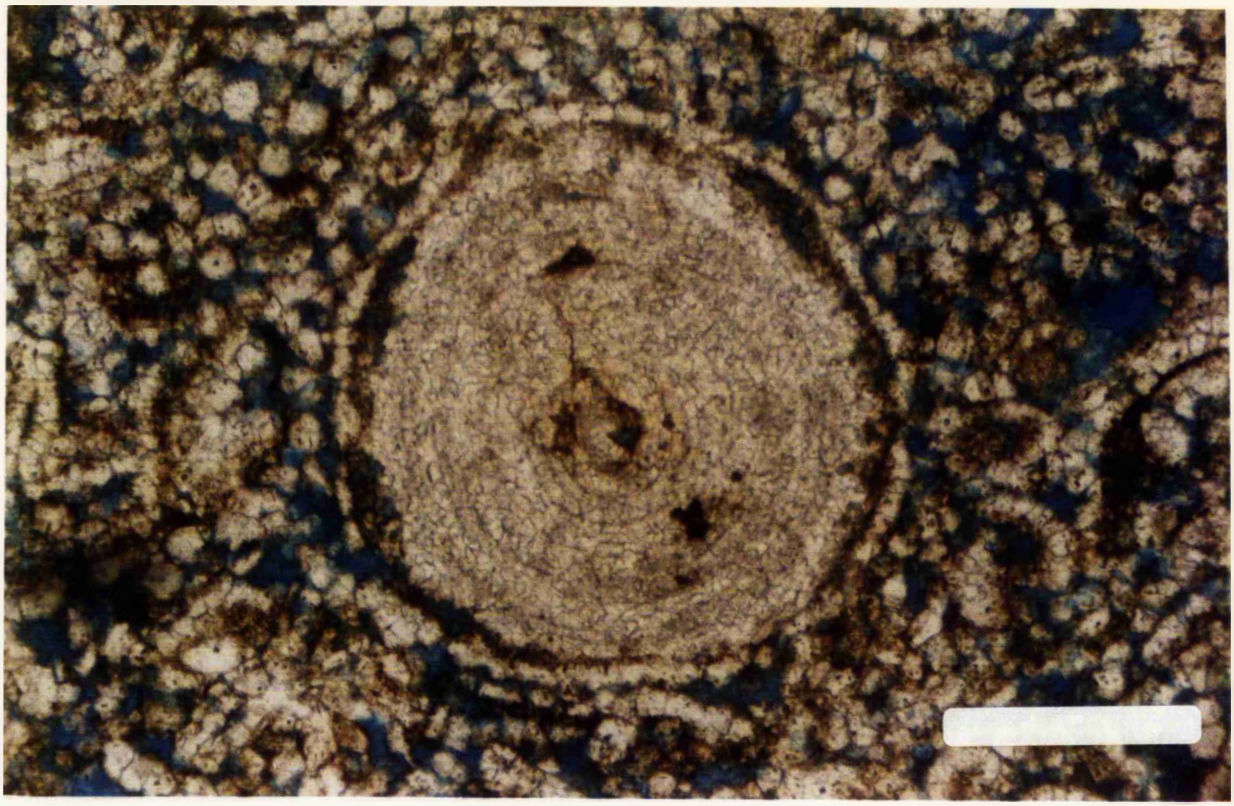

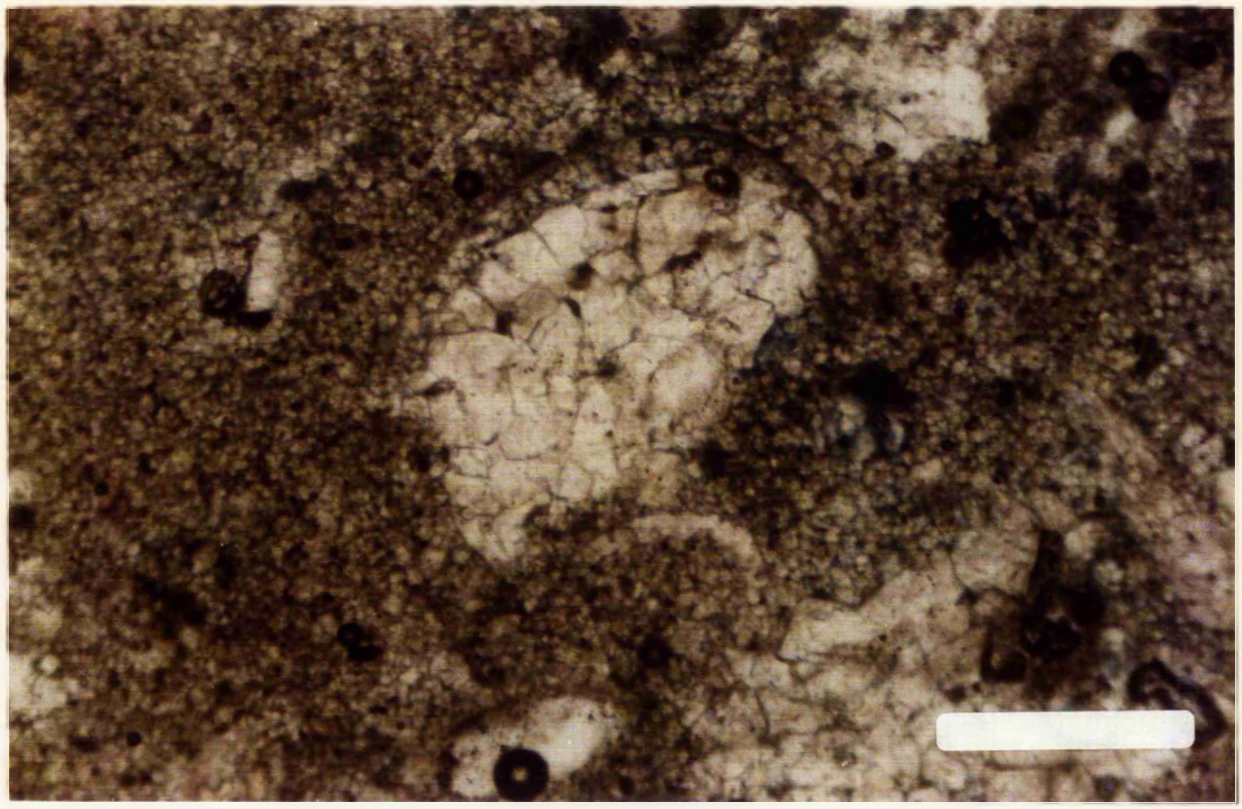

Probably, only types 1 and 7 occur singly while the rest of the dolomitization fabrics are transitional from one to another.

The "contrary dolomitization" fabric of Shukla has not been identified in the Euphrates Limestone Formation.

3.3.3. DOLOMITE DISTRIBUTION

According to their dolomitization these cores from the eight wells fall into three areas as follows:-

3.3.3.1. Area 1

This area is represented by cores **G, H,** and **C.** In these cores the Euphrates Limestone Formation is usually covered by the Dhiban Anhydrite Formation, and the top is formed of very fine crystalline limestone with anhydrite cement. Downward to 2/3 of the thickness of the formation, the limestone contains less than 10% dolomite. In the lower 1/3 of the formation the limestone is devoid of any dolomite and in most cases formed of wackstone-mudstone limestone with blocky calcite cement which reflects the fresh water diagenesis **(Fig 3.38).**

3.3.3.2. Area 2

This area is represented by core **E,** and can be regarded as a transitional zone, because the upper third is still dolomitic limestone, but more dolomitized than the previous area. The upper third of the formation contains up to 40% dolomite underlain by 4 metres of

Fig 3.35 Photomicrograph of completely dolomitized carbonate sediments. The boundary of the grain is still recognizable. But the grain itself is hardly recognizable. Plane polarized light. Scale bar is 0.35mm.

Fig 3.36 Microphotograph shows complete alteration of the original texture. No sign of bioclasts or lithoclasts. White areas are anhydrite cement. Plane polarized light. Scale bar is 0.35mm.

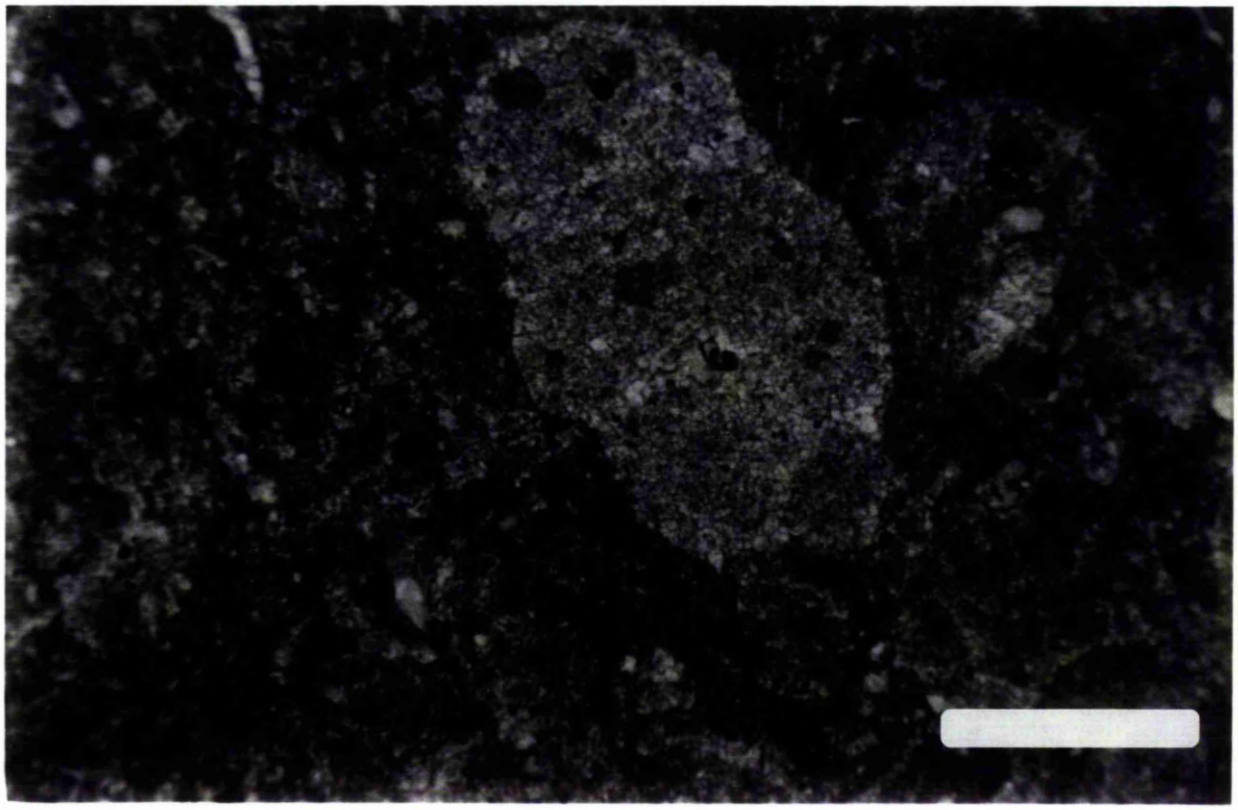

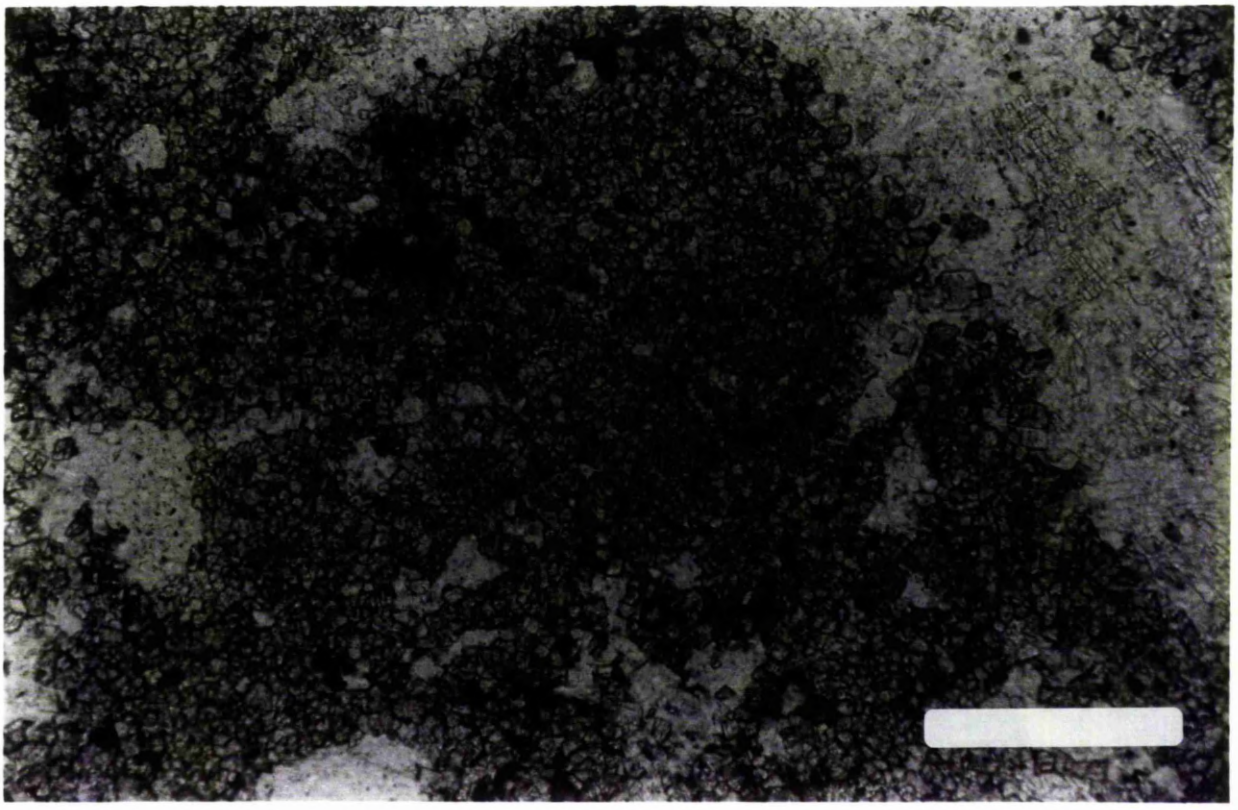

Fig 3.37 SEM photomicrograph of coarse dolomite rhombs (50-80 microns). These dolomite rhombs fill a mold (type 8). These dolomite crystals have curved edges, they probably represent saddle dolomite.

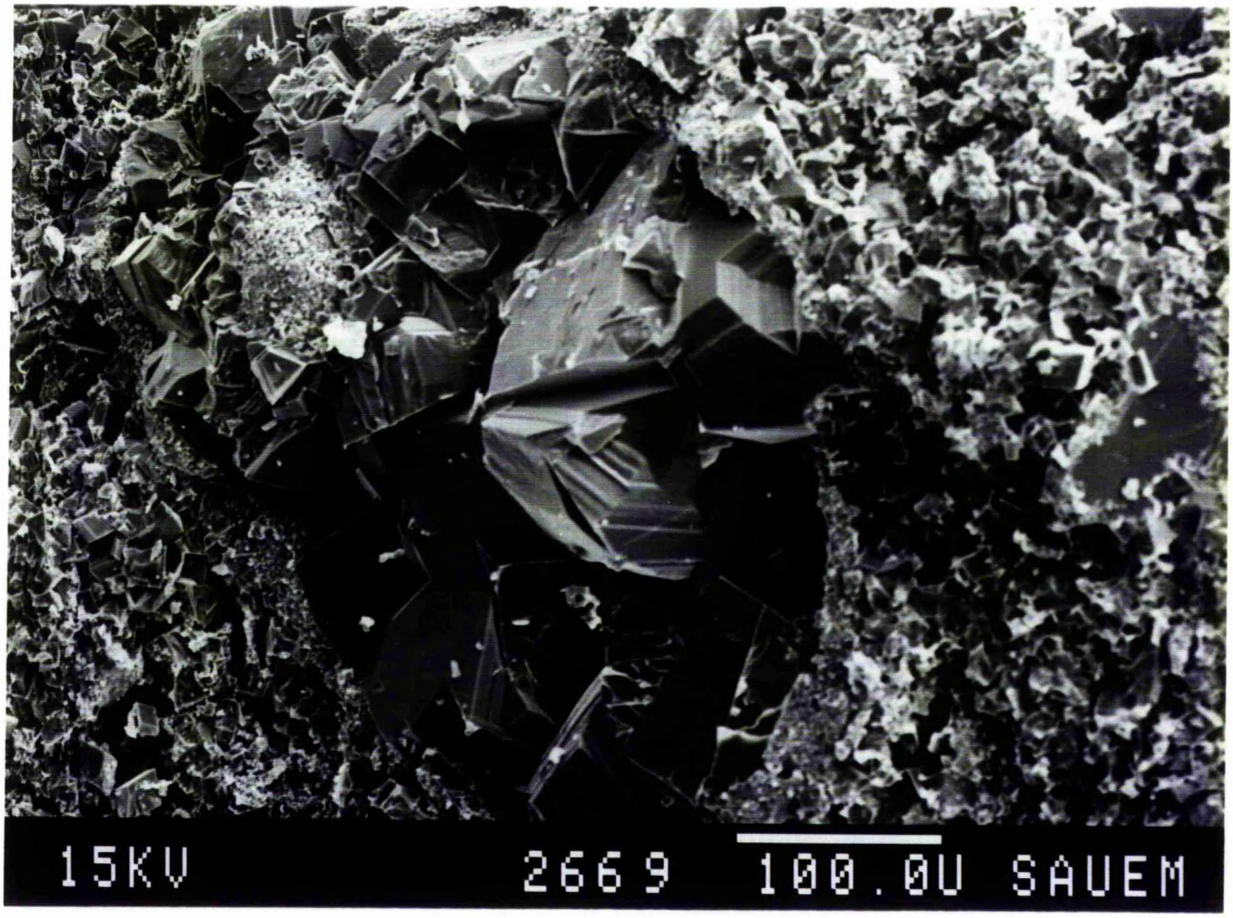
15KV
2669
100.0U SAUEM

partially dolomitized limestone, followed by 3 metres of dolomitic limestone, then followed by a thick bed of dolomite and calcitic dolomite (6 metres). This micritic dolomite contains various percentages of anhydrite as cement, filling, and replacement. This thick dolomite bed is followed by a bed of 2 metres of dolomitic limestone which in turn (by comparison with core **H**) is followed by limestone.

3.3.3.3 Area 3

This area is represented by the cores **A**, **B**, and **D** which are similar to each other, and core **D** will be taken as a representative of this area.

The top metre of the Euphrates Limestone Formation lying below massive anhydrite of the Dhiban Formation is formed of nodular dolomite and a chicken-wire textured anhydrite in which the anhydrite nodules are large and surrounded by a very fine crystalline to cryptocrystalline dolomite. The rest of the formation is very porous dolomite, which contains various percentages of anhydrite. In the middle of the dolomite sequence the anhydrite becomes more abundant and forms thin beds of one metre thick at different intervals (**Fig 3.38**).

There is a great thickening of the Euphrates Limestone Formation in this area. The thickened part is formed of oolitic fossiliferous dolomite. At the bottom of this dolomite there is an alternation of dolomite and dolomitic limestone. In the dolomitic limestone the anhydrite is usually rare, whereas in the dolomite sequence the anhydrite is very abundant (**Fig 3.38**).

From the above it is clear that dolomitization of the Euphrates Limestone Formation increases to the southeast, but

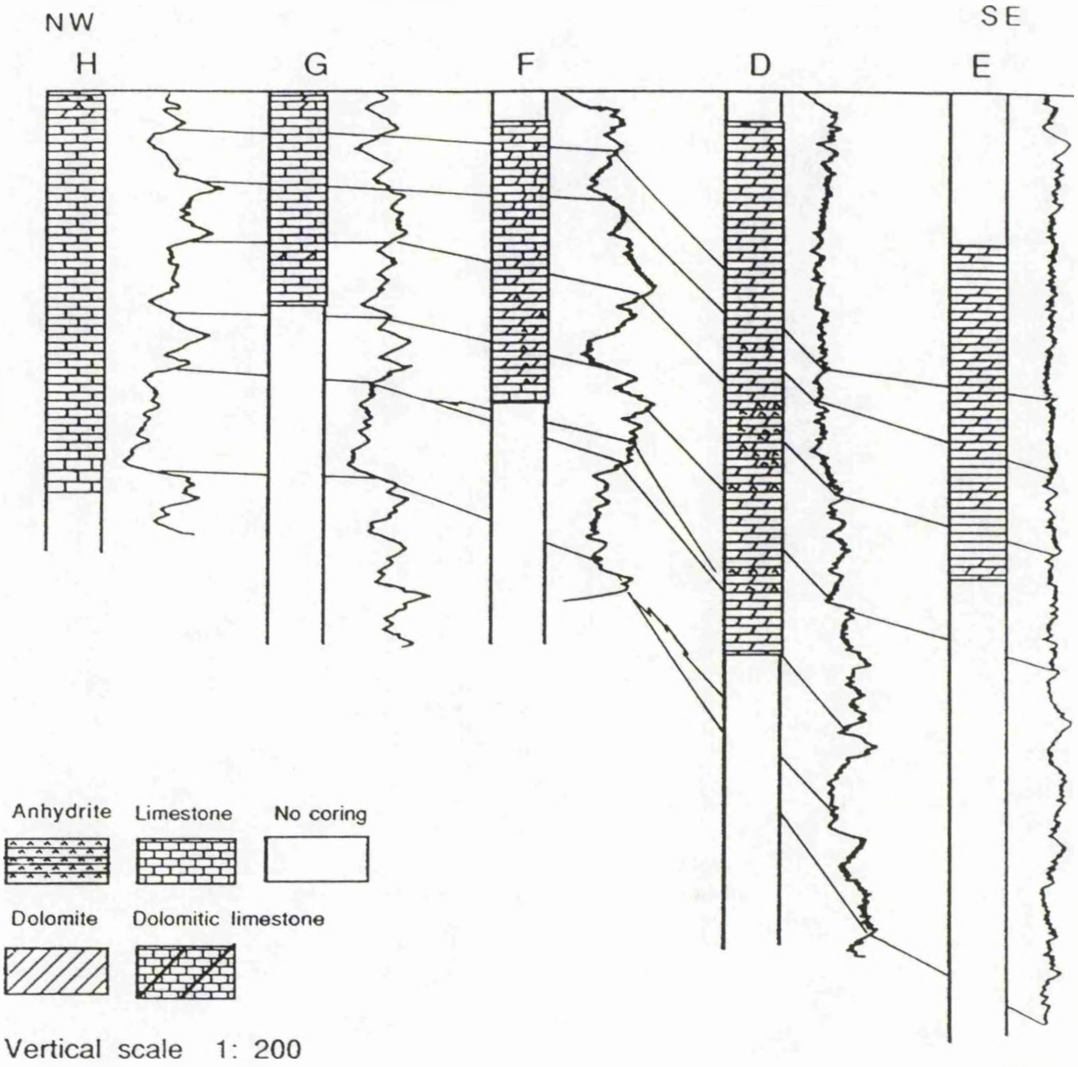

Fig 3.38 Correlation diagram showing different areas of dolomitization, extensive in the southeast and partial in the northwest. Gamma ray logs are not of the same quality because they were run at different times.

in most cases dolomitization is restricted to the upper part of the formation (**Fig 3.38**).

3.4. HOLLOW DOLOMITE RHOMBS

3.4.1. INTRODUCTION

In the present study dolomite rhombs with incomplete centres have been found to be very abundant in the Euphrates Limestone Formation, Lower Miocene, Iraq. They are readily seen under the petrographic microscope and further details are revealed under the SEM.

The composition and structure of these rhombs have been investigated by cathodoluminscence (CL) and the microprobe (EMPA). A variety of shapes of partially complete crystals of dolomite may be recognized. It is found that the "hollow" dolomite rhombs are usually associated with completely dolomitized limestone together with the presence of abundant secondary anhydrite and in a porous facies.

Similar phenomena have been reported from different part of the world in rocks of different ages (**Folk and Siedlecka, 1974; Land *et al*,1975; Weaver, 1975; Weaver and Beck, 1977; Gidman, 1978; Dunham and Oslon, 1980; Clark, 1980; Sibley, 1982; Schenk and Richardson, 1985; Rosen and Holdren, 1986; Pierre and Rouchy, 1988**).

It is suggested that the presence of trapped fluid inclusions or other more subtle defects in the lattice allowed selective dissolution of parts of the rhombs.

The sediment in which the hollow dolomite rhombs are found underwent a series of diagenetic processes as listed below:-

1. Formation of micritic envelopes and isopachous cement.
2. Dolomitization of the oolitic grainstone sediments contemporaneous with the deposition of gypsum and anhydrite.
3. Dissolution of the remenant calcite.
4. Compaction.
5. Introduction of the anhydrite cement as filling and replacement.
6. Dissolution of the dolomite rhombs.
7. Hydrocarbon emplacement as a final diagenetic process.

The hollow dolomite rhombs are found in vugs and pores in the grainstone/packstone fossiliferous oolitic dolomite. The original sediment was a well sorted oolite (**Fig 3.39**). The sediment underwent marine diagenesis indicated by the presence of micritic envelopes and the isopachous crust cement around the grains. This is followed by the dolomitization of the carbonate sediments, then followed by the dissolution of the grain centres which may have been caused by meteoric diagenesis. Crystals grown during marine diagenesis were influenced and controlled by the composition of the marine water, in contrast crystals growing during metoric diageneis are controlled by terristerial derived waters (**Fig 3.52**). Compaction followed causing the breakage of grains. Following or contemporaneous with dolomitization some dissolution of calcite took place leaving for example some hollow ooids (**Fig 3.39**). Anhydrite cement was then introduced to the sediment filling the oolites cores and various pores (**Fig 3.40**).

The introduction of the anhydrite cement caused a reduction in the porosity. At the same time it replaced the dolomite as evidenced by the presence of dolomite relics associated with the anhydrite cement. The hollow rhombs post-date the anhydrite cement because none of the hollow are filled with anhydrite (**Fig 3.41**). Some of the hollow rhombs are filled with hydrocarbon (**Fig 3.42**). Hydrocarbon emplacement postdate the hollow dolomite formation and, therefore, represents the final stage of diagenesis.

3.4.2. HOLLOW RHOMBS DESCRIPTION

Incomplete crystallization or partial dissolution?

Hollow dolomite rhombs are clearly visible under the microscope and scanning electron microscope (SEM) (**Figs 3.42, 3.43**). The rhombs are euhedral and range between 10 and 50 microns in size. It may be suggested that the rhombs owe their present form due to incomplete crystallisation , and indeed some of the edges have a distinct angularity (**Fig 3.44**). On the other hand, others are especially irregular and have a distinct appearance of dissolution, in addition the structure of more complex rhombs suggest that it is a dissolution phenomenon caused by reaction with composition of diagenetic waters rather than incomplete recrystallisation. There has been no collapse even though the rhombs are very fragile (**Fig 3.45**). In the case of the Euphrates Limestone Formation dissolution may have been effected by massive reduction of the salinity due to fresh water flushing during the period of regression or uplift following the Jeribe Formation.Various types of hollow rhombs denote different types of dissolution.

The first stage is shown when the outer surface is slightly etched (**Fig 3.43b**) then attack seems to have been concentrated on a very small hole developed at the middle of the rhomb face (**Fig 3.43b**). The small hole then enlarged by dissolution of the core of the rhomb or by etching along narrow zones leaving eventually a small central island (**Fig 3.47**). Some of the etching takes the form of a thin spherical cavity while the centre of the rhomb remains (**Fig 3.48**).

Etching may occur in zones leaving a hollow frame within a frame (**Fig 3.49**). As a final stage the rhomb centres were completely dissolved leaving only thin rims (**Fig 3.50**). The diameter of the hollow centres varies in size between 10-25 microns. These hollows contribute to the microporosity (the pores it form is called intracrystalline poprosity) of the dolomite rocks and in most cases are empty, but in certain instances are filled with hydrocarbon deposits (**Fig 3.42**). They may form conduits for fluid percolation through the rock (**Schenk and Richardson, 1985**). **Weaver and Beck (1977)** reported hollow dolomite rhombs from early to middle Miocene. Many cases have been reported from Eocene and Miocene, which probably indicates that the condition favourable for the formation of the hollow dolomite rhombs during these periods was widespread (**Land *et al*, 1975; Pierre and Rouchy, 1988**).

Trapping of samples of diagenetic waters which aided dissolution and partial reprecipitation are found as a trials of fluid inclusion in the partially hollow dolomite rhombs. More work on the composition of these inclusions could aid the identification of the diagenetic fluids.

Fig 3.39 Photomicrograph shows oolitic grainstone dolomite; white area is anhydrite filling the dissolved dolomite; dark area is interparticle porosity; oolites are well sorted with isopachous cement. Plane polarized light. Scale bar is 0.35mm.

Fig 3.40 Photomicrograph of the sediment texture in which the hollow dolomite rhombs occur; white area is anhydrite filling the inter and intraparticle porosity. Oolites surrounded by isopachous cements. Plane polarized light. Scale bar is 0.35mm.

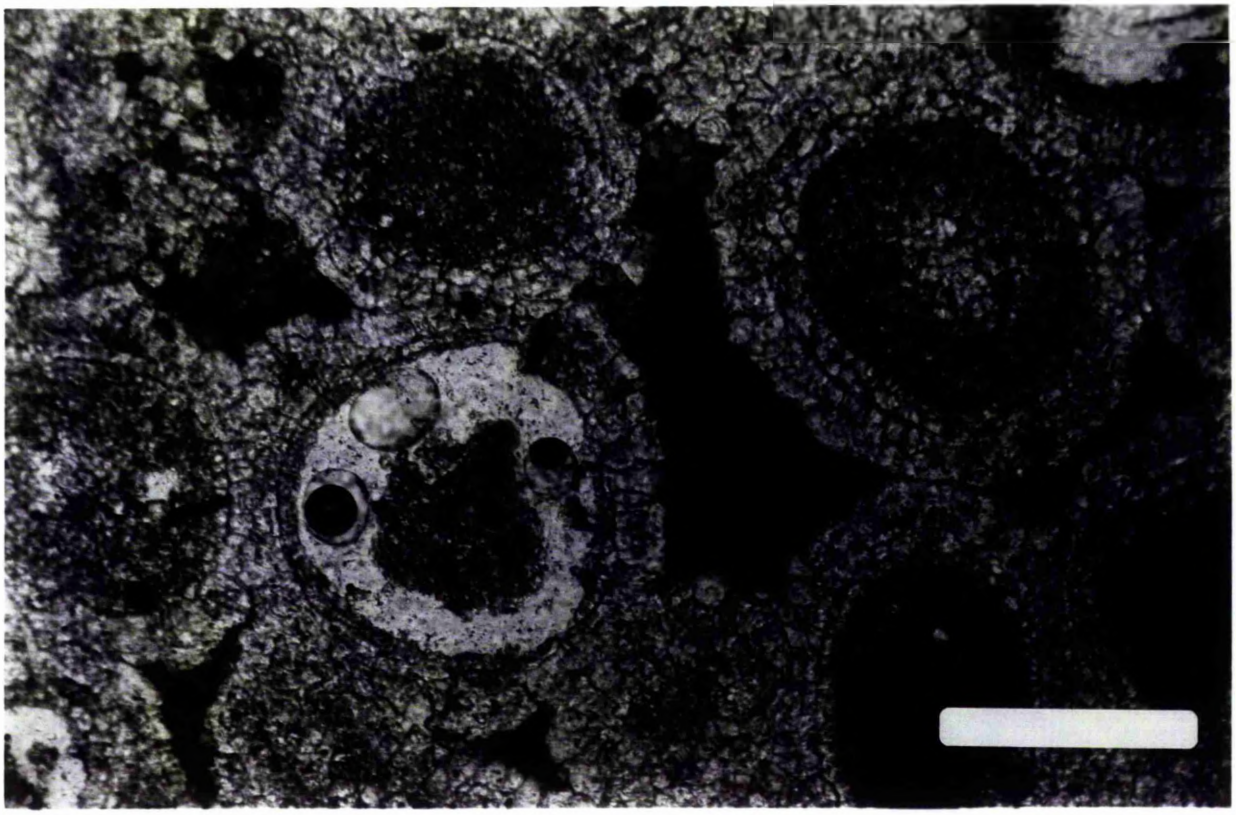

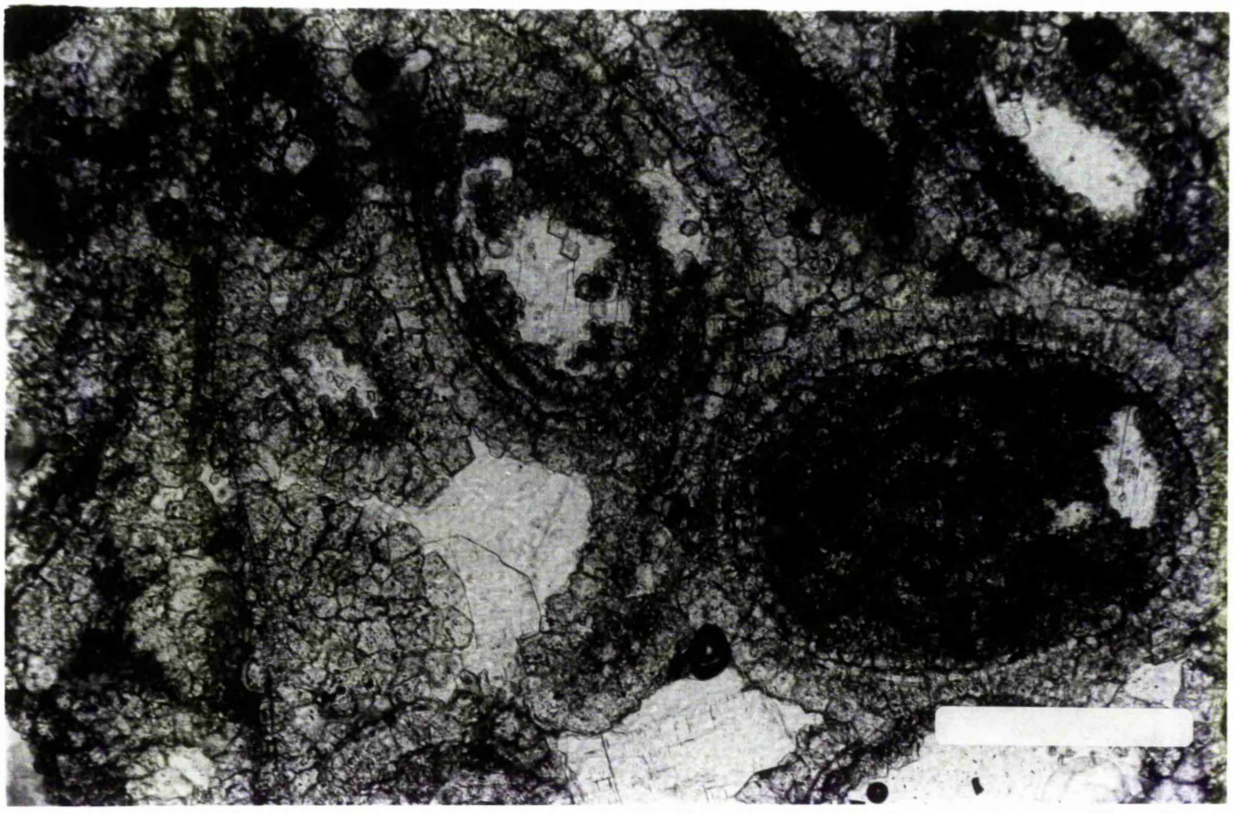

Fig 3.41 SEM photomicrograph of hollow dolomite rhomb overlying anhydrite cement (top right) without being filled with anhydrite, indicating a later stage of dissolution after the inroduction of the anhydrite.

Fig 3.42 Photomicrograph of hollow dolomite rhomb filled with hydrocarbon, white large area representing anhydrite, black areas represent pore spaces. Plane polarized light. Scale bar is 0.875mm.

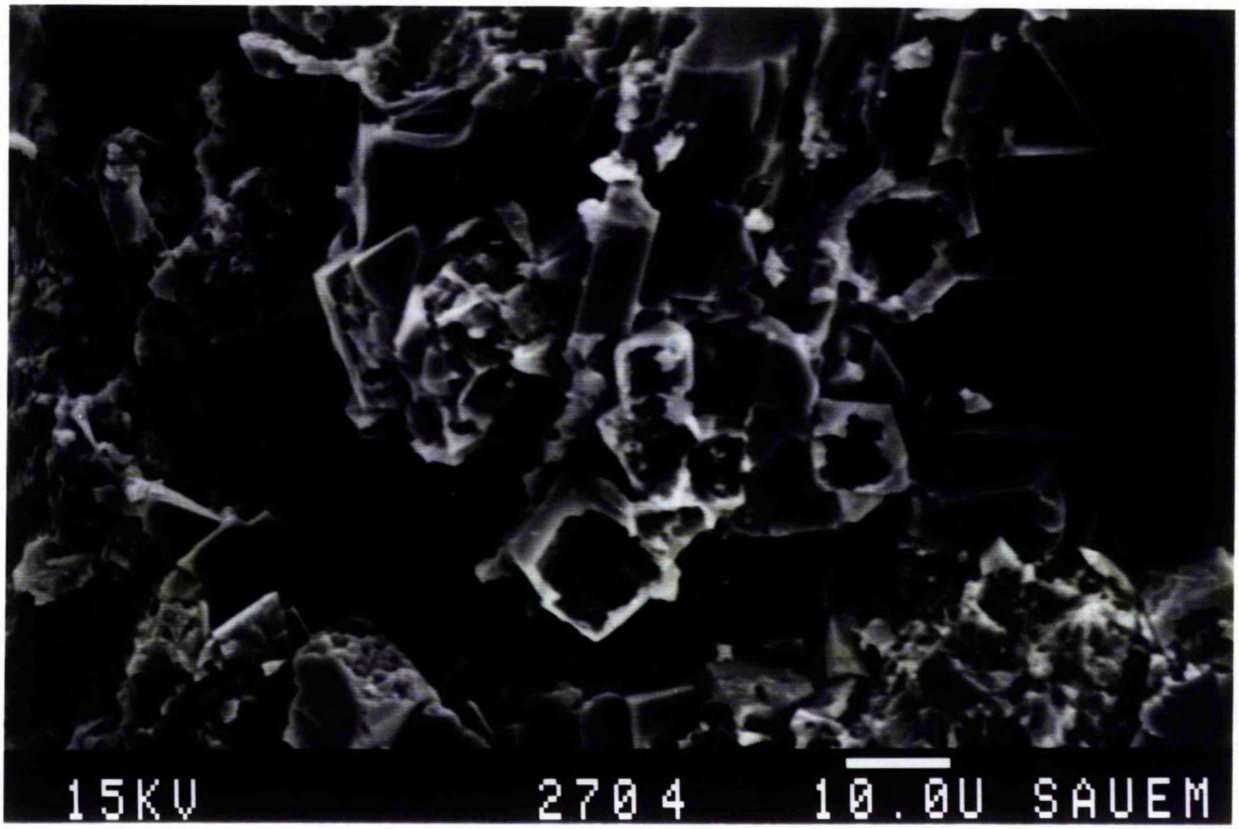
15KV
2704
10.0U SAUEM

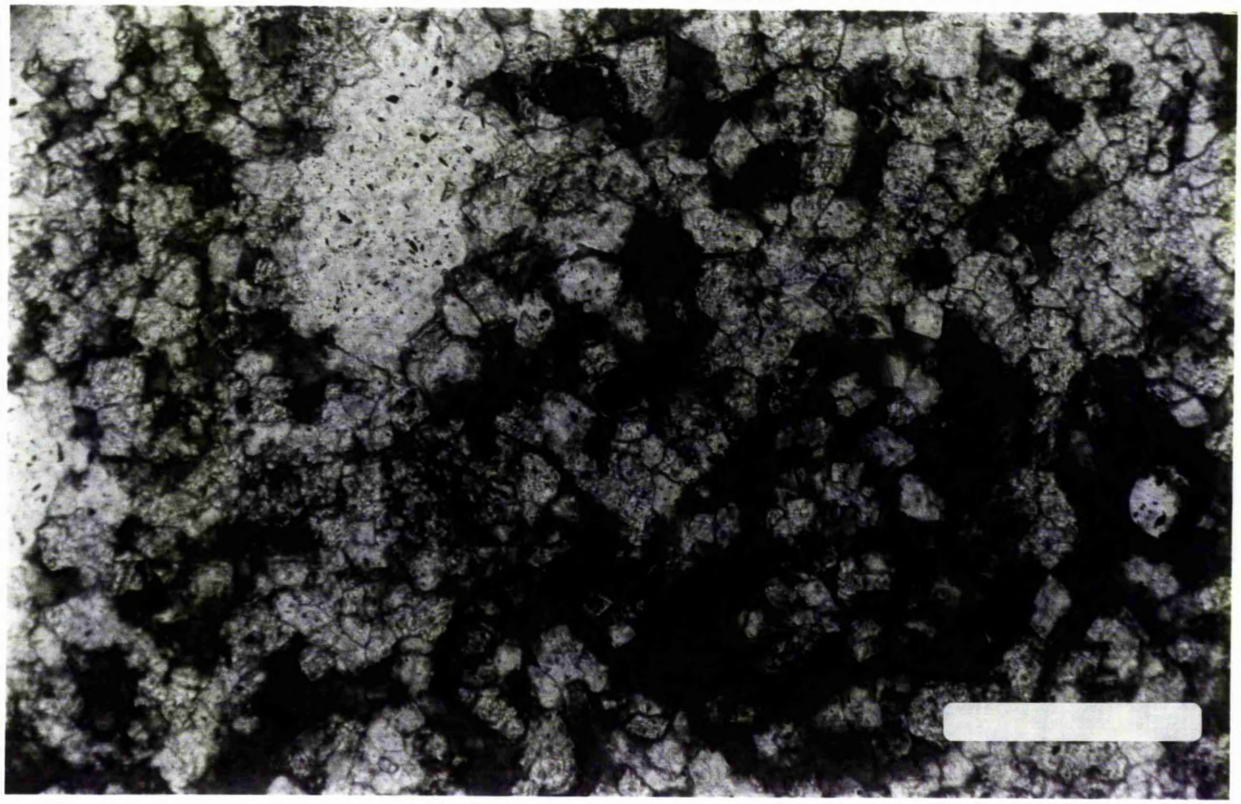

Fig 3.43a Photomicrograph of hollow dolomite rhombs present in the intraparticle porosity. Plane polarized light. Scale bar is 0.35mm.

Fig 3.43b SEM photomicrograph of slightly etched surface of dolomite rhomb (arrow) representing the first stage of dissolution of rhombs, other stages can be noticed in the photograph.

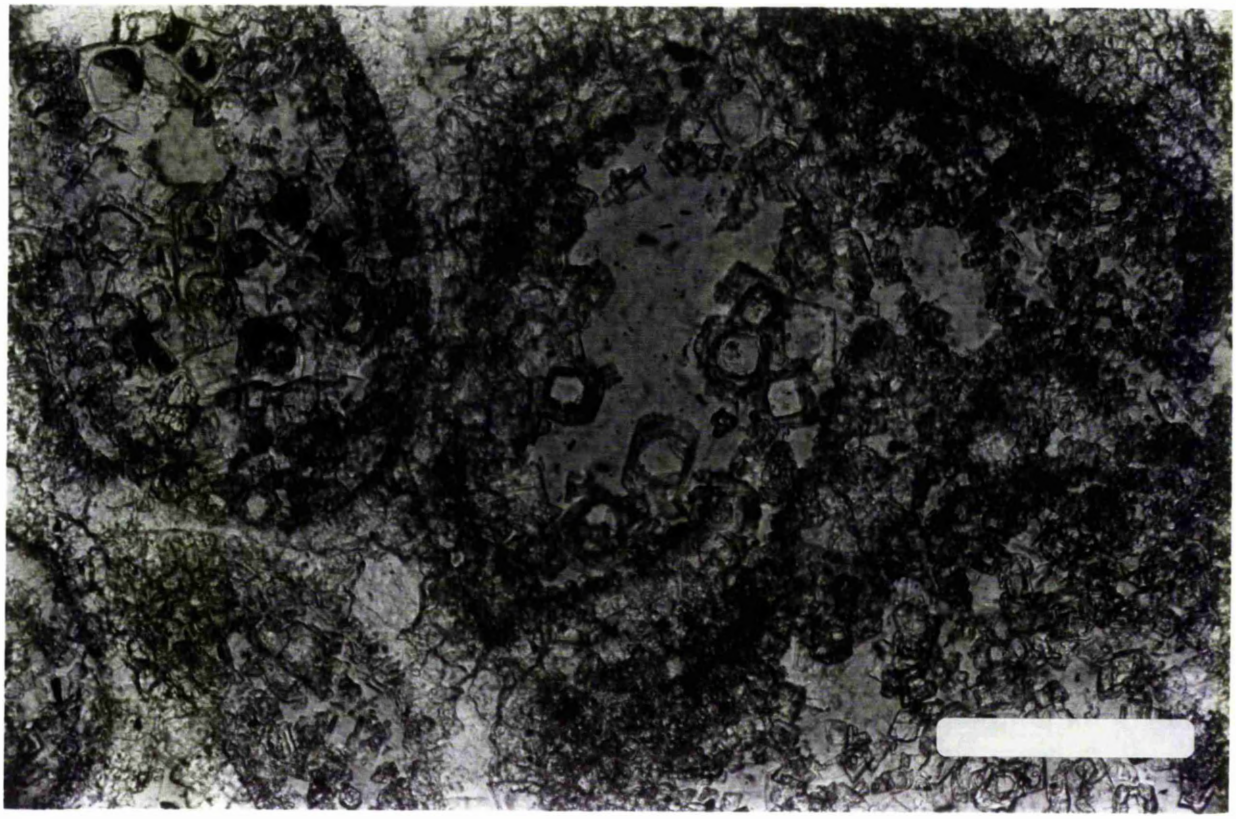

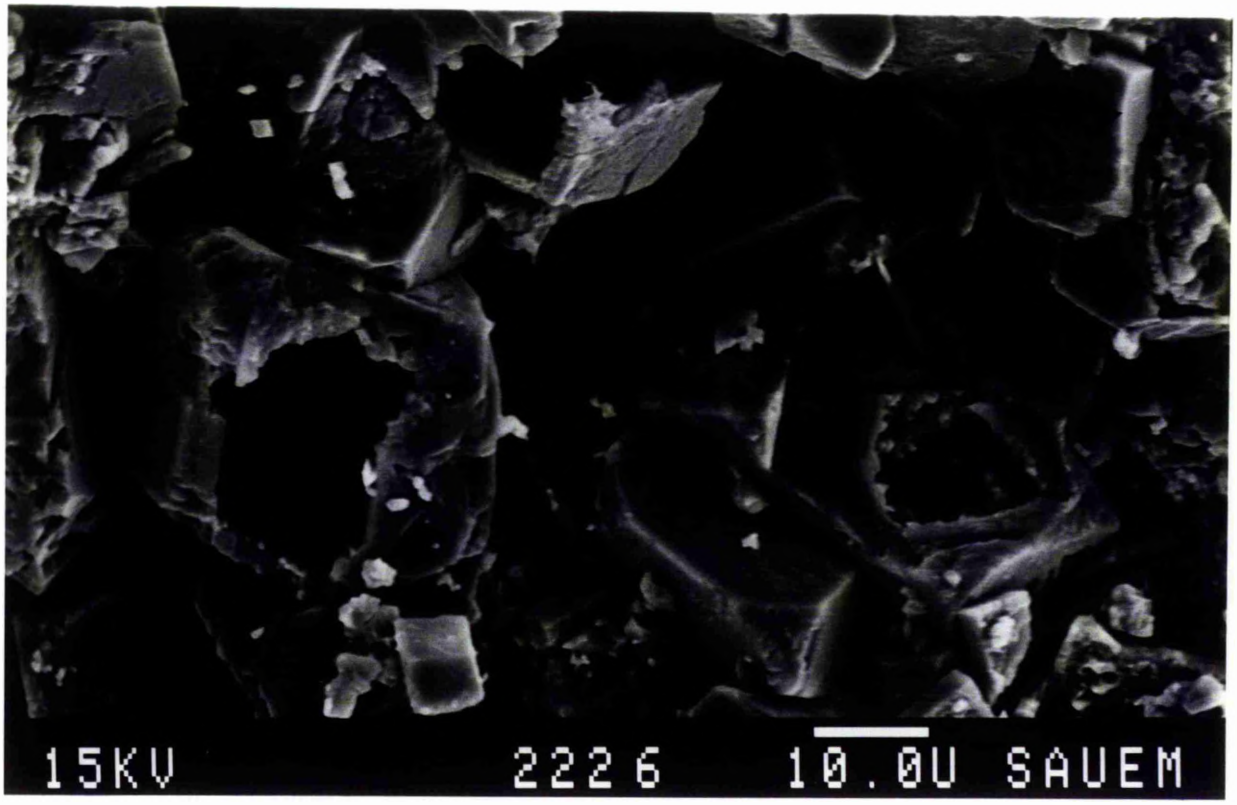
15KV
2226
10.0U SAUEM

Fig 3.44 SEM photomicrograph of a hollow rhomb dissolved in the centre with partially dissolved zones surrounding the centre. This rhomb lies inside a vug.

Fig 3.45 SEM photomicrograph of a dolomite rhomb which has been dissolved leaving only a very narrow outer rim.

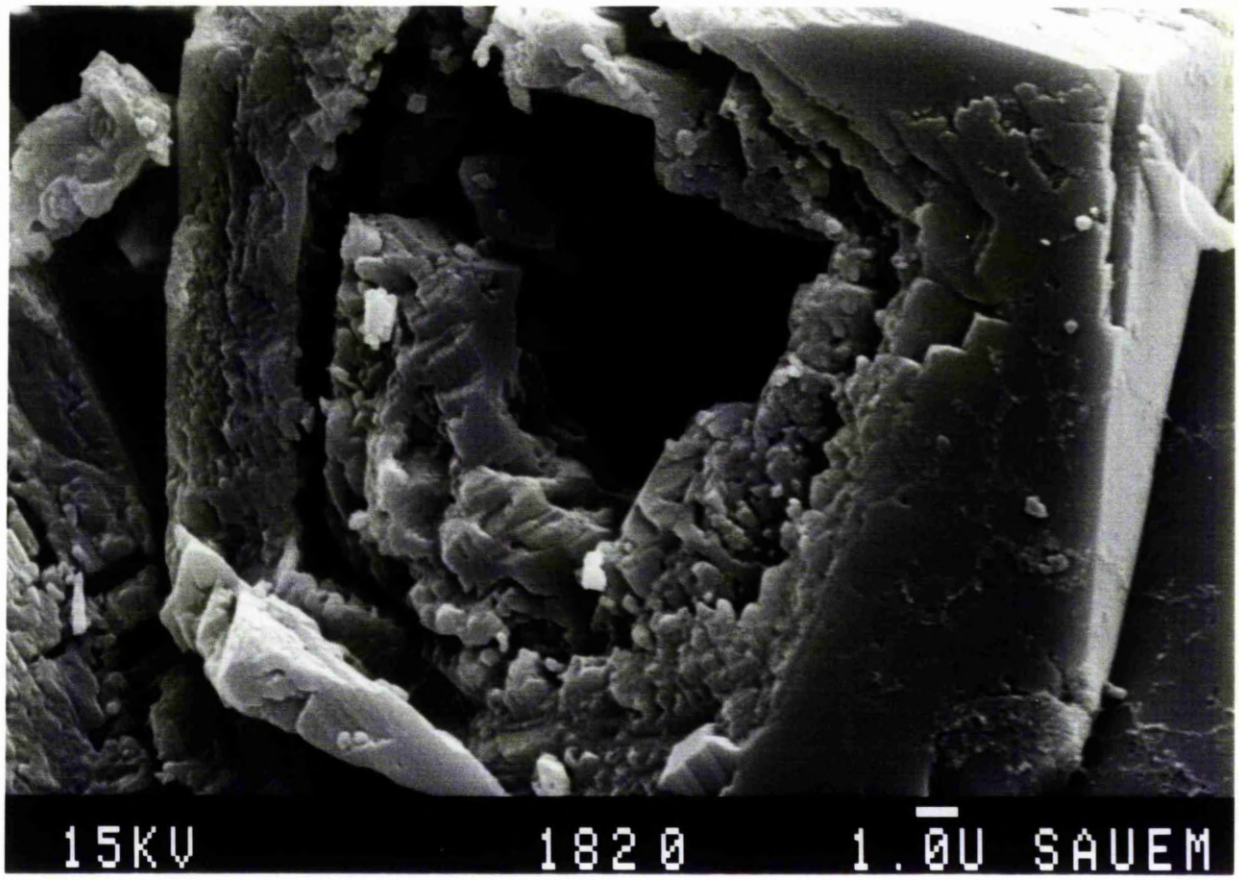
15KV 1820 1.0U SAUEM

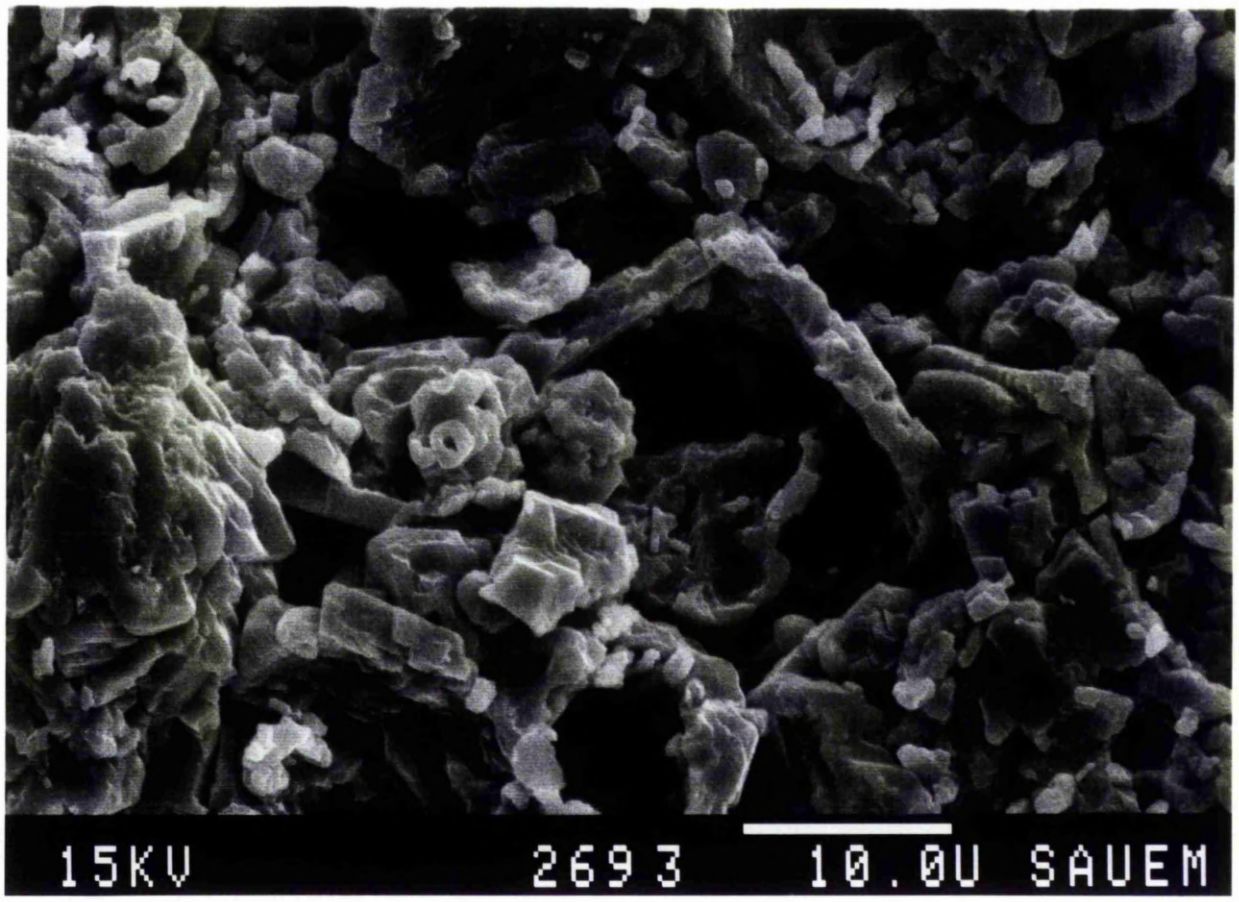
15KV 2693 10.0U SAUEM

Fig 3.46 SEM photomicrograph of a hollow dolomite rhomb with a circular hole in the centre, representing the initial stage of dissolution.

Fig 3.47 SEM photomicrograph of a dolomite rhomb dissolved from the centre but a small core remains.

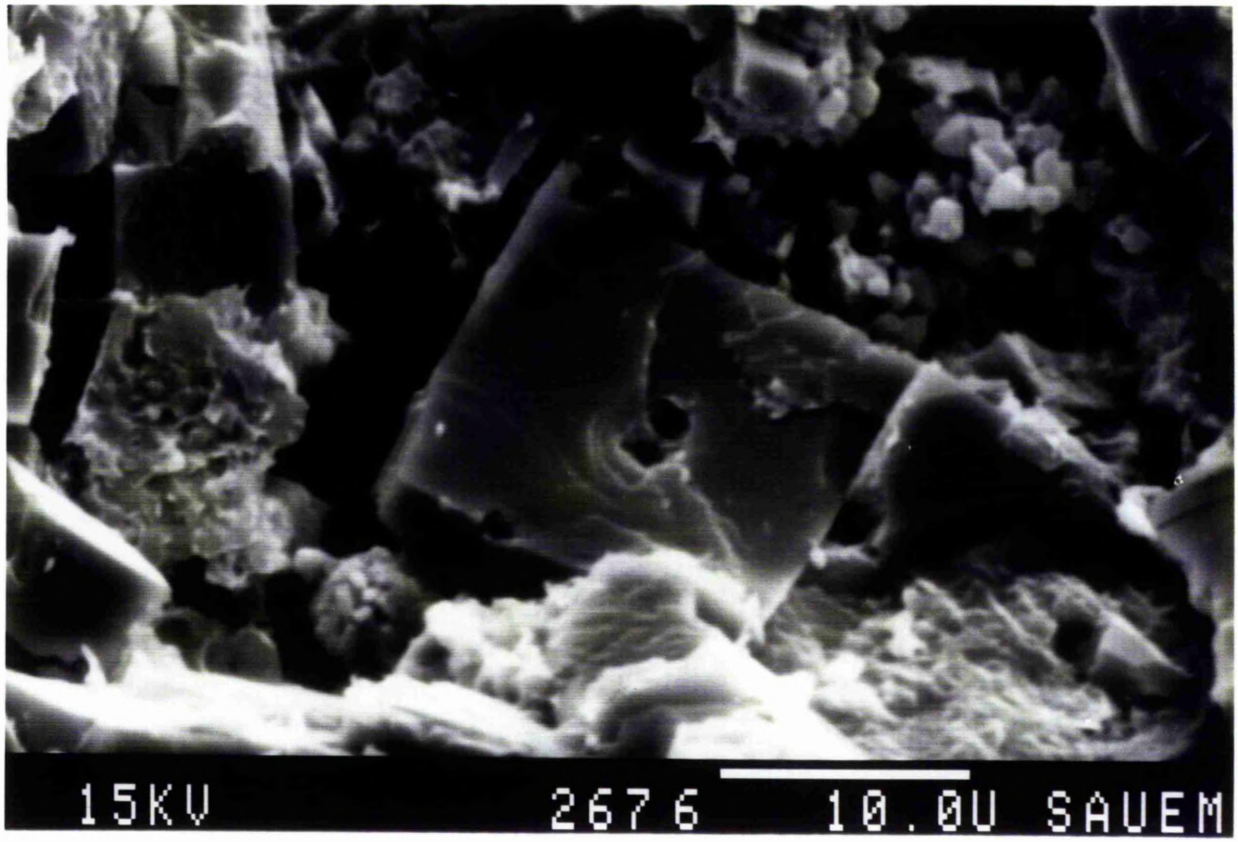
15KV 2676 10.0U SAUEM

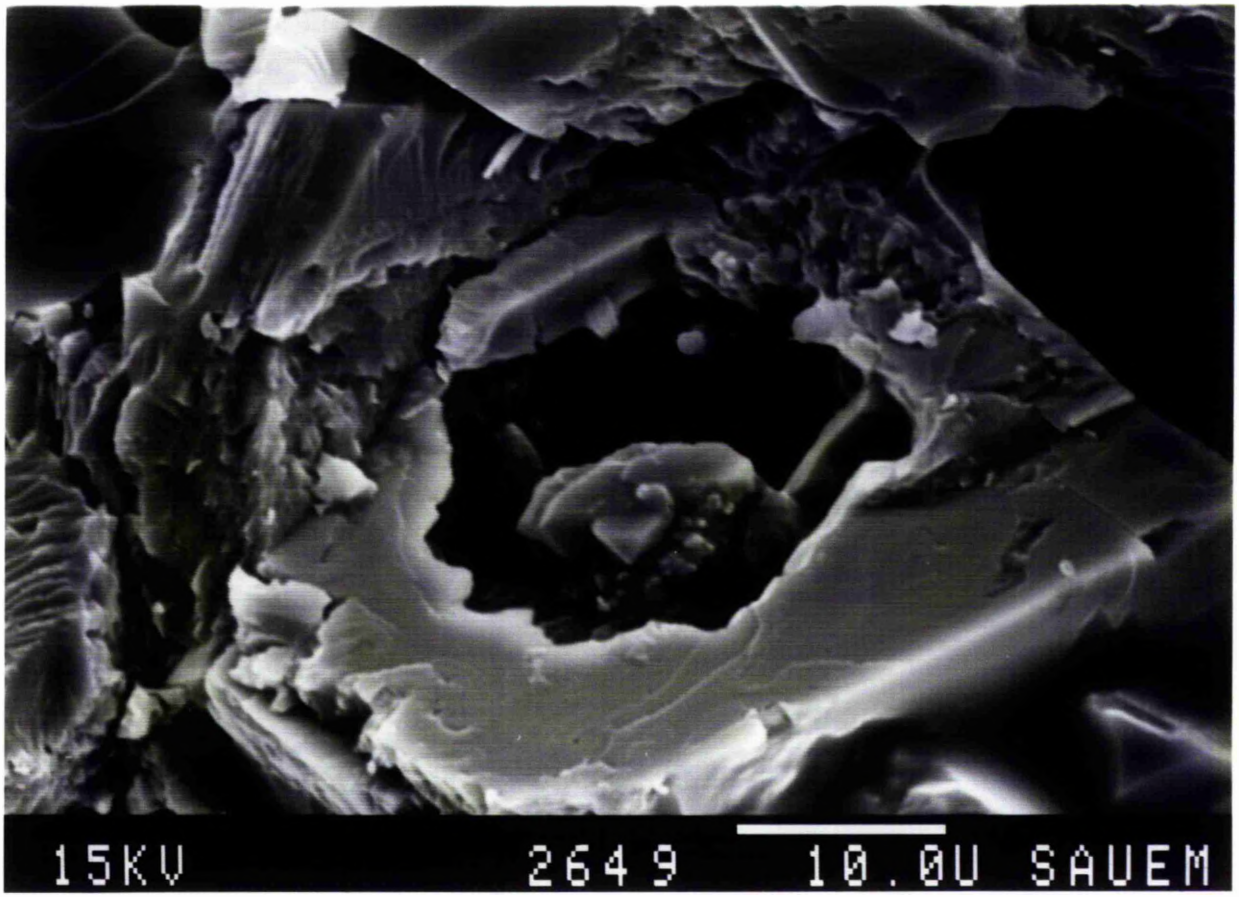
15KV 2649 10.0U SAUEM

3.4.3. DISCUSSION AND CONCLUSIONS

In considering the origin of the hollow rhombs of dolomite the following are the pertinent facts.

1. No zoning or compositional differences are found in surviving rhombs.
2. No mineral inclusions occur in most undissolved rhombs but a few bear tiny fluid inclusions toward the middle of the crystals.
3. Hollow rhombs are found in a facies which contains also abundant anhydrite either as nodules or as cement. In addition the formation is overlain by massive anhydrite beds.

Lithological and isotopic evidence points to the dolomite of the Euphrates Limestone Formation as having formed in an overall sabkha environment. Through the rock sequence of the Euphrates Limestone Formation and above there is a trend to greater salinities culminating in the massive anhydrite of the Dhiban Anhydrite Formation.

Ordering of sabkha dolomite is progressively increased with aging of the crystals (**McKenzie, 1981**). However in the sabkha environment periodic flushing of fresh water from for example rain storms would produce schizohaline conditions (**Folk and Land, 1975**). In such a situation the Mg/Ca ratio in solution is increased by the removal of calcium during anhydrite or gypsum precipitation. This, together with a tremendous reduction in salinity by the accession of meteoric waters predisposes the precipitation of dolomite. With considerable

Fig 3.48 SEM photomicrograph showing the dissolution of a dolomite rhomb leaving a partly etched centre.

Fig 3.49 SEM photomicrograph of a dolomite rhomb etched in zones and retaining crystal faces on the inner "shell".

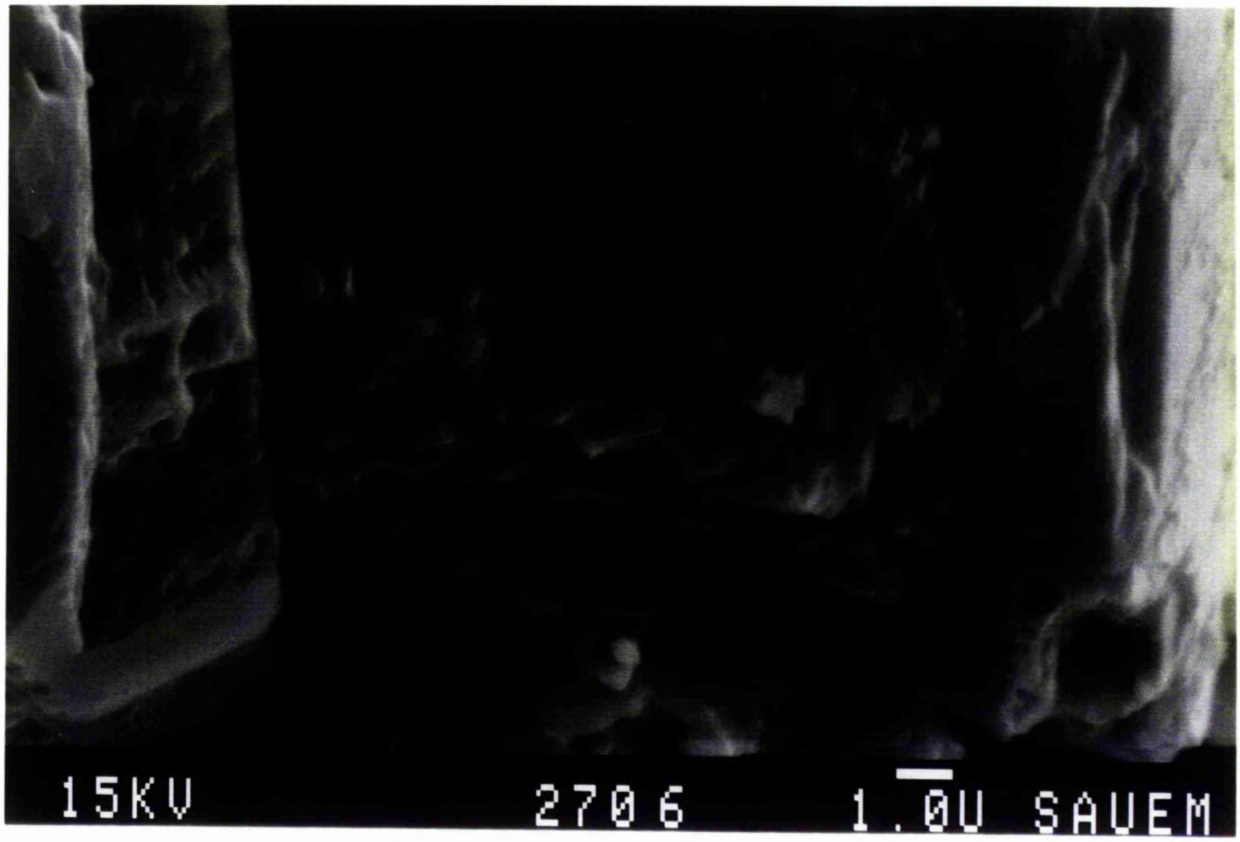
15KV
2706
1.0U SAUEM

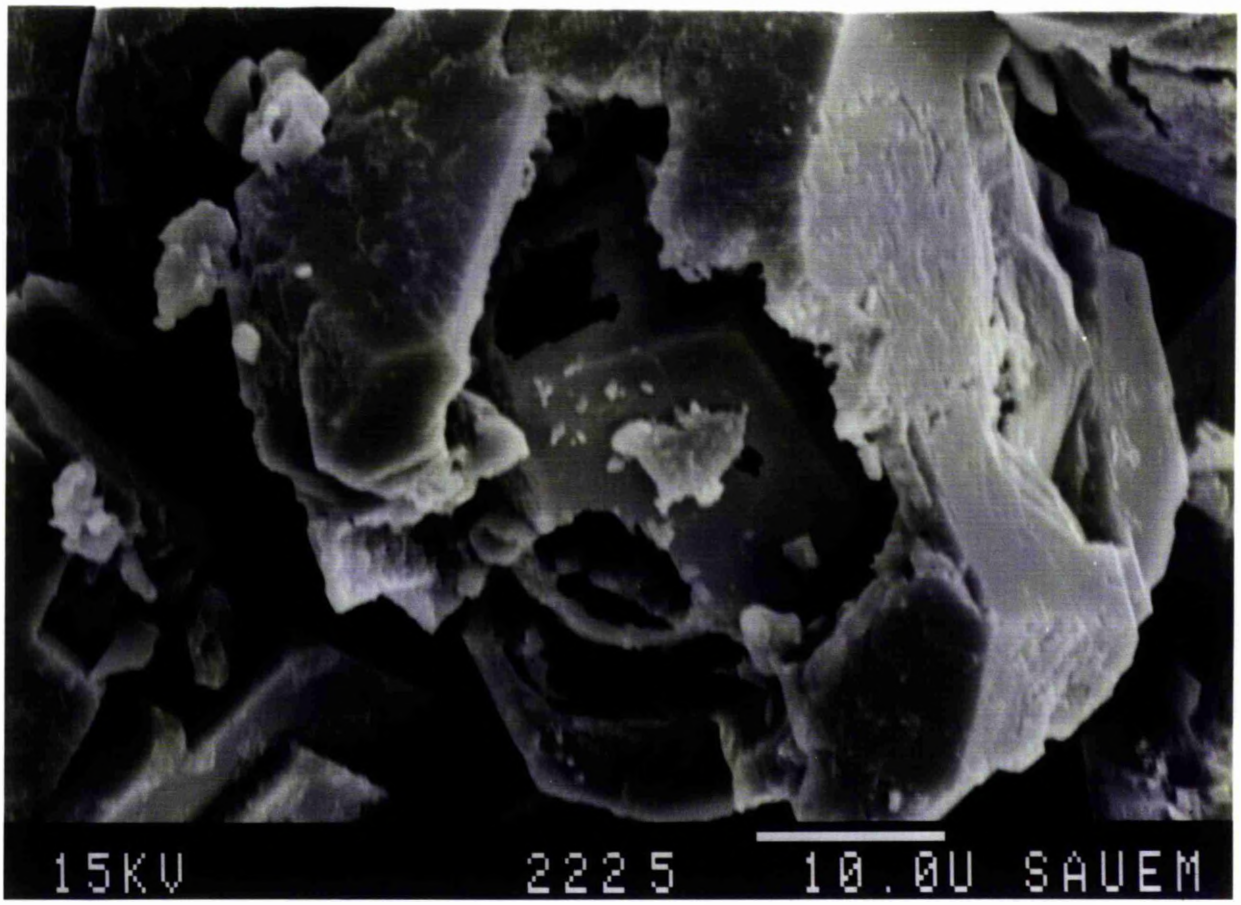
15KV
2225
10.0U SAUEM

Fig 3.50 Photomicrograph of hollow dolomite rhombs in which only the rims remain. Plane polarized light. Scale bar is 0.17mm.

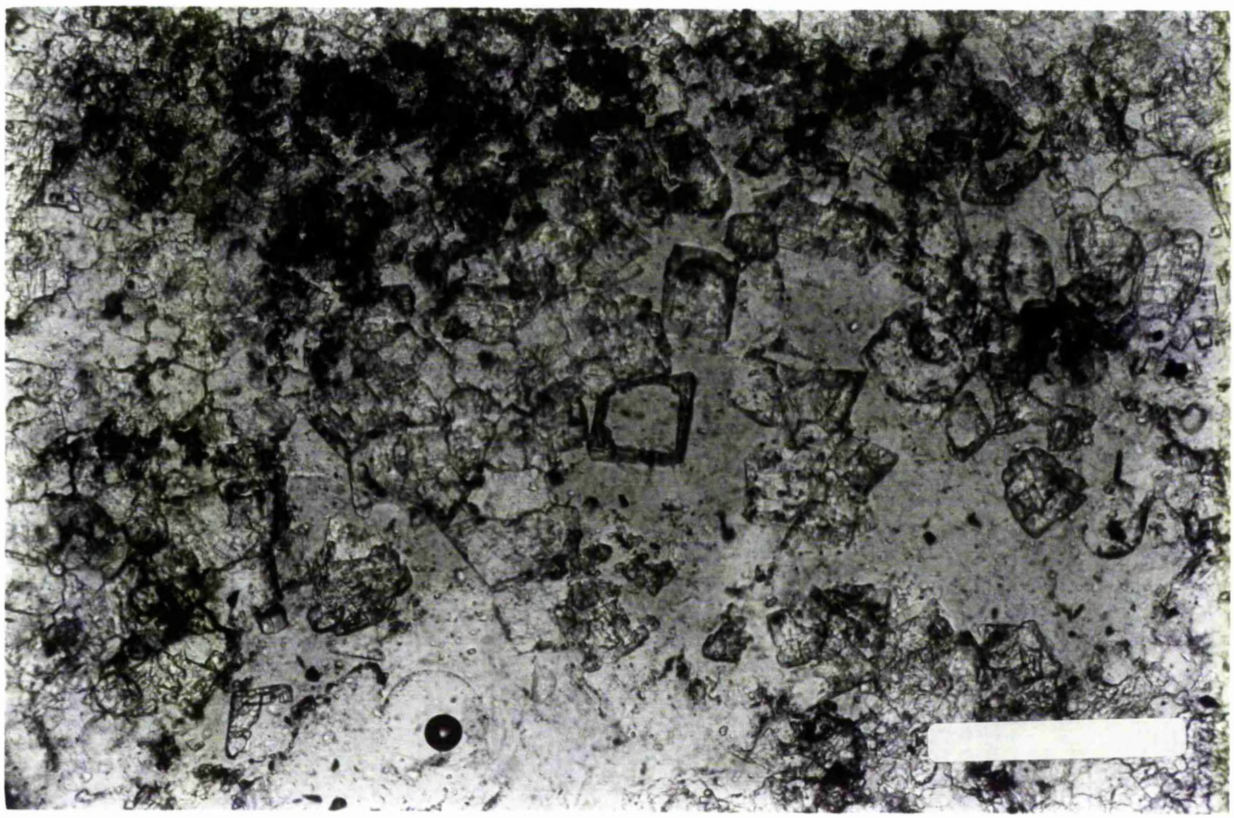

dilution well ordered, clear, limpid, crystals are formed (**Folk and Land, 1975**) (**Fig 3.51**).

It has been found that there is a direct correlation between the frequency of flooding, composition of the interstitial brines, and the distribution of the diagenetic minerals developed (**Butler, 1969**). Therefore, in such a case, the alternation of low ordered and well ordered limpid dolomite will be expected.

The suggestion that hollow rhombs might be due to the dissolution of an early anhydrite nucleus within resistant rims of limpid dolomite (**Folk and Siedlecka, 1974; Rosen and Holdren, 1986**) seems untenable in the case of the Euphrates Limestone Formation because of the pervasive presence of unaffected anhydrite within the Formation and above. Furthermore complete lack of zoning and compositional differences also rules out the likelihood that it was magnesian calcite that was dissolved (**Gidman, 1978**).

We are therefore left with the possibility that selective dissolution took place due to structural rather than compositional differences (**Busenberg and Plummer, 1982**). Preferential dissolution has been produced experimentally on dolomite rhombs and **Herman (1982)** suggested that attack was concentrated on energetically favoured sites in the lattice where defects occurred. These could be subtle structural effects not easily detected or equally in the present case they could have been caused by the presence of fluid inclusions in the centres of crystals or, if freshening of waters was repeated, by alternating zones in the rhombs.

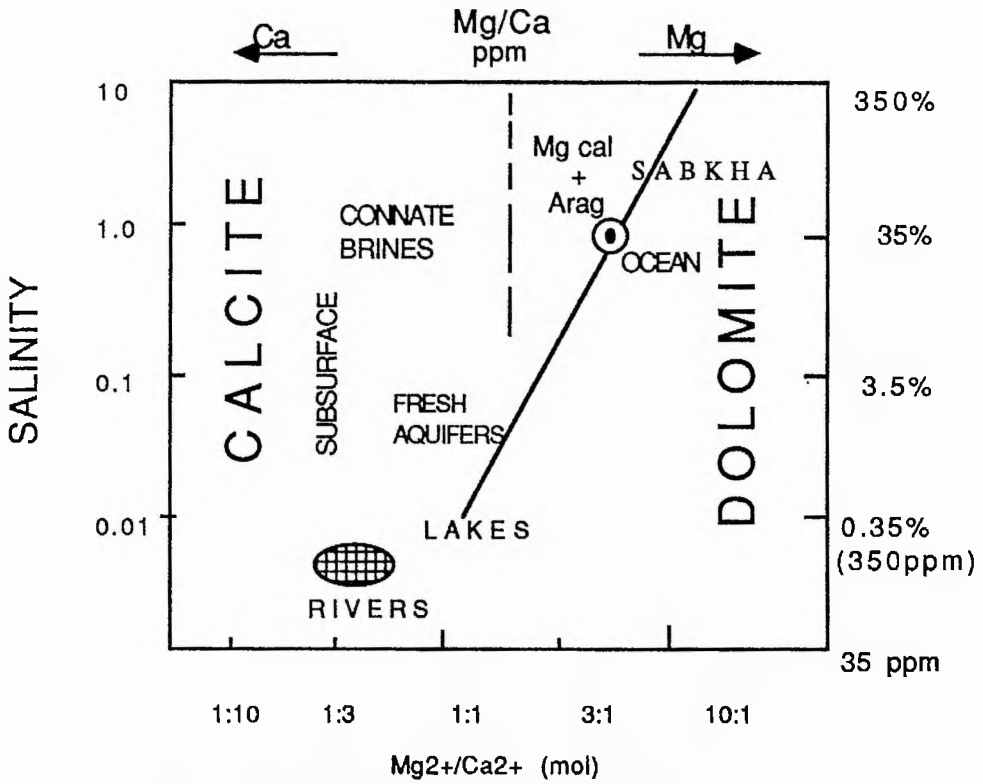

Fig 3.51 Fields of occurrence of common natural waters plotted as graph of salinity versus Mg/Ca ratio. (from Folk and Land 1975)

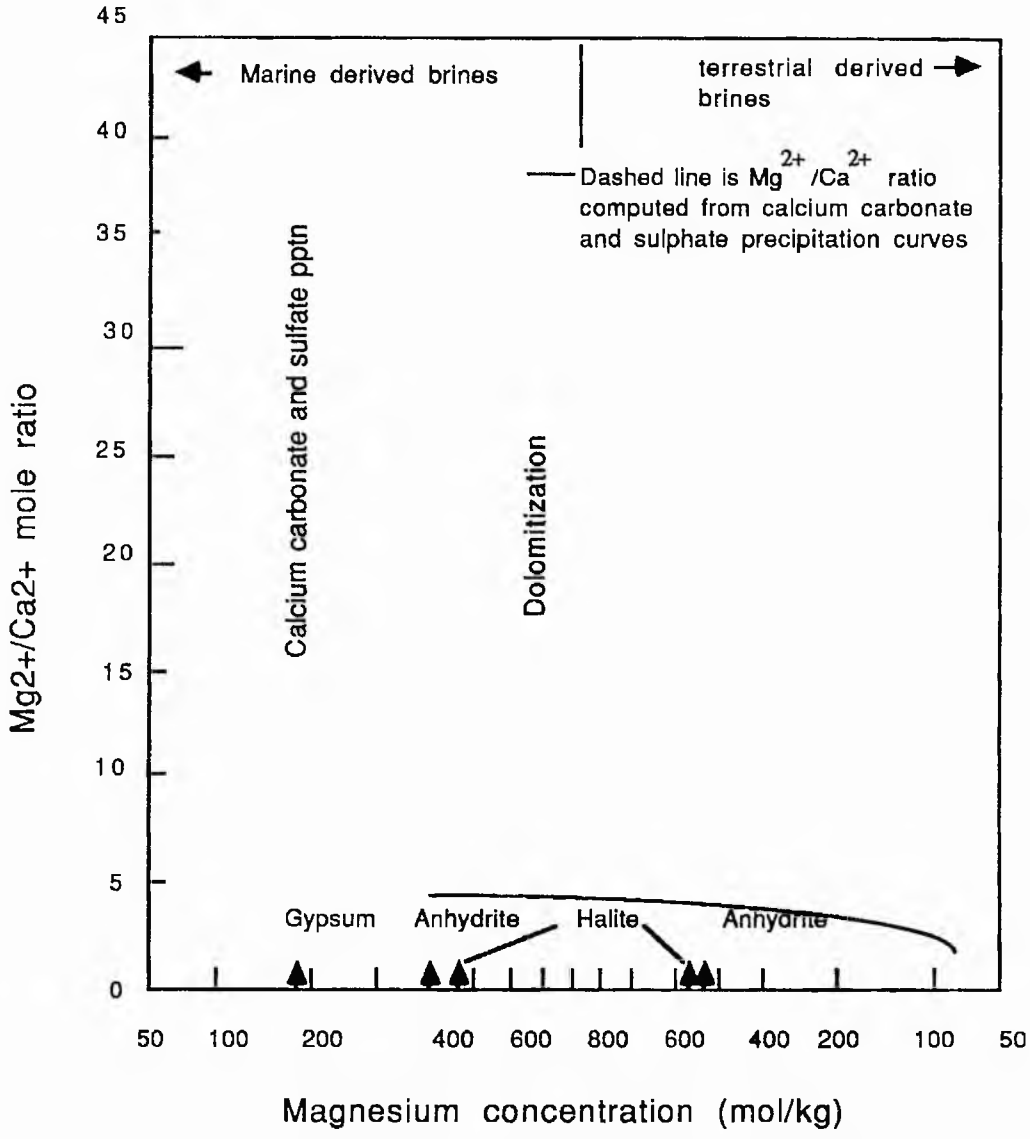

Fig. 3.52 Mg^{2+}/Ca^{2+} ratio as a function of Mg concentration for Abu Dhabi sabkha (Butler,1969).

CHAPTER 4
GEOCHEMISTRY

INTRODUCTION

The origin of dolomite in sedimentary rocks is a matter of controversy. Recent studies have shown that the dolomite forms from solutions of different origin (as indicated by isotopic composition) under a range of environmental conditions. Dolomites have been found in diverse Recent sediments in the Coorong, in Australia (**Alderman and Skinner, 1957; Skinner *et al*, 1963; Von Der Borch and Jones, 1976**), under the sabkha surface and in the high algal flats in the Arabian Gulf (**Wells, 1962; Shearman, 1963; Kinsman, 1964**); in the playa environment as in Deep Spring Lake California (**Jones, 1961, 1965**); in supratidal flats on Bonair Islands, Netherlands Antilles (**Deffeys *et al* , 1964, 1965; Hsu and Siegenthaler, 1969**); on Andros Islands at the Bahamas Banks (**Shinn, 1964; Shinn *et al*, 1965**); on the bottom of some freshwater lakes, and as a precipitate in some caves and freshwater springs as well as in the subsurface where mixing of fresh and salt waters occurred as in the Hope Gate formation, on the north coast of Jamaica (**Land, 1973**); in the Middle Ordovician Champlainian series of southern Wisconsin (**Badiozamani, 1973**). Dolomite found in the above examples represents a variety of environments, and either formed in shallow marine areas with restricted circulation such as lagoons

or supratidal areas in which the sea water becomes concentrated by evaporation, or from meteoric ground water: this indicates the need for special modification of the parental waters. The association of presently forming dolomite with anhydrite deposits and hypersaline environment is regarded as a bias of the Recent environment which is not shared by ancient dolomites (**Hardie, 1987**).

Fuchtbauer (1972) has reported that almost stoichiometric and nearly well ordered dolomite is related to evaporitic conditions and the presence of anhydrite. Recent studies shed doubt about the dolomite formed in the sabkha environment and whether the dolomite formed from direct precipitation or by replacement (**Hardie, 1987**). Also questioned is the evidence used to support the replacement origin of the dolomite. An alternative origin for the dolomite formation is offered is direct precipitation, known from other modern sabkha and saline lakes, and which is consistent with experimental evidence. At lower temperature dolomite could only form by direct precipitation.

Replacement of dolomite, at low temperature requires very long reaction times (10^4 years). This requirement can only be met in a very large regional water flow system, either marine or nonmarine (**Hardie, 1987**). Dolomite in the present study shows the evidence of replacement of the original carbonate sediments, evidence that came from dolomitization of the original fossil skeletons which are known not to be formed as dolomite. No ferroan dolomite is found in the Euphrates Limestone Formation

and iron concentration is very low. Suggesting non oxidizing condition of the formation.

4.1 ORDERING

The degree of dolomite ordering was estimated by dividing the intensity of the ordering line (015) by that of the diffraction peak (110) (**McKenzie, 1981; Goldsmith and Graf, 1958a**).

The degree of ordering also can be estimated from the presence or absence of the major peaks of reflections (006, 015 , 110, 030, 0012), and their intensities. The weakness of order reflection can be a consequence of the substitution of Mg in dolomite by Mn or Fe (**Goldsmith and Graf, 1958b**).

The dolostone in the southeast area has a high degree of ordering ranging between 0.4-0.7 and in one single case up to 0.93. The dolomite in the northwest area has a very weak degree of order (Appendix 2).

4.2. STOICHIOMETRY

Dolomite stoichiometry was determined by the XRD methods of **Lumsden and Chimahusky (1980)** in which the calcium content in the dolomite is related to the d(104) spacing (**Goldsmith and Graf, 1958b**).

The X-ray patterns were used to measure the amount of excess calcite in the dolomite lattice. Excess calcite in non stoichiometric dolomite causes a shift in the main dolomite peak (104). For each of the Euphrates Limestone Formation samples the position of (104) peak was measured with reference to the salt internal standard, the mole % of the $CaCO_3$ was determined (**Appendix 2**).

Dolomite in the southeast area is nearly stoichiometric and ranges from 50 to 51.7 mole % $CaCO_3$ (**Appendix 2**). Dolomite in the central and northwestern areas is calcium-rich and ranges from 52 to 58 mole % $CaCO_3$, the degree of calcium enrichment covaries with the content of the separate calcite phase (**Fig 4.1**).

The $Ca_{50}Mg_{50}$ dolomite composition is associated with the presence of anhydrite as found by **Fuchtbauer (1972)**. The association of calcite with calcium rich dolomite also agrees with previous observations in the Middle Jurassic Great Estuarine Group in NW Scotland (**Andrews *et al*, 1987**). Complete dolomitization is accompanied by the formation of nearly stoichiometric dolomite, and is probably due to the persistence of condition favourable for dolomite formation (**Andrews *et al*, 1987**).

The bulk percentage of the dolomite per sample was calculated by comparing the unknown sample with standard of known dolomite contents (**Royse *et al*, 1971; Tennant and Berger, 1957**). **Royse *et al*** method is more precise than the other method, especially at the low and high D/D+C ratios graph (**Fig 4.2**). For quantitative determination of the percentages of the dolomite in a mixed calcite dolomite samples the peak height ratio was used in conjunction with graphs by **Tennat and Berger (1957)**; **Royse *et al*, (1971)**. The 104 peaks are chosen because they have greater intensity for dolomite and calcite respectively, and they are free from interference by other peaks. Accuracy of this method of dolomite versus calcite determination

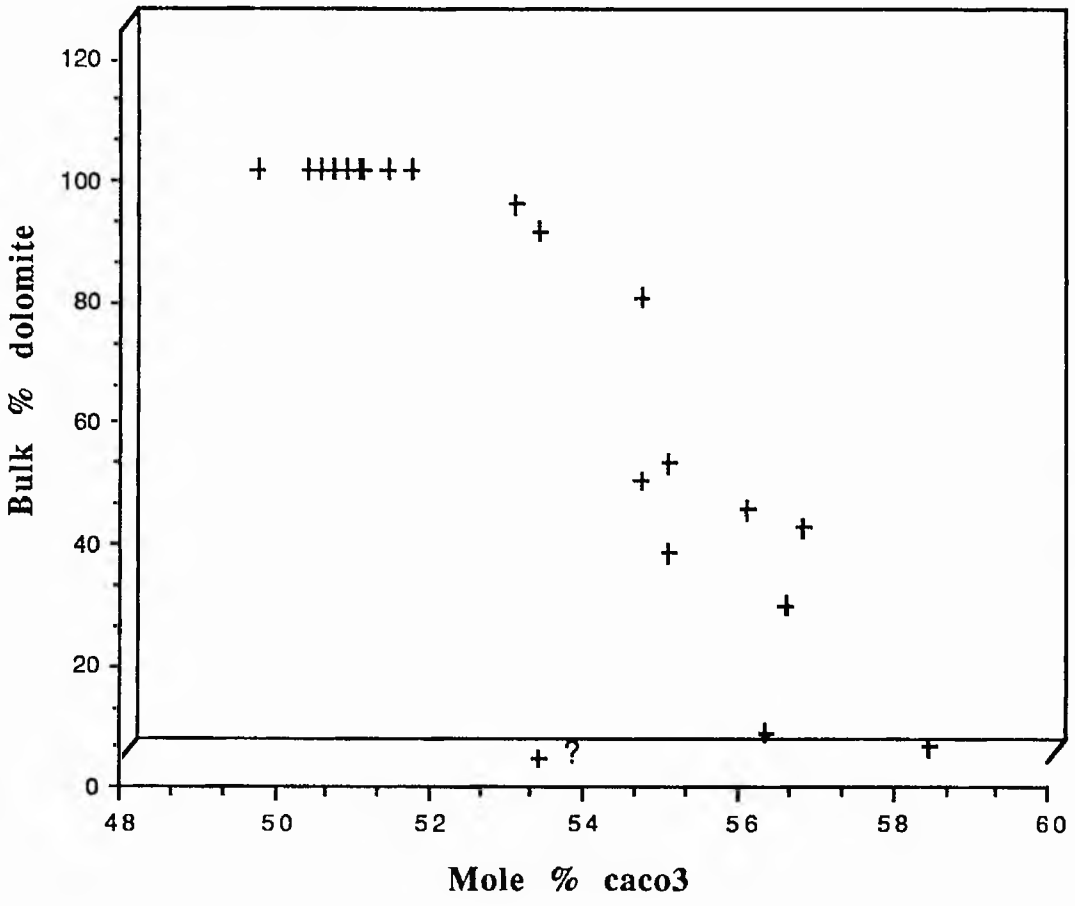

Fig 4.1 A plot of bulk dolomite prcentage against the mole percentages in the dolomite lattice.

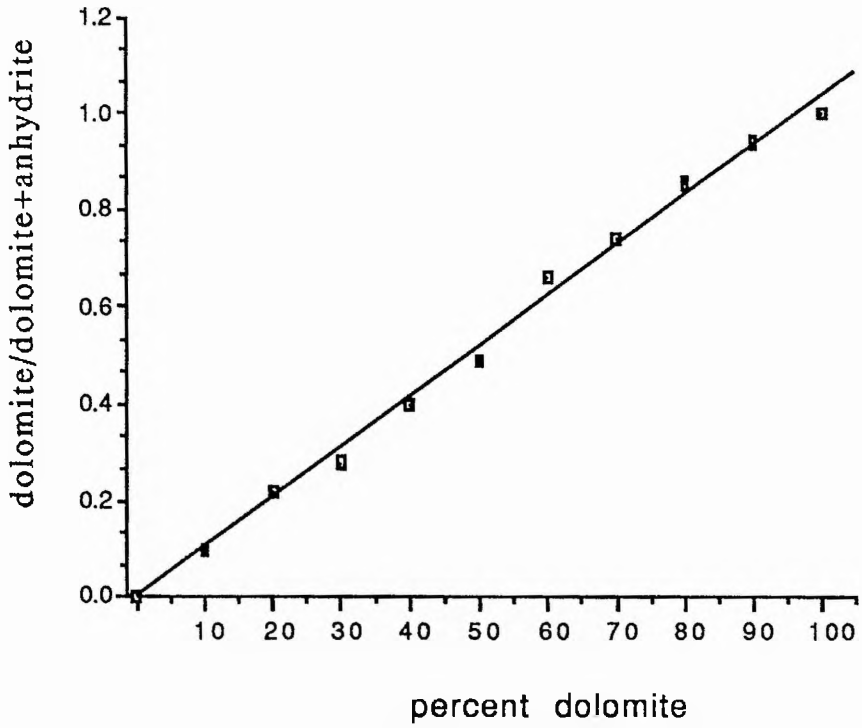

Fig 4.2 Graph used to calculate the percentages of dolomite in a mixture of dolomite and anhydrite

has been found to be within 6% of the dolomite at 95% confidence level (**Royse *et al*, 1971**). Another standard curve was also prepared used to calculate the percentage of dolomite in a mixture of anhydrite and dolomite (**Fig 4.2**).

4.3. GEOCHEMICAL RESULTS

4.3.1 Mineralogical composition

Mineral percentages are calculated from X-ray diffraction results and presented as percentages versus depth to show their variations with depth **Fig. (4.3)** shows that dolomitization of the Euphrates Limestone Formation in core **D** is complete except at the lower part of the section where the limestone percentage is high and dolomitic limestone is formed. The anhydrite percentage fluctuates with depth, but becomes very high at certain depths to form thin beds of nodular anhydrite and dolomite (**Fig 4.3**). At this core the anhydrite disappears at the bottom of the section and partial dolomitization is noticed. This probably occurred because the dolomitizing solution was no longer supersaturated with respect to anhydrite to precipitate anhydrite. Three thin anhydrite beds can be seen (**Fig 4.3**), which from petrographic identification are associated with a very fine crystalline dolomite. These beds probably mark the position of very saline environment during the deposition of the Euphrates Limestone Formation. The sequence of these beds probably indicate a cyclic sea level fall or may be due to the closure of the lagoon during the deposition of the Formation.

In core **E** complete dolomitization is clear (**Fig 4.4**) in which calcite is absent. High anhydrite percentage is seen at the top of

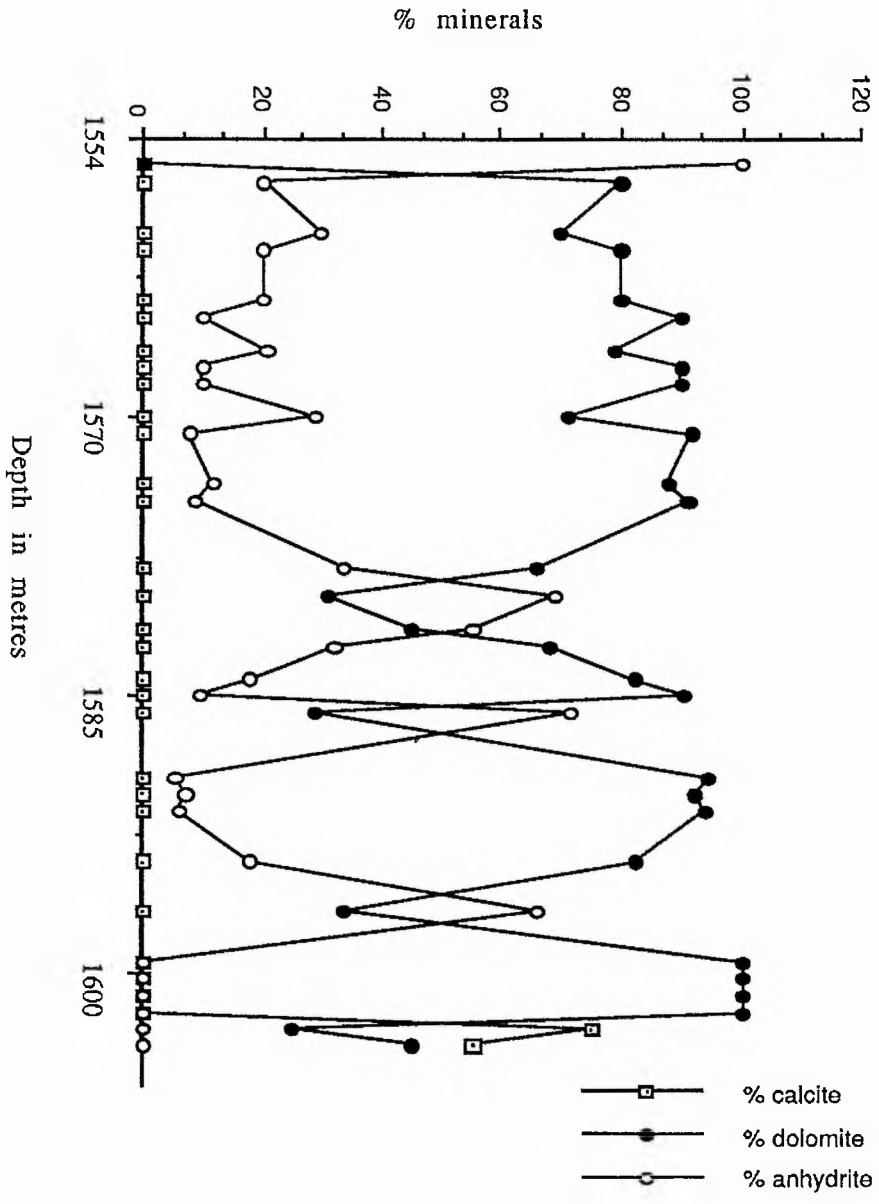

Fig 4.3 Diagram showing the variations of mineral percentages with depth in core D.

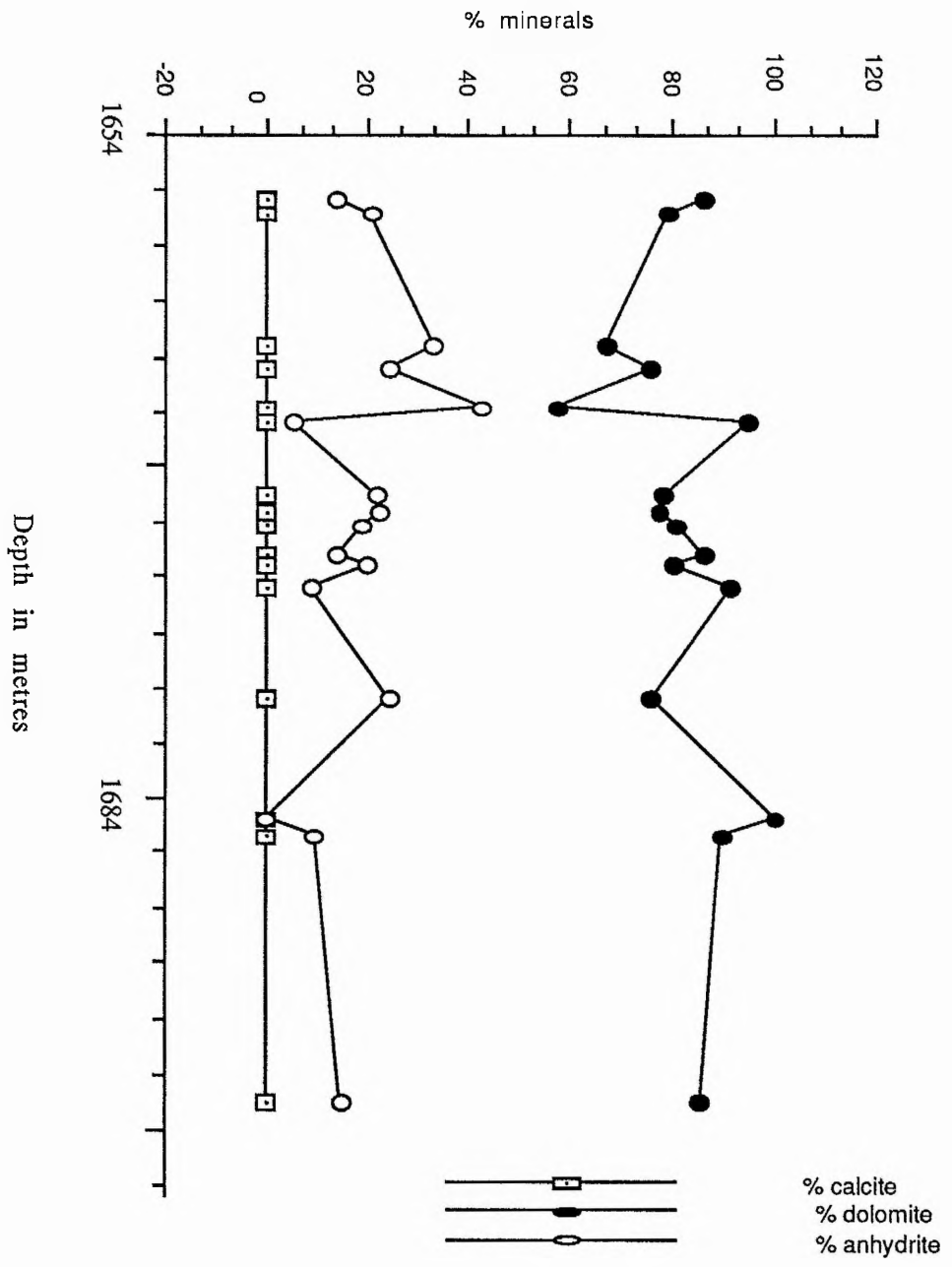

Fig 4.4 Diagram showing the variations between the mineral percentages with depth in core E.

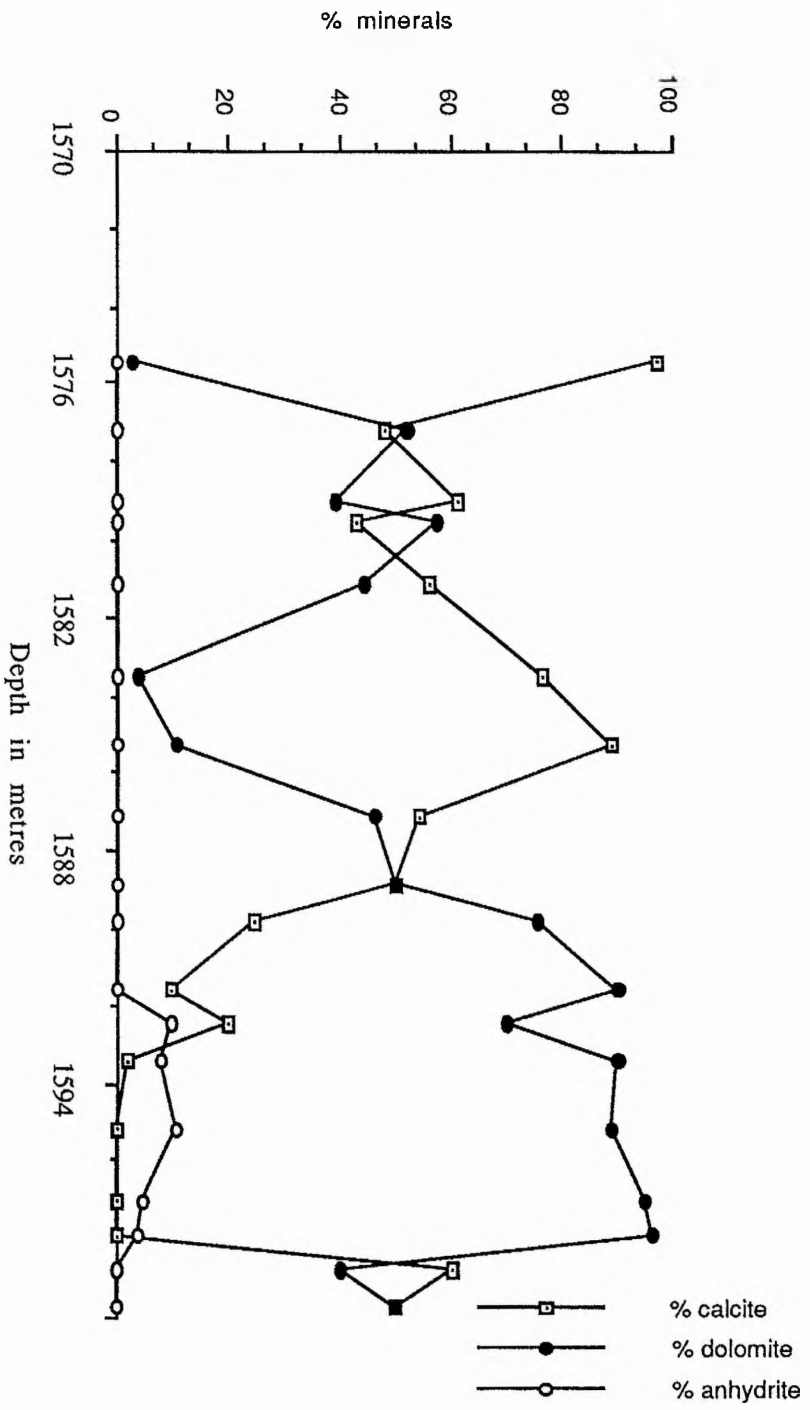

Fig 4.5 Diagram showing the variations of mineral percentages with depth in core F.

the section and then remains constant with a lower value through out. There are two high anhydrite percentages which probably correlate with the anhydrite beds in core **D**. These beds may mark an increase in salinity of the environment at the time of the deposition of the Euphrates Limestone Formation due to the closure of the lagoon. Core **F** represents a transitional stage between cores **D** and **E**, and between cores **G** and **H**. Below the top of the formation there is a dolomite and dolomitic limestone bed. This bed is followed by limestone partially dolomitized. Then at the bottom of the section there is a thick dolomite bed associated with a low percentage of anhydrite. This dolomite bed is followed by a dolomitic limestone and limestone bed. From correlation with the other wells there are no dolomites below this bed (**Fig 4.5**).

Core **G** graph shows that there is a bed of dolomite two metres below the top of the Euphrates Limestone Formation and another bed in the middle of the section (**Fig 4.6**). Apart from that, dolomitization is partial and very limited. There is no anhydrite in this section, the rock is mainly composed of limestone in which molds and vugs are filled with calcite cements.

In core **H** the Formation is covered with anhydrite bed which is the usual case, below which a bed of dolomite of one metre thick with very few skeletal fragments undolomitized. Below the dolomite bed the Formation is only partially dolomitized; anhydrite is absent through out this core (**Fig 4.7**).

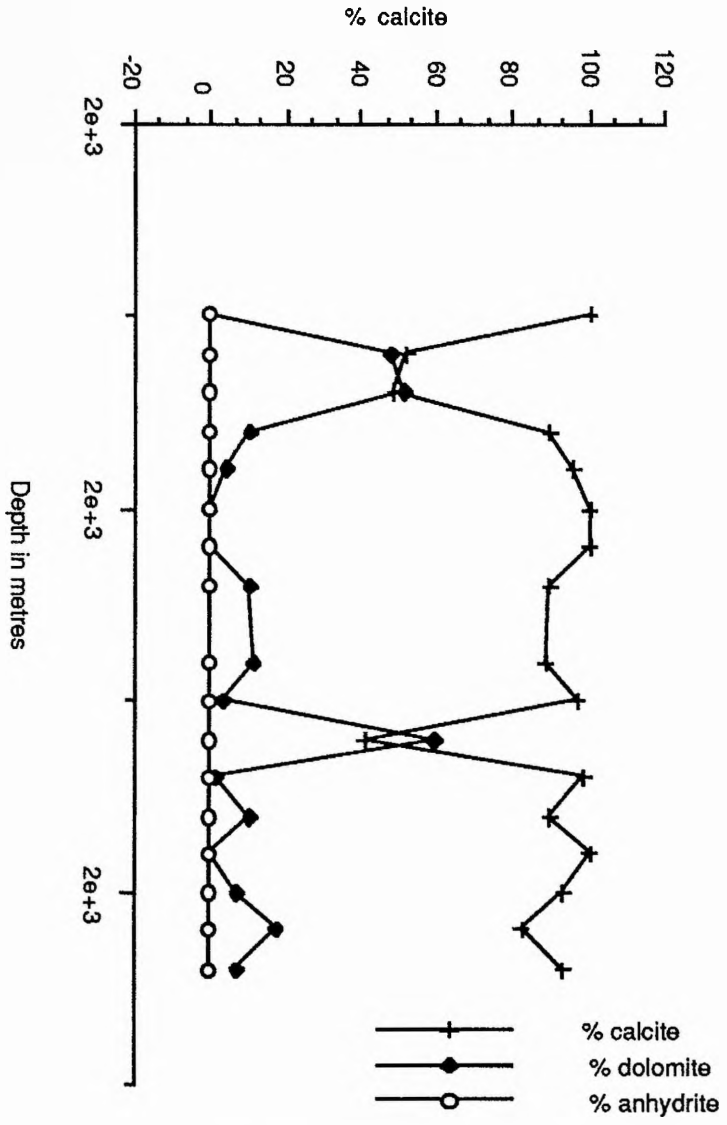

Fig 4.6 Diagram showing the variations of mineral percentages with depth in core G

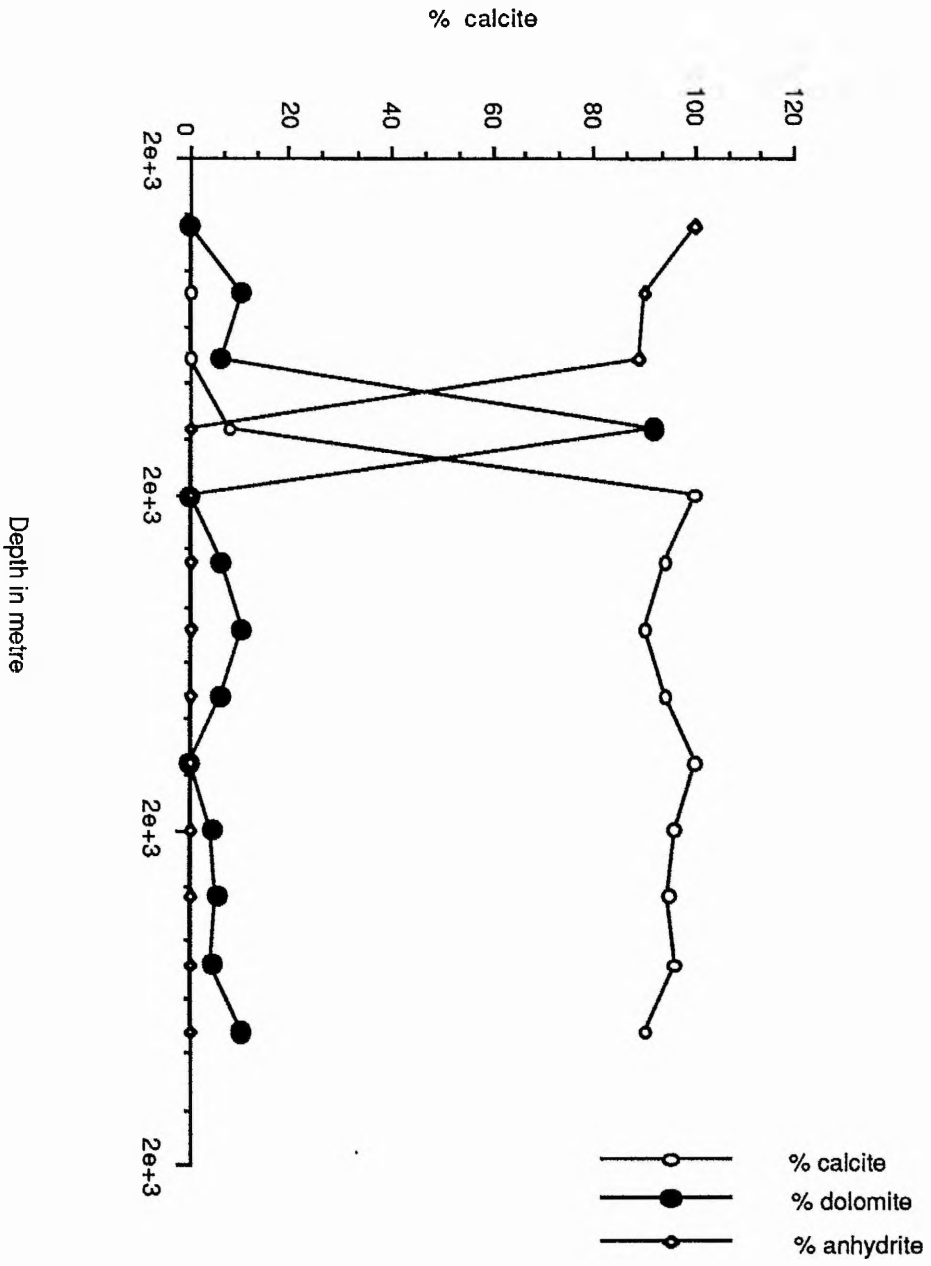

Fig 4.7 Diagram showing the variations of mineral percentages with depth in core H.

4.3.2. Trace elements

The objective of the analyses was to monitor any systematic variation with depth of the studied area. Trace elements analysis of the core samples are carried out using the X-ray fluorescence instrument by analysing the self-supporting pellets (**Appendix 6**).

Sample preparation was made according to standard procedure in the department. Discussion will be limited to Sr, Ba, Pb, Cu, Ni, and Cr.

4.3.2.1 Strontium

Strontium concentration measurement in core **D** showed a high values (557± 297.6, n=23) **Appendix 6**. In general the Sr values are high correlated with most ancient dolomite (200 ppm) (**Weber, 1964c**). These values match with the Holocene values of 500-600 ppm (**Land, 1973**).

It was concluded that early diagenetic dolomite contains higher Sr concentration (10-600 ppm) than later diagenetic ones (**Viezer and Demovic, 1974**). Therefore, the high value of the Euphrates Limestone Formation dolomite may be used as an indicator of an early diagenesis. The dolomitization process is known to lead to the removal of Sr from the formed dolomite and only a small concentration will remain (**Al Hashimi, 1976**). In the present study the Sr content is high (**Appendix 6**) which probably indicates that the dolomitizing solution may be highly concentrated with Sr. It is known that supersaline brines are saturated with Sr.

Kinsman (1969) indicated that Sr/Ca ratio is higher in hypersaline brines than in the freshwater. In this case it might be expected that dolomite deposited from hypersaline brines would contain higher Sr^{2+} concentrations similar to that of dolomite formed in equilibrium with sea water. This type of dolomite as suggested by Behrens and **Land (1972)** should contain 600-700 ppm. This high value of Sr^{2+} concentration is found in the Euphrates Limestone Formation, and if the suggestion is correct , then Sr concentration can be used as an indication that Euphrates Limestone Formation dolomite was formed from hypersaline brines. The Sr^{2+} concentration in core **E** is even higher than in core **D** (1520 ±1178.4 ppm) with very high value of 19181 ppm which was not included in the calculations. This very high value is associated with celestite ($SrSO_4$) (**Appendix 3**).

Core **G** is partially dolomitized, the Sr concentration is quite lower than the previous cores (387.8 ± 61.2 ppm, n=11). The high anomalous values were not included in the calculation (2690, and 745 ppm).

These lower values contradict the fact that limestone should contain higher Sr concentration than dolomite . Probably the increased exposure of the limestone to fresh water, with its attendant recrystallization, resulted in its lower Sr^{2+} contents (**Sears and Lucia, 1980**).

4.3.3. STABLE ISOTOPES

Isotopic analysis were carried out on samples from the Euphrates Limestone formation subsurface cores, from the Jambur field. The powder was finely ground and heated to 450°C in a vacuum for 30 minutes in order to remove the organic matter. Carbon dioxide gas was extracted from samples by reacting them with 100% phosphoric acid in a vacuum at 25°C (**McCrea, 1950**), in mixed samples the CO_2 gas aliquot after 20 minutes were taken to represent calcite, and the aliquot of CO_2 gas evolved between 20 minutes and complete reaction was taken to represent dolomite (**McKenzie, 1981**). The collected carbon dioxide was analysed on VG Isogas Sira10 spectrometer with a working standard calibrated against NBS20; values are corrected using standard procedures and then presented as parts per thousands relative to PDB standard (**Craig, 1957**).

Theoretically dolomite which has been formed in isotopic equilibrium should be enriched in $\acute{O}^{18}O$ by 4 to 7‰ relative to calcite (**Epstein *et al*, 1964; O'Neil and Epstein, 1966**).

Experimental studies at low temperature (25 to 78.6° C) have indicated that $\acute{O}^{18}O$ enrichment of dolomite in equilibrium with syngenetic calcite is in the range of 3 to 4 ‰ (**Fritz and Smith, 1970**).

Hydrothermal studies (**Katz and Matthews, 1977**) showed that secondary dolomitization is a dissolution-precipitation process, which involves the crystallisation of an intermediate phase.

No systematic stable isotope trend was observed with depth or core location, consequently, all of the data are considered as a single ensemble.

Dolomite $\acute{O}^{13}C$ analyses are uniformly high in the range 1.23 to +3.5‰ (mean 1.96± 0.99 ‰, 1 n=15) except for one value of -0.16 ‰. The dolomite $\acute{O}^{18}O$ shows a range of +0.23 to +3.57 ‰ (1.95 ±1.066 ‰, n= 15) (**Appendix 5**).

The analyses of calcite for oxygen and carbon isotopes show $\acute{O}^{13}C$ in the range of +0.6 to +3.25‰ (mean 1.84 ±1.16 ‰, n= 15) and $\acute{O}^{18}O$ in the range -1.28 to -0.26‰ (mean -0.81 ± 0.68‰, n=17) Note that the mean $\acute{O}^{13}C$ values are equal within the error.(**Appendix 4**).

The dolomite-calcite pairs from Euphrates Limestone Formation give an average of $\Delta^{18}O$ dol-cal 3.79‰ (n=4) and $\acute{O}^{18}O$ is systematically lower in $\acute{O}^{18}O$ of calcite than dolomite, similar to values discussed earlier for other environmenmts.

4.3.4 STABLE ISOTOPE RATIO

4.3.4.1 OXYGEN ISOTOPES

Normal marine sediments have an isotopic composition of oxygen (-2 to 0‰), the $\acute{O}^{18}O$ of the dolomite of the present study is in the range of +0.23 to 3.57‰ (**Fig 4.9**) which is clearly heavier than most the normal marine sediments, and it is as

heavy as some Recent hypersaline dolomite (**Land, 1980; McKenzie, 1981**).

Accepting the dolomite fractionation factor of 3‰ (**Fritz and Smith, 1970; Land, 1980**), the oxygen isotope value to be expected of dolomite from dolomitization of normal marine carbonates in the presence of sea water should be in the range of 1 to 3‰ , thus, the Euphrates Limestone Formation dolomite is either formed from normal sea waters or from hypersaline brines. As discussed previously, the Dorag or mixing model for

Go to page 93 please,

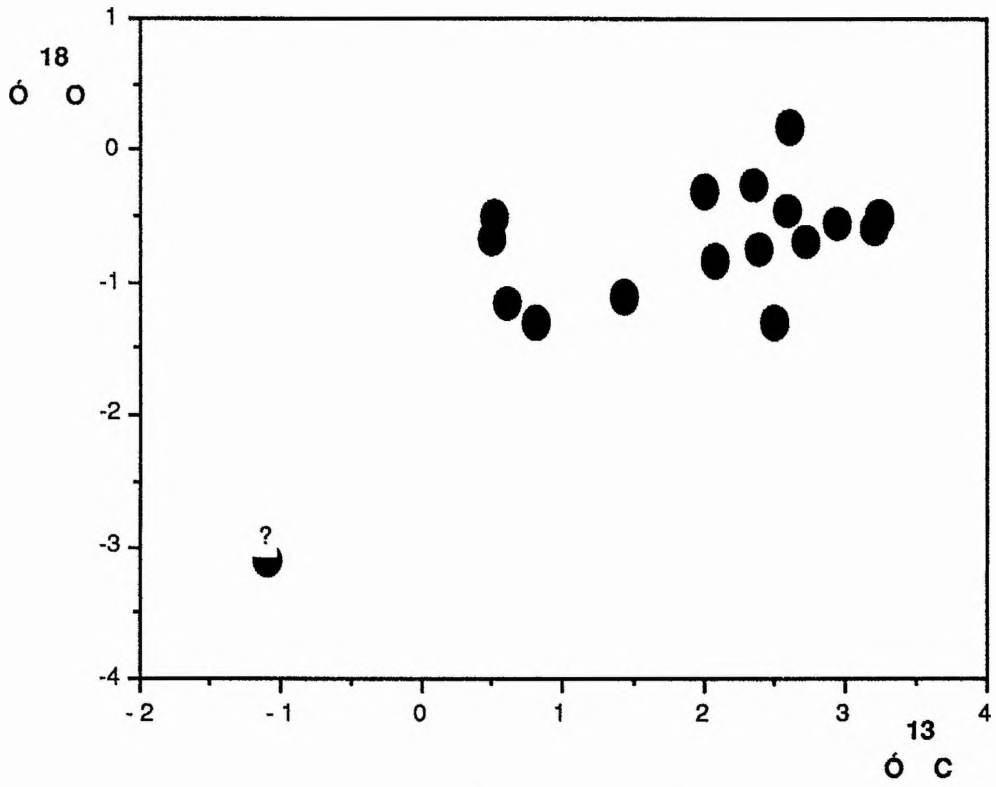

Fig 4.8 plot of Ó ^{18}O and Ó ^{13}C of calcite in Euphrates Limestone Formation.

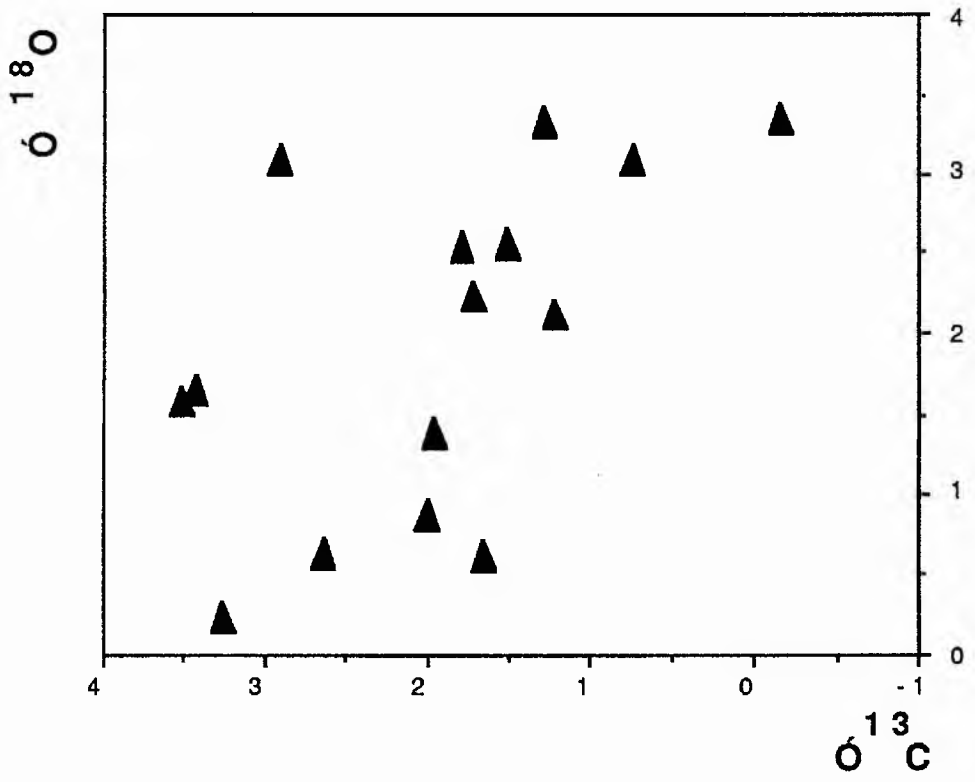

Fig 4.9 $Ó^{18}O$ and $Ó^{13}C$ plot of dolomite in the Euphrates Limestone Formation.

dolomitization invokes the participation of meteoric fluids which are generally of lower $\acute{O}^{18}O$ than sea water. The data reported here show that $\acute{O}^{18}O$ increased during dolomitization, to values excceding those typical of normal marine sediments. It is suggested therefore that this dolomite probably formed as a result of reaction of hypersaline brines with marine carbonates.

Anhydrite nodules and chicken-wire texture are known to be a significant features of the sabkha environment which are seen in the Euphrates Limestone Formation. All these factors suggest that dolomite formed as a product of sabkha environment diagenesis. The present isotope results compare closely with those of the Abu Dhabi Sabkha dolomite (**Fig 4.10**). They are consistent with the observation that Holocene hypersaline dolomites are enriched in $\acute{O}^{18}O$ relative to the precursor carbonates by 2 to 4‰ (**Land, 1980**) and 3.2‰ (**McKenzie, 1981**).

The calcite $\acute{O}^{18}O$ values of the present study are in the range of -1.28 to 0.26‰ (-0.81 ± 0.68 ‰, n= 17) (**Fig 4.8**), which indicate precipitation from a normal marine sediments (0 to 0.2‰ Hudson, 1977).

4.3.4.2 CARBON ISOTOPES

The dolomite $\acute{O}^{13}C$ values of the present study range from +1.23 to +3.5‰ (mean 1.95 ± 0.99‰, n= 15) while the calcite $\acute{O}^{13}C$ values are from 0.65 to +3.25‰ (1.84 ± 1.16 ‰, n= 17); these results clearly indicate that the overall carbon isotope composition has changed very little during the diagenesis of the limestone. On a large (basinwide) scale the carbon system has

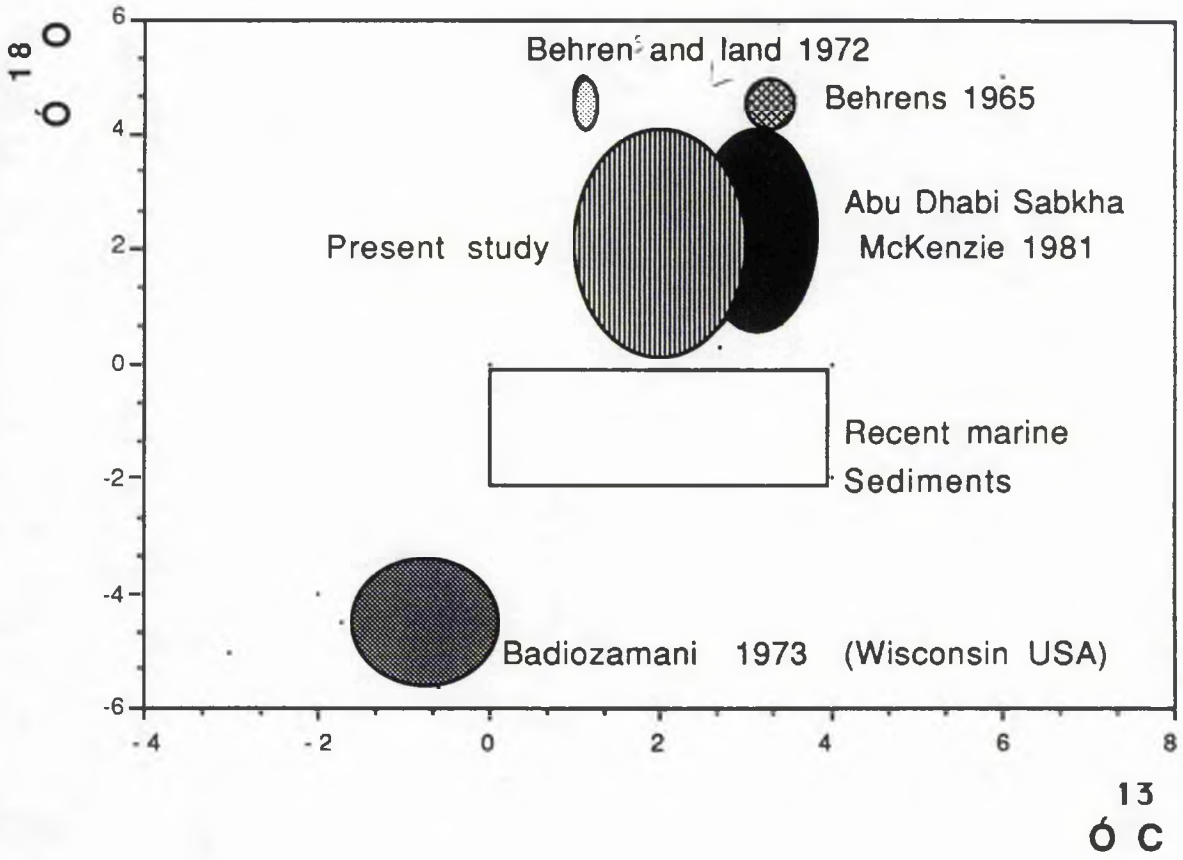

Fig 4.10 Plot of stable isotopes of different types of dolomites compared with Euphrates Limestone Formation.

been closed or in dynamic equilibrium, although carbon isotope mobility on a small scale is possible.

Normal marine sediments have $\delta^{13}C$ values in the range of 0 to +4‰ PDB (**Fig 4.10**) (**Keith and Weber, 1964; Hudson, 1977**). Therefore, the setting of these sediments was probably a normal marine environment which may have undergone heating during the isolation of the lagoon from the main sea. Fossil assemblages and the lithology indicate that the facies were deposited in a partially restricted lagoon (**Bellen, 1959**).

4.4. GENERAL DISCUSSION AND CONCLUSIONS

Fig 4.10 clearly shows different oxygen isotope range for different types of dolomite and carbonate sediments.

As has been discussed dolomite can be formed under different circumstances from solutions which vary in their oxygen isotopic composition. However, if the oxygen isotopes value is taken as an indicator or a function of temperature or evaporitic concentration, it follows, that dolomite can form from different types of waters. Dolomite with heavy $\delta^{18}O$ values has been reported from mid Pacific atolls (**Berner, 1965**) with values reaching 4.5‰. This dolomite is believed to be precipitated by reaction of supersaline evaporated brines with buried skeletal limestone.

Dolomites from sabkha environment in the Arabian Gulf have been reported with relatively heavy $\delta^{18}O$ values 1.35 to 3.91‰ (**McKenzie, 1981**). On the other extreme; a dolomite with very light $\delta^{18}O$ (-4.47‰) has been reported from Middle Ordovician dolomite (**Badiozamani, 1973**). The latter author

believed that dolomitization occurred as a result of mixing of ground meteoric water with sea water in the Phreatic zone (**Dorag Model**).

Normal marine sediment $\acute{O}^{18}O$ value lie in the range -2 to 0‰ PDB (**Fig 4.10**). It is well known that evaporation causes a preferential depletion in the light isotopes (which become enriched in the vapour phase), consequently the remaining water will be isotopically heavier. Dolomite formed from the evaporation of sea water is commonly associated with anhydrite and gypsum precipitated from hypersaline solution (**Friedman and Sanders, 1967**). However, a close lateral and vertical or temporal relationship commonly exists between dolomite and evaporite deposits (**Friedman, 1980**).

There are indications outlined below that the present dolomites have been deposited in a lagoonal environment in which the lagoon was separated from the open sea and evaporation tookplace. After the deposition of the Euphrates Limestone Formation a more restricted environment existed and for a long time (deposition of the Dhiban Ahydrite Formation). The top of the Euphrates Limestone Formation is covered by a massive bed of anhydrite with chicken-wire texture, a significant feature of the sabkha environment. Dolomite associated with anhydrite filling pores, and replacing the sediments can be taken as evidence of hypersaline environment existence. Evidence of carbonate replacement by dolomite is shown by dolomitization of skeletal debris and fossil skeletons.

It is fairly well known that skeletons are not formed of dolomite. All the evidences suggest that dolomite could be formed by the reaction of the hypersaline brines percolating underneath the surface with the carbonate sediments.

Dolomite of the present study observed especially in the higher primary porosity southeast area of the field, found to have high $\acute{O}^{18}O$, to be well ordered, nearly stoichiometric and associated with calcium-sulphate minerals (anhydrite and gypsum) which all indicate that this dolomite has been formed from hypersaline brines acting in the sabkha environment or restricted lagoon (which possibly persisted for a long time).

CHAPTER 5

DIAGENESIS

5.1 INTRODUCTION

Diagenesis in carbonate sediments include essentially the transformation of the unstable minerals into stable limestone or dolomite. The definition of the diagenesis according to the AGI Glossary of Geology is " *All the chemical, physical, and biological changes undergone by a sediment after its initial deposition (i.e after it has been reached its final resting place in the current cycle of erosion, tranformation, and deposition) and during and after its lithification, exclusive of surfacial alteration (weathering and metamorphism)*".

This process includes, the dissolution, neomorphism and replacements of unstable minerals, grain compaction as well as the lithification by precipitation of the void filling cements (**Scoffin, 1987**). The Euphrates Limestone Formation has been subjected to a variety of diagenetic processes, including cementation, dissolution, compaction, neomorphism precipitation of evaporite, and dolomitization. Dolomitization will be dealt with in chapter 6.

Early diagenetic processes which are very evident in the Euphrates Limestone Formation are, the formation of the micritic envelopes, and the deposition of isopachous crust cement. These features are characteristic of early marine phreatic diagenesis. This diagenesis has been very well established in Holocene sequences, with regard to cementation,

interaction of mineral phases, interstitial pore fluids, and the role of algae and fungi (**Bricker, 1971; Friedman *et al.*, 1974; Bathurst, 1975; and Longman, 1980**).

5.2 Types of diagenesis

There are four major types of diagenetic environments, marine phreatic, meteoric phreatic, vadose, and mixing zone.

These zones are classified according to the types of fluids , and the absence or presence of air in the pore spaces. Each of those zones may be subdivided into two or more subdivisions on the basis of the flow rates of water through them, and the water saturation with respect to $CaCO_3$ (**Longman, 1980**).

The main two types of environments which will be discussed in this chapter and are relevant to the Euphrates Limestone Formation are the marine and meteoric environments.

5.2.1 Marine diagenesis

The marine diagenetic environment is one in which all the pores in a sediment or rock are filled with normal marine sea water. Two zones are found, the stagnant marine phreatic in which there is little water circulation, and the active marine phreatic zone in which water circulation is extensive and cementation usually occurs.

5.2.1.1 Cementation

5.2.1.1.1 Micritic envelopes

Studies have demonstrated that carbonate grains usually are bored by different organisms (algae, fungi, and bacteria) in

the photic zone forming holes of 6 to 10 microns in diameter. **Bathurst (1966)** and **Monty (1967)** have recorded bored carbonate grains from the Gulf of Batabano and the Bahamas respectively.

The endolithic algae cause strong damage to all types of carbonate grains , skeletal, oolitic, and peloidal. Grains are riddled with holes and as a result are particularly liable to abrasion, the consequences of this are seen in the Bimini lagoons, Bahamas, where it was found that the most densely bored grains are also the most rounded (**Bathurst, 1967**).

Micritic envelopes are produced by the filling of the bores made by algae and fungi, following death and decay, by micritic aragonite or high magnesian calcite in tubes by a process still unknown (**Bathurst, 1975**). The dark colour of these envelopes on some of the grains results from pyrite, iron oxides, or probably from undistinctive organic matter. Most micritization occurs near the sediment/ water interface **(Kobluk and Risk, 1977)**, but it may also occur more than a metre beneath the interface (**May and Perkins, 1979**).

The algal borings have been used as a depth indicator, reduction in abundance is to be expected with depth, and great abundance of the algal bored grains in sediments indicates a depth less than 15-18m (**Swinchatt, 1969**).

In the Euphrates Limestone Formation the micritic envelopes are very abundant in cores **D , E,** and **F** in the grainstone and packstone facies, where they are clearly seen.

5.2.1.1.2 Isopachous crust cement

Precipitation of cements can only proceed in pore waters that are supersaturated with respect to calcium carbonates, consequently the process is limited to the shallow, near surface, waters of tropical or subtropical seas (**Bathurst, 1983**). Calcium carbonate grains are dissolved in cold waters as shown by **Alexandersson (1975)** on the sea floor of Skeggarak.

Evidence available so far indicates that the most active cementation has occurred where the waters were turbulent but the sediments were stable. For example where **Ginsburg and Schroeder (1973)** recorded it in the Cup reef of Bermuda and **Macintyre (1977)** on the fore reef slopes at Galatea, near Panama. **Kaldi and Gidman (1982)** showed that isopachous crust cement precipitated as dolomite in the Permian magnesian limestone both centrifugally and centripetally on the grains in the mixing zone.

Magnesian calcite and aragonite are the dominant cements precipitated in active marine phreatic environments, Magnesium calcite is usually formed as micritic or steep sided rhombic crystals distributed as isopachous crusts around the grains (**Alexandersson, 1972; James *et al*, 1976; Macintyre, 1977**).

The isopachous cement present in the Euphrates Limestone Formation is of the equal thickness type (but unequal ones are not uncommon) around the grains and in all cases is of

Fig 5.1 SEM photomicrograph shows isopachous crust cement surrounding the grain and it is completely dolomitized. The interior is still empty, dolomite crystals grew on the wall of the grain.

Fig 5.2 Photomicrograph of fibrous isopachous cement forming a mesh-like needle texture. Plane polarized light. Scale bar is 0.17mm.
N.B.(Later identified as wall structure of formaninifera).

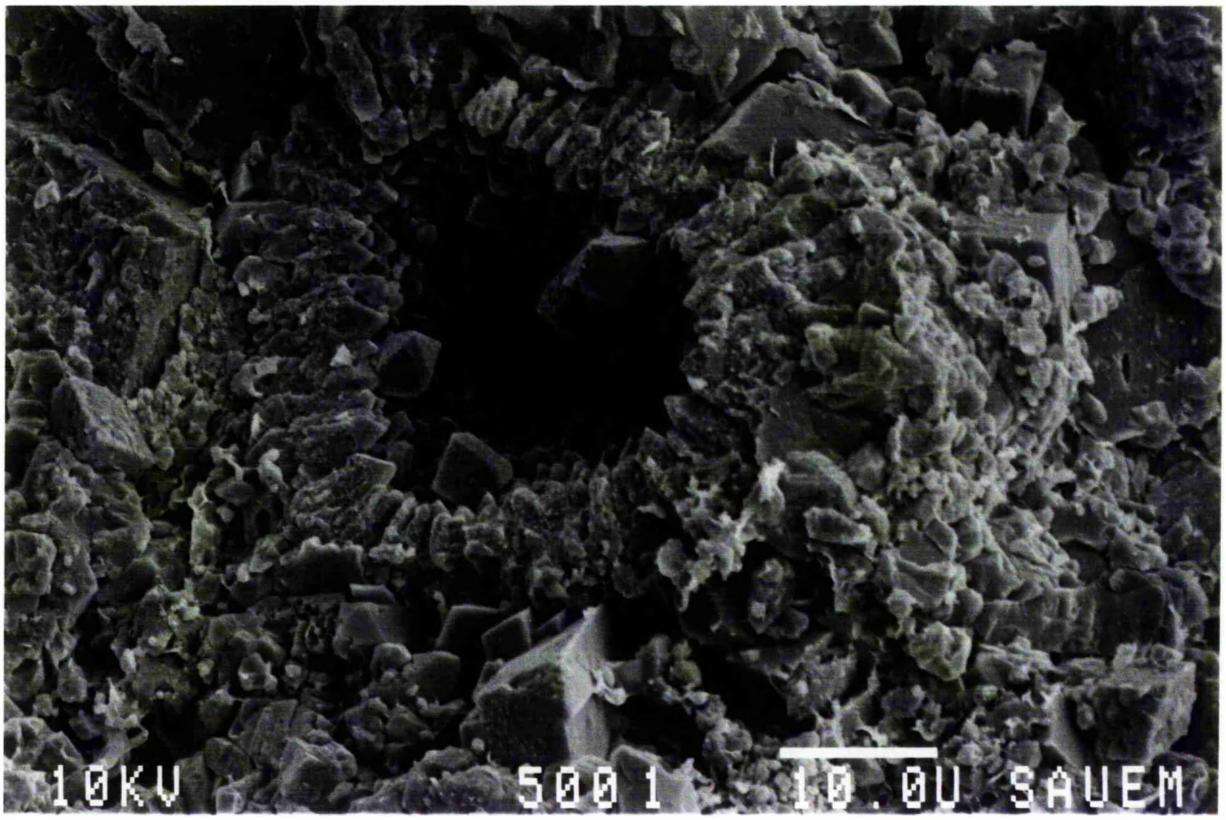
10KV
5001
10.0U SAUEM

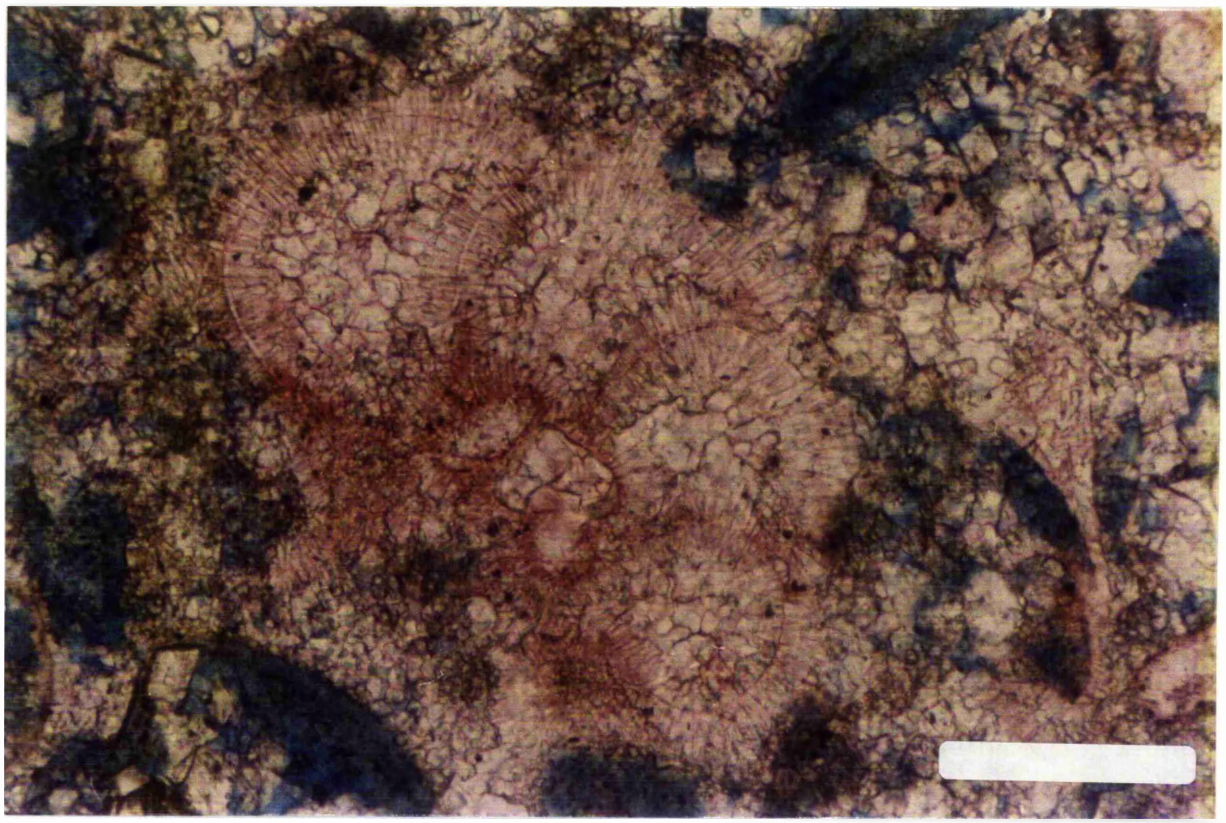

Fig 5.3a SEM photomicrograph of calcite cement filling pore with a very distinctive layering structure.

Fig 5.3b SEM photomicrograph of calcite cement filling a fracture. This cement also shows the same distinctive type of layering sructure as in Fig 5.3a.

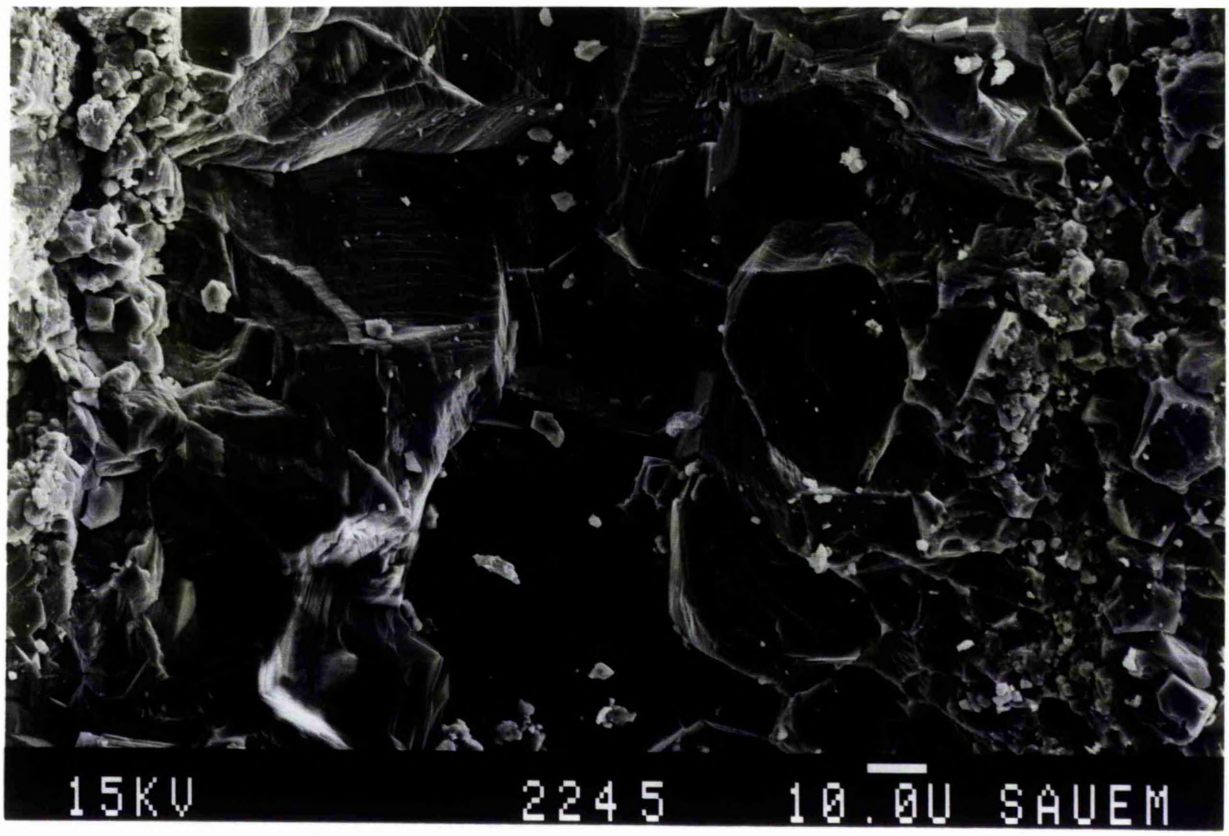
15KV 2245 10.0U SAUEM

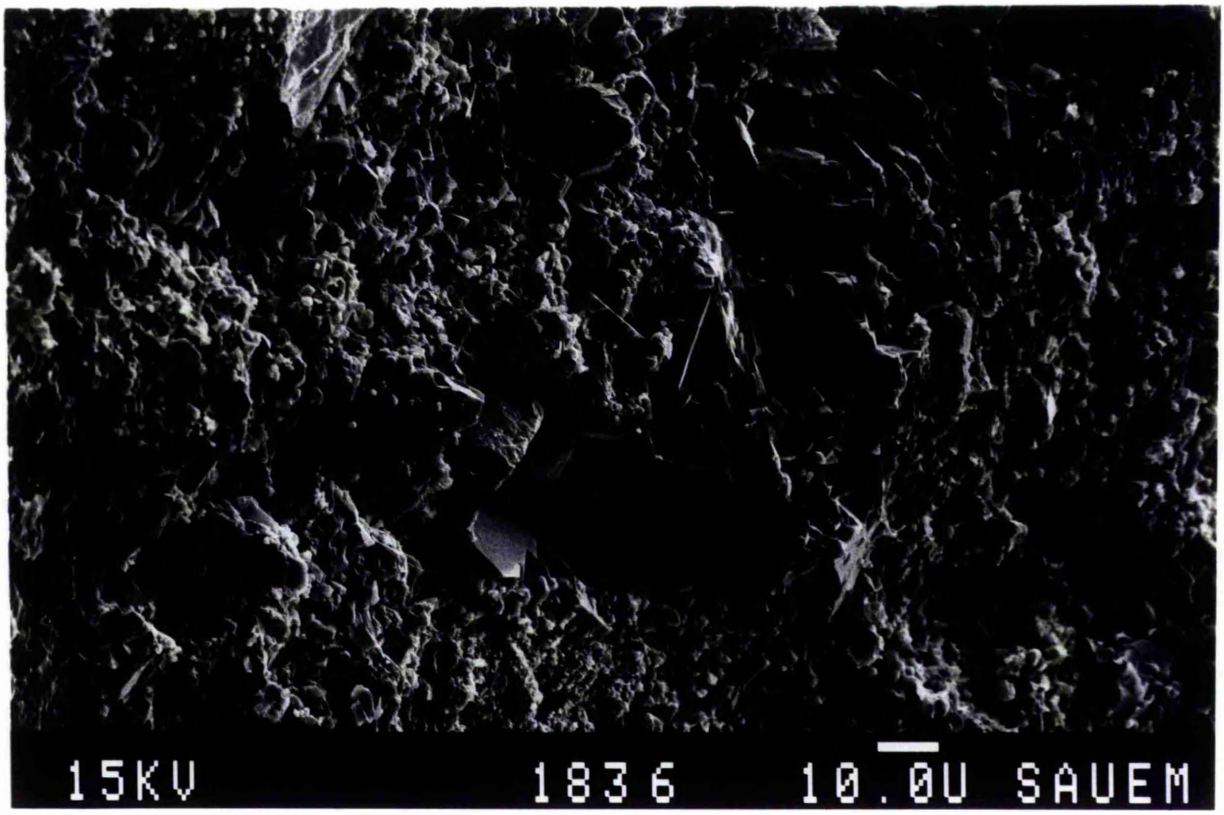
15KV 1836 10.0U SAUEM

centrifugal type. This type of cement is completely dolomitized in the Euphrates Limestone Formation especially in cores A, B, D, E, (**Fig 5.1**) and it is found surrounding the micritic envelopes and associated with it.

It is important to note here that if the isopachous crust cement was formed after the dissolution of the grains it would be reasonable to expect a centripetal cement on the grains , therefore, it must have formed before the dissolution. Dolomite cement is found filling the intergranular porosity. This dolomite in some places is completely dissolved forming excellent intergranular (interparticle) porosity. This kind of dolomite cement is coarse to medium and interlocking without any noticable microscopic intercrystalline porosity. But the intercrystalline porosity is very clear under the SEM.

The above two types of the diagenetic products shows that the Euphrates Limestone Formation have been subjected to the early marine diagenesis.

5.2.1.1.3 Other calcite cements

Different types of calcite cement are found in the Euphrates Limestone Formation (**Fig 5.3a, 5.3b**). The first type is found as a fracture filling in the form of large crystals of 100 microns in size. This kind of cement is sometimes formed of ferroan calcite and some times is of nonferroan calcite, the ferroan calcite in some instances has been replaced by anhydrite and/or by K-feldspar. This type of cement has a straight crystal boundaries, very few inclusions and it does not coarsen toward the centre of a vug.

Fig 5.4 Photomicrograph of fibrous crust cement around a skeletal grain, the thickness of the fibrous crust is not equal. It postdates the fracturing. Mosaic calcite cement has healed the fracture (arrow). Plane polarized light. Scale bar is 0.35mm.

Fig 5.5 Photomicrograph shows grapestone, the interior of the grains were dissolved and filled with anhydrite (white area). The pores between grains were also leached and filled with anhydrite. Plane polarized light. Scale bar is 0.35mm.

Fig 5.6 Photomicrograph of a syntaxial calcite cement grown over an echinoderm fragment .Large crystal of quartz present at the bottom of photograph. Plane polarized light. Scale bar is 0.35mm.

Fig 5.7 Photomicrograph of hollow dolomite rhombs inside a dissolved ooids. These hollow rhombs form an intracrystalline porosity in a mesh-like texture. Plane polarized light. Scale bar is.0.35mm.

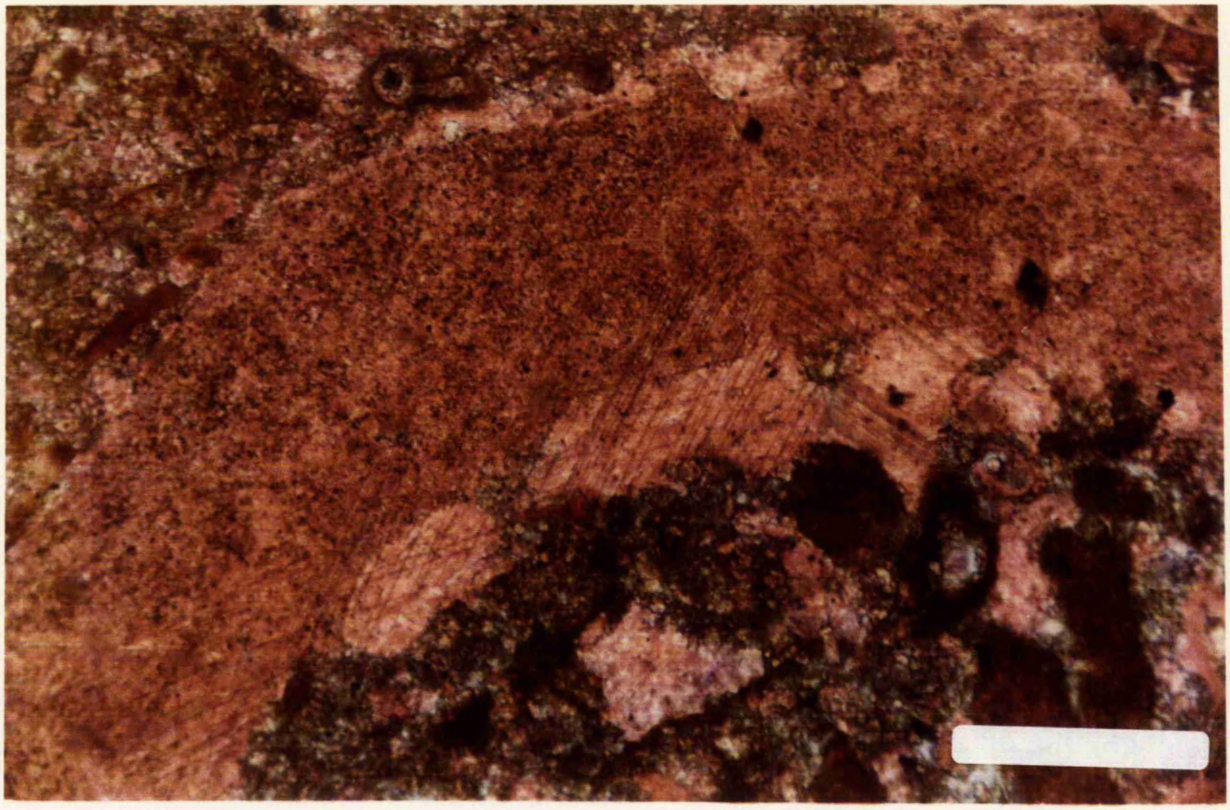

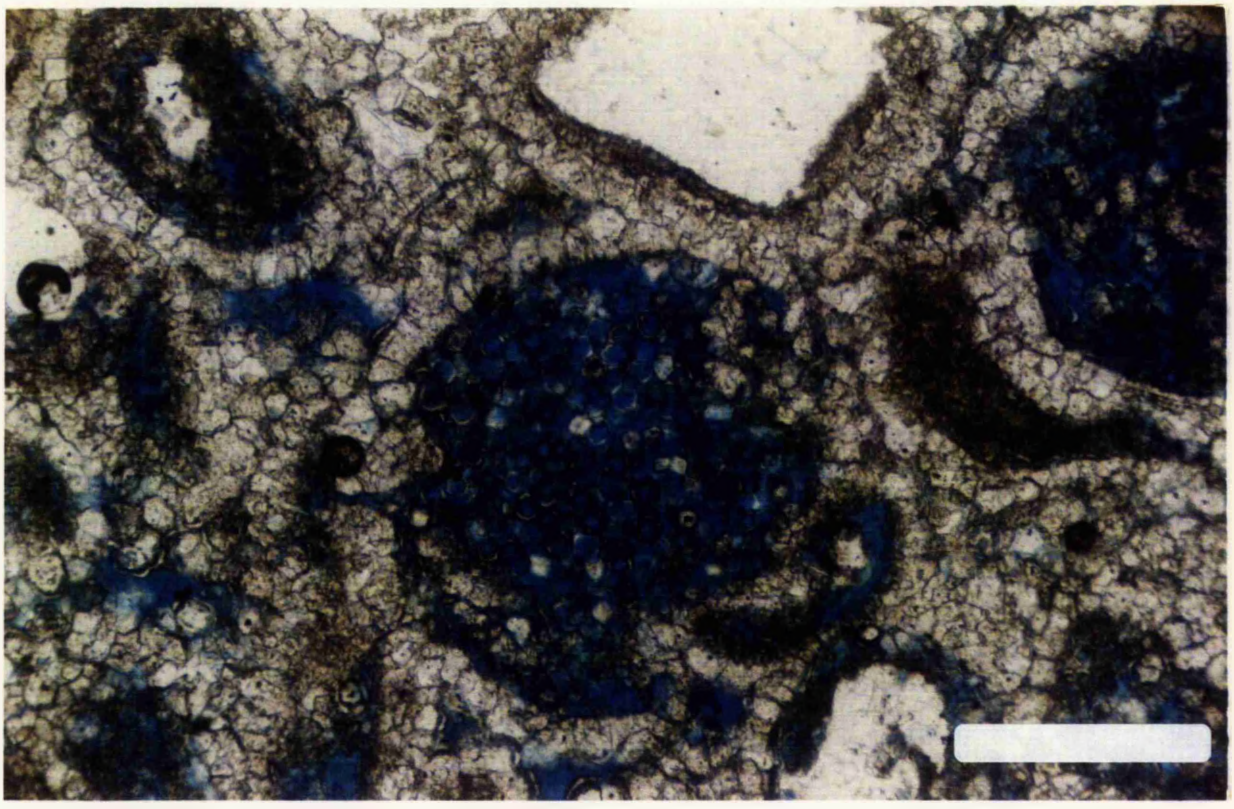

It is therefore, indicative of a late subsurface diagenetic calcite cement (**Loucks and Budd, 1980**). In the Euphrates Limestone Formation this type of cement is found in the mudstone, wackestone facies sediments which are partially dolomitized in cores **F, G**, and **H**.

Some of the calcite blocky cement is found riddled with fine micritic calcite crystals, probably indicating that the blocky cement in these cases is of replacive or recrystallized in origin.

Isopachous fibrous crystals have been found in the mudstone, wackestone facies and sometimes form a mesh work of needles (**Fig 5.2**). The fibrous texture may be still recognizable, in spite of neomorphism to calcite (**Longman, 1980**).

Some of the oolitic and bioclastic grains are found to be held together to form grapestone (**Fig 5.5**) which have been found to result from the cementation of the oolitic and bioclastic grains by algal mat in the shallow lagoons **(Illing, 1954)**.

5.2.2 Meteoric water diagenesis

Marine carbonate sediments may become bathed in the meteoric realm after sea regression, tectonic uplift or coastline progradation. All the pore spaces are filled with fresh (usually meteoric) water.

Diagenesis in this environment may result in leaching in the zone of solution. Principal factors governing fresh water phreatic diagenesis are type and rate of ground water

movements, variation in the freshwater strength (**Badiozamani, 1973**), and salinity, and chemical composition (**Bathurst, 1983**).

Meteoric (fresh) water leaching is probably the main porosity creating factor in the sedimentary basin of a marginal shallow marine platform. If the sediments were cemented before leaching, then selective leaching of the bioclasts and the ooids centres will occur. An excellent intragranular porosity will form. But if the sediments were uncemented varying degrees of vadose compaction may occur causing overpacking of grains and in some cases complete obliteration of the depositional intergranular porosity (**Clark, 1979**).

Intragranular cementation in the active saturated zone may be accompanied by neomorphism of the grains. Syntaxial overgrowths on echinoderm fragments (**Fig 5.6**) and interlocking equant calcite crystals which coarsen toward the pore centres are typical products in the active phreatic zone. In the Euprates Limestone Formation the most significant petrographic feature indicating meteoric (freshwater) diagenesis is the moldic porosity which resulted from dissolution of the carbonate grains.

Moldic porosity is common throughout the whole dolomite section in cores **D**, **E**, and **F**. In these cores, the oolitic fossiliferous grainstone facies cortices of ooids have been dissolved forming oomoldic porosity. In other cases the cortices of the ooids remain undissolved, but in the intermediate cases, cortices are partially dissolved leaving

either micrite or coarser dolomite; the coarse undissolved dolomite crystals themselves have been extensively leached (hollow dolomite rhombs) to form a mesh like texture (**Fig 5.7**).

Oomoldic fabrics have been interpreted to form from dissolution of aragonite ooids. The moldic porosity in the dolomite section in the Euphrates Formation ranges from 0 up to 19% (point counts) (**Appendix 6**).

Meteoric (freshwater) diagenesis has been reported to result in the precipitation of cements which occlude the intergranular and intragranular porosities, but no such cements were found in the dolomite section of the Euphrates Limestone Formation. The dissolution of grains probably occurred in the undersaturated zone of the meteoric phreatic environment (**Longman, 1980**), where the water entering from the vadose zone has not dissolved enough carbonate to become saturated.

Preservation of the interior of some oolitic grains in the Euphrates Limestone Formation suggests that these grains were entirely of low magnesium micrite prior to dissolution. Phreatic meteoric zone has been found to be the stabilization zone as compared to the vadose zone (**Land, 1970; Stenein and Matthews, 1973; Stenein, 1974**).

5.3 Compaction

The grains in the oolitic fossiliferous grainstone facies of the Euphrates Limestone Formation have been subjected to mechanical compaction. Crushed grains, interpenetration of grains, and coalescence of some grains have been seen. The

shape of the grains has been highly modified by compaction. Mechanical compaction and crushing of grains is reported to be more pronounced in the grainstone facies (**Meyers, 1980**) but mechanical compaction in biomicrite is normally not detectable (**Pray, 1960; Bathurst, 1975, and Steinen, 1978**).

Signs of compaction in the wackestone and mudstone facies in the Euphrates Limestone Formation are evidenced by the presence of the horizontal orientation of the bioclastic grains (**Fig 5.8**). The compaction in the Euphrates Limestone Formation occurred after the formation of the isopachous crust cement and before any other type of cement. It has been reported that uncemented voids in Recent sediments are obliterated very early under very little overburden (**Coogan, 1970: Shinn *et al*, 1980**). The compacted grains are very highly packed in some cases, because there was no cement precipitated prior to compaction, and thus compaction has occurred at an early stage of the diagenesis.

Fig 5.8 Photomicrograph of a horizontally oriented grains. This orientation indicates the effect of compaction on the sediments Plane polarized light. Scale bar is 0.875mm.

Fig 5.9 Photomicrograph of a grain in grainstone facies which was broken due to compaction. The fracture was healed by anhydrite cement. White areas are anhydrite cement. Plane polarized light. Scale bar is 0.35mm.

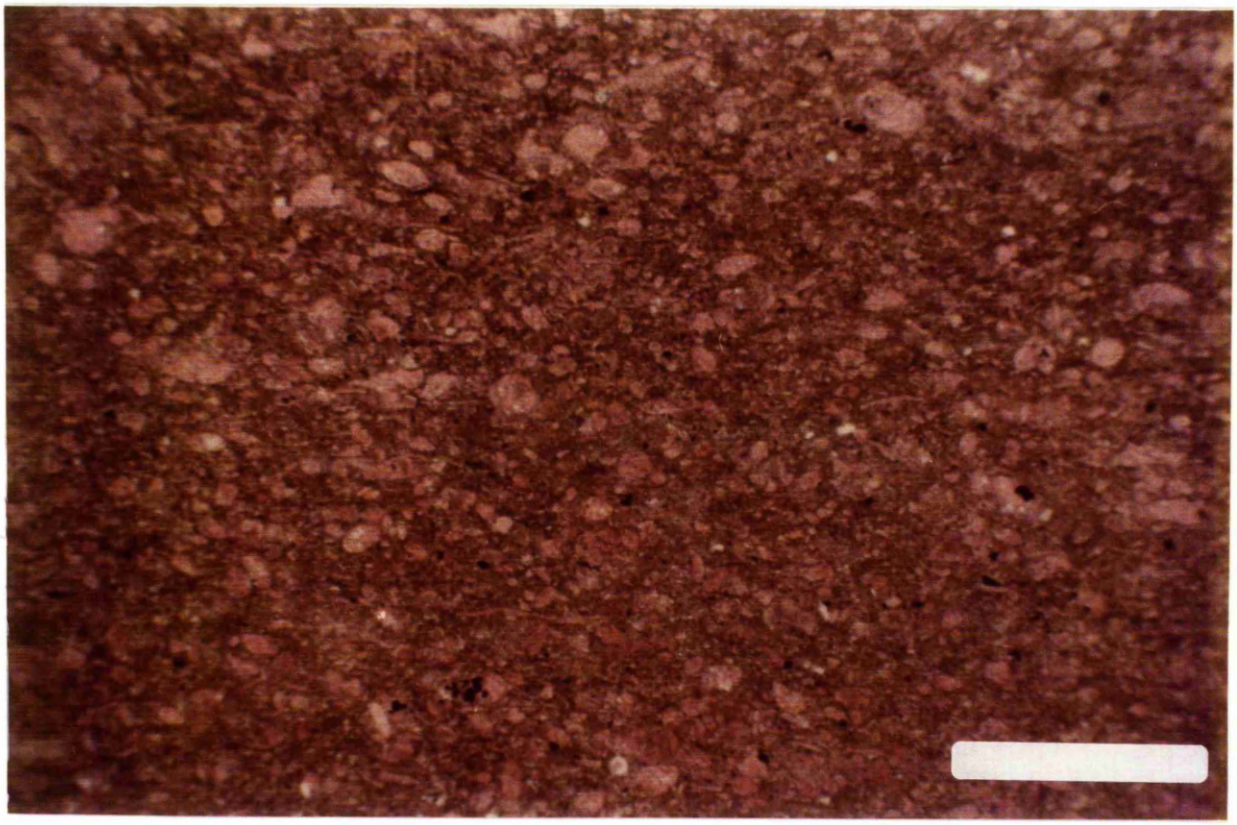

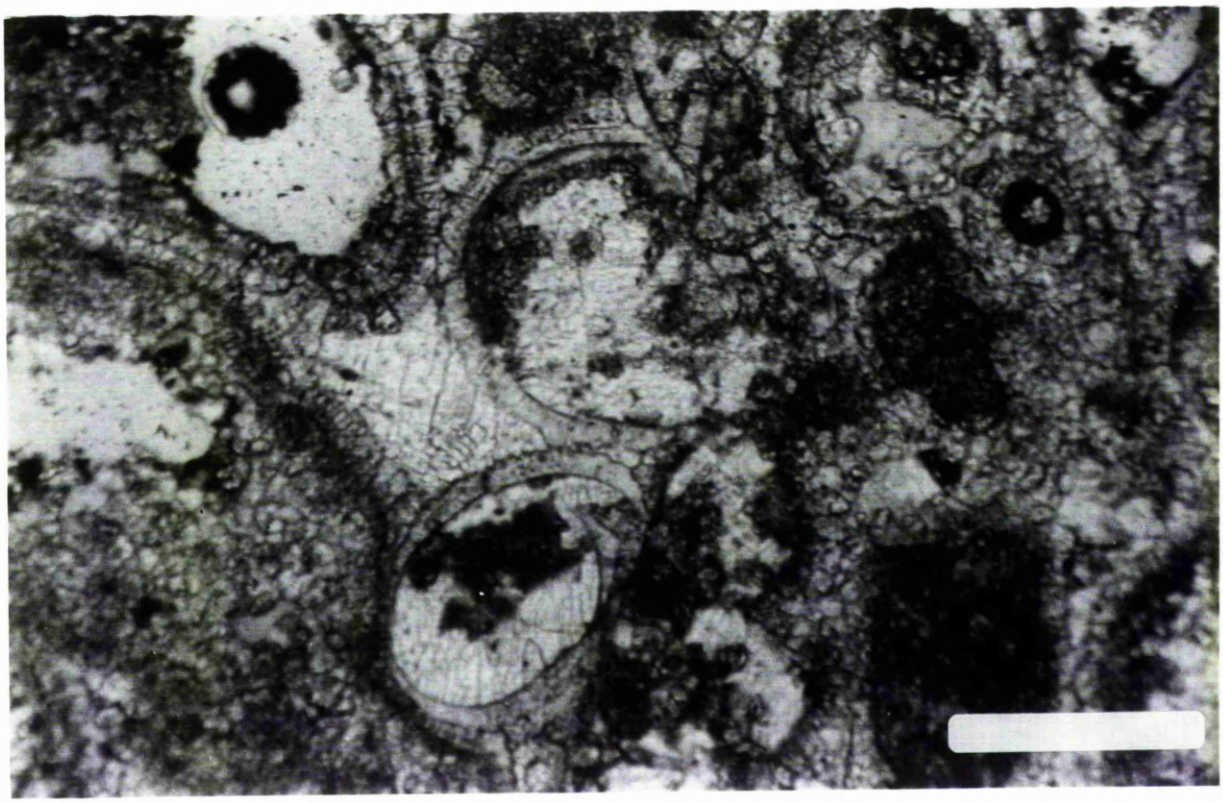

The dolomite cement did not heal the fractures formed during the breakage of the grains, therefore, dolomite formation was before the compaction. On the other hand the anhydrite cement has grown over the fracture surface indicating that the anhydrite cements were deposited after compaction (**Fig 5.9**).

5.2.4 Anhydritization

Anhydritization of the sediments is very strongly pronounced in the Euphrates Limestone Formation.

Most of the moldic, intergranular, and intragranular porosity and to some extent vuggy porosity is filled with anhydrite cement which in some cases drastically reduces the porosity of the oolitic fossiliferous grainstones.

This extensive anhydritization is thought to have formed when the sediments fractured directly against sulphates, causing easy flow of $CaSO_4$ bearing solution. On the other hand extensive replacement of the dolomite by anhydrite occurs in the dolomite mudstone facies in Euphrates Limestone Formation, the anhydrite replaces the dolomite either as a discrete crystals or as nodules.

The evidence of the replacive origin of those nodules is the ubiquitous occurrence of isolated sometime corroded dolomite crystals with the anhydrite.

Anhydrite nodules are very common in the upper part of the cores, and formed when the discrete crystals grew

Fig 5.10 Core sample show anhydrite nodules which replaced the dolomite and coalesced to form a larger nodule. Boundaries between the nodules still can be seen. Scale bar is 2.2cm.

Fge 5.11a Chicken-wire texture which is characteristic of sabkha environment. The black areas are dolomite and represent the boundaries between the small nodules; the white areas are anhydrite. Note that the nodules are very clear with no dolomite upon them. Scale bar is 2.5cm.

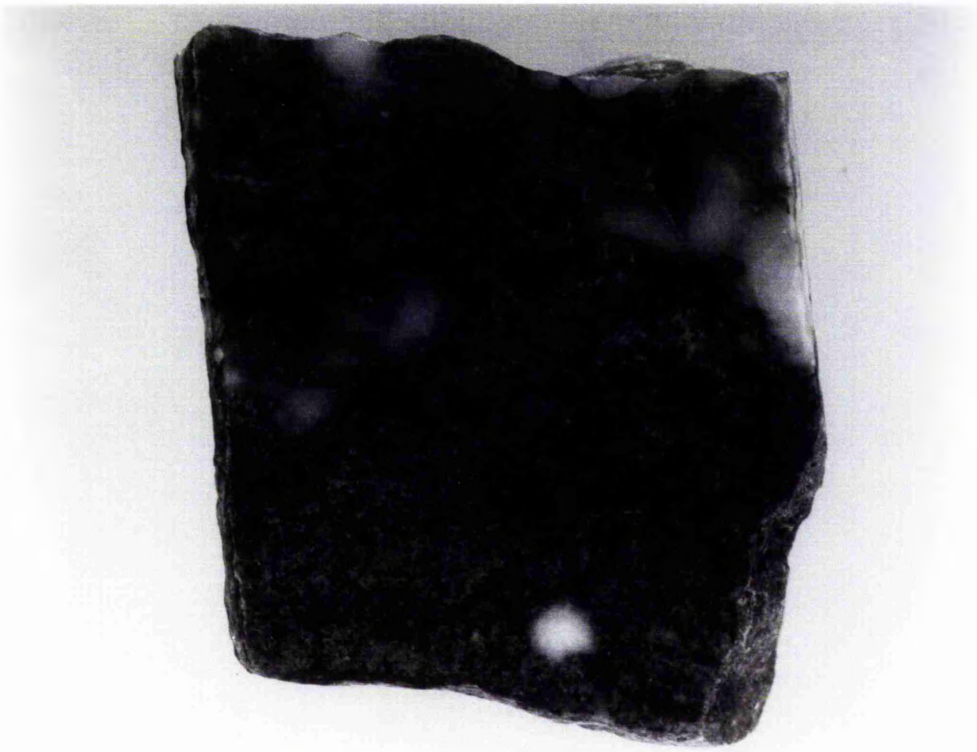

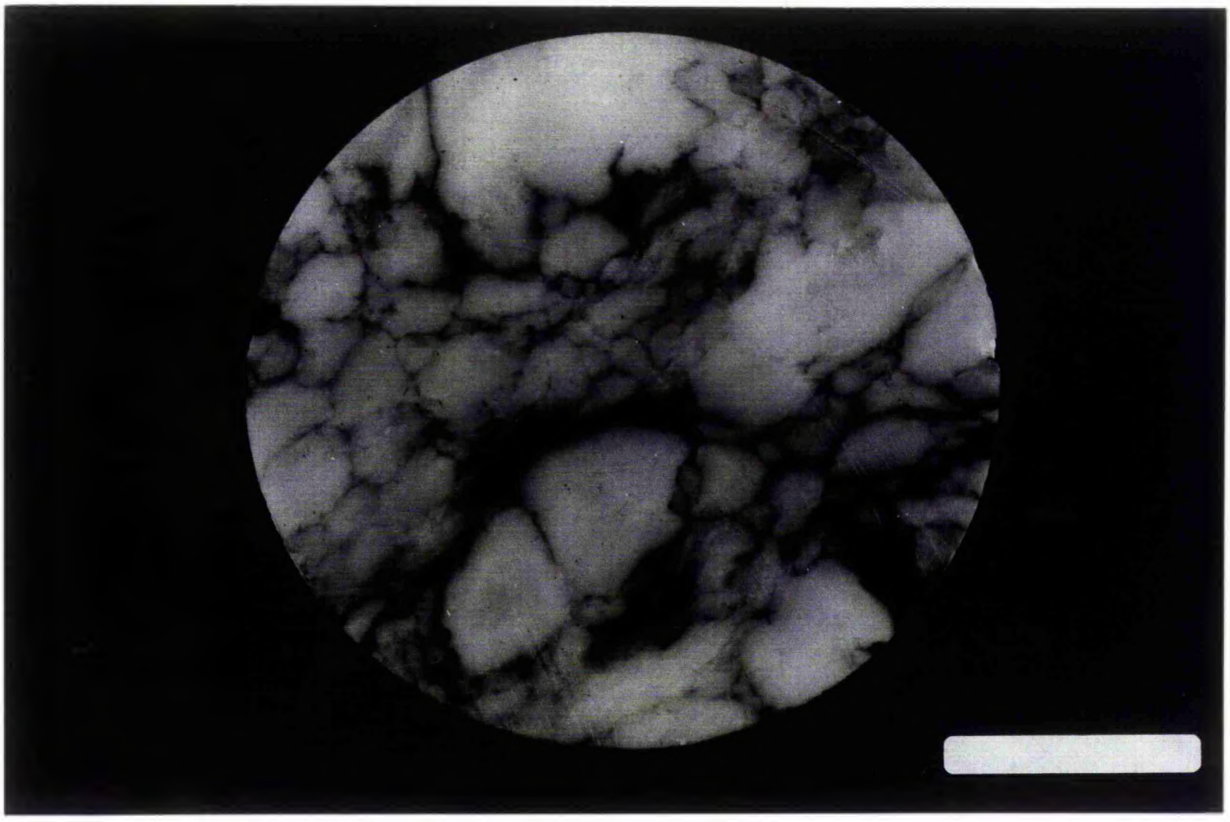

Fig 5.11b SEM photomicrograph of anhydrite texture which is formed of lath shape crystals.

Fig 5.11c SEM photomicrograph of a large block of anhydrite cement. The anhydrite is highly leached. Cleavage lines are clear.

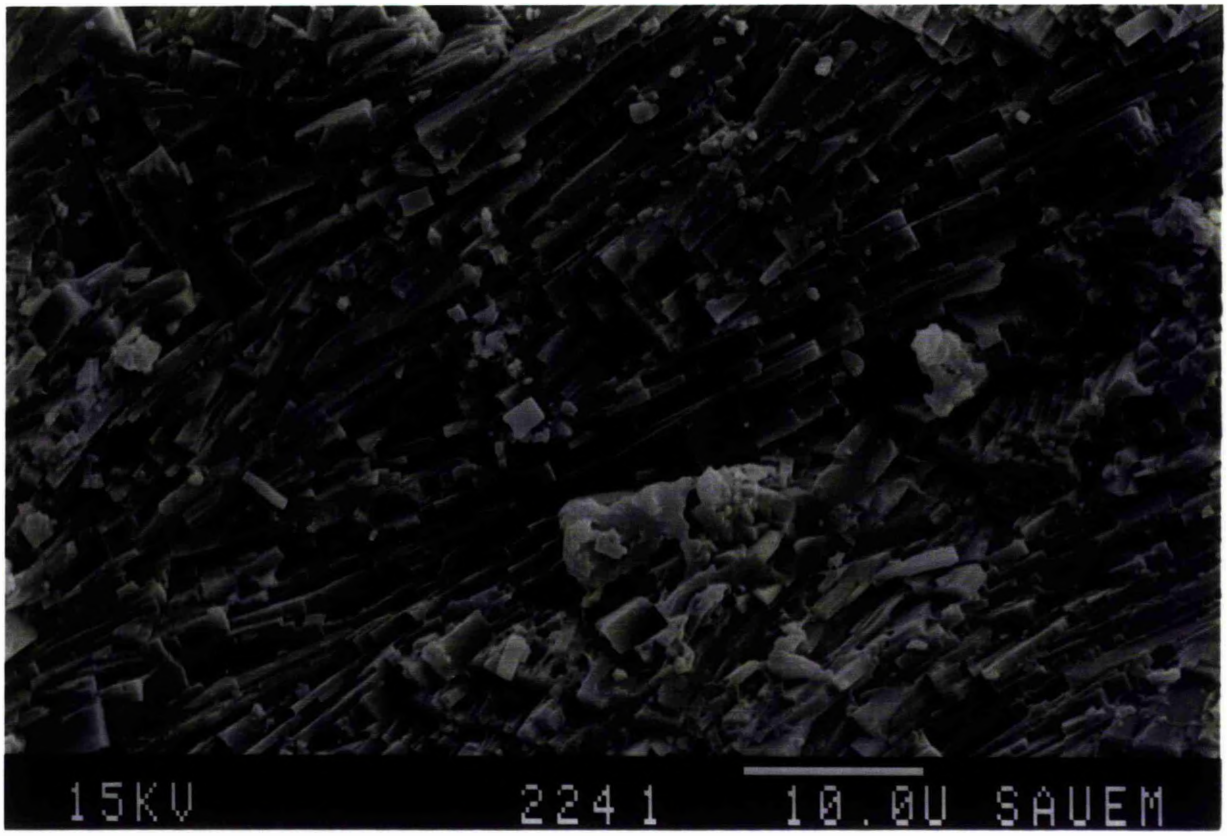
15KV
2241
10.0U SAUEM

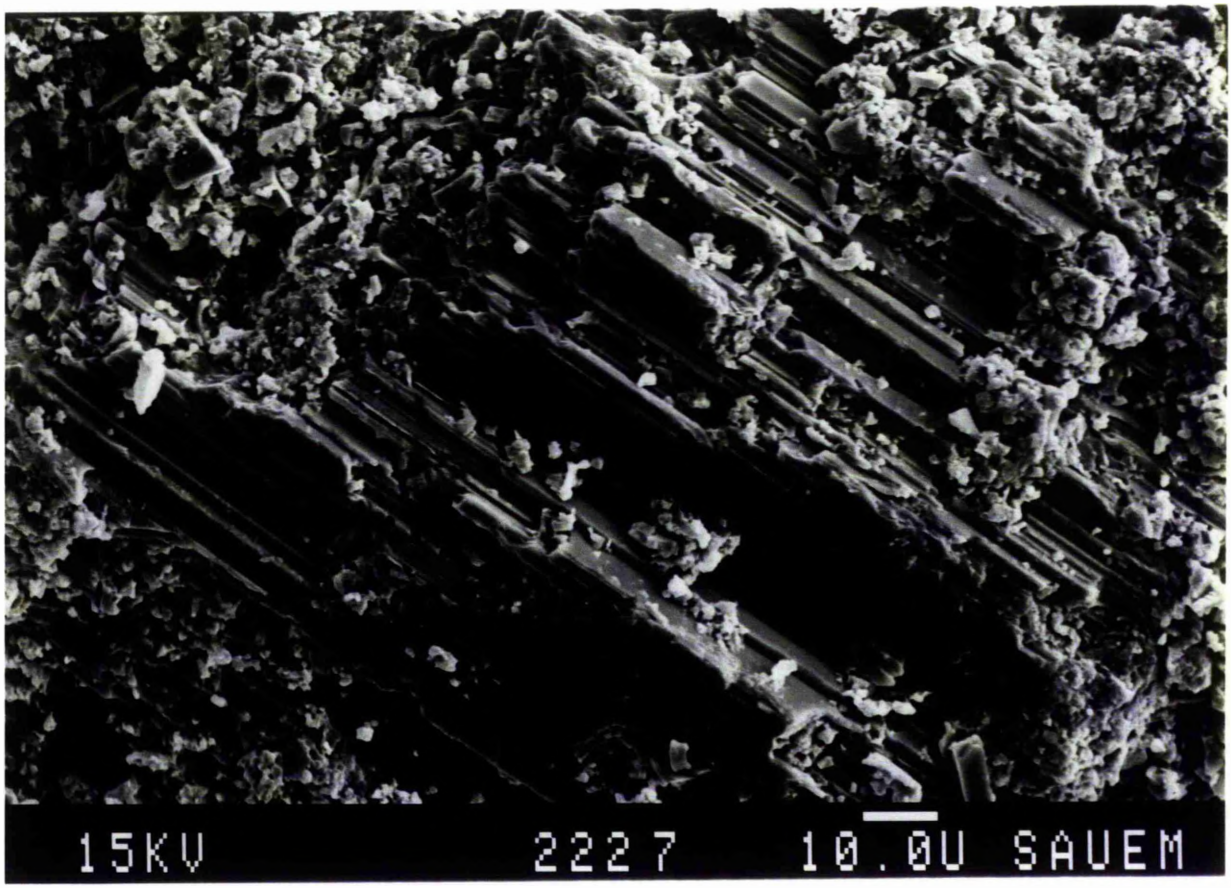
15KV
2227
10.0U SAUEM

together to form a large nodule, and this with further replacement formed a solid masses of anhydrite.

Large anhydrite nodules formed by coalescence of a number of smaller nodules, and the dust line of the boundaries which separated the small ones still can be seen (**Fig 5.10**). Such boundary films have been reported from the sabkha of Abu Dhabi (**Butler *et al.*, 1982**). According to **Shearman (1978)** the structure of coalescing anhydrite nodules is formed as a diagenetic feature after original discoidal gypsum crystals. Gypsum crystals which neomorphosed to anhydrite still can be seen in the dolomite with their original shape..

A chicken-wire texture is formed as a result of extensive replacement (**Fig 5.11a**). Usually the chicken-wire texture rocks have no dolomite relics in them. Instead it is formed of pure white anhydrite nodules. Such texture is reported to be formed due to displacement growth in sabkhas (**Shearman, 1966**). These nodules are clearly formed during late diagenesis.

Other different types of anhydrite cements have been formed in the Euphrates Limestone Formation. Sometimes these types remain unaltered and some times they are replaced by other minerals as shown in **Fig 3.11b, 3.11c**.

5.2.5 Celestitization

Celestite is found primarily near the sites of anhydrite and early dolomite formation (Muller, 1962). Celestite has been recorded as a common minor mineral of the coastal sabkha and

Fig 5.12a SEM photomicrograph of large crystals of celestite embedded in the dolomite matrix.

Fig 5.12b SEM photomicrograph of celestite crystals of euhedral shape embedded in a dolomite, associated with a barite crystal (arrow).

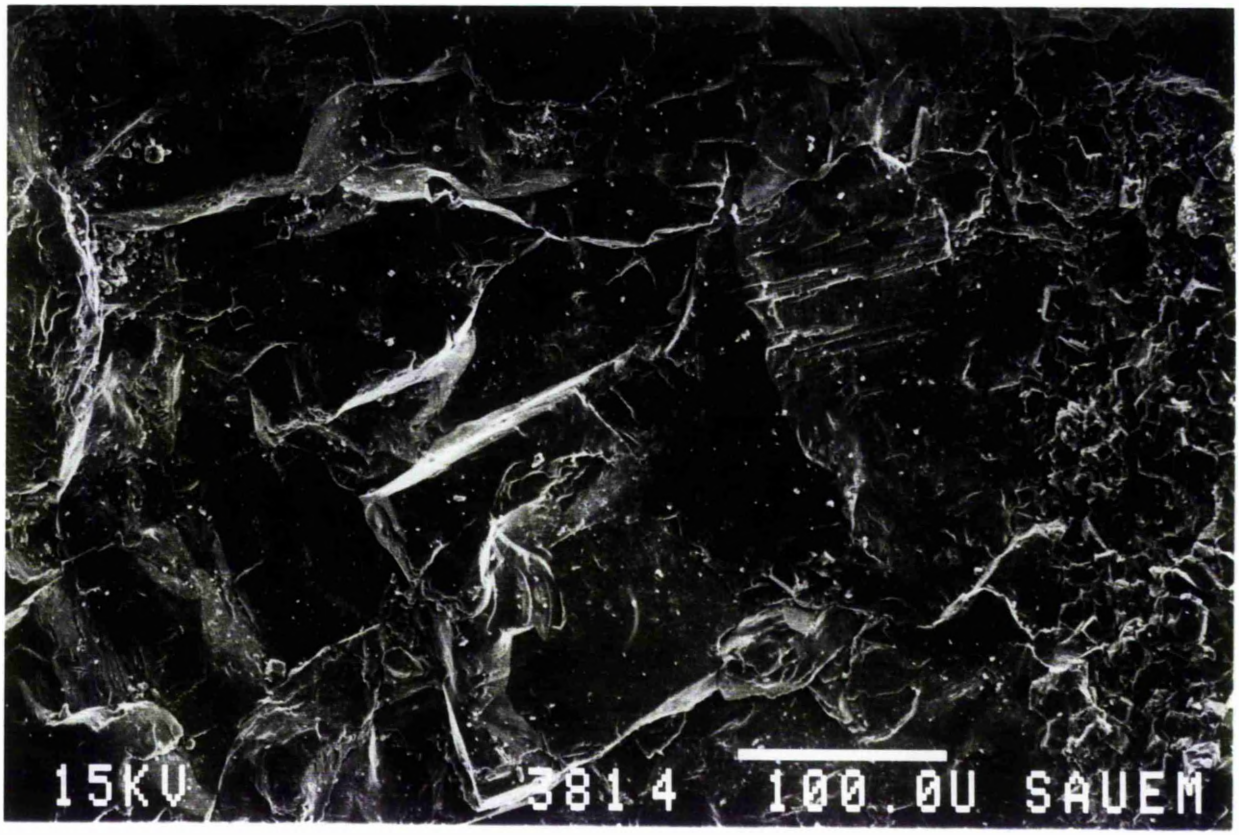
15KV
3814
100.0U SAUEM

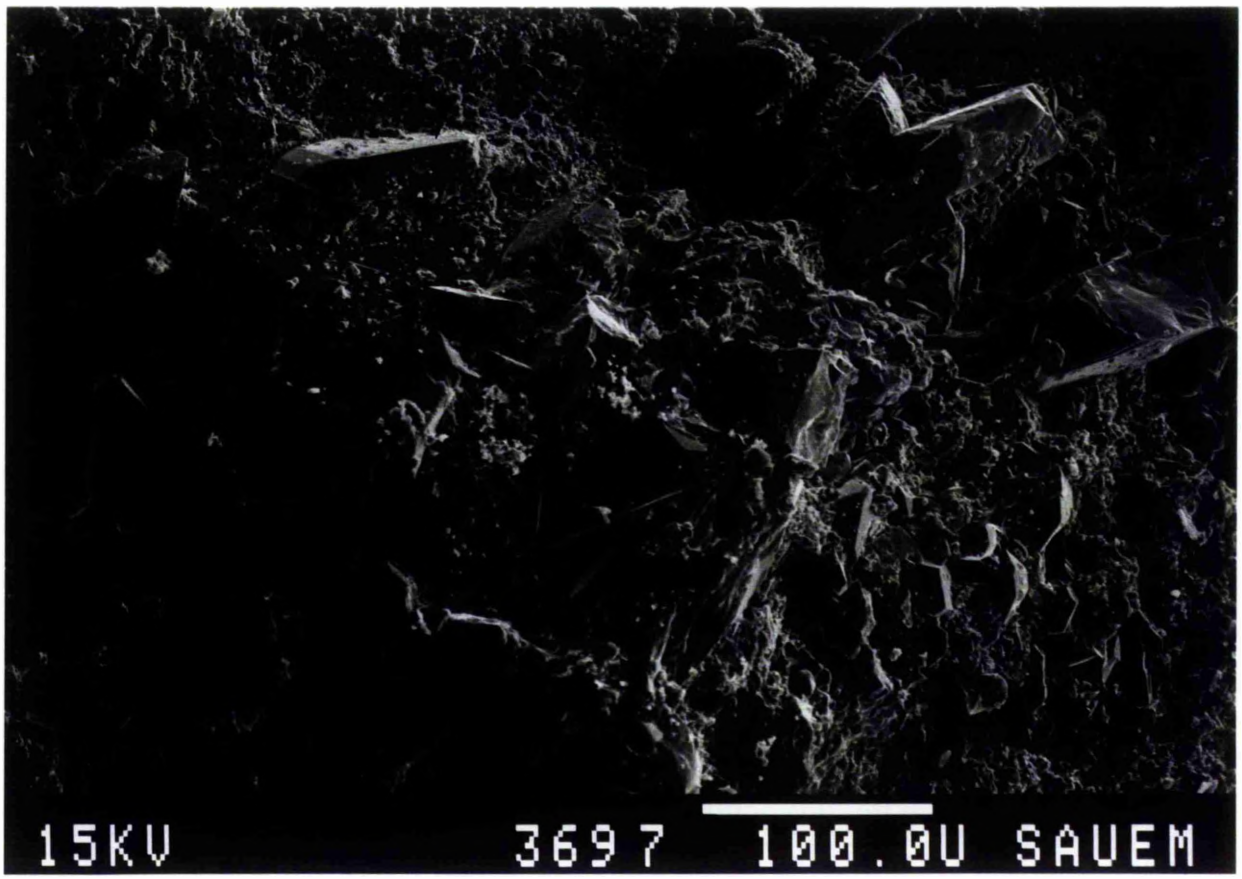
15KV
3697
100.0U SAUEM

most abundant in the intense dolomitization areas (**Kinsman, 1969**).

Celestite in the Euphrates Limestone Formation formed as large subhedral crystals about 300 microns or as aggregates of 150 microns(**Fig 5.12a**).

Radial celestite aggregates up to 10 cm in diameter found in chalk in Lower Tertiary limestone of Libya, have been interpreted as replacement. Skeletal limestone with small lenses of celestite enclosing relics of fossils have been described frequently (**Schmidt, 1961**). Celestite is also reported as a replacement and as a cement in the Gigas beds of northwest Germany (**Schmidt, 1965**).

Some strontium may be freed during the formation of calcite or dolomite from aragonite. Another possibility is that the SO_4^{2-} resulting from dissolution of anhydrite by ground water would produce a solution which saturated with $SrSO_4$ but undersaturated in $CaSO_4$ (**Olaussen, 1981**).

Barite occurs in isolated clear porphyrotopes of 1 mm long. In the Euphrates Limestone Formation it formed as longitudinal euhedral crystals of 90 microns long associated with celestite (**Fig 5.12b**).

5.2.6 Pyritization

Pyrite is known as a typical authigenic mineral, in association with the bacterial reduction of sulphates in gypsum. (**Tucker, 1981**).

In the Euphrates Limestone Formation pyrite is found in various forms, the first form is framboidal, within intercrystalline porosity in the dolomite (**Fig 5.13, 5.14**).

The size of the framboids ranges generally between 10 to 40 microns in diameter but smaller sizes are not uncommon. The framboids are formed of aggregates of spherical micro concretions of pyrite. The regular forms of these framboids has led to the suggestion that they have an organic origin related to the action of sulphate-reducing bacteria.

Vaughan and Turner (1980) suggested that framboids are formed due to release of detritally introduced iron, which reacted with the sulphide produced by the sulphate reduction beneath the surface (**Berner, 1971**) .

The framboidal pyrite is generally regarded as early in the diagenetic history yet they postdate dolomite formation (**Fig 5.14**). Considerable quantities of pyrite are distributed throughout the formation in the form of extremely small framboidal pyrite (**Fig 5.13**).

The second form of pyrite found in the formation is the cubic form which is of 2 microns in size and the edges of these cubic forms are not very sharp suggesting that they have suffered some kind of corrosion (**Fig 5.15**). This form is found in the pores within the calcite cement (core **F**).

Finally, the last form is the pyritohedral form, the size of which ranges between 2 to 4 microns. This type is found in the chamber of foraminiferal tests. It seems that there are two generations , the first one is corroded, and the second one with

Fig 5.13 SEM photomicrograph of framboidal pyrite. Note that there are different sizes of the framboids.

Fig 5.14 SEM photomicrograph of framboidal pyrite in close up view, the framboids are filling the pores between the dolomite crystals. They postdate the dolomite formation.

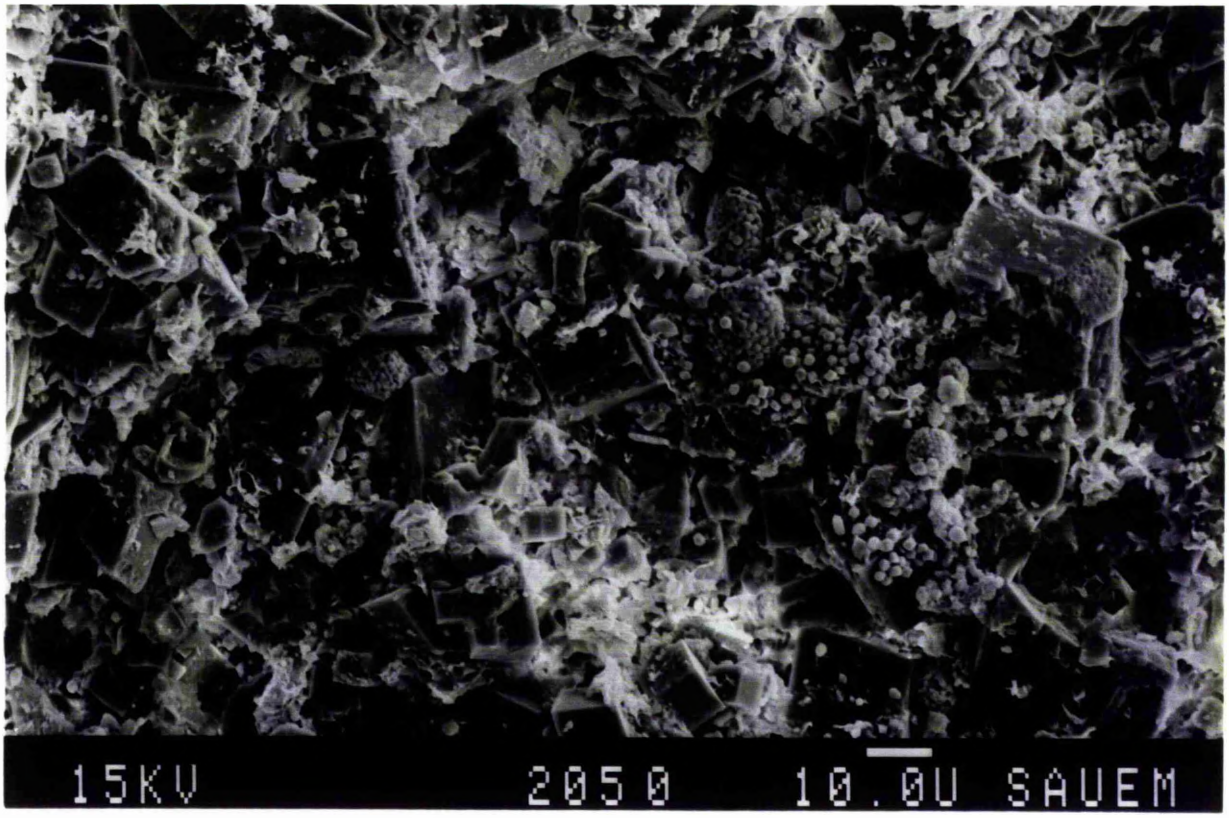
15KV 2050 10.0U SAUEM

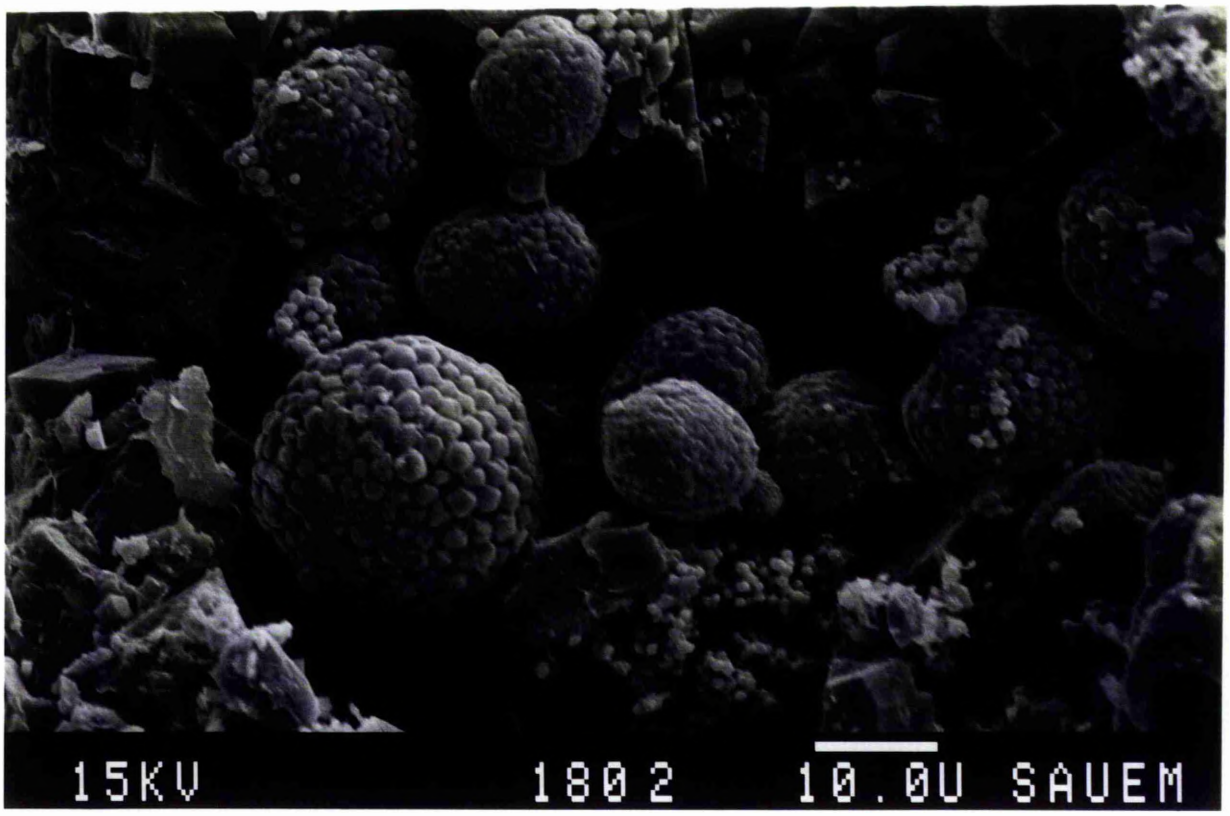
15KV 1802 10.0U SAUEM

Fig 5.15 SEM photomicrograph of cubic pyrite form, the pyrite filling vugs in the calcite cement; pyrite is corroded on the edges of the cubes.

Fig 5.16 SEM photomicrograph showing pyritohedral form of pyrite filling mold of skeletal grain. There are two different sizes and forms; some have sharp edges, the others are corroded.

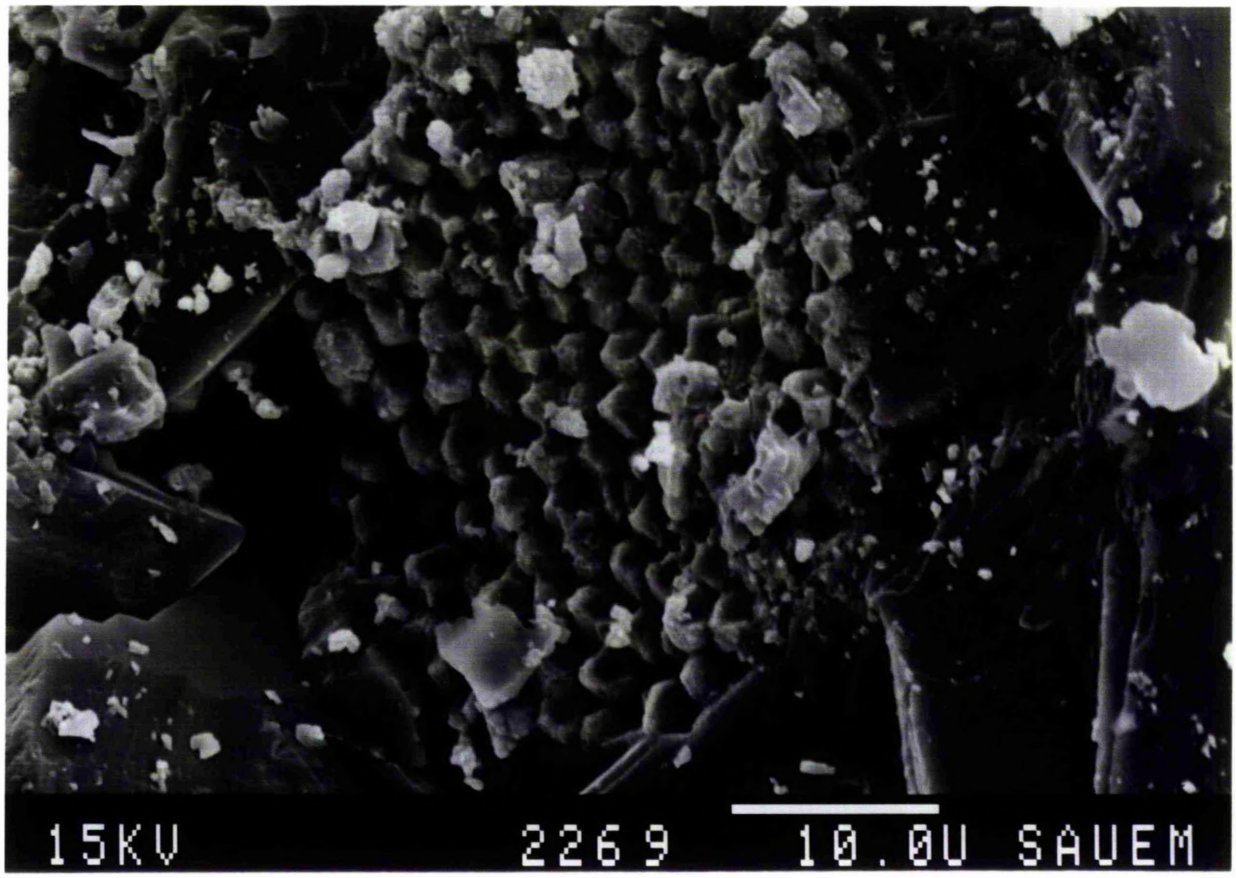
15KV 2269 10.0U SAUEM

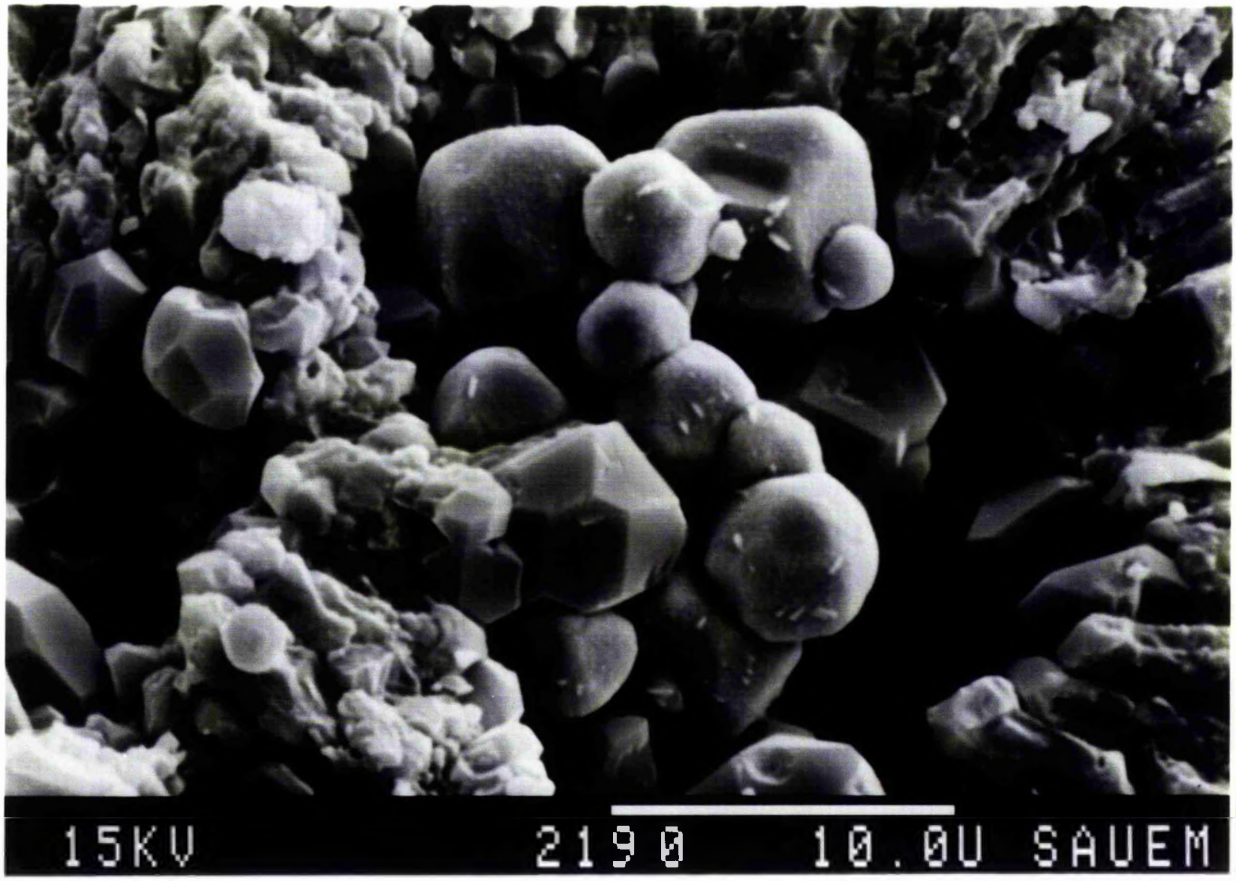
15KV 2190 10.0U SAUEM

clear, and sharp edges, therefore, may be they were formed at two different times (**Fig 5.16**).

Some of the other forms which are not very common is the replacement of the skeletal fragments. Pyrite is found over some of the anhydrite cement which suggest that pyrite formation is spread over some time.

5.3 Timing of the diagenesis

The Euphrates Limestone Formation has been subjected to intensive diagenetic processes, these processes can be arranged in the chronological order as follows:

1.Marine diagenesis, including the formation of the micritic envelopes and the isopachous fibrous crust cement is the first diagenetic process.

2.Then, the sediments were subjected to dolomitizing solutions which led to pervasive dolomitization in the southeast part of the studied area, and partial dolomitization in the northwest part. At this stage probably some of the grains were not completely dolomitized.

3. Dolomitization was followed by meteoric diagenesis which leached the undolomitized parts of the grains and resulted in the formation of the oomoldic and vuggy porosity in the southeast part of the studied area.

4. Then, the sediments were buried and compacted, the compaction led to breakage and in some cases interpenetration of the grains.

5. Anhydrite cement was precipitated, and healed the fractures and filled the leached parts (vugs and molds).

6. Another episode of leaching and probably karstification has occurred, caused the corrosion of the dolomite crystals and formed the hollow dolomite rhombs (see chapter 3).
7. Hydrocarbon emplacement regarded as a final stage of diagenesis.

Pyritization probably occurred after the dolomitization and the dissolution of the sediments, because it is found between and upon dolomite rhombs. It is also found filling the molds and vugs. Some pyrite cement was also found associated with anhydrite which indicates that pyritization probably spread over some time.

a Episodes of diagenesis

1	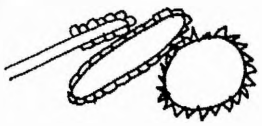	Isopachous cement+micritic envelopes
2		Dolomitization
3	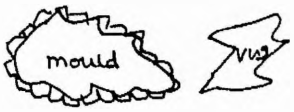	Dissolution producing vugs
4		Burial compaction
5	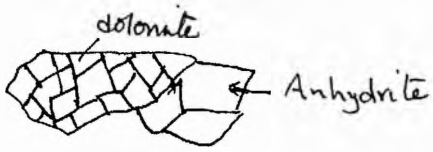	Anhydrite filling moulds
6	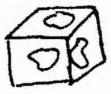	More leaching creating hollow dolomite rhombs
7		Hydrocarbon emplacement

B- Location of the diagenetic episodes

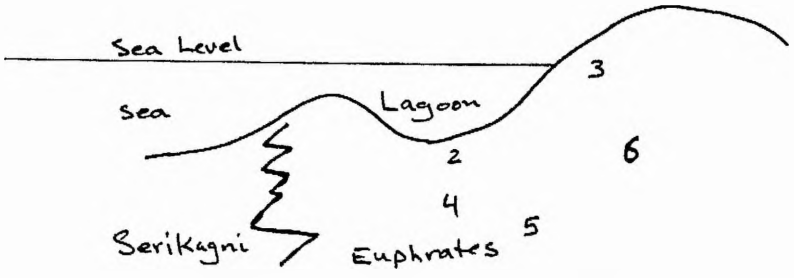

Fig 5.16b Schematic diagram of diagenesis of the Euphrates Limestone Formation.

5.4 Porosity

5.4.1 Introduction

In this study the focus will be on the porosity types in the Euphrates Limestone Formation and the description of these types. The relationships of porosity to diagenesis is also highlighted. Porosity percentages have been calculated from thin sections using the point count method, the thin sections having been impregnated with coloured epoxy resin. Three hundred points were measured at 0.3 mm intervals using a Swift automatic point counter.

Primary porosity in carbonate rocks may be very high (60% or more in lime mud), but this will be quickly reduced at early stages due to diagenesis. In certain cases and due to leaching of some carbonate components or recrystallization new voids will be created, to form secondary porosity. The secondary porosity may be later destroyed partially or completely by cementation.

The most widely used classification is the one made by **Choquette and Pray (1970)** in which porosity types are divided into three basic types, each of which has been further divided:

1. Fabric dependent/ selective porosity
2. Non fabric selective porosity
3. Porosity which may or may not be fabric selective

The fabric selective porosity is present in the Euphrates Limestome Formation as follows;

5.4.2 Intragranular (intraparticle) porosity

This porosity is formed within individual grains or particles e.g inside the shell of a foram or mollusc (**Fig 5.17, 5.18**). This type of porosity generally is primary, but sometimes it secondary, formed by the leaching of the cement or the matrix. It is regarded as the least important type of porosity in carbonate rocks. Preserved porosity of this type in ancient shallow water carbonates is generally association with arid climates as shown by recurring associate of evaporite with primary porosity in the rock record (**Longman, 1981**).

From the point count results made on the cores of the Euphrates Limestone Formation this type of porosity is very scarce and ranges between 0.33 to 3.66 % of the total porosity.

5.4.3 Intergranular (interparticle) porosity;

This type is defined as the porosity between the grains and/or particles. It is a primary type and formed during final sedimentation of detrital particles. On the other hand it can also can form by matrix or cement dissolution. In the present study several types of this porosity are noticed, between ooids, and skeletal grains in grainstone facies. The percentages of this porosity in the present study ranges between 0.66 to 6.3 % which is not high. Recovery efficiency from a reservoir with intergranular porosity is found to be largely dependent on pore shape and size which in turn are controlled to some extent by grain size and grain shape (**Longman, 1981**). In some instances this porosity is very much reduced due to cementation by anhydrite or dolomite cements

Fig 5.17 SEM photomicrograph showing intraparticle porosity. The pores are still open although a few are partially filled with cement (arrow). Quartz crystals have overgrown on the top of the dolomite which means that they formed after dolomitization.

Fig 5.18 Photomicrograph showing intraparticle porosity which has been left open (arrow). Plane polarized light. Scale bar is 0.35mm.

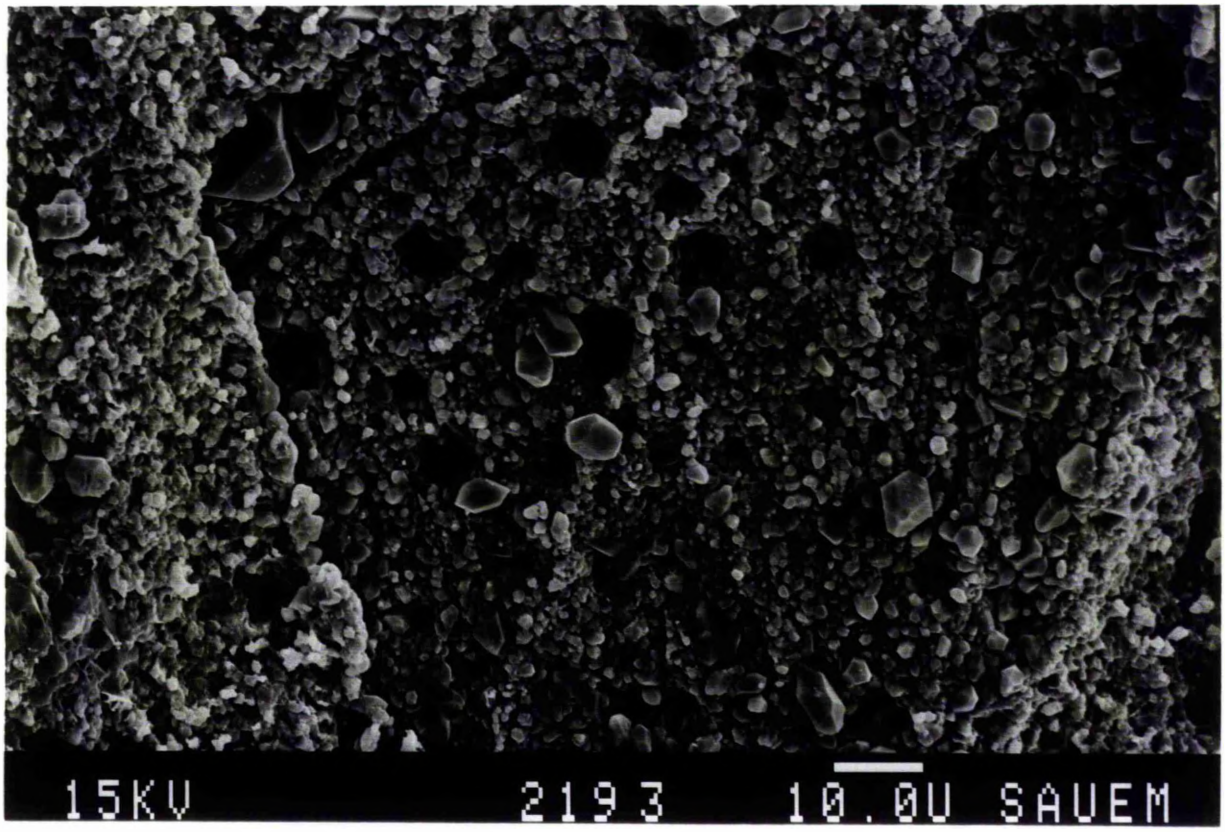
15KV
2193
10.0U SAUEM

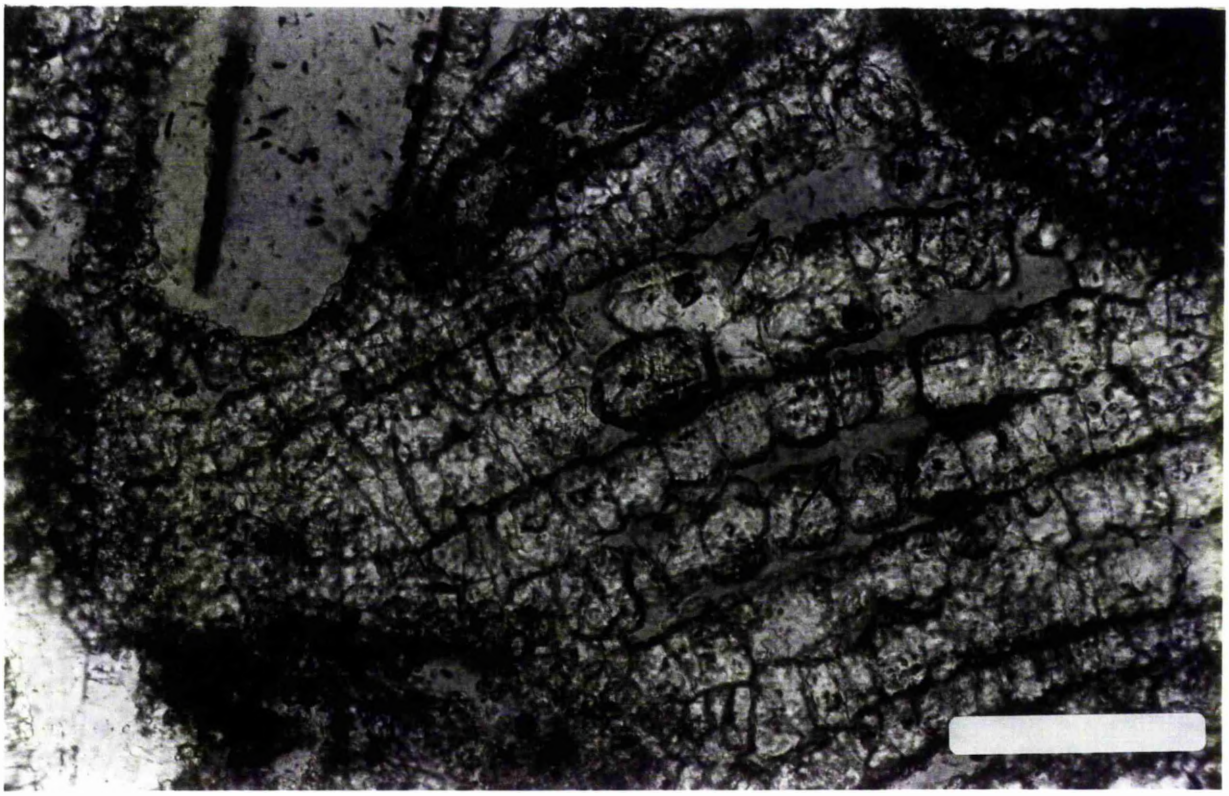

Fig 5.19a Photomicrograph of interparticle pores filled with dolomite crystals. This dolomite filling reduced the interparticle porosity. Plane polarized light. Scale bar is 0.875mm.

Fig 5.19b Photomicrograph of interparticle pores filled with anhydrite cement. The anhydrite filling reduced the interparticle porosity. Plane polarized light. Scale bar is 0.875mm.

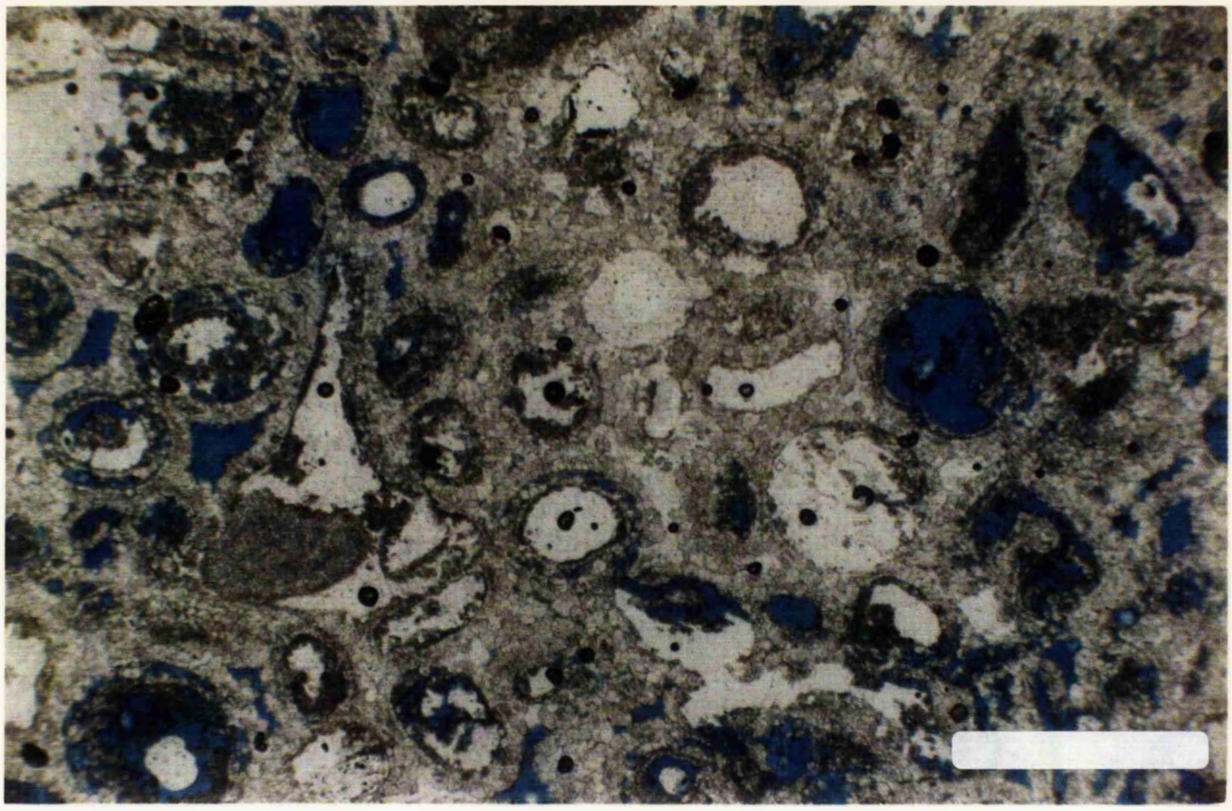

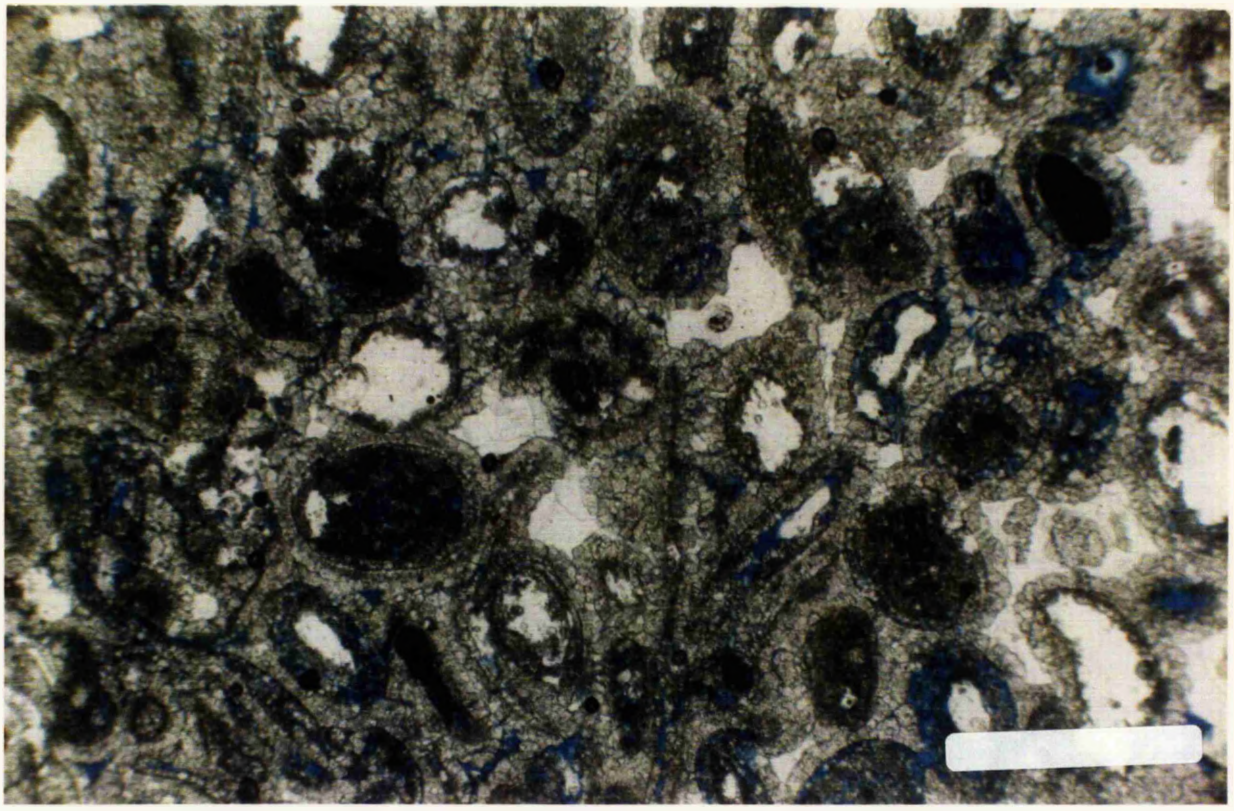

(**Fig 19a, 19b**) but in other instances this primary porosity may be enhanced due to enlargements by dissolution around the original pores. This type when found is called enhanced porosity (**Longman, 1981**). It was not described by **Choquette and Pray (1970)** who included it in the vuggy porosity. This type is very clearly noticed in the Euphrates Limestone Formation.

5.4.4 Intercrystalline porosity;

This type of porosity defines the porosity between crystals relatively similar in size and crystals that have grown in place e.g. in some dolomite, evaporites and recrystallized components. This is usually secondary. Dolomite intercrystalline porosity may also form by partial dolomitization and dissolution of the remaining calcite, or by burial dolomitization (**Fig 5.20**). Such porosity may sometimes be filled with later cements such as anhydrite (**Fig 5.21**). It is high localy in core A (12.3±5.2% in amount) and in core **D** (9±15.5% in amount) in the Euphrates Limestone Formation. It is very well developed and in some cases has been enlarged to form vugs. Permeabilities in rocks with intercrystalline porosity are strongly controlled by size of the crystals, the finer the grains the lower the permeabilities (**Fig 5.24, 5.25, 5.26**) and **Appendix 6**.

Fig 5.20 SEM Photomicrograph showing intercrystalline porosity. The pores in the dolomite crystals form intracrystalline porosity (arrow).

Fig 5.21 SEM photomicrograph of intercrystalline porosity; although some pores have been filled with anhydrite.

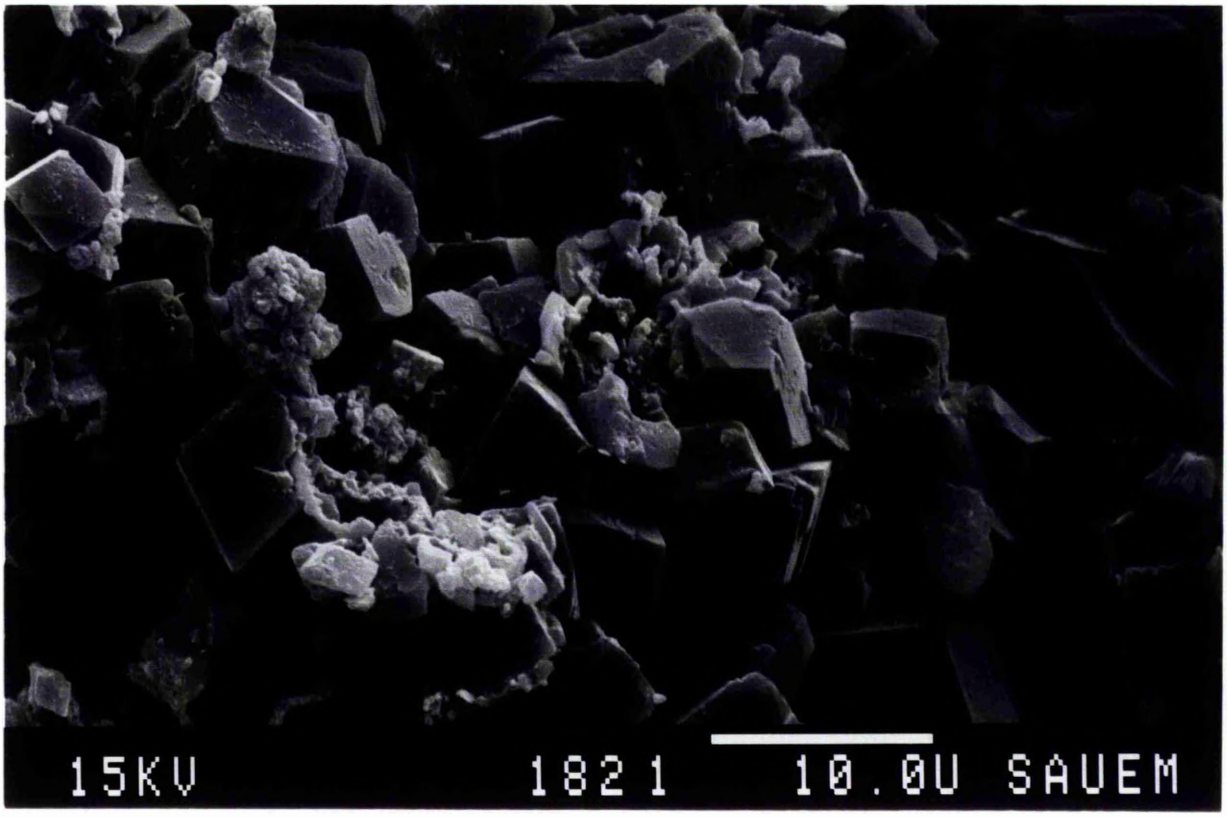
15KV
1821
10.0U SAUEM

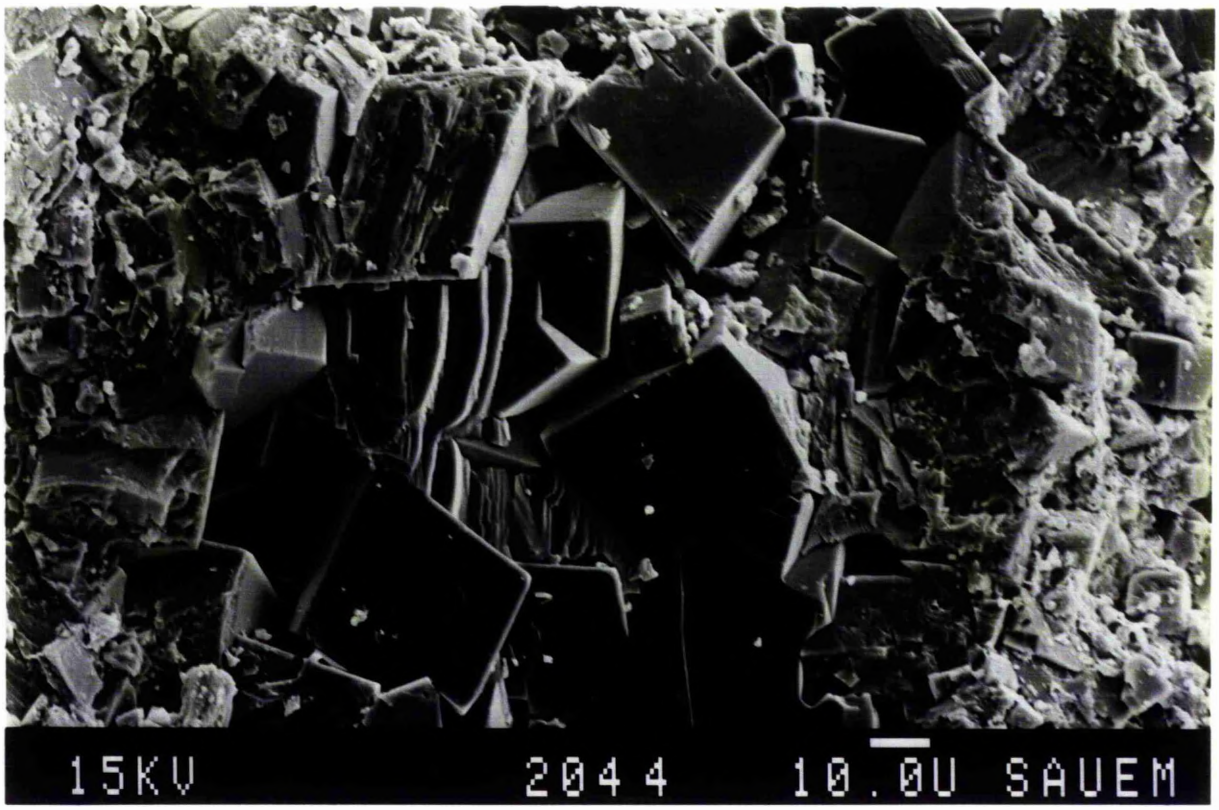
15KV
2044
10.0U SAUEM

Fig 5.22 SEM photomicrograph of dolomite crystals showing intracrystalline porosity formed due to leaching of the dolomiter rhombs. The pores are still open. Intercrystalline pores are also present.

Fig 5.23 SEM photomicrograph of intracrystalline porosity. The pores are extensively enlarged due to dissolution forming micropores (arrow).

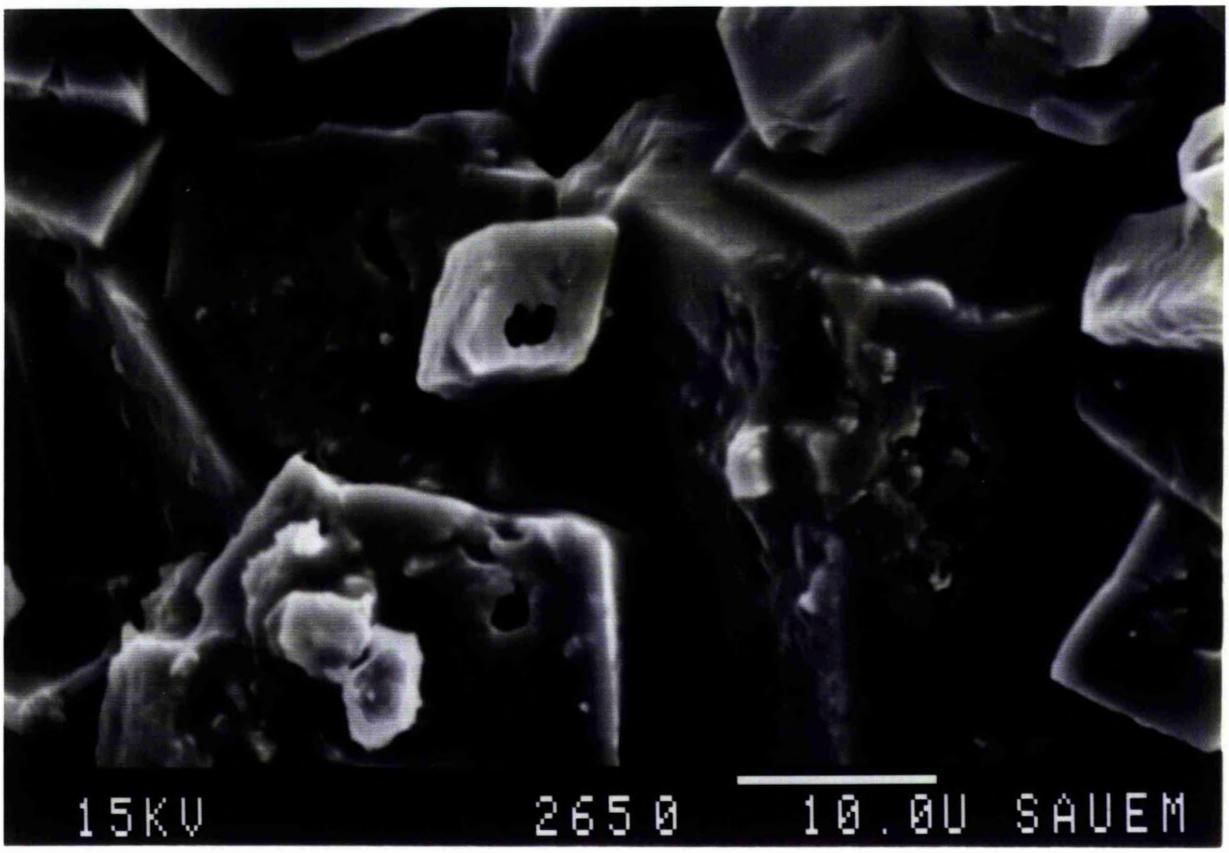
15KV
2650
10.0U SAUEM

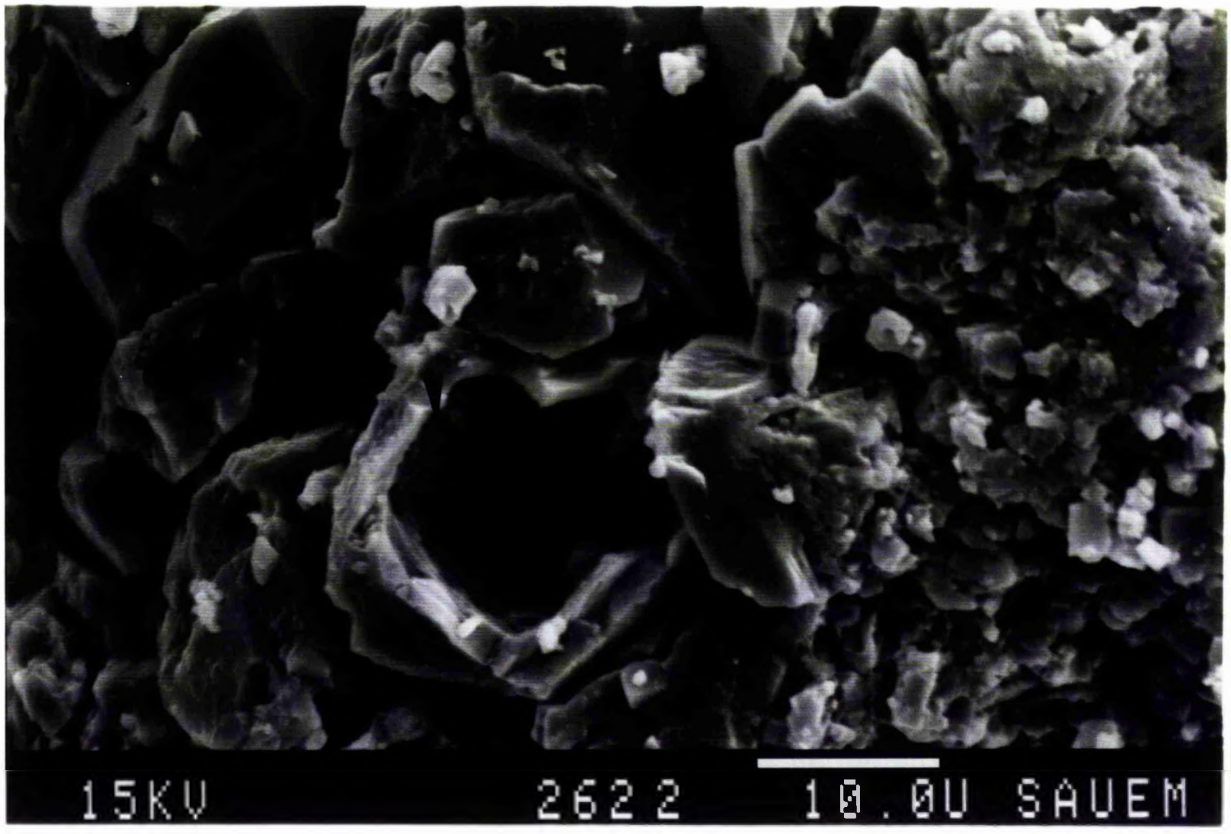
15KV
2622
10.0U SAUEM

Clay mineral growth may reduce this porosity, and chlorite and illite clay minerals are found occluding the intercrystalline porosity (**Fig 5.31, 5.32**). In some cases pores are filled with framboidal pyrite.

5.4.5 Intracrystalline porosity;

Defined as the porosity inside crystals , this type was not described by **Coquette and Pray (1970)**. It is very clear and important in the Euphrates Limestone Formation. It formed where the dolomite crystals were dissolved at their centres (**Fig 5.22, 5.23**), and it forms a substantial amount in cores **B**, **D**, and **E** (**Fig 5.24, 5.25, 5.26**).

Intracrystalline porosity in the Euphrates Limestone Formation is associated with dolomite, and very well developed in core **E** in which it reaches 15% (**Fig 5.26**).

5.4.6 Moldic porosity;

This kind of porosity is formed by selective dissolution or leaching of grains in a rock, most commonly caused by removal of aragonite in corals, molluscs, or ooids from a calcite cemented limestone (**Fig 5.27**).

Much moldic porosity forms by leaching by phreatic and vadose freshwater. Conditions for calcite cementation and leaching of the aragonite are found in many freshwater regions near the

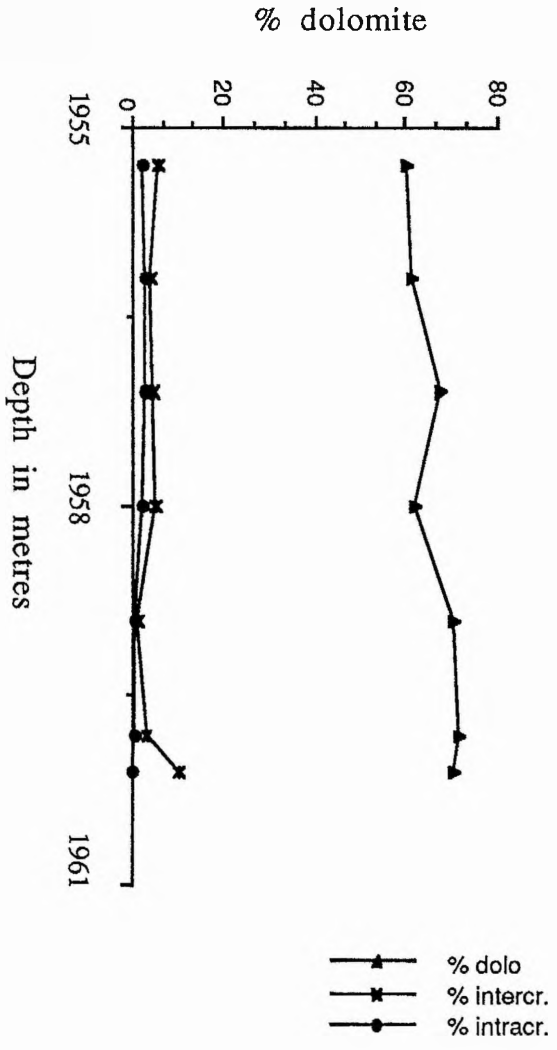

Fig 5.24 Graph showing the relationship betwwen the dolomite percentages, intercrystalline, and intracrystalline porosities in core B

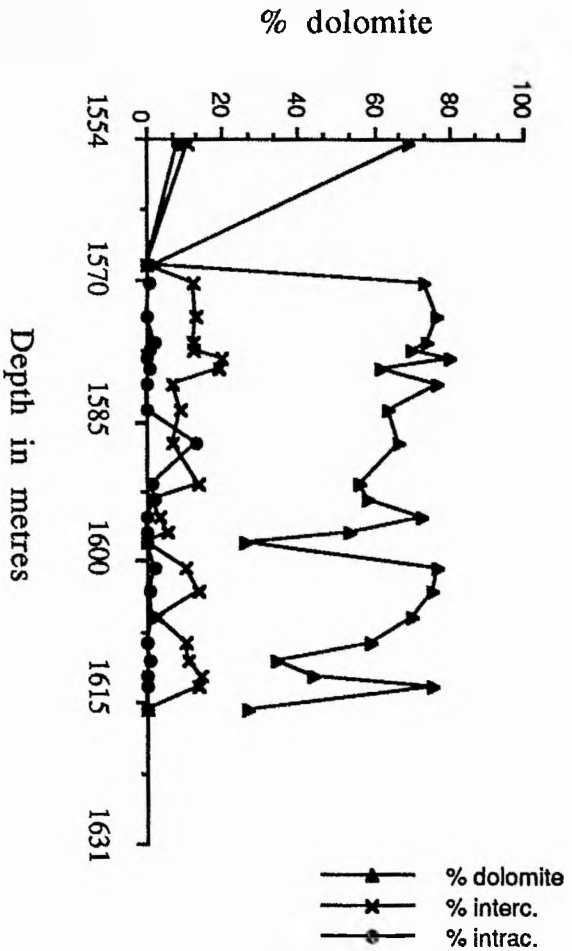

Fig 5.25 Graph showing the realtionship between the dolomite percentages, intercrystalline and intracrystalline porosities in core D

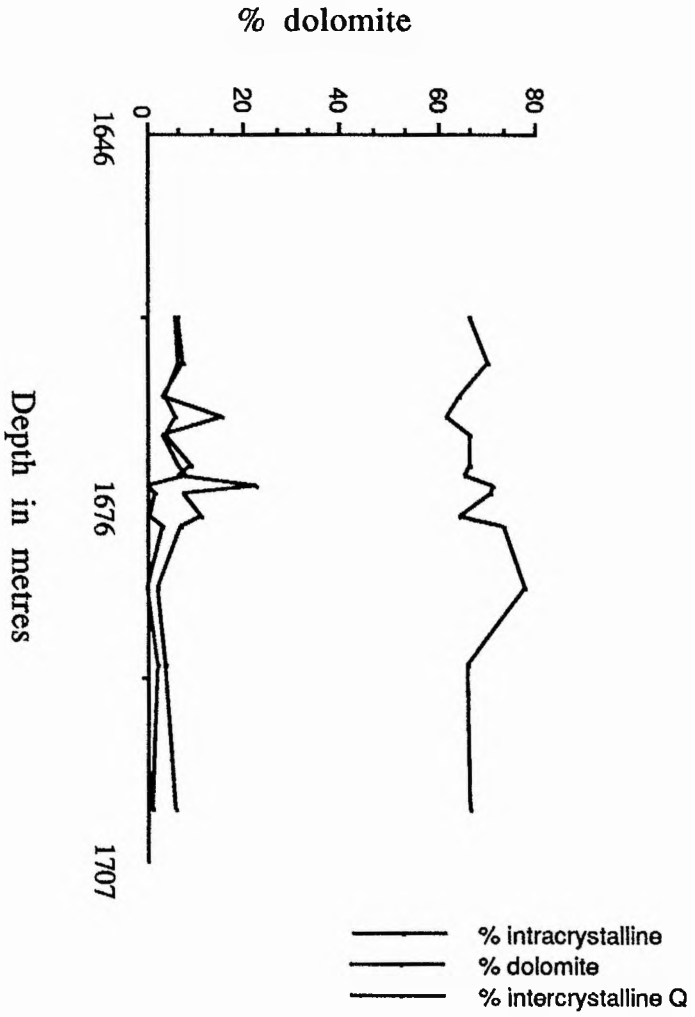

Fig 5.26 Graph showing the relationship between the dolomite percentages, intercrystalline and intracrystalline porosities in core E

earth surface. Some moldic porosity forms in the subsurface associated with the dewatering of shales.

In the Euphrates Limestone Formation moldic porosity is found especially in the oolitic fossiliferous grainstone facies in the dolomite section.

The moldic porosity in the Euphrates Limestone Formation is sometimes greatly reduced due to anhydrite cementation. It was found that this type of porosity is very important in the hydrocarbon reservoirs.

5.4.7 Vuggy porosity;

Secondary vugs and voids are formed by post depositional processes, which produced voids (**Fig 5.28**) usually larger than the normal primary pores (**Murray, 1960**). They are irregular, and represented by holes cutting across grains and/or cement boundaries which are large enough to be visible in the naked eye.

Vugs or voids are formed due to solution and they are not fabric selective; the vugs may be in some cases interconnected to form channels. Vugs are usually important in limestones that have been subaerially exposed and leached. They are formed in the freshwater vadose and some meteoric (freshwater) phreatic environments. Like moldic, vuggy porosity requires at least a semi-lithified limestone and a solution undersaturated in calcium carbonates, but unlike the moldic porosity, vuggy porosity generally forms in a homogeneous limestone or dolomite. This type of porosity is

Fig 5.27 SEM photomicrograph of moldic porosity. The mold of the foram is still open. An euhedral calcite crystal sealed one of the pores.

Fig 5.28 SEM photomicrograph of vuggy porosity in limestone . The size of the vug of irregular shape is about 40 microns. Salt crystals can be seen (arrow).

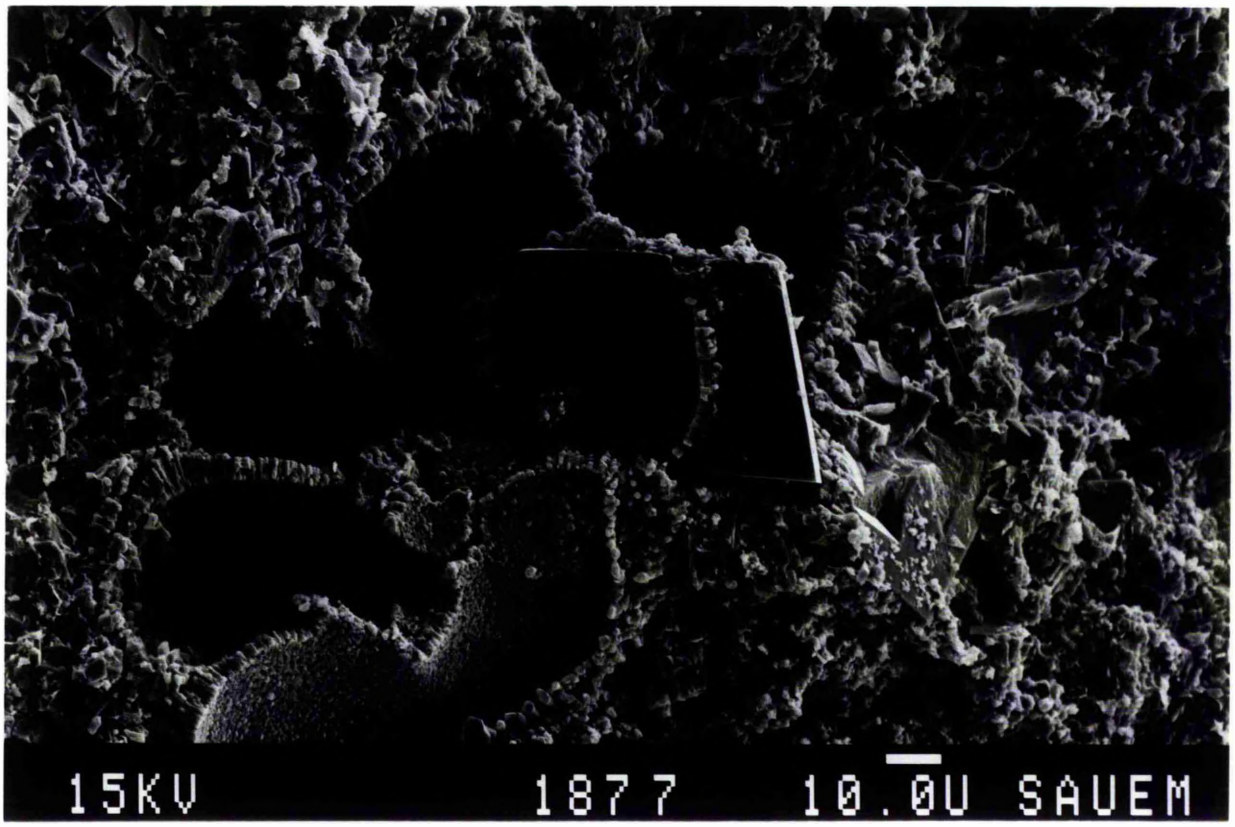
15KV 1877 10.0U SAUEM

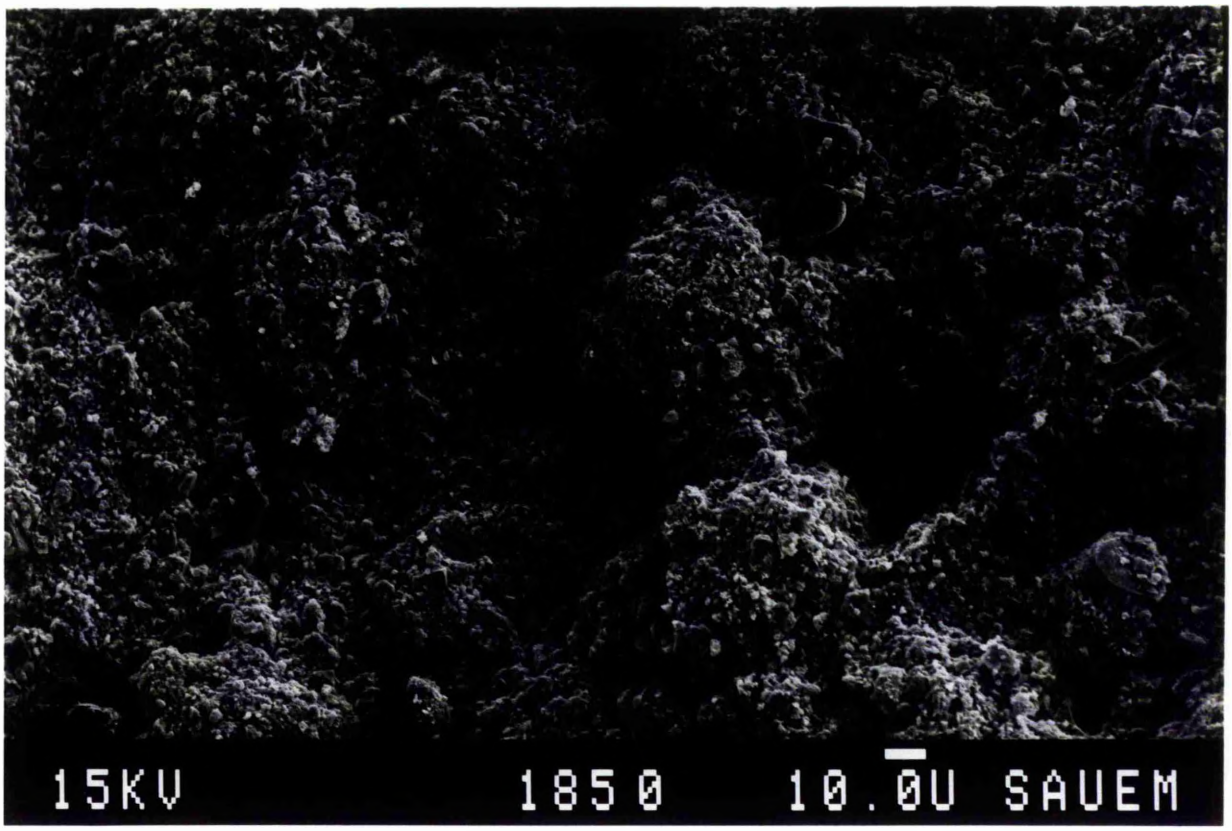
15KV 1850 10.0U SAUEM

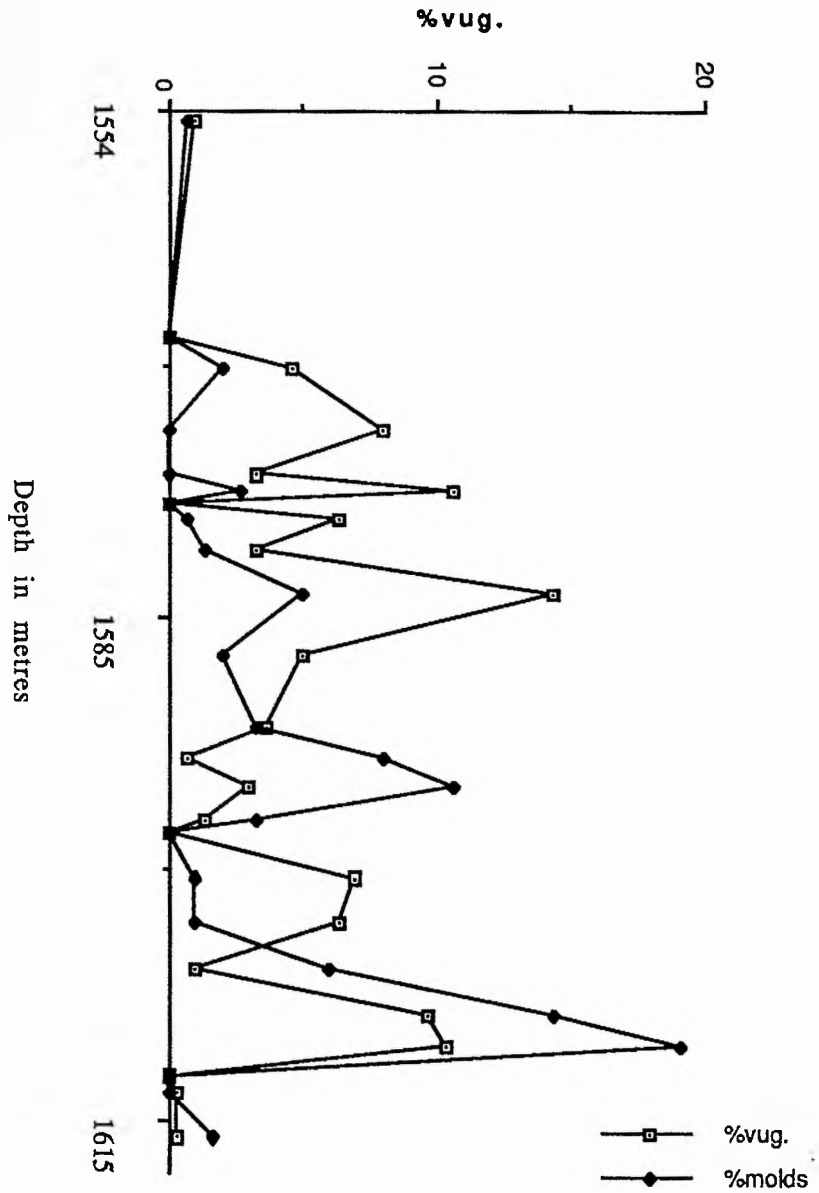

Fig 5.29 Depth versus vuggy and moldic porosities in core D.

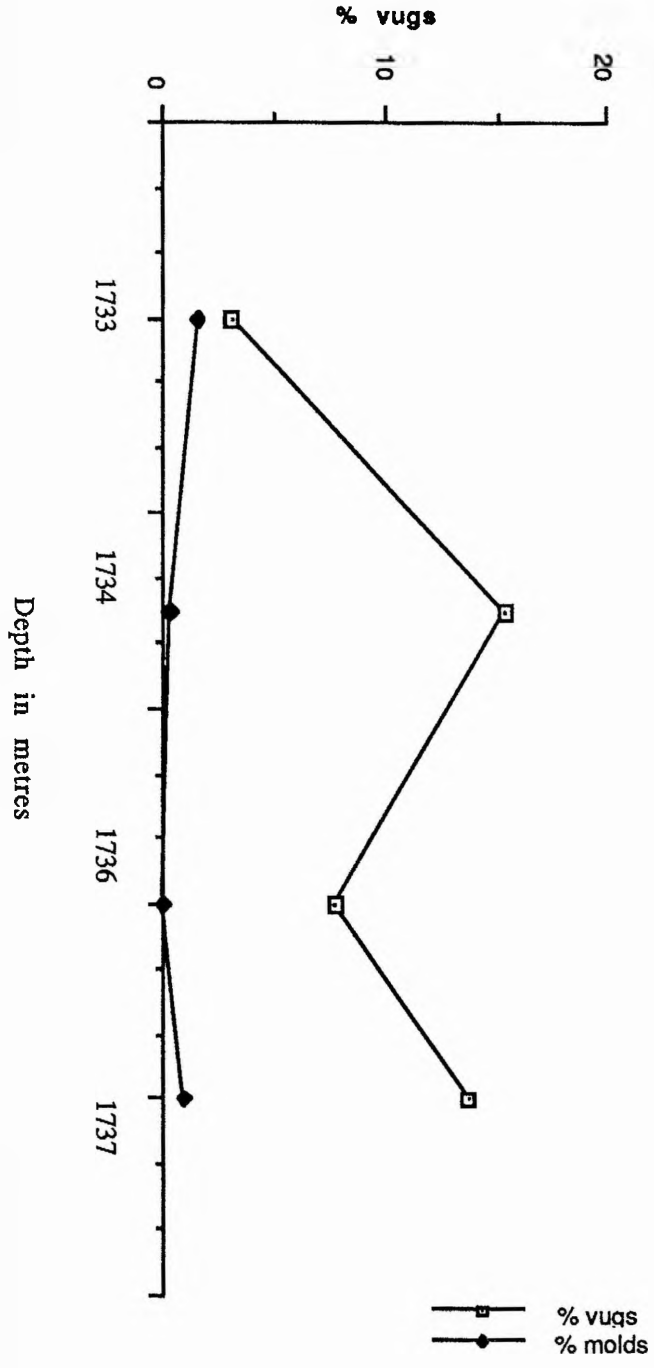

Fig 5.30 Depth versus vuggy and moldic porosities in core A

Fig 5.31 SEM photomicrograph shows a rounded vug with growth of a clay mineral.

Fig 5.32 SEM photomicrograph of chlorite crystals bridging the pores and vugs among the dolomite crystals.

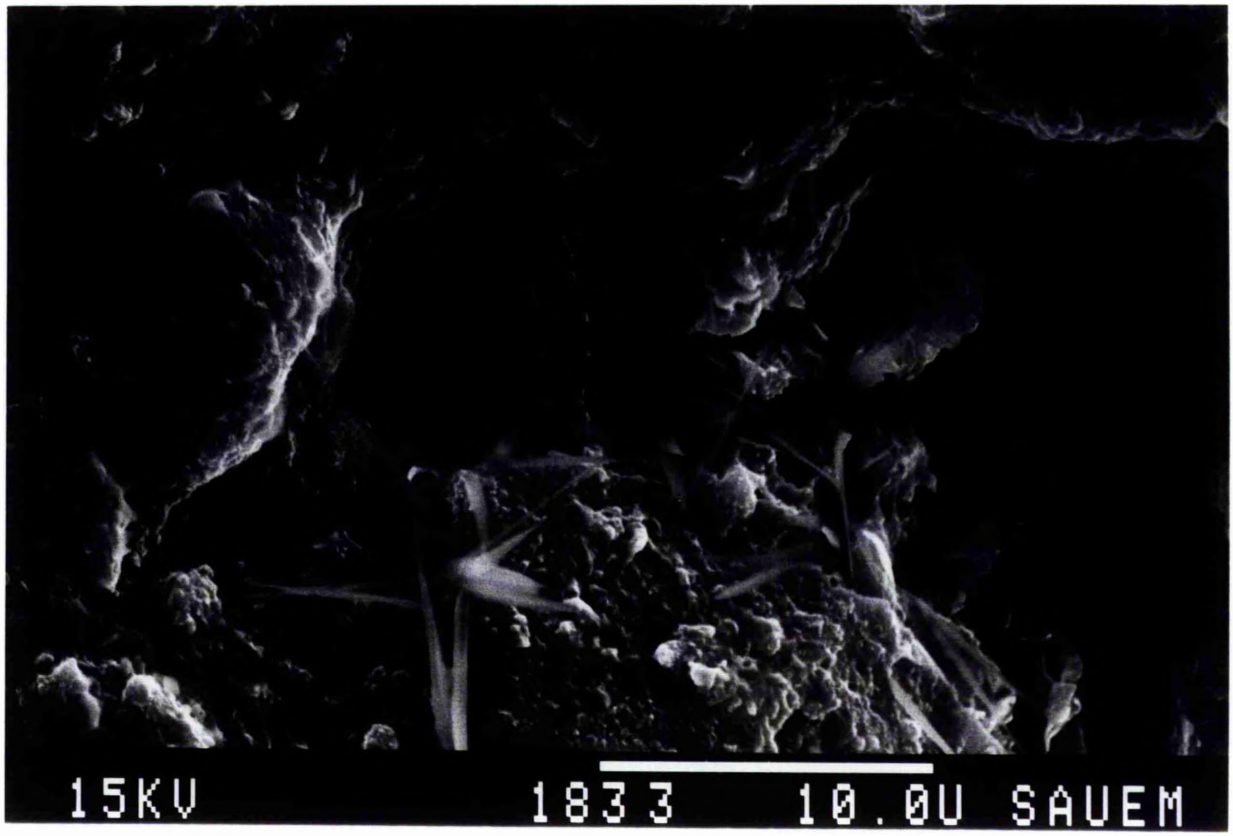
15KV
1833
10.0U SAUEM

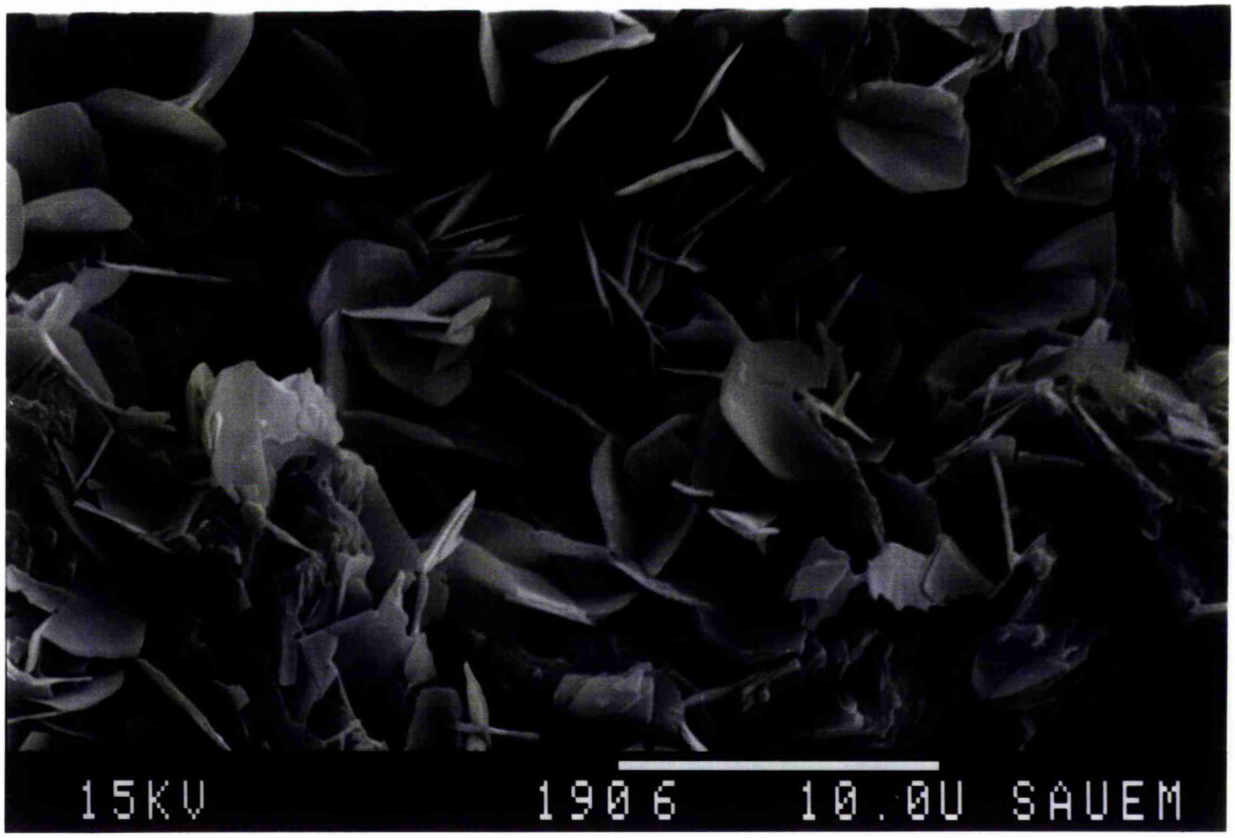
15KV
1906
10.0U SAUEM

Fig 5.33 SEM photomicrograph of clay minerals forming a network over a vug in the dolomite and bridging the intercrystalline pores.

Fig 5.34 SEM photomicrograph of gypsum laths filling vugs in dolomite.

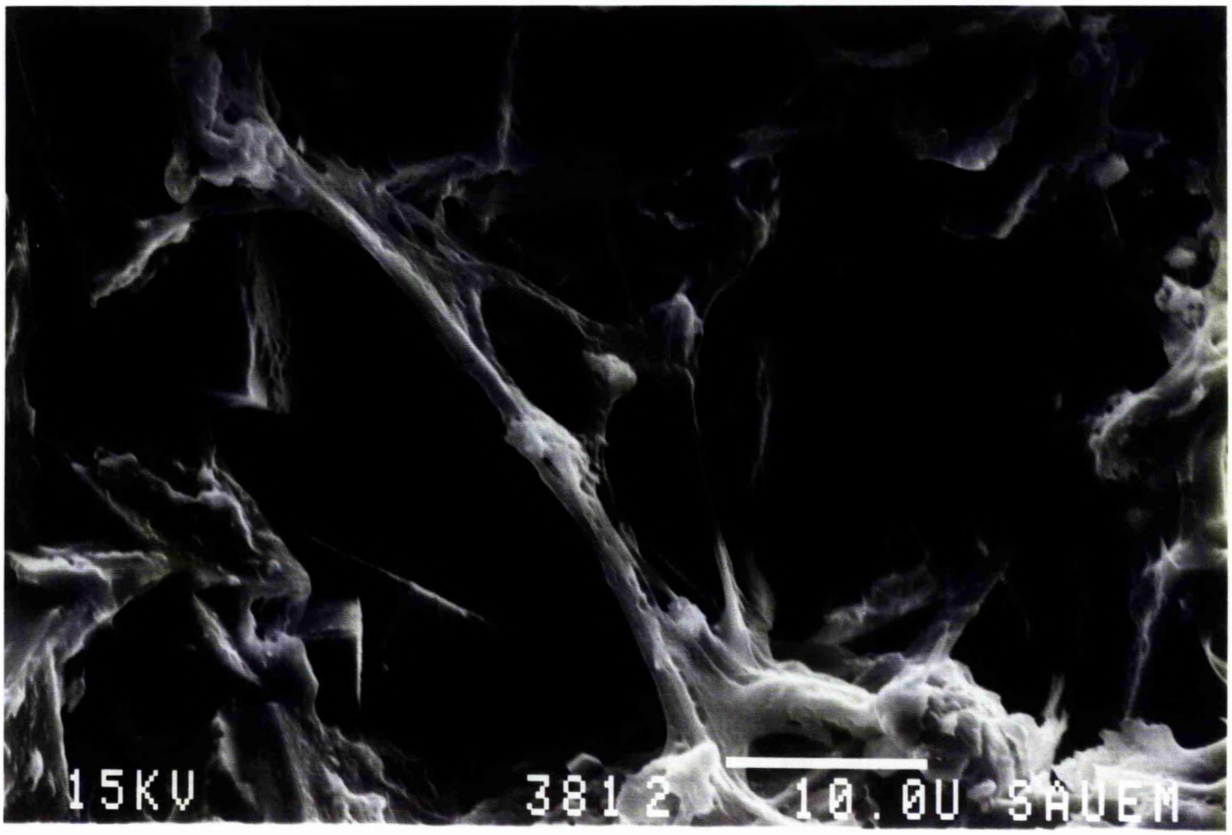
15KV
3812
10.0U SAUEM

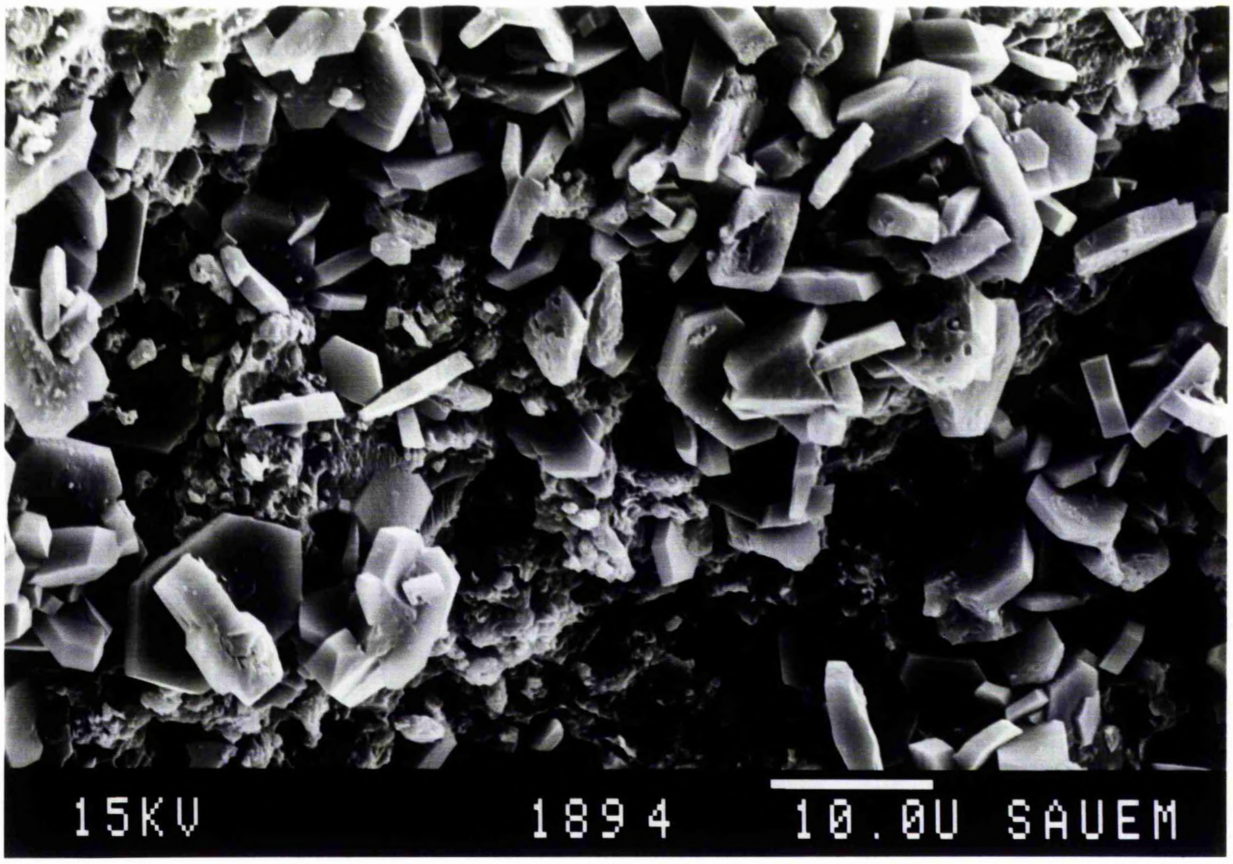
15KV
1894
10.0U SAUEM

represented in the Euphrates Limestone Formation and reaches an average of 9.9% (core **B**), and 4.2±4 in other cores (**Fig 5.29 to 5.30**).

Vugs are formed within the interlocking dolomite mosaic; they are open and in some cases are interconnected. This type of vugs probably formed by dissolution of non dolomitized patches of calcite.or they formed as an earlier vug that was not cemented during dolomitization.

The vugs are formed in some cases due to enlargement of some intercrystalline porosity, and in other cases due to enlargement of the interparticle or intergranular porosity. In some cases this porosity is filled with clay minerals (**Fig 5.31, 5.32, 5.33**) and other cases with gypsum (**Fig 5.34**). Their sizes reach 750 microns in length.

5.4.8 Fracture porosity

This type is not a fabric selective. The best fractures are related to subsurface fracturing and faulting.

Usually, fractures formed early in reefs or shallow water carbonates are filled quickly with sediments.

In the Euphrates Limestone Formation fracture porosity is not very effective. Fractures are very small and not filled by sediments, therefore, they either formed after the precipitation of cements or perhaps during coring or sample preparation.

Fig 5.35 SEM photomicrograph of microfracture in the calcite cement. The fracture is still open and postdates the calcite cementation. There are two places showing previous fractures filled and completely healed (arrow).

Fig 5.36 SEM photomicrograph showing fractures formed due to leaching of anhydrite cement. The leaching runs along parallel lines which probably represent cleavages. Small ones joined to form a larger fracture.

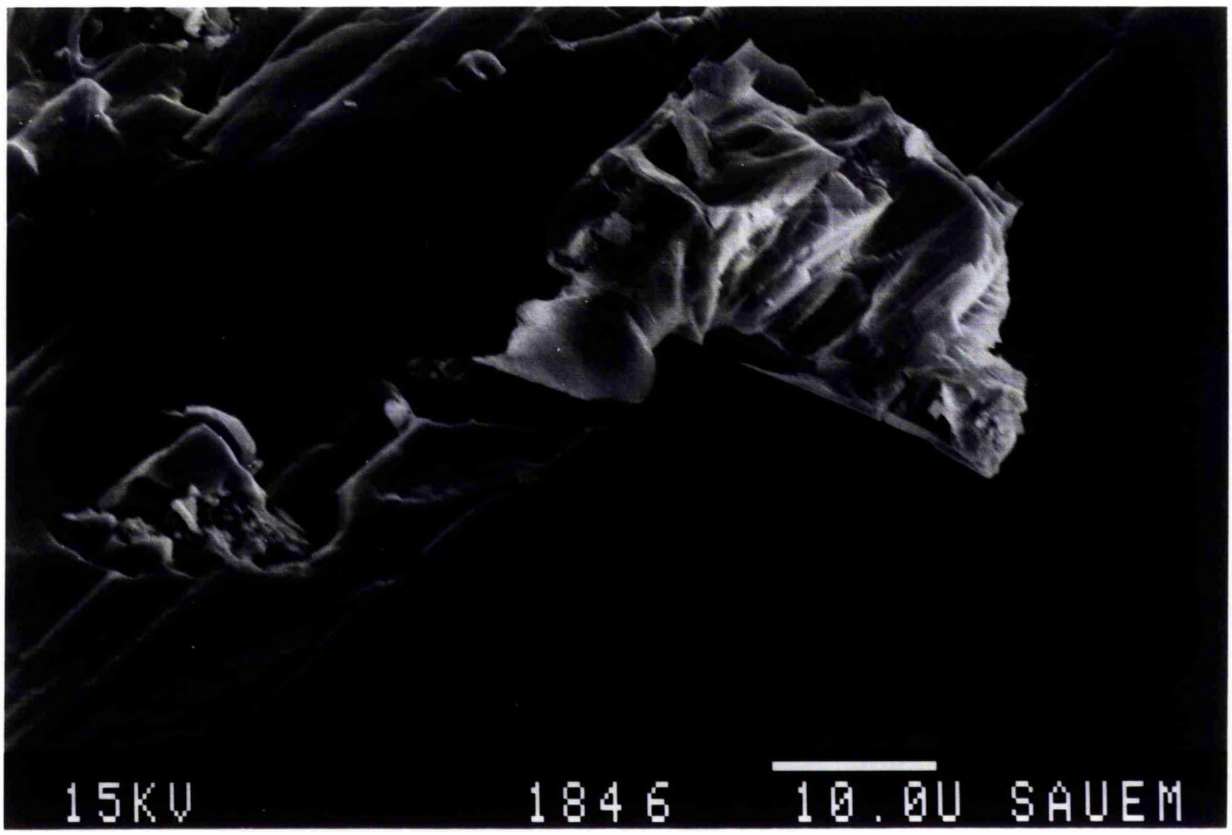
15KV
1846
10.0U SAUEM

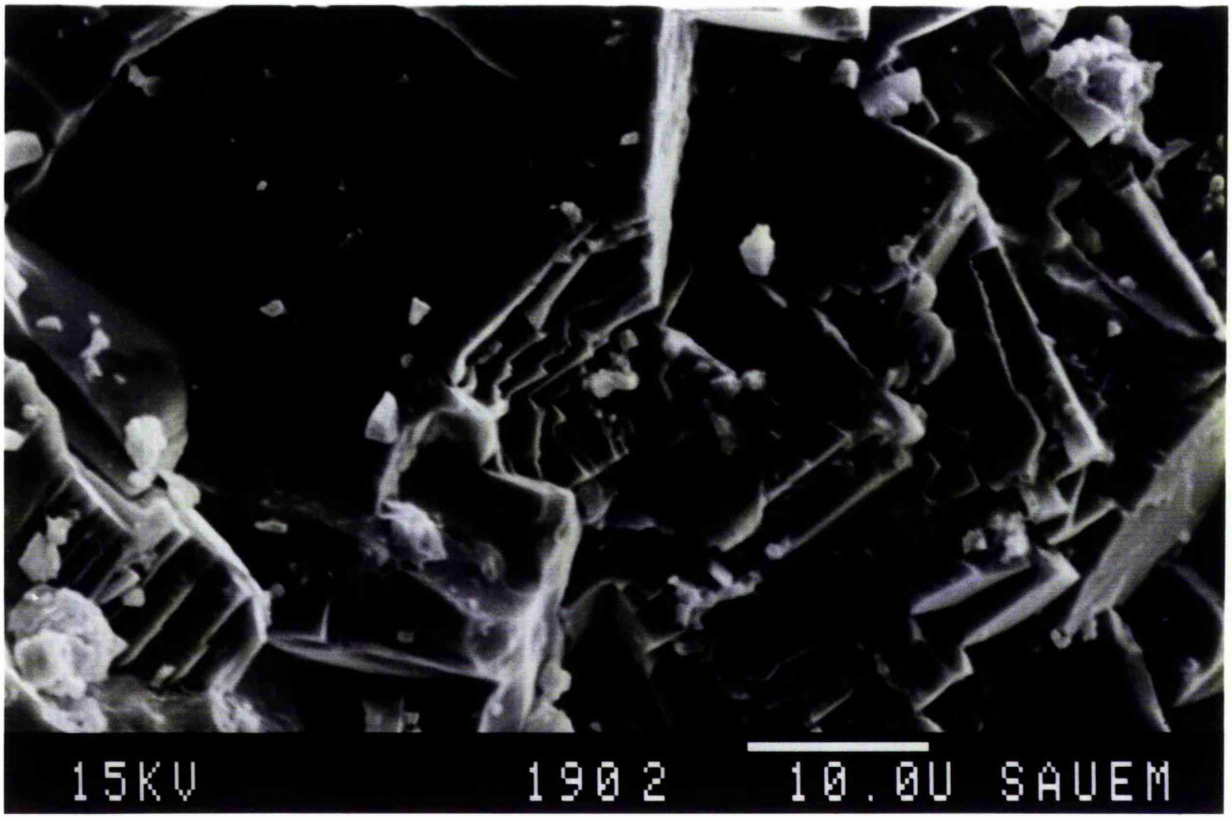
15KV
1902
10.0U SAUEM

Another type of fracture is found crossing the calcite filling cements, and these microfracture are not filled with later cements. They are original fractures formed after calcite cement precipitation (**Fig 5.35**).

Another type of fracture porosity detected in the Euphrates Limestone Formation is the dissolution fracture found in the anhydrite cement (**Fig 5.36**). In this case fractures are aligned in parallel probably following the cleavage of the anhydrite. These small fractures are joined together to form larger fractures.

5.4.9 Discussion

The overall total porosity in the Euphrates Limestone Formation is very good in cores **A, B, C, D, E,** and **F** (**Fig 5.37 to 5.42**), but the total porosity in the cores G, and H is very poor and negligible.

The total porosity in cored section of core A is very good with the average of 20 % value, but becomes very high (38%) at the depth of 5697.5m (**Fig 5.37**). These high total porosities are mainly related to very high intercrystalline porosity which was enlarged due to rock dissolution gave a high vuggy porosity as well .

In core **B** the average total porosity is 19 % (**Fig 5.38**). The two high values 27.32 %, and 24.65 % are mainly related to high intercrystalline porosity. In the first case the high value is due to the presence of vuggy, intercrystalline and intraparticle porosities (**Fig 5.38**).

Fig 5. 39 shows the trend of porosity in core **C**. Generally the total porosity is low. Although the rock is formed almost of dolomite at the depth of 1706m (87 % dolomite and 11.6 % anhydrite). The porosity is still low, because the texture of the dolomite is formed of very fine crystalline interlocking dolomite.

The higher porosity values are related to very low percentages of anhydrite cement (0.33, 4.3) and the presence of higher intercrystalline and vuggy porosity.

Lower porosities occur when the limestone percentage is increased and the dolomite decreased with or without very low percentages of anhydrite cement. The last high value in **Fig 5.39** is mainly related to vuggy and intercrystalline porosity. The rock at this depth is mainly composed of dolomite with 17.5% anhydrite and a lower amount of calcite (4.66%).

Fig 5.40 shows porosity percentage with depth in core **D**. The low values are always associated with high percentages of anhydrite. High values in most cases are related to high intercrystalline and vuggy porosities, which indicate the high effect of dolomitization and rock dissolution. The last porosity value in **Figure 5.40** is related to high percentage of calcite and partially dolomitized rock, in which porosities in general in the Euphrates Limestone Formation are very low.

Fig. 5.41 shows very high porosity in core **E** . The rock is totally dolomitized. The total porosity is mainly related to the occurrence of the four main types of porosities. The intercrystalline, intracrystalline (which in this core

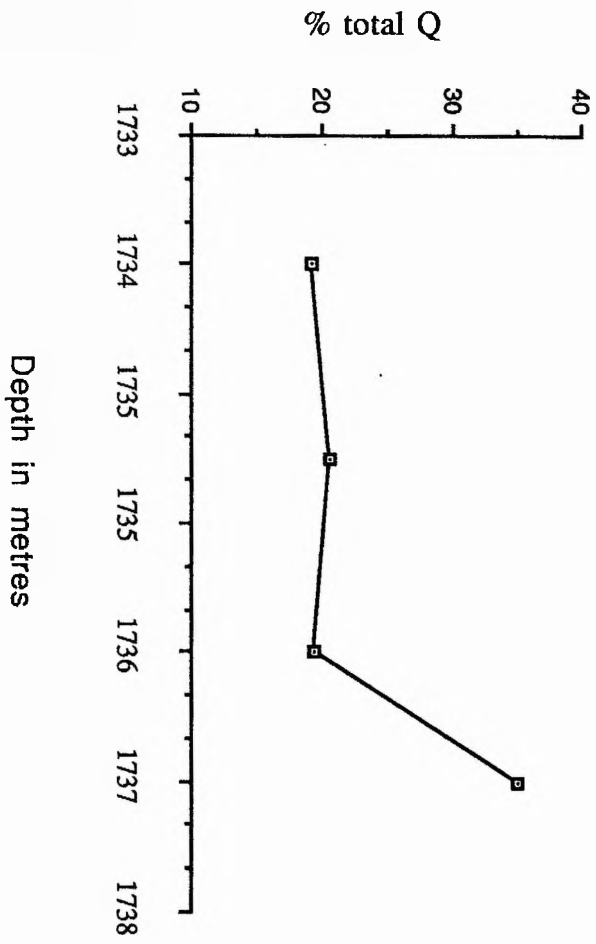

Fig 5.37 Graph showing the relationship between the total porosity (point count) and depth in core A

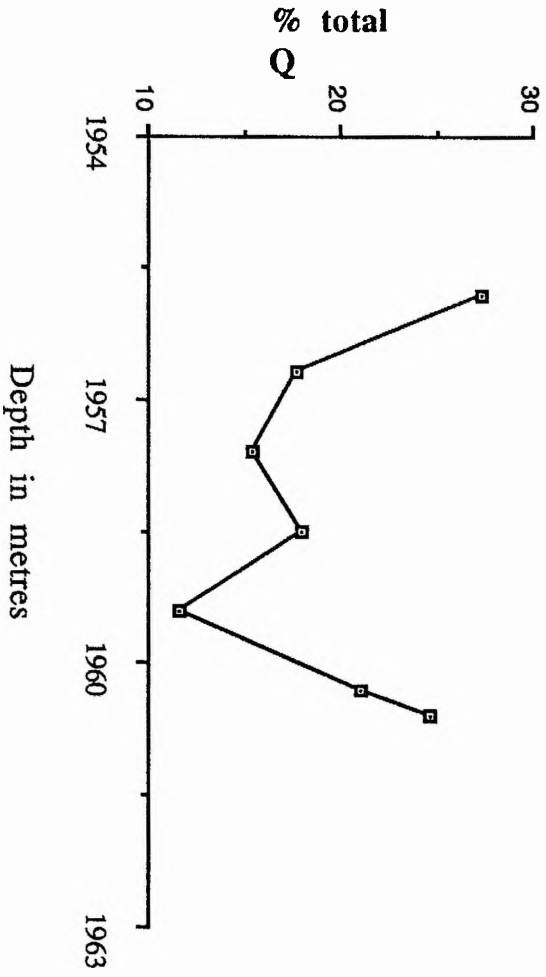

Fig 5.38 Graph showing the relationship between the total porosity (point count) and depth in core B

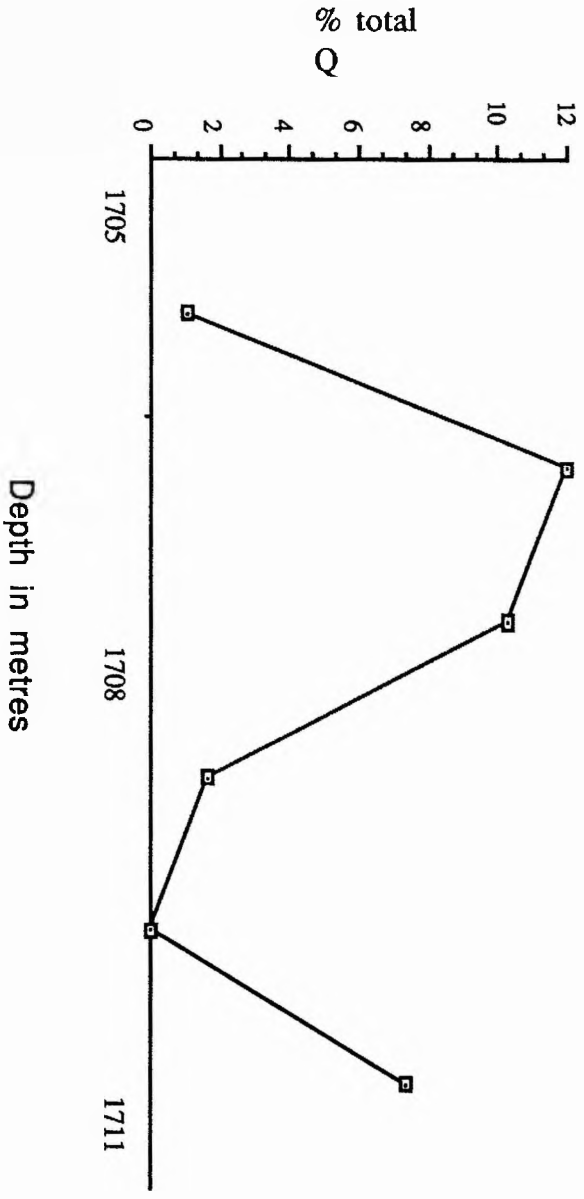

Fig 5.39 Graph showing the relationship between the total porosity and depth in core C

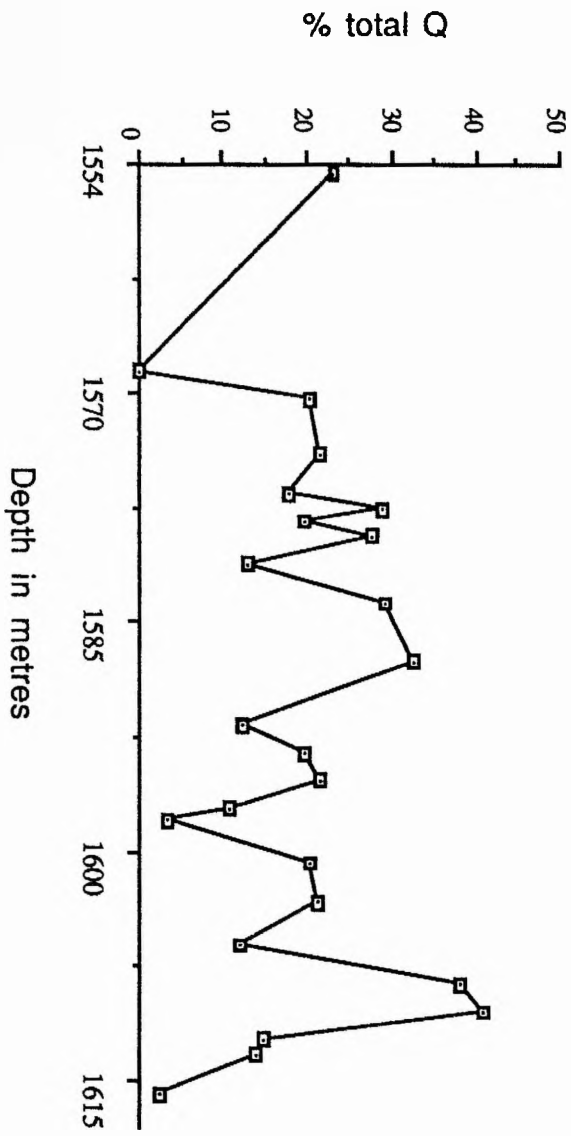

Fig 5.40 Graph showing the relationship between the total porosity (point count) and depth in core D

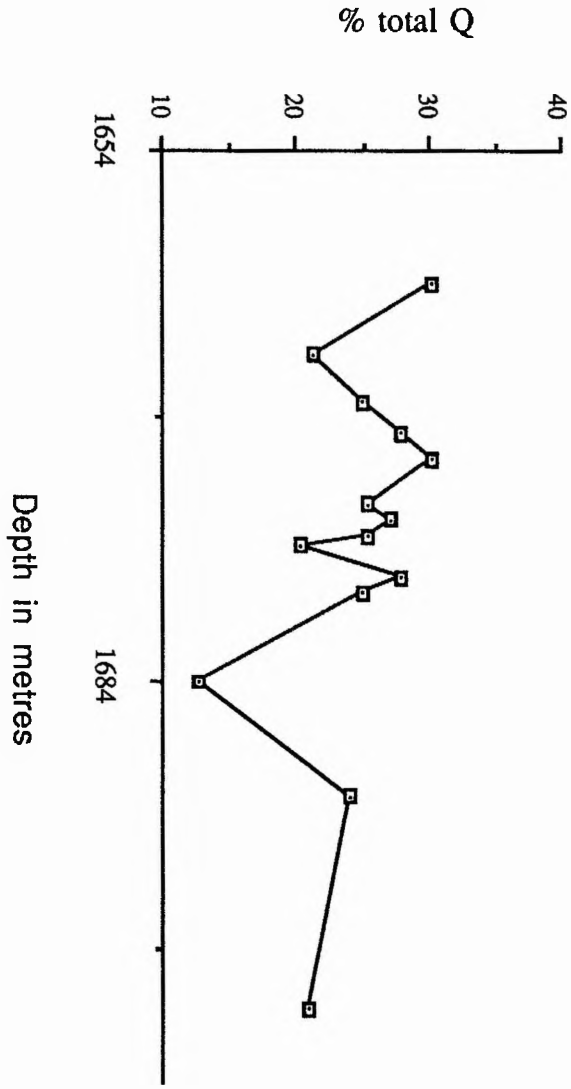

Fig 5.41 Graph showing the relationship between the total porosity (point count) and depth in core E

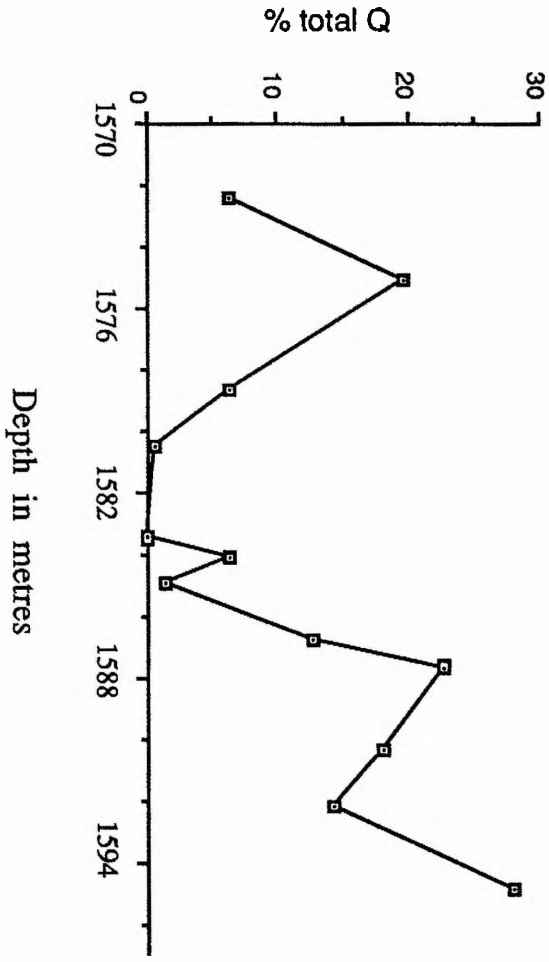

Fig 5.42 Graph showing the relationship between the total porosity (point count) and depth in core F

produces a high value in the top part of the core), moldic, and vuggy porosities (**Appendix 6.5**).

The low value at 1684 m is related to the absence of the intracrystalline and lower intercrystalline and moldic porosities.

The presence of anhydrite which fills the interparticle pores is also added to the factors lowering the porosity at this depth. The intracrystalline porosity in this core is important and reached a value of 15% at the depth of 1670 m.

The total porosity in core **F** in general is low. The low values in the middle of **Fig 5.42** are related to the limestone which is formed of fine crystalline algal mudstone in which the molds are filled with mosaic calcite cement.

Dolomitization is partial in this core and the dolomite percentages in the best case reachs the value of 22.33%.

Below these values a high porosity is related to the high dolomitization of the rock which has very high intercrystalline and moldic porosities (**Fig 5.42**).

CHAPTER 6
DOLOMITE MODELS

6.1 Introduction

Dolomites have been found in diverse Recent sediments; in hypersaline supratidal flats, on the bottom of some freshwater lakes, and as a precipitate in some caves and freshwater springs as well as in the subsurface where mixing of fresh and salt waters occurred. It has been reported that many dolomites owe their origin to the reaction between calcium carbonate and hypersaline brines (see page 74).

Documentation of the growth of the dolomite crystals in hypersaline setting, has come from the study of recent tidal flats and sea side marginal pools along the Arabian Gulf and the Red sea (**Dunham and Olson, 1980**). Dolomite forms as a primary precipitate i.e has nucleated and grown in open water, in a few areas of the world. In the Coorong region of south Australia, fine grained whiting containing dolomite has been observed. In the Baffin Bay area, thin beds of pure dolomite interbedded with terrigenous muds have been found, and interpreted as a primary dolomite, or as result of the total replacement of carbonates.

There is however general agreement that dolomite in ancient rocks is a replacement product, and that a relatively insignificant amount of ancient dolomite is truly primary (**Zenger *et al*, 1980**).

A great variety of models for dolomite formation have been suggested to explain the origin of different types. The models will

be discussed with the aim of choosing the most appropriate to explain the dolomite of the Euphrates Limestone Formation.

6.2 Types of models

A number of conditions are required for any valid model of dolomitization. The conditions required, very simply are, a source for Mg^{2+}, a delivery mechanism to bring the Mg^{2+} and a small amount of CO_3 ions to the dolomitization site, and finally the solution must have a composition conducive to dolomitization (**Morrow, 1982b**). The more important factors which control dolomitization process are, temperature, solution composition, and the rate of crystallization. The major models set up for dolomite formation and which will be discussed here are; the **hypersaline model (Primary precipitation, Seepage reflux , Capillary concentration, and evaporative pumping models) and the non-hypersaline model (mixing or Dorag model).**

6.2.1 Hypersaline model:

Many supratidal sediments of the tropics contain dolomites as very small rhombs usually replacing fine grained aragonite. In arid regions (e.g. Arabian Gulf) this dolomite is usually found within the soft sediments in the intertidal and low supratidal areas of the tidal flats. Whereas in humid climates (Caribbean) the dolomites occur more commonly as a surfacial crust on supratidal flats. During early diagenesis the nucleation rate of dolomite is high due to the easy access of magnesian ions through the soft sediments. For this reason the crystal size generally is small, but it

may increase by subsequent crystal enlargement (**Laporte, 1967**).

6.2.1.1 Primary precipitation

Precipitation of the primary dolomite from normal sea water in the present seas in not known. However, some evidence suggests that primary dolomite could be precipitated from brackish and hypersaline lakes (**Hardie, 1987**).

A primary dolomite has been claimed to have formed beneath the Baffin Bay in Holocene sediments (**Behren and Land, 1972**). The idea of primary dolomite, was accepted before the 60s, whereas the same idea was discounted after the 60s and 70s. Any way even if primary dolomite was formed in the past, it does not represent a significant contribution to the mass of ancient dolomites (**Chilingar *et al*, 1979**).

6.2.1.2 Seepage reflux

Seepage reflux was the first model proposed for dolomitization on a large scale (**Adams and Rhodes, 1960; King, 1947; Chilingar and Bissell, 1961; and Friedman and Sanders, 1967**) and as a major factor of dolomitization of the bedded Permian carbonates of west Texas.

The theory behind the model is that the evaporative shelf lagoon is isolated from the open sea by a shelf edge barrier reef, after which continuous evaporation produces highly alkaline, heavy, hot ($35^{o}C$ and above) and carbon dioxide free hypersaline brines. Precipitation of anhydrite and gypsum decreases the Ca^{2+}

concentration in the solution and consequently increases the Mg^{2+}/Ca^{2+} ratio to a value which may be several times (9.0) higher than in normal sea water.

Dolomite is formed because the higher Mg/Ca ratio overcomes the inhibiting effects of salinity (**Morrow, 1978**). These heavy brines are thought to sink and move in a seaward direction along the lagoon. The driving force for such seepage reflux is the greater density of the lake or the lagoon water over sea water. These refluxing brines continue to supply the Mg^{2+} for dolomitization and also remove the Ca^{2+} which occurs through a process of carbonate replacement.

Adams and Rhodes (1960) concluded that fossil lagoonal brines and filling of halites and anhydrite in the dolomite pores is a proof of the brine invasion, and any similar dolomite would have a comparable origin. This theory is supported by many authors. **Deffeys *et al* (1965)** claimed that this process is actually operating at the present on Bonair Island.

But **Lucia (1968)** found no dolomite in the subsurface in the Pekelmeer (Island of Bonair), therefore, Lucia observations are at variance with the seepage refluxion theory. Low permeability of the fine grained muds of this type of environment make it difficult to understand how enough Mg can be provided for the formation of thick sequences of early diagenetic dolomite.

6.2.1.3 Capillary concentration

Dolomite crusts are found on Bonair island, and as a well known feature of some sabkha e.g. as reported in the Arabian Gulf,

Trucial Coast , and from the Florida-Bahama areas. The origin of these dolomite crusts has been ascribed to a process of capillary concentration (**Shin and Ginsburg, 1964; Illing *et al*,1965**).

The theory behind the formation of the dolomite crusts claims that the strong evaporation of the interstitial pore water near the surface of supratidal flats causes a subsurface flow of the sea water in the landward direction beneath the sabkha in order to replace the water that lost by evaporation.

The Ca^{2+} is continuously removed from the solution by the formation of sulphate minerals and this will increase the Mg^{2+}/Ca^{2+} ratio in the lagoon. It is suggested that Mg^{2+} then reacts with the carbonate sabkha sediments (aragonite) to form dolomite.

The Ca- excess of the dolomites is influenced by the chemistry of the solutions, especially by the salinity; There an excess of calcium in this type of dolomite when first formed but with increasing aridity and salinity the Ca-excess in the dolomite lattice decreases as shown in the different modern examples.

During diagenesis, however the calcian excess decreases; this decrease is greater in porous rocks than rocks with low porosity and permeability.

6.2.1.4 Evaporative pumping

Hsu and Siegenthaler (1969) proposed the evaporation pumping model as an alternative to the seepage reflux process of dolomitization. This model is based on a series of experiments in the laboratory.

The theory of this model is that evaporative action on the sabkha provides the energy for the landward movement of subsurface marine waters during dry periods, in an arid coastal region underlain by sediments with saline pore water.

The basin would be separated from the sea by a barrier, therefore, the great water influx through the subsurface carbonates in the barrier would cause dolomitization. The process perhaps slows down when the basin fills with salts and porosity is very low.

Hsu and Siegenthaler suggested that the result of this process is the precipitation of evaporitic crusts on tidal flats. Some Recent and ancient dolomites are thought to have originated in this way (**Bathurst, 1975**).

6.2.2 Non hypersaline (Mixing Model)

Hypersaline models cannot be applied to all types of dolomites, especially those which are not associated with evaporites or lack the evidence of supratidal environments.

An alternative approach was needed; therefore much attention has been given to the effects of mixing waters which have different PCO2 values (**Holland *et al.*, 1964; Runnels, 1969; Matthews, 1971; Plummer, 1975**). **Hanshaw *et al.*, (1971)** proposed that dolomite could form from brackish water in a mixing zone where the Mg/Ca ratio is greater than 1:1.

In this subsurface zone, cyclic flow of water is important to nucleate dolomite crystals. The supply of magnesium leads to dolomitization.

The great advantage of the mixing model is that very large scale dolomitization may result at the junction of the fresh phreatic and marine ground water realms (**Leeder, 1982**).

Modern examples of dolomitization at these junctions are known in the Jamaican and Florida aquifers (**Land, 1973; Hanshaw *et al*, 1971; Randazzo and Heckey, 1978**). The most popular type of mixing model was named the Dorag, the Persian word for hybrid.

6.2.2.1 Dorag model

Badiozamani (1973) studied the mixing of ground meteoric water with sea water and concluded that a mixture which contains between 5% and 30% sea water is undersaturated with respect to calcite, but may be many times supersaturated with respect to dolomite, and will result in dolomite precipitation. This model is known as **Dorag model**, and was applied by Badiozamani to the Middle Ordovician Champlainian series of the southern Wisconsin.

At progressively reduced salinities dolomite is able to nucleate at low Mg^{2+}/Ca^{2+} ratios approaching 1:1 and when the rate of crystallization is low.

The dolomite spar and microspar crystals that are thought to result from the mixing process are perfectly formed, clear and, if precipitated in cavities euhedral. They show perfect stoichiometry because of slow precipitation (**Leeder, 1982**).

The absence of impurities in the fresher waters may allow clean, inclusion free rhombs of well ordered dolomite to form.

These limpid dolomite crystals are less soluble than most sedimentary dolomites (**Scoffin, 1987**).

Land (1973) reported that the mixing waters are the mechanism responsible for dolomitization of the Pleistocene reef rocks in Hope Gate Formation, the north coast of Jamaica. His idea was that a mixture of meteoric water with as little as 3% sea water would be oversaturated with respect to dolomite.

6.3 Euphrates Dolomitization Model

The evidence for persistent hypersalinity in any depositional environment is shown by the presence of evaporite minerals associated with very finely crystalline dolomite (**Dunham and Olson, 1980**). In the present study the Euphrates Limestone Formation dolomite is strongly associated with evaporite minerals as cement, nodules, and replacement, and the formation is covered by a massive anhydrite bed. A restricted fauna, and birds eye structure, features of typical hypersaline origin dolomites are present in the formation. (**Laporte, 1967**). Therefore, it is very clear that any model to be proposed for Euphrates dolomitization should involve hypersaline diagenesis except perhaps for minor occurrences of very fine dolomite usually found at the very top of the formation and which may have formed as a primary precipitate.

The dolomite is not mimetic of the precursor carbonates, therefore it is not of a dissolution precipitation process. On the other hand the second generation of dolomite is limpid and was probably precipitated as cavity fillings or as a cement (which have

been found to be formed from meteoric waters on cave walls (**Vernon, 1965**).

Some of the dolomite of the Euphrates Limestone Formation is very fine crystalline especially at the top of the formation (Core **D**), and associated with anhydrite nodules. Some of the dolomite can be of replacive origin because it replaced all the ooids and the skeletal fragments, none of which is known to be formed as dolomite, but all originally formed as calcite and aragonite and were later replaced by dolomite after deposition and cementation. In modern carbonate terrains, ooids predominate in areas of hypersaline waters (**Lees, 1975**) such as the Gulf of Suez. (**Friedman and Sanders, 1978 p.53**) in the Arabian Gulf (**Loreau and Purser, 1973**).

The presence of ooids has been used as an empirical indicator of elevated salinities and temperatures. Examples of ooids include those of Whitehall Formation, Upper Cambrian-Lower Ordovician, (**Rubin and Friedman, 1977**) and they are found in the Euphrates Limestone Formation. Presence of stromatolites has been interpreted as indicating a hypersaline facies (Tribes Hill Formation, **Braun and Friedman, 1969, and Friedman and Braun, 1975; Whitehall Formation, Rubin and Friedman, 1977**). The Euphrates Limestone Formation contains indications of stromatolites.

In core **D** dolomitization is pervasive and no calcite has been found at all in the upper 2/3 of the Euphrates Formation (except at the bottom of the core). In some cases the dolomite crystals are of large size which probably indicates (neomorphism)

recrystallization. The porosity of this upper part is very high. The oolitic fossiliferous grainstone texture of the precursor carbonate is obliterated but still identifiable.

The isotopic data have shown that the average $\delta^{13}C$ of the dolomite is (1.96 ± 0.99 ‰) and the average $\delta^{18}O$ is (1.95 ± 1.01‰). The isotope data are much heavier than those of mixing zone dolomite (Land, 1973, 1875) but they do resemble the isotopic values associated with sabkha environments. Correspondence is even closer when it is recognized that like the Abu Dhabi sediments the Euphrates dolomites will have become slightly lighter with age as they equilibrate with lighter waters (McKenzie, 1981).

Dolomite also shows a good stoichiometry, and is relatively well ordered. The dolomite in core D is very porous and nearly stoichiometric. The decrease of the Ca excess in the dolomite lattice may be taken as an indicator of high aridity and salinity aided by the high porosity of the sediments.

Euphrates Formation dolomite may have been formed as a syngenetic dolomite. This is indicated by the presence of very fine dolomite lacking any skeletal fragments, or even any dust lines which may be an indicative of presence of skeletal precursor. This type of dolomite is usually found interbedded and interfingered with marine evaporites (Friedman and Sanders 1967, see Hardie, 1987).

The dolomite of the Euphrates Formation is not epigenetic because it is not localized by faults or fractures. Dolomitization occurred after the formation of the isopachous crust cement which

is a characteristic feature of the marine phreatic diagenesis (Friedman and Sanders 1967) and present in almost all the carbonate grains of the Euphrates Limestone Formation.

Paleogeographic studies have shown that the Euphrates Limestone Formation was deposited in a restricted lagoon separated from the sea by a barrier reef. With time conditions became more arid and led to the deposition of the Dhiban Anhydrite Formation, with alternating massive anhydrite and limestone.

The most favourable model for the Euphrates Limestone Formation is regarded the seepage reflux model which operated during the persistence of lagoonal conditions; later, during the formation of the sediments of the Dhiban anhydrite formation further hypersaline brines percolated down from the sabkha environments.The ability of the seepage reflux model to produce massive dolomites has been questioned but Sears and Lucia (1980) concluded that magnesium supply from a reflux model is 1000 times greater than from mixing model. They also suggested that reflux by hypersaline brines was necessary to produce massive dolomite in the Niagara reefs; such massive dolomite are also found in the Euphrates Limestone Formation. The Euphrates Limestone Formation(like the Niagara sediments, shows evidence of later mixing indicated by strong dissolution effects and the formation of limpid crystals recognized here as of a later, second generation.

Because the Euphrates Limestone Formation dolomite is close to ideal stoichiometry and displays well ordered structure, it

Because the Euphrates Limestone Formation dolomite is close to ideal stoichiometry and displays well ordered structure, it seems reasonable to conclude that the Euphrates dolomites were initially enriched in $Ó^{18}O$ but subsequent diagenesis (aging) resulted in the present stoichiometry, and a slight reduction in the oxygen isotope value.

In summary most of the dolomite of the Euphrates Limestone Formation was formed by hypersaline solutions developed first in a lagoon affected by strong evaporation; second by solutions formed in the sabkha environment in which the overlying Dhiban evaporites accumulated.

In view of the present knowlege, limpid dolomite has taken as a product of the mixed water environment. If this is true there must have been a phase of mixing of freshwater and marine water.

CHAPTER 7

SUMMARY AND CONCLUSIONS

Euphrates Limestone Formation of Lower Miocene age is encountered at depth in Jambur area in a structure extending in a general NW-SE direction.. Eight cores (A, B, C, D, E, F, G, and H) were examined during the present study and a total of 170 samples were collected from these cores.

The Euphrates Limestone Formation is overlain by Dhiban Anhydrite Formation which is itself overlain by the transgressive Jeribe Limestone Formation.

Tertiary sediments were laid down in a broad basin trending in general NW-SE direction. This basin was formed during the upper Cretaceous and continued throughout Tertiary times. Facies distribution in the trough was controlled by a series of shoals and islands along the eastern shore of the trough. These shoals and islands separated the open sea in the west from a more or less lagoonal area to the east or northeast.

At the end of the Oligocene a regression occurred in the Kirkuk area which is marked by a conglomerate separating the Euphrates Limestone Formation from the Anah Formation.

An important transgression followed and introduced the Lower Miocene sediments including the Euphrates Limestone Formation which was deposited in a belt varying in width between 10-20 Km in Kirkuk area.

Toward the west of this area the off-shore equivalent Serikagni Formation was laid down. These two formations were

deposited in a shallow sea which was bordered by fairly wide lagoon. To the west of the coast line and seawards, the top of the Euphrates Limestone Formation passes laterally into Dhiban Anhydrite Formation. A complete succession of Euphrates, Dhiban, and Serikagni is found in Injana, Pulkhana, and Jambur areas.

Precipitation of the Dhiban Anhydrite Formation is thought to be due to complete or partial closure of the exit between the lagoon and the open sea.

The Dhiban Anhydrite Formation shows frequent facies change which may be caused be the oscillation in the depth of the sea. Evaporite sedimentation was followed by a major transgression probably caused by the opening of the barrier between the lagoon and the open sea.

A short period of regression at the end of Lower Miocene occurred in Kirkuk area resulting in the erosion of exposed Eocene and some Oligocene formations and L Miocene.

The Euphrates Limestone Formation is composed of different facies, grainstone, packstone, wackestone, mudstone, and boundstone which are in all cases fossiliferous. These facies indicate that the formation was deposited in a shallow marine environment.

Three different types of the dolomite texture have been described in the present study according the dolomite crystal size; fine (4-10 microns), medium (10-30 microns), and coarse (50-100 microns). and these are termed **A**, **B**, and **C** respectively.

Dolomite has been classified into eight different dolomitization fabrics according to the degree of dolomitization. Type 1

represents the onset of dolomitization, type 2 in which the ground mass is completely dolomitized whereas the bioclastic and lithoclastic grains are not, type 3 in which the groundmass is completely dolomitized and the skeletal grains are partially dolomitized, type 4 in which dolomitization is so intensive that the internal structure of the skeletal grains is obliterated, type 5 in which dolomitization has obliterated the boundaries of the grains, type 6 in which dolomitization has completely obliterated the boundaries of the grains and only the ghosts of the grains can be seen, type 7 in which dolomitization has completely altered the original structure of the original sediments, type 8 in which the dolomite also fills the voids and vugs. These types are compared with **Shukla (1980)** types.

Dolomitization is extensive and pervasive in cores **A, B, D, E** in southeast of the studied area, and partly in **F** in the centre, but very weak and partial in cores **G**, and **H** to the northwest of the studied area. Therefore , three different areas are identified in the present work and these are named area 1 (in the southeast), area 2 (in the centre), and area 3 (in the northwest)

From petrographic studies hollow dolomite rhombs have been identified and found abundant in the Euphrates Limestone Formation. These rhombs can be easily seen under the optical microscope, and their detail under the scanning electron microscope. A variety of shapes of partially and completely dissolved dolomite rhombs have been recognized. The hollow rhombs are found associated with totally dolomitized and porous sediments and with abundant anhydrite cement. The selective

dissolution took place due to structural rather than compositional differences. It is suggested that the presence of trapped fluid inclusions or other more subtle defects in the lattice allowed selective dissolution of parts of the rhombs. Some of the hollow dolomite rhombs are filled with hydrocarbon, whereas in other cases they are empty. These hollow dolomite crystals can contribute to the total porosity in the Euphrates Limestone Formation.

Geochemical studies show that the dolomite is well ordered in the southeast part of the studied area. Nearly stoichiometric dolomite has been found in the present study which falls in the range of 49.66 to 51.7 mole % CaCO3, but in the central and northwest part there is a calcium-rich dolomite which ranges from 52 to 58 mole % CaCO3. The proportion of calcium in the dolomite lattice correlates with the higher amount of remnant calcite.

Anhydrite is present as thin beds in core **D** and at the top throughout the studied area. Anhydrite beds are also present in core **E** within the formation and thought correlatable with the beds in core **D**. The anhydrite percentages decrease toward the central area (**core F**), and are very low to absent in cores **G** and **H** except at the top of the formation which is usually covered by anhydrite beds.

Trace elements studied in the present work show that the dolomite contains an exceptionally high concentration of strontium. At 260-800 ppm.the very high values recorded are thought to be associated with the mineral celestite.

The high concentration of strontium is thought to be due to hypersaline brines responsible for dolomite precipitation which were also enriched in strontium.

The limestones of the Euphrates Limestone Formation contain an unusually low strontium concentration. This is thought probably due to the exposure of the limestone to freshwater, during the regression at the end of L. Miocene.

Oxygen isotopes show that the dolomite contains a relatively high values of oxygen isotopes ranging from 0.23 to 3.57‰. These are clearly heavier than most of the normal marine sediments and are as heavy as the present Recent hypersaline dolomite. The heavy isotopes values suggest that the dolomite of the present study has been formed by hypersaline solutions produced in a lagoonal environment which has undergone strong evaporation and later from hypersaline brines of the Dhiban sabkha environment that percolated downward through the underlying carbonate sediments and caused diagenetic replacement.

The Euphrates Limestone Formation has been subjected to a variety of diagenetic processes, including cementation, dissolution, compaction, neomorphism, precipitation of evaporite and dolomitization.

Marine diagenesis in the Euphrates Limestone Formation is evident from the presence of the micritic envelopes and isopachous crust cement, a characteristic feature of this type of environment and diagenesis.

Very high moldic porosity and dissolution, coupled with mosaic and syntaxial cements are indications of the meteoric phreatic environment and diagenesis.

Some compaction is indicated by grain breakage and interpenetration of some grains.

Anhydrite cementation is very extensive in the southern area but very scarce in the northwest area.

Dissolution of the anhydrite cement created a high moldic and vuggy porosity. Pyrite of different forms is found and probably formed over some time.

Various types of porosity are seen in the Euphrates Limestone Formation including intercrystalline, intracrystalline, interparticle, intraparticle, moldic, vuggy, and fracture porosity. The overall porosity is high in the southeast part of the studied area and negligible in the northwest part (cores **G**, and **H**). Intercrystalline porosity forms an important part of the overall porosity in certain cases and reaches up to 15 % (core **E**). Only dolomite at the upper part of the formation may have formed as direct precipitate. The dolomite generally in the present study is believed to have formed due to an evaporation process, which produced hypersaline brines. Downward percolation of these brines caused diagenetic replacement of the carbonate sediments. In terms of models, the characteristics described in the present study suggest that most of the dolomite formed due to hypersaline environments which persisted for a long time.

The suggested model is one of seepage reflux, followed by a sabkha environment, and much later by schizohaline conditions.

REFERENCES

Adams, J. E. and Rhodes, M. L., 1960. Dolomitization by seepage refluxion. Bull. Am. Assoc. Petrol. Geologists, v. 44: p. 1912-1920.

Alderman, A. R. and Skinner, H. C. W., 1957. Dolomite sedimentation in the southeast of south Australia. Am. J. Sci., v. 255: p. 561-567.

Alexandersson, T., 1975. Marks of unknown carbonate-decomposing organelles in Cyanophyte borings. Nature, v. 254, 212, p. 237-238.

Alexandersson, T., 1972. Intragranular growth of marine aragonite and Mg-calcite: evidence of precipitation from suprsaturated sea water: Jour. Sed. Petrology, v. 42, p. 441-446.

Al Hashimi, w.S., 1976. Significance of strontium distribution in some carbonates rocks in the Carboniferous of Northumberland, England. Jour. Sed. Petrology, v. 46, p. 369-376.

Al Naquib, K. M., 1959., Geology of the Southern area of Kirkuk Liwa, Iraq:1st Arab Petroleum cong. (Cairo), Proc, p. 1-50.

Andrews, J. E., Hamilton, P. J. and Fallick, A. E, 1987. The geochemistry of early diagenetic dolostones from a low salinity Jurassic lagoon. Jour. Geol. Soc., London, v. 144, p. 687-698.

Badiozamani, K., 1973. The Dorag dolomitization Model-Application to the Middle Ordovician of Wisconsin. Jour. Sed. Petrology, v. 43: p. 65-984.

Badiozamani, K., and Thorstenson, D.C., 1977. Experimemtal carbonate cementation, salinity, temperature and vadose phreatic effects. Jour. Sed. Petrology, v. 47, p. 529-557.

Bathurst, R. G. C., 1967. Oolitic films on low energy carbonate sand grains, Bimini lagoon, Bahamas. Marine Geol., v. 5, p. 89-109.

Bathurst, R. G. C., 1983. Early diagenesis of carbonate sediments *in*:: Parker, A. and Sellwood, B. W. (eds.), Sediment diagenesis. Reidel Publishing Company, p. 349-377.

Bathurst, R. G. C., 1966. Boring algae, micritic envelopes and lithification of molluscan biosparites: Geol. Jour., v. 5, p. 15-32.

Bathurst, R. G. C., 1975. Carbonate sediment and their diagenesis, 2nd ed.: Elsevier, Amsterdam, 658 p.

Bellen, R. C. Van. 1959. Lexique Stratigraphique International ASIE Fasc.10a Centre De La Recherche Scientifique. Paris, p. 333.

Berner, R. A. 1965. Dolomitization of the Mid Pacific Atolls. Science, v. 147: p. 1297-1299.

Berner, R. C., 1970. Sedimentary pyrite formation. Am. J. Sci. v. 208, p.1-23.

Berner, R. A., 1971. Principles of Chemical sedimentolgy. McGraw-hill, New York, N, Y., 240 P.

Behrens, E. W. and Land, L. S., 1972. Subtidal Holocene dolomite, Baffin Bay, Texas, Jour. Sed. Petrology, v. 42: p. 155-161.

Braun, M. and Friedman, G. M., 1969. Carbonate lithofacies and environments of the Tribes Hill Formation (Lower Ordovician.) of the Mohawk Valley, New York: Jour. Sed.Petrology, v. 39, p.113-135.

Bricker, O. P., 1971. Carbonate cements: John Hopkins Press, Baltimore, Md., 360p. Hopkins Univ., 376 p.

Buday, T., 1980. Regional Geology of Iraq. Baghdad-Mosul. p.445.

Busenberge, E. and Plummer, L. N. 1982. The kinetics of dissolution of dolomite in CO2-H2O system at 1.5 to 65°C and 0 to 1 ATM PCO_2. Am. J. Science, v. 282, p. 45-78.

Butler, G. P., 1969. Modern evaporite deposition and geochemistry of coexisting brines, the sabkha, Trucial Coast, Arabian Gulf: Jour. Sed. Petrology, v. 39, p. 70-89.

Butler, G. P., Harris, P. M., and Kendall, C. G. St. C., 1982. Recent evaporite from the Abu Dhabi Coastal flats. *in* : Depositional and diagenetic spectra of evaporites: A core workshop. SEPM., No.3, p. 33-64.

Chafetz, H. S., McIntosh, A. G., and Rush, P. T. 1988. Freshwater phreatic diagenesis in the marine realm of Recent Arabian Gulf carbonates. Jour. Sed. Petrology, v. 58, no. 3, p. 433-440.

Chilingar, G., and Bissell, H. J., 1961. Dolomitization by seepage refluxion (Discussion). Bull. Am. Assoc. Petrol. Geologists, v. 45 (5), p. 679-681.

Chilingar, G. V., Zenger, D. H., Bissell, H. S., And Wolf, ., 1979. Dolomites and dolomitization. *in* : Larsen, A. G., and Chilingar, G. V. (eds.). Diagenesis in sediments and sedimentary rocks; Dev. in Sedimentology, v. 25, Elsevier, Ametwrdam, p. 423-536.

Choqutte, P. W., and Pray, L. C., 1970. Geologic nomenclature and classification of the porosity in sedimentary carbonates: Bull. Am. Assoc. Petrol. Geologists, v. 54, p. 207-250.

Clark, D. N., 1979. Patterns of porosity and cement in ooid reservoir in Dogger (Middle Jurassic) of France: Discussion, Bull. Am. Assoc. Petrol. Geologists, v. 63, p. 676-679.

Clark, D. N., 1980. The diagenesis of the Zechstein carbonate sediments. *in*: The Zechstein Basin. Fuchtbauer, H., and Peryt, T. Stuttgart,1980. p. 167-203.

Clark, D. N., and Tullbacka, L., 1980. The Zechstein deposits of southern Denmark. *in* : The Zechstein Basin, Fuchtbauer, H., and Peryt T. (eds). Stuttgart, 1980. p. 205-231.

Coogan, A. H., 1970. Measurements of compaction in oolitic grainstone; Jour. Sed. Petrology, v. 40, p. 921-929.

Ctyrocky, P ,and Karim, S. A., 1971a. Stratigraphy and paleontologyof the Oligocene and Miocene strata near Anah, Euphrates valley. NIMCO Report, SOM. library, No. CZ104, Baghdad.

Craig, H., 1957. Isotopic standards for carbon and oxygen, correction factors for mass spectrometric analysis of carbon dioxide. Geochim Cosmochim Acta, v. 12, p. 133-49.

Deffeyes, K. S., Lucia, F. J. and Weyl, P. K.,1964. Dolomitization: observations on the Island of Bonaire, Netherland Antilles. Science, v. 143: p. 678-9.

Deffeyes, K. S., Lucia, F. J. and Weyl, P. K., 1965. Dolomitization of the Recent and Plio-Pleistocene sediments by marine evaporative waters on Bonaire, Netherlands Antilles. *in* : L. C. Pray and R.C. Murray (eds.). Dolomitization and limestone diagenesis; Soc. Econ. Palaeon. Mineral. Spec. Publ., No.13, p. 71-88.

Dickson, J. A. D., 1965. A modified staining technique for carbonates in thin section. Nature, 205, 587.

Dorobek, S. l. , and Read, J. F., 1986. Sedimentology and Basin evolution of the Siluro-Devonian Elderberg goup, central Appalichians. Jour. Sed. Petrology, v.56, p.601-613.

Dickson, J. A. D., 1966. Carbonate identification and genesis as revealed by staining. Jour. Sed. Petrology, v. 36, p. 491-505.

Drever, J. I.,1982. Geology of natural waters.USA. Prentice-Hall international Inc.

Dunham, J. B., Oslon, F. R. 1980. Shallow subsurface dolomitization of subtidally deposited carbonate sediments in the Hanson Creek Formation (Ordovician-Silurian) of central Nevada *in* : Zenger, D. H., Dunham,J. B. and Ethington, R. L. (eds.). Concepts and models of dolomitization. Soc. Econ. Paleon. Mineral. Spec.Publ. No. 28, p.139-161.

Dunham, R. J., 1962. Classification of carbonate rocks according to depositional texture. *in* : W.E. Ham (ed.), Classification of carbonate rocks. Am. Assoc. Petrol. Geologists Mem. 1, p. 108-121.

Dunnington, H. V., 1958. Generation, migration, accumulation, and dissipation of oil in Northern Iraq. *in* ; Weeks, G. L. (ed). Habitate of Oil, a symposium. Am. Assoc. Petrol. Geologists. Tulsa. p. 1194-1251.

Dunnington, H. V., 1967. Stratigraphic distribution of oil fields in Iraq, Iran, Arabia Basin. Jour. Inst. Petrol., v. 53, p.129-161.

Dunnington, H. V., 1967. Aspects of diagenesis and shap changes in the stylolitic limestone reservoirs: World petroleum Cong., 7th, Mexico City, 1967, Proc., v. 2, p.339-352.

Epstein, S., Graf, D. A., and Degens, E. T., 1964. Oxygen isotope, studies on the origin of dolomites. *in* : Craig, H., Miller, S.L., and Wasserburg, G.J. (eds.), Isotopic and cosmic chemistry: North Holland Publ. Co., Amsterdam, p. 169-180.

Evan, G. , and Shearman, D. J., 1964. Recent celestite from the sediments of the Trucial Coast of the Arabian (Pertian) Gulf. Nature, 202, p. 385-386.

Folk, R. L., and Land, L. S., 1975. Mg/Ca ratio and salinity: two controls over crystallization of dolomite : Bull. Am. Assoc. Petrol. Geologists, v. 59, p. 60-68.

Folk, R. L., and Siedlecka, A., 1974. The Schizohaline environment; its sedimentary and diagenetic fabrics as exemplified by Late Paleozoic rocks of Bear Island, Svalbard, Sed. Geology, v. 11, P. 1-15.

Friedman, G. M. and Braun, M., 1975. Shoaling and tidal deposits that accumulated marginal to the Proto-Atlantic ocean: the Tribes Hill Formation (Lower Ordovician) of the Mohawk Valley, New York. *in* : R. N. Ginsburge (ed.), Tidal deposits; a casebook of Recent examples and fossil counterparts: Springer-Verlag, New York-Hiedel bege-Berlin, p. 307-314.

Friedman, G. M., Amiel, A. J., And Schneidermann, N., 1974. Submarine cementation in reefs: example from Red Sea: Jour. Sed. Petrology, v. 44, p. 816-825.

Friedman, G. M. and Sanders, J. E., 1978. Principles of sedimentology. John Wiley and Sons, New York, 795p.

Friedman, G. M.1980. Dolomite is an evaporite mineral, evidence from the rock record and from the sea marginal ponds of the Red Sea. *in* : Zenger, D. H., Dunham, J. B. and Ethington, R. L. (eds.), Concepts and models of dolomitisation. Soc. Econ. Paleon. and Mineral. Spec. Publ., No. 28, p. 69-80.

Friedman, G. M. and Sanders, J. E., 1967. Origin and occurrence of dolostones: *in.*: G.V. Chilinger, H. J. Bissell and R. W. Fairbridge (eds.). Carbonate rocks, origin, occurrence and classification. Elsevier, Amsterdam, P. 267-348.

Friedman, G. M., 1964. Early diagenesis and lithification in carbonate sediments. Jour. Sed. Petrology, v. 34, p. 777-813.

Friedman, G. M., Gebelein, C. D., and Sanders, J. E. ,1971. Micritic envelopes of carbonate grains are not exclusively of photosynthetic algal origin: Sedimentology, v.16, P. 89-96.

Fritz, P. and Smith, D. G. W., 1970. The isotopic composition of secondary dolomites. Geochim. Cosmochim. Acta, v. 34: p.1161-1173.

Fuchtbauer, H.,1974. Sediments and sedimentary rocks. 2nd Ed.: Halsted Press,New York, 464 PP.

Fuchtbauer, H. and Goldschmidt, H., 1965. Beziehungen Zwishchen Calciumgehalt und Bildungsbedingungen der dolomite. Geo Rundschau, v. 55, p. 29-40.

Fuchtbauer, H., 1972. Influence of salinity on carbonate rocks in the Zechstein Formation, Northwestern Germany.*in* : G. Richter-Bernburg (ed.), Geology of saline deposits., Unesco, Paris, p. 23-31.

Gidman, J., 1978. Diagenesis of cored Pleistocene carbonate, Great Abaco Island, Little Bahamas Bank. (Unpubl.Ph.D.Thesis), University of Liverpool.

Ginsburg, R. N., and Schroeder, J. H., 1973. Growth and submarine fossilization of algal Cup reefs, Bermuda. Sedimentology, v. 20, p. 575-614.

Goldsmith, J. R. and Graf, D. L., 1958a. Structural and compositional variations in some natural dolomite. Jour. Geology, v. 66, p.678-693.

Goldsmith, J. R. and Graf, D. L.,1958b. Relation between lattice constants and composition of the Ca-Mg carbonates. American Mineralogist, v. 43, p. 84-101.

Hanshaw, B. B., Back, W. and Deike, R. G., 1971. A geochemical hypothesis for dolomitization by ground water. Econ. Geol. v. 66, p. 710-724.

Hardie, L. C., 1987. Perspectives; dolomitization: A critical view of some current views. Jour. Sed. Petrology, v. 57 (1), p.166-183.

Hay, J. T. C., and Hart, R. E., 1959. Final report on well Anah 2. MPC Repor, INOC library, No FWR7, Baghdad.

Heckel, P. H., 1983. Diagenetic model for carbonate rocks in Midcontinent Pennsylvanian Eustatic Cyclothems: Jour. Sed. Petrology, v. 53 (3), p. 0733-0759.

Herman, S. J., 1982. The dissolution kinetics of calcite, dolomite, and dolomitic rocks in CO2- water system. Unpubl. Ph.D. Thesis, The Pennsylvania State University.

Henson, F. R. S., 1950. Cretaceous and Tertiary reef formation and associated sediments in Middle East. Bull. Am. Assoc. Petrol. Geologists : v. 34 (2), p. 215-238.

Henson, F. R. S., 1951. Observation on the geology and petroleum occurrences of the Middle East, Proc. Third World Petrol. Cong. Sec. 1B, p.118-140.

Holland, H. D., Kirsipu, T. V., Huebner, J, S. and Oxburgh, U. M.,1964. On some aspects of the chemical evolution of cave water. J. Geol., v. 72, p. 36-67.

Hudson, J. D., 1977. Stable isotopes and limestone lithification. Jour. Geol. Soc., London, v. 133, p. 637-660.

Hsu, K. J., and Siegenthaler, C., 1969. Preliminary experiments on hydrodynamics movement induced by evaporation and their bearing on the dolomite problem. Sedimentology, v.12, p. 11-25.

Illing, L.V., 1954. Bahamian calcareous sands. Bull. Am. Assoc. Petrol. Geologists, v. 38, p.1-95.

Illing, L. V., Wells, A. J., and Taylor, J. C. M., 1965. Penecontemporaneous dolomite in the persian (arabian) Gulf. *in* : Pray, L. C., and Murray, R. C. (eds.), Dolomitization and limestone diagenesis: Soc. Econ. Paleon. Mineral. Spec. Publ., No. 13, p. 89-111.

James, N. P., Ginsburg, R. N., Marszalek, D. S., and Choquette, P. W., 1976. Facies and fabric specificity of early subsea cements in shallow Belize (British Honduras) reefs. Jour. Sed. Petrology, v. 46, p. 523-544.

Jones, B. F., 1961. Zoning of saline minerals at Deep Spring Lake, California. U.S., Geol. Surv., Profess. papers, 424-B: 199-209.

Jones, B. F.,1965. The hydrology and mineralogy of Deep spring lake, Inyo County, California. U.S. Geol. Survey, Profess. Papers, 205-A:1-56.

Jumaily, R, Al., 1974. Report on the Regional geological mapping of the area of the Iraqi-syrian border-T1 oil pumping station (western Desert). NIMCO Report, SOM library, Baghdad.

Kaldi, J., and Gidman, J., 1982. Early diagenetic dolomite cements, examples from the Permian Lower Magnesian limestone of England and the Pleistocene carbonates of the Bahamas. Jour. Sed. Petrology, v. 52(4), p. 1073-1085.

Katz, A., and Matthews, A., 1977. The dolomitization of $CaCO_3$: An experimental study at 252-295°C, Geochim. Cosmochim. Acta, v. 41, p. 297-308.

Keith, M. L., and Weber, J. n., 1964. Carbon and oxygen isotopic composition of selected limestones and fossils. Geochim. Cosmochim. Acta, v. 28, p. 1787-816.

King, R. H., 1947. Sedimentation in Permian Castile Sea. Bull. Am. Assoc. Petrol. Geologists, v. 31, p. 470-477.

Kinsman, D. J . J., 1964. Recent carbonate sedimentation near Abu Dhabi, Trucial Coast, Arabian Gulf. Thesis, Imp. Coll. Sci. Technol., Unpublished.

Kinsman, D. J. J., 1969. Modes of formation, sedimentary associations, and diagenetic features of shallow-water and supratidal evaporites: Bull. Am. Assoc. Petrol. Geologists, v. 53, p. 830-840.

Kinsman, D. J. J., 1969. Interpretation of Sr^{2+} concentration, in carbonate minerals and rocks. Jour. Sed. Petrology, v. 39, p. 486-508.

Kinsman, D. J. J., 1966. Gypsum and aragonite of Recent age, Trucial Coast, Persian (Arabian) Gulf. *in* : Second symposium on salt, J. L. Rau (ed.)., Cleveland Northern Ohio Geol. Soc. Ohio, p. 302-326.

Kobluk, D. R., and Kahle, C. F.,1978. Geological significance of boring and cavity dewelling marine algae : Bull Can. Petrol.Geology, v. 26, P.362-379.

Kobluk, D. R., and Risk, M. J., 1977. Micritization and carbonate grain binding by endolithic algae: Bull. Am. Assoc. Petrol. Geologists, v. 61, P. 1069-1082.

Land, L. S., 1966. Diagenesis of metastable skeletal carbonates. Thesis, Lehigh Univ. , Pa., 141pp.

Land, L. S., 1967. Diagenesis of skeletal carbonates. Jour. Sed. Petrology, v. 37, p. 914-930.

Land, L. S., 1970. Phreatic versus vadose meteoric diagenesis of limestones; evidence from a fossil water table. Sedimenetology, v.14, p.175-185.

Land, L. S., 1973a. Contemporaneous dolomitization of Middle Pleistocene reefs by meteoric water, North Jamaica. Bull.Marine Sci. Gulf Caribb., v. 23, p. 64-92.

Land, L. S., 1973b. Hollocene Meteoric dolomitization of Pleistocene limestone, N. Jamaica. Sedimentology, v. 20, p. 411-424.

Land, L. S., Salim, M. R. I. and Morrow, P. W. 1975. Paleohydrology of ancient dolomites: Geochemical Evidence: Bull. Am. Assoc. Petrol. Geologists, v. 59. p. 1602-1625.

Lands, L. S., 1980. The isotopic and trace element geochemistry, the state of art. *in* : Zenger, D.H., Dunham, J. B. and Ethington, R. L. (eds.) Soc. Econ. Paeontol. Mineral. Spec. Publ. No. 28, p. 87-110.

Laporte, L. F., 1967. Carbonate deposition near mean sea level and resultant facies mosiac: Manlius Formation (Lower Devonian) of New York State. Bull. Am. Assoc. Petrol. Geologists, v. 51, p. 73-101.

Leeder, M. R., 1982. Sedimentology: London, George Allen and Unwin, 344p.

Lees, A., 1975. Possible influence of salinity on modern shelf carbonate sedimentation; Marine Geology, v. 19, p.158-198.

Lloyd, R. M., 1966. Oxygen isotopes enrichment of sea water by evaporation. Geochim. Cosmochim. Acta, v. 30, p. 801-814.

Longman, M. W., 1980. Carbonate diagenetic textures from near-surface diagenetic environments: Bull. Am. Assoc. Petroleum Geologists, v. 64, p.461-487.

Longman, M. W., 1981. Carbonate diagenesis as a control on stratigraphic traps. AAPG. Education Course Note Series No. 21, 159p.

Loucks, R. G., and Budd, D. A., 1981. Diagenesis and reservoir potential of the Upper Jurassic Smackover Formation of south Texas: Tran. Gulf. Coast Assoc. Geol. Soc., 31st. Ann. Mtg., p. 339-346.

Loreu, J. P., and Purser, B. H., 1973. Distribution and ultrastructure of Holocene ooids in the (Arabian) Persian Gulf. *in* : Purser, B. H. (ed.), the Persian Gulf: Holocene carbonate sedimentation in a shallow epicontinental sea. Springer-Verlag, New York-Heidelberg-Berlin. p.279-328.

Lucia, F. J., 1968. Recent sediments and diagenesis of south Bonair, Netherlands Antilles. Jour. Sed. Petrology, v. 38, p. 845-858.

Lumsden, D. N., and Chimahusky, J. S., 1980. Relationship between dolomite non-stoichiometry and carbonate facies parameters. *in* : Zenger, D. H., Dunham, J. B. and Ethington, R. L. (eds). Concepts and models of dolomitization. Soc. Econ. Paleon. Mineral. Spec. Publ., No. 28, p.123-37.

Macintyre, J. G., 1977. Distribution of submarine cements in a modern Caribbean fringing reef, Galeta point., Panama. Jour. Sed. Petrology, v. 47, p. 503-516.

Matthews, R. K., 1971. Diagenetic environment of possible importance to the explanation of cementation fabric in subaerially exposed carbonate sediments. *in* : O. P. Bricker (ed.), Carbonate cements. John Hopkins Press, Baltimore, Md., p.127-132.

May, T. A., and Perkins, R. D., 1979. Endolithic infestation of carbonate substrate below the sediment-water interface. Jour. Sed. Petrology, v. 49, p. 357-377.

McCrea, J. M., 1950. The isotopic chemistry of carbonates and paleotemperature scale: Jour. Chem. Phys., v. 18, p. 849-857.

McKenzie, J. A., Hsu, K. J. and Schneider, J. F., 1980. Movements of subsurface waters under the sabkha, Abu Dhabi, and its relation to evaporative dolomite genesis: *in* : D. H. Zenger, J. B. Dunham and R. L. Ethington, (eds), Concepts and models of dolomitization. Soc. Econ. Paleon. Mineral. Spec. Publ. No.28, p. 11-30.

McKenzie, J. A.,1981. Holocene dolomitization of calcium carbonate sediments from the coastal sabkhas of Abu Dhabi, UAE. A stable isotope study. Jour. Geology, v. 89, p. 185-98.

Meyers, W. J., 1980. Compaction in Mississippian skeletal limestones, southern New Mexico. Jour. Sed. Petrology, v. 50, p. 457-474.

Monty, C. L. V., 1967. Distribution and structure of Recent stromatolitic algal mats, Eastern Andros Island, Bahamas. Ann. Soc. Geol. Belg., v. 90, p. 55-100.

Morrow, D. W.,1982b. Dolomitization models and Ancient dolostone. Geoscience Canada. v. 9, p. 94-107.

Morrow, D. W., 1978. The influence of the Mg/Ca ratio and salinity on dolomitization in evaporite basins: Bull. Can. Petrol. Geology, v. 26, p. 389-392.

Murray, R. C., 1960. Origin of porosity in carbonate rocks. Jour. Sed. Petrology, v. 30, no. 1, p. 59-84.

Olaussen, S., 1981. Formation of celestite in the Wenlock, Oslo Region, Norway, evidence for evaporite depositional environment. Jour. Sed. Petrology, v. 51 (1), p. 37-46.

Oldershaw, A. E. and Scoffin, T. P. , 1967. The source of ferroan and non-ferroan calcite cement in the Halkin and Wenlock Limestone. Geol. J., v.5, p. 309-320.

O'Neil, J. R., and Epstein, S., 1966. Oxygen isotope fractionation in the system dolomite-calcite carbon dioxide: Science, v.152, p. 198-201.

Pierre, C., and Rouchy, J. M., 1988. Carbonate replacement after sulphate evaporites in the Middle Miocene of Egypt. Jour. Sed. Petrology, v. 58, p. 446-456.

Pingitore, N. E. JR., 1976. Vadose and phreatic diagenesis: processes, products and their recognition in corals. Jour. Sed. Petrology, v. 46, p. 985-1006.

Plummer, L. N., 1975. Mixing of sea water with calcium carbonate ground water. Geol. Soc. Am., Mem., v.142, p. 19-236.

Pray, L. C., 1960. Compaction in calcilutites (abs.). Bull. Geol. Soc. America., v. 71, p.1964.

Prazak, J., 1974. Stratigraphy and paleontology of the Miocene of the Western Desrt, w.Iraq. NIMCO Report, SOM library, Baghdad.

Radke. B. M., 1978. Carbonate sedimentation in tidal and epeiric environments and diagenetic overprints: The Ninmaroo Formation (Upper Cambrian-Lower Ordovician), Central Australia. Ph.D. Diss., Rensselaer Polytechnic Institute, Troy, N. Y. 254p.

Randazzo, A. F., and Hickey, E. W., 1978. Dolomitization in the Florida aquifer. Am. Jour. Sci. v. 278, p. 1177-1184.

Rosen, M. R., and Holdren, G. R. JR., 1986. Origin of dolomite cement in Chesapeake Group (Miocene) siliciclastic sediments: An alternative model to burial dolomitization. Jour. Sed. Petrology, v. 56 (6), p. 788-798.

Royse, C. R., Wadell, J. S. and Petersen, L. E., 1971. X-Ray determination of calcite-dolomite: An evaluation. Jour. Sed. Petrology, v. 41, p. 483-88.

Rubin, D. M., and Friedman, G. M., 1977. Intermittently emergent shelf carbonates: an example from the Cambro-Ordovician of eastren New York State. Sed. Geology, v. 19, p. 81-106.

Runnells, D. D., 1969. Diagenesis, chemical sediments, and the mixing of natural waters. Jour. Sed. Petrology, v. 39, p. 1188-1201.

Schenk, C. J., and Richardson, R.W., 1985. Recognition of interstitial anhydrite dissolution. A case of secondary porosity, San Andres Limestone, New Mexico and Upper Minnetasa

Formation, Wyoming. Bull. Am. Assoc. Petrol. Geologists, v. 69 (7), p.1064-1076.

Schmidt, V., 1965. Facies, diagenesis and related reservoir properties in the Gigas beds (Upper Jurassic), northweastern Germany. *in* : Pray, L. C., and Murray, R. C.(eds.). Dolomitization and limestone diagenesis: Soc. Econ.Paleon. Mineral. Spec. Publ., No. 13, p.129-168.

Schreiber, B. C., Roth, M. S., and Helman, M. L., 1982. Recognition of primary facies characteristics of evaporites and the differentiation of these forms from diagenetic overprints. *in*:: Depositional and diagenetic spectra of evaporites: A core workshop. SEPM., No. 3, p. 33-64.

Scoffin, T. C., 1987. An introduction to carbonate sediments and rocks. Chapman and Hall, New York. p.33

Shearman, D. J., 1963. Recent anhydrite, gypsum, dolomite and halite from the coastal flats of the Arabian shore of the Arabian Gulf. Proc. Geol. Soc. London, 1607: p. 63-65.

Shearman, D. J., 1966. Origin of marine evaporites by diagenesis. Trans Inst. Mining Metall. Trans., v. 75B, p. 208-215.

Shearman, D. J., 1978. Evaporite of coastal sabkha in: W. E. Dean, and Schreiber (eds.). Marine evaporites. Soc. Econ. Paleontol. Mineral. Notes, No. 4, p. 6-42.

Sears, S. O., and Lucia, F. J., 1980. Dolomitization of northern Michigan Niagara reefs by brines refluxion and fresh water/ seawater mixing. *in* : Zenger, D. H., Dunham, J. B., and Ethington, R. L. (eds.). Concepts and models of dolomitization. Soc. Econ. Paleon. Mineral. Spec. Pub., No.8, p. 215-235.

Shinn, E. A., 1964. Recent dolomite, Sugarloaf Key. *In* : Guide book. for field Trip No.1. Geol. Soc. Am. Convention on 1964. Geol. Soc. Am. New York, N. Y., p.62-67.

Shinn, E. A., Ginsburg, R. N. and Lloyd, R. M., 1965. Recent supratidal dolomite from Andros Island, Bahamas. *in*: L.C. Pray and R. C. Murray (eds.), Dolomitization and limestone diagenesis: Soc. Econ. Paleon. Mineral., Spec. Publ., No. 13, p.112-123.

Shinn, E. A., Robbin, D. M., And Steinen, R. P., 1980. Experimental compaction of lime sediments : Am. Assoc. Petrol. Geologists and Soc. Econ. Paleon. Mineral. Ann. Mtg. Abstracts with Program, Denver, p. 783.

Shinn, E. A., 1983. Bridges, fenstrae, shrinkage pores, and loferites: A re-evaluation. Jour. Sed. Petrology, v. 52 (2), p. 619-628.

Shukla, V., 1980. Dolomotization in the Lockport Formation, Middle Silurian, in New York. Unpub. Ph.D. Thesis. Rensselaer Polytechnic Institute, Troy, N. Y.192p.

Shukla, V., and Friedman, G. M., 1983. Dolomitization and diagenesis in a shallowing upward sequence. the Lockport formation (Middle Sil.).: Jour. Sed. Petrology, v. 53, P. 0703-0717.

Sibley, D. F., 1982. The origin of common dolomite fabric; clues for the Pliocene. Jour. Sed. Petrology, v. 52, p. 1087-1100.

Sibley, D. F., and Gregg, J. M. 1987. Classification of dolomite rock textures. Jour. Sed. Petrology, v. 57, p. 967-975.

Siedlecka, A., 1972. Length-slow chalcedony and relics of sulphates-evidence of evaporitic environments in the Upper Carboniferous and Permian beds of Bear Island, Svalbad. Jour. Sed. Petrology, v. 42, p.812-816.

Skinner, H. C. W. , Skinner, B. J. and Rubin, M. , 1963. Age and accummulation rate of dolomite bearing carbonate sediments in south Australia. Science, v. 139, p. 335-336.

Steinen, R. P., and Matthews, R. K., 1973. Phreatic versus vadose diagenesis: Stratigraphy and mineralogy of a cored borehole on Barbados, West Indies, Jour. Sed. Petrology, v. 43, p.1012-1020.

Steinen, R. P., 1974. Phreatic and vadose diagenetic modification of Pleistocene limestone: petrographic observations from subsurface of Barbados, West Indies. Bull. Am. Assoc. Petrol. Geologists, v. 58, p.1008-1029.

Steinen, R. P., 1978. On the diagenesis of lime mud: Scanning electron microscopic observations of subsurface material from Barbados, WI. Jour. Sed. Petrology, v. 48, p. 1139-1147.

Supko, P. R., 1977. Subsurface dolomites; San Salvador, Bahamas. Jour. Sed. Petrology, v. 47, p. 1063-1077.

Swett, K., 1965. Dolomitization, silicification, and calcitization pattern in Cambro-Ordovician oolites Northwest Scotland. Jour. Sed. Petrology, v. 35 (4), p. 928-938.

Swirydczuk, K., 1988. Mineralogical control on porosity type in upper Jurassic Smackover ooid grainstone, southern Arkansas and northern Louisiana. Jour. Sed. Petrology, v. 58 (2), p. 339-347.

Tennant, C. B., and Berger, R. W., 1957. X-Ray determination of dolomite-calcite ratio of a carbonate rock. American Mineralogist, v. 42, p. 23-29.

Thrailkill, J., 1971. Carbonate deposition in Carlsbad caves. Jour. Sed. Petrology, v. 79, p. 683-695.

Tucker, M. E., 1981. Sedimentary petrology: an introduction. Blackwell Scient. Publication. 252p.

Vernon, R. H., 1969. The geology and hydrology associated with a zone of high permeability (Boulder Zone) in Florida. Soc. Mining Enginers. A. I. M. E., preprint 69-Ag-12.

Vaughan, D. J., and Turner, P., 1980. Diagenetic, Magnitization and mineralization of the Marl Slate. *in* : Fuchtbauer, H. and Peryt. T. (eds.).. The Zechstein Basin with emphasis on carbonate sequences. Stuttgart. p. 73-90.

Veizer, J., and Demovic, R., 1974. Strontium as a tool in facies analysis. Jour. Sed. Petrology, v. 44, p. 93-115.

Von Der Borch, C. C., and Jones, J. B. , 1976. Spherular modern dolomite from Coorong area, South Australia. Sedimentology, v. 23.

Ward, C. W., and Halley, R. B.,1985. Dolomitization in a mixing zone of near-seawater composition, Late Pleistocene, North eastern Yucatan Peninsula. Jour. Sed. Petrology, v. 55 (3), p. 0407-0420.

Weaver, C. E.,1975. Construction of limpid dolomite: Geology 3, p.425-428.

Weaver, C. E., and Beck, K. C., 1977. Miocene of the southeastern United States: A model for chemical sedimentation in a Peri-marine environment: Developments in Sedimentology No. 22: Amsterdam, Elsevier, 234p.

Weber, J. N., 1964c. Trace element composition of dolostones and dolomites and its bearing on the dolomite problem. Geochim. Cosmochim. Acta V. 28, p. 1817-1868.

Wells, A. J.,1962. Recent dolomite in the Arabian Gulf. Nature, 194: 274-275.

Wood, G. V., and Armstrong, A. K., 1975. Diagenesis and stratigraphy of the Lisburne Group Limestones of the Sadlerochit mountains and adjacent areas, north eastern Alaska. Geol. survey. prof. papers, 857, p. 1-41.

Zenger, D. H., Dunham, J. B., and Ethington, R. L., (eds.),1980. Concepts and models of dolomitization. Soc. Econ. Paleon. Mineral. Spec. Pub. No. 28, 320p.

Appendix 1 . Description of the methods and techniques used during the present work.

1.1 Staining

Chemical staining of thin section involve reaction of the solution with the minerals which will produce a coloured precipitate on the surface of the stained mineral surfaces , and that make them easily recognizable.

The thin section to be stained was left uncovered. Staining was carried out by using a solution of Alizarin Red S (0.2 gm of Alizarin Red S in 100ml of 1.5% hydrochloric acid) and potassium ferric cyanide (2 gm in 100 ml of 1.5% hydrochloric acid), the two solutions were mixed together in the proportion of two parts by volume of potassium ferric cyanide solution to three parts by volume of Alizarin Red S solution (Dickson, 1965, 1966). The sections were immersed in the combined solution for 30-40 seconds and rinsed with distiled water. In order to get a bright colour of stained sections, they were reimmersed for 10 seconds in a solution of Alizarin Red S, then the sections were finally rinsed with distiled water and dried as quickly as possible and covered. Calcite stains pink, ferroan calcite appear mauve to royal blue. Dolomite on the other hand is unstained, and ferroan dolomite stains to a pale to deep turquoise colour. Dickson (1966) pointed out that Alizarin Red S can differentiate between different bioclasts stains with different intensities, depending on their structure and the size of the crystallites.

1.2 scanning Electron Microscope (SEM)

Fresh specimens were taken for use on the scanning Electron Microscope (SEM), these specimens were cleaned with Dichloride methanole (Methylen Chloride CH_2CL_2). by immersing them in the solution for twenty four hours. If they are clean they were rinsed with water and dried in an oven. If they were not cleaned then immersion was repeated until they become clean. The samples with hydrocarbons needed several immersions before they were clean. The clean specimens were dried and mounted on certain stubs with a glue, then coated with a gold coating (5nml) thick.

1.3 Mass spectrometry

Dolomite and calcite samples were analysed for oxygen and carbon isotopes. The powder was finely grounded and heated to 450°C in a vacuum for 30 minutes in order to remove the organic matter. The carbon dioxide was extracted from samples by reacting them with 100% phosphoric acid in a vacuum by using the McCrea (1950) method at 25°C.

For samples which are mixture of calcite and dolomite, the gas evolved between 0-20 minutes of reaction was taken to represent the calcite. The gas evolved between 20 minutes and 72 hours reaction taken to represent the dolomite (Mckenzie, 1980). The recovered carbon dioxide gas was analysed on a Micromass isotope ratio mass spectrometer and reported as % PDB.

1.4 X-Ray difraction

Samples were ground to mean particle diametre 0f 5-10 microns grain size using a tungsten carbide mortar or the agate mortar, a certain amount of the powdered specimens was put in the sample holder and packed carefully with their surface as even as possible to get the best results. care must be taken in order not to damage the crystlllite because that will broaden the diffraction.

Analyses were made on a Phillips-PW 1010 X-Ray diffractometer with a monochromator Cu K radiation. A tube rating of 18 MA and a detector voltage of 36 KV were used. Sensitivity of $4x10^2$ trace on a scan between 5-70° at speed of 1°/ min. The quantitative analyses was made by the identification of the peaks, the measurement of 2Ø° and convertion of them to lattice spacing.

The position of the diffraction peaks is taken as the position of the point of greatest intensity. Dolomite, anhydrite and calcite percentages were calculated by using standard curve made up using internal standard minerals.

1.5 X-Ray fluorescence

Trace elements analysis was made on a pressed powder disc prepared for the better international standard by pressing 5 tons a powder mixed with 7-10 drops of movial plastic solution as a binder which will produce a stable self- supporting pellets. These pellets were placed in the oven until they dry and analysed against international standard samples using Phillips PW 1212

X-ray fluorescence spectrometer. The elements are excited with Rh tube and analysed with either L1F 200 or L1 f220 crystals. The apparent fluorescence values (AFV) are calculated for the better international standard by inverting the normal matrix correction against their intensities.

All intensities are calculated in terms of ratios to a monitor in the first sample position to eliminate the effects of machine drift. For consistency all calculations are performed by an on-line microcomputer.

1.6 Point count

This method has been chosen for petrographic study of the porosity with the light microscope. Three hundred poins were measured at 0.3 mm interval using a Swift automatic point counter. The results are tabulated in certain tables and the porosity percentages were calculated following the methods in Carver (1957).

Appendix 2 Table Showing the values of the mole percentages of $CaCO_3$ in the dolomite , the weight percentages of the dolomite in the core samples, and the ordering number of the dolomite samples of the Euphrates Limestone Formation.

Sample Number	Mole % $CaCO_3$	Weight % dolomite	Ordering No.
1R1	-	100	0.54
IR2	51.03	100	0.53
IR4	50.80	100	0.44
IR5	50.66	100	–
IR6	50.66	100	–
IR7	51.00	100	–
IR8	51.33	100	–
IR9	50.33	100	–
IR10	–	100	–
IR11	51.66	100	–
IR12	51.03	100	0.93
IR13	56.00	44	–
IR14	55.33	92.00	–
IR15	–	21.00	–
IR16	–	22.50	–
IR17	–	96.50	–
IR19	51.33	100	–
IR22	50.66	100	0.46
IR23	51.00	100	–
IR24	51.00	100	–
IR25	50.33	100	–
IR26	50.50	100	0.56
IR27	50.80	100	0.45
IR28	51.33	100	–
IR29	51.30	100	0.4
IR30	51.33	100	–
IR31	50.66	100	–
IR33	51.03	100	0.43
IR34	50.50	100	0.54
IR35	50.33	100	–
IR37	50.80	100	0.46
IR38	50.00	100	0.38
IR39	49.66	100	–
IR41	50.66	100	–
IR42	51.00	100	–

Sample Number	Mole % $CaCO_3$	Weight % dolomite	Ordering No.
IR43	50.66	100	–
IR45	50.80	100	0.46
IR46	50.80	100	0.48
IR47	50.66	100	–
IR48	50.00	100	–
IR49	51.03	100	0.47
IR50	50.33	92.00	–
IR51	50.00	100	–
IR53	–	100	0.50
IR54	51.00	100	–
IR55	50.66	100	–
IR56	–	100	0.59
IR57	52.00	100	–
IR59	50.66	100	0.60
IR62	–	100	0.70
IR63	–	100	–
IR64	–	49.00	–
IR65	–	100	–
IR66	51.03	100	0.40
IR67	–	100	–
IR68	–	100	0.45
IR69	56.73	41.00	–
IR70	–	54.00	–
IR71	50.80	100	0.44
IR72	50.80	100	0.44
IR73	51.33	100	–
IR75	51.00	100	–
IR76	50.33	–	–
IR77	50.80	100	0.52
IR79	–	–	0.39
IR80	–	100	0.46
IR82	50.66	100	–
IR84	50.80	100	0.48
IR85	50.80	100	0.50
IR86	–	100	0.89
IR87	–	100	0.45
IR88	51.03	100	0.47
IR89	50.66	100	–
IR90	50.33	100	–
IR91	50.00	100	–
IR92	–	100	–
IR93	51.00	100	–

Sample Number	Mole % $CaCO_3$	Weight % dolomite	Ordering No.
IR94	50.33	100	–
IR95	58.33	<4.00	–
IR96	–	76.00	–
IR97	–	54.00	–
IR98	–	55.00	–
IR99	–	40.00	–
IR100	–	57.00	–
IR101	–	45.50	–
IR102	53.33	90.00	–
IR103	56.00	44.00	–
IR104b	–	33.80	–
IR105	–	2.500	–
IR106	–	3.500	–
IR107	–	44.99	–
IR109	55.00	51.50	–
IR110c	50.66	100	–
IR111	55.00	89.00	–
IR113	–	100	–
IR114	50.66	100	–
IR115	51.00	100	–
IR116	53.00	94.00	–
IR117a	–	100	–
IR117b	54.66	79.00	–
IR118a	55.00	37.00	–
IR118b	54.66	49.00	–
IR119	–	0.00	–
IR120	–	47.50	–
IR121	–	5.00	–
IR122	58.33	5.00	–
IR123	–	5.00	–
IR124	–	5.00	–
IR125	–	0.00	–
IR126	–	12.50	–
IR127a	–	12.00	–
IR128	–	9.50	–
IR129	–	64.30	0.55
IR130	–	4.00	–
IR132	–	0.00	–
IR133	–	4.50	–
IR134	56.50	28.00	–
IR135	56.23	7.00	–
IR137	–	100	–

Sample Number	Mole % $CaCO_3$	Weight % dolomite	Ordering No.
IR138	–	82.00	0.43
IR139	–	<5.00	–
IR140	–	>90.00	0.52
IR141	–	10.00	–
IR142	–	7.00	–
IR143	–	0.00	–
IR145	–	Trace	–
IR146	–	33.80	–
IR147	–	10.50	–

Appendix 3 Trace element concentration of the samples of the Euphrates limestone Formation at Jambur Field.

Sample	Sr	Ba	Pb	Zn	Cu	Ni	Cr
IR2	3275	793	28	24	9	9	0
IR4	414	0	1	0	0	18	0
IR5	520	0	2	-	-	-	-
IR6	506	129	9	-	-	-	-
IR7	502	0	7	-	-	-	-
IR8	449	0	3	-	-	-	-
IR10	237	212	4	-	-	-	-
IR12	-	26	-	64	32	3	0
IR13	8094	226	16	-	-	-	-
IR15	696	0	0	13	0	11	0
IR19	582	747	18	-	-	-	-
IR22	133	0	7	1	0	5359	-
IR22w	19867	147	7	-	-	-	-
IR23	133	32	10	-	-	-	-
IR26	749	22	0	9	0	11	4
IR27	1116	235	8	14	0	10	0
IR29	2630	157	1	7	2	2	0

Sample	Sr	Ba	Pb	Zn	Cu	Ni	Cr
IR30	844	73	40	-	-	-	-
IR31	446	49	7	-	-	-	-
IR33	490	0	01	9	0	2	0
IR34	348	0	17	8	0	0	0
IR37	338	158	75	0	2	0	
IR38	336	0	02	1	0	5	0
IR41	654	904	23	-	-	-	-
IR43	751	940	22-	-	-	-	
IR45	853	597	57	25	0	3	0
IR46	889	0	13	0	0	4	-
IR48	383	32	11	-	-	-	-
IR49	286	150	604	7	0	8	0
IR50	743	614	52	-	-	-	-
IR54	329	11	3	-	-	-	-
IR55	1316	306	34	-	-	-	0
IR56	7371	-	8	-	-	-	-
IR59	512	157	56	25	0	2	0

Sample	Sr	Ba	Pb	Zn	Cu	Ni	Cr
IR62	733	0	22	15	5	1	0
IR65	332	0	1	18	0	0	0
IR66	191	118	6	33	2	14	41
IR69	411	0	1	27	0	17	46
IR71	1046	0	14	7	0	4	0
IR72	728	0	9	14	0	3	0
IR76	1074	0	5	-	-	-	-
IR77	804	0	0	11	0	1	0
IR79	970	0	7	10	0	0	0
IR80	270	-	14	-	-	-	-
IR84	2390	0	9	5	2	0	0
IR85	813	0	12	10	2	0	0
IR86	595	0	1	5	0	1	0
IR87	2419	0	5	3	2	3	0
IR88	4883	0	24	4	8	3	0
IR89	2136	-	7	-	-	-	-
IR91	1642	605	24	-	-	-	-

Sample	Sr	Ba	Pb	Zn	Cu	Ni	Cr
IR93	1918	1135	20	-	-	-	-
IR95	271	0	13	4	0	3	0
IR107	333	0	20	14	251	20	0
IR122	745	0	3	30	213	962	-
IR124	434	-	6	26	0	8	0
IR125	382	0	0	5	0	1	0
IR126	-	0	-	7	0	19	0
IR127a	2690	0	0	8	0	20	7
IR128	302	0	5	4	0	8	0
IR129	377	0	14	17	5	34	39
IR130	532	-	4	7	0	27	21
IR132	387	0	3	8	0	4	0
IR133	380	0	0	10	17	14	0
IR134	343	0	1	15	0	25	23
IR135	353	0	0	9	0	12	0
IR137	179	50	0	11	0	2	0
IR140	237	0	0	34	10	14	22

Sample	Sr	Ba	Pb	Zn	Cu	Ni	Cr
IR144	318	0	0	9	0	5	0
IR145	836	0	0	9	0	4	0

Appendix 4 Isotopic composition of calcite from the Euphrates Limestone formation at Jambur Field.

Sample number	$\delta^{13}C$	$\delta^{18}O$
IR15	0.5	-0.66
IR69	0.61	-1.16
IR95	2.08	-0.83
IR102	0.8	-1.3
IR107	2.5	-1.3
IR120	3.25	-0.5
IR122	0.51	-0.5
IR125	2.6	-0.44
IR126	2.61	0.18
IR128	2.35	-0.26
IR132	1.43	-1.1
IR134	-1.1	-3.1
IR135	2.0	-0.3
IR140	2.95	-0.55
IR143	2.72	-0.68
IR144	2.39	-0.73
IR145	3.2	-0.60

Appendix 5 Isotopic composition of dolomite samples from the Euphrates Limestone Formation at Jambur Field.

Sample number	$\delta^{13}C$	$\delta^{18}O$
IR12	1.96	1.38
IR27	2.9	3.1
IR33	1.23	2.13
IR49	0.75	3.10
IR69	2.0	0.88
IR72	3.34	1.65
IR77	2.63	0.63
IR88	3.51	1.59
IR94	-0.61	3.35
IR95	3.26	0.23
IR111	1.72	2.23
IR122	1.28	3.32
IR134	1.66	0.62
IR135	1.51	2.57
IR138	1.79	2.54

Appendix 6 Results of 300 point counts to calculate the porosity percentages in the studied cores.

Tp Total porosity
Vp Vuggy porosity
Mp moldic porosity
Iec Intercrystalline porosity
Iac Intracrystalline porosity
Ieg interparticle porosity
Iag intracrystalline porosity

Appendix 6-1 porosity percentages in core A

	Porosity types						
Sample	**Tp**	**Vp**	**Mp**	**Iec**	**Iac**	**Ieg**	**Iag**
IR1	19.19	3.00	1.6	14.3	0.33	0.33	2.33
IR2	20.65	15.33	0.33	4.33	0.33	0	0
IR3	19.32	7.66	1	18.66	0.33	1	0
IR4	34.98	13.66	1	18.66	0.33	1	0

Appendix 6-2 Porosity percentages of core B

	Porosity types						
Sample	**Tp**	**Vp**	**Mp**	**Iec**	**Iac**	**Ieg**	**Iag**
IR5	27.32	5.0	2.66	6	2.33	4.0	7.33
IR6	17.64	1.66	5	4.33	2.66	1.33	2.66
IR7	15.32	0.33	2.0	5.0	2.66	4.0	1.33
IR8	17.98	2.66	0	5.33	2.33	3.66	4.0
IR9	11.65	5.66	3.0	1.0	0.66	1.0	0
IR10	20.98	7.66	7.33	3.0	0.33	2.0	0.66
IR11	24.65	5.33	4.66	10.0	0	3.33	1.33

Appendix 6-3 Porosity percentages of core C

	Porosity types						
Sample	**Tp**	**Vp**	**Mp**	**Iec**	**Iac**	**Ieg**	**Iag**
IR12	1.0	0	0	1.0	0	0	0
IR13	11.98	1.66	0	5.0	0.66	0	1.33
IR14	10.32	3.66	0	6.33	0	0	0.3
IR15	1.66	0	0	1.66	0	0	0

IR16	0	0	0	0	0	0	0
IR17	7.33	5	0	2.33	0	0	0

Appendix 6-4 porosity percentages of core D

	Porosity types						
Sample	**Tp**	**Vp**	**Mp**	**Iec**	**Iac**	**Ieg**	**Iag**
IR20	20.32	4.66	2	12.0	1	0.66	0
IR22	28.96	10.66	2.66	12.0	0.66	1.66	0.66
IR24	21.33	8.0	0	13.0	0.33	0	0
IR27	17.66	3.33	0	12.0	2.33	0	0
IR29	19.66	0	0	19.66	0	0	0
IR30	27.64	6.33	0.66	19.0	0.66	0.66	0.33
IR32	12.99	3.33	1.33	7.0	0.33	1.0	0
IR35	29.32	14.33	5.0	9.0	0	0.33	0.66
IR37	23.31	1.0	0.66	10.66	8.33	1.33	1.33
IR39	32.66	5.0	2.0	7.00	13.0	2.0	3.66
IR43	12.32	3.66	3.3	14.0	1.33	0	0
IR45	19.65	0.66	8.0	1.66	2.0	6.33	1.0
IR47	21.31	3.0	10.66	3.66	0.33	0	3.66
IR49	10.98	1.33	3.33	5.33	0.33	0.66	0
IR53	20.33	7.0	1.0	10.0	2.33	0	0
IR59	11.99	1.0	6.0	2.66	1.33	1.0	0
IR62	37.98	9.66	14.33	10.0	0.33	3.66	0
IR64	40.98	10.33	19.0	10.66	0.66	0.33	0
IR66	14.66	0	0	14.66	0	0	0
IR67	13.99	o.330	13.66	0	0	0	0
IR69	0.66	0	0.66	0	0	0	0
IR70	2.29	0.33	1.66	0.33	0	0	0

Appendix 6-5 porosity percentages of core E.

	Porosity types						
Sample	**Tp**	**Vp**	**Mp**	**Iec**	**Iac**	**Ieg**	**Iag**
IR71	30.31	5.66	7.33	6.0	6.66	4.0	0.66
IR73	21.3	2.66	3.33	6.33	7.66	0.66	0.66
IR76	24.98	3.33	10.66	3.66	3.33	3.0	1.0
IR78	27.81	1.0	3.66	5.66	15.33	1.66	0
IR80	30.31	4.66	11.0	3.66	3.33	6.0	1.66

IR83	25.31	0	5.33	9.0	6.66	2.66	1.66
IR84	26.99	1.33	10.0	6.33	8.0	1.0	0.33
IR85	25.33	3.0	0	22.33	0	0	0
IR86	20.31	0	9.66	7.66	1.66	1.33	0
IR88	27.98	6.33	6.33	11.33	0.66	1.33	2.0
IR89	24.98	3.66	7.33	7.0	3.33	2.66	1.0
IR91	12.65	2.33	3.33	2.33	0	3.33	1.33
IR93	23.97	1.66	12.66	3.66	2.33	3.0	0
IR94	20.98	4.33	6.66	5.66	1.33	3.0	0

Appendix 6-6 porosity percentages of core F.

	Porosity types						
Sample	**Tp**	**Vp**	**Mp**	**Iec**	**Iac**	**Ieg**	**Iag**
IR95	6.3	0	2.0	4.3	0	0	0
IR98	19.66	2.33	0.33	17.0	0	0	0
IR102	6.33	0	0	6.33	0	0	0
IR104a	o.66	0	0	0.66	0	0	0
IR106	0	0	0	0	0	0	0
IR107	6.33	0	0	6.33	0	0	0
IR108	1.33	0	0.33	1.0	0	0	0
IR110	10.99	0	0	10.66	0	0	0
IR110c	22.66	1.33	6.66	10.33	3.33	1.0	0
IR113	17.99	1.0	0.66	16.33	0	0	0
IR115	14.33	2.0	4.33	8.0	0	0	0
IR117a	28.0	1.0	3.0	24	0	0	0

Appendix 6-7 porosity percentages of core G.

	Porosity types						
Sample	**Tp**	**Vp**	**Mp**	**Iec**	**Iac**	**Ieg**	**Iag**
IR119	0	0	0	0	0	0	0
IR120	1.0	0	0	0	0	0	0
IR122	0	0	0	0	0	0	0
IR123	0	0	0	0	0	0	0
IR124	0	0	0	0	0	0	0
IR125	0	0	0	0	0	0	0
IR126	0	0	0	0	0	0	0
IR127a	0	0	0	0	0	0	0

IR128	0.66	0.66	0	0	0	0	0
IR129	0.33	0.33	0	0	0	0	0
IR130	0	0	0	0	0	0	0
IR131	0	0	0	0	0	0	0
IR131	0	0	0	0	0	0	0
IR132	0.33	0.33	0	0	0	0	0
IR133	0	0	0	0	0	0	0
IR134	0	0	0	0	0	0	0
IR135	i.33	1.0	0	0	0	0	0.33

Appendix 6-8 porosity percentages of core H.

			Porosity types				
Sample	**Tp**	**Vp**	**Mp**	**Iec**	**Iac**	**Ieg**	**Iag**
IR137	0	0	0	0	0	0	0
IR138	7.99	3.0	0.33	4.66	0	0	0
IR139	0	0	0	0	0	0	0
IR140	0	0	0	0	0	0	0
IR141	0.33	0.33	0	0	0	0	0
IR142	1.66	0.33	0	1.33	0	0	0
IR143	0.66	0.33	0	0.33	0	0	0
IR144	0	0	0	0	0	0	0
IR145	0	0	0	0	0	0	0
IR146	0	0	0	0	0	0	0
IR147	0.66	o.66	0	0	0	0	0

Appendix 7 Percentages of the major rock constituents as calculated using x-ray diffraction analyses of the Euphrates Limestone Formation core samples from Jambur field.

	percentages		
Sample Number	calcite	dolomite	anhydrite
IR2	0	92	8
IR4	0	81	19
IR5	0	76	24
IR6	0	47	53
IR7	0	74	26
IR8	0	69	31
IR10	0	91	9
IR12	-	100	0
IR13	0	100	0
IR15	80	20	0
IR19	0	80	20
IR22	0	70	30
IR23	0	80	20
IR26	0	80	20
IR27	0	90	10
IR29	0	79	21
IR30	0	90	10
IR31	0	90	10
IR33	0	71	29
IR34	0	92	8
IR37	0	88	12
IR38	0	91	9
IR41	0	66	34
IR34	0	31	69
IR45	0	45	55
IR46	0	68	32
IR48	0	82	18
IR49	0	90.5	9.5
IR50	0	28.5	71.5
IR54	0	94.5	5.5
IR55	0	92.5	7.5

	percentages		
Sample Number	calcite	dolomite	anhydrite
IR56	0	94	6
IR59	0	82	18
IR62	0	34	66
IR65	0	100	0
IR66	0	100	0
IR67	0	100	0
IR68	0	100	0
IR69	75	25	0
IR70	55	45	0
IR71	0	86	14
IR72	0	79	21
IR76	0	67	33
IR77	0	76	24
IR79	0	57	43
IR80	0	95	5
IR84	0	78	22
IR85	0	77	23
IR86	0	81	19
IR87	0	86	14
IR88	0	80	20
IR89	0	91.5	8.5
IR91	0	76	24
IR92	0	100	0
IR93	0	90	10
IR94	0	85	15
IR95	97	3	0
IR97	48	52	0
IR99	61	39	0
IR100	43	57	0
IR101	55.5	44.5	0
IR104	76	4	0
IR105	89	11	0
IR107	54	46	0
IR109	50	50	0
IR110	25	75	0

	percentages		
Sample Number	calcite	dolomite	anhydrite
IR111	10	90	0
IR112	20	70	10
IR113	2	90	8
IR115	0	89	11
IR117a	0	95	5
IR117b	0	96	O
IR118a	60	40	0
IR118b	50	50	0
IR119	100	0	0
IR120	52.5	47.5	0
IR121	49	51	0
IR122	90	10	0
IR123	96	4	0
IR124	100	0	0
IR125	100	0	0
IR126	90	10	0
IR127a	88.5	11.5	0
IR128	97	3	0
IR129	41	59	0
IR130	98.5	1.5	0
IR131	90	10	0
IR132	100	0	0
IR133	93.5	6.5	0
IR134	82.5	17.5	0
IR135	93.5	6.5	0
IR136a	0	0	100
IR136b	0	10	90
IR137	0	11	89
IR138	8	92	0
139	100	0	0
IR140	94	6	0
IR141	90	10	0
IR142	94	6	0
IR143	100	0	0
IR144	96	4	0

	percentages		
Sample Number	calcite	dolomite	anhydrite
IR145	94.5	5.5	0
IR146	96	4	0
IR147	90	10	0